Author:
Koptelov, Anatoly

Title:
Autonomous and objective characterisation of composite precursors in manufacturing

AUTONOMOUS AND OBJECTIVE CHARACTERISATION OF COMPOSITE PRECURSORS IN MANUFACTURING

Anatoly Koptelov

A dissertation submitted to the University of Bristol in accordance with the requirements for award of the degree of Doctor of Philosophy in the Faculty of Engineering

September 2021

Word Count: 49334

ABSTRACT

Any composite manufacturing method requires an application of a carefully designed consolidation process to ensure the suppression of voids in the laminate, establish bonding in laminate layers and prevent dimensional or fibre-path defects. The optimisation of consolidation processes relies on the characterisation of the composite precursors' deformability. There are multiple mechanisms occurring in consolidation and various experimental programmes have been suggested in the literature to describe these mechanisms and deduce relevant material properties. The selection of a testing methodology often relies on an initial hypothesis or prior knowledge regarding the deformation modes. This may be a source of significant errors. This research poses questions on the testing rationales, on subjectivity in material testing and on how data-rich programmes should be designed.

The proposed solution to the consolidation characterisation problem is a real-time adaptive testing strategy that enables a "conversation with the material" – flexible autonomous steering of a testing programme reacting on the obtained output. Such system is implemented within this research and is called adaptive consolidation sensor framework. The system's algorithm is set to analyse composite precursor's feedback to compression in real time and to track characteristic signatures relevant to existing consolidation models. Based on that feedback the framework formulates a load programme for the test in a reactive manner. The developed testing system focuses on the identification of the underlying physical mechanisms rather than material properties identification in a rightly or wrongly assumed resin flow mode.

To validate the proposed testing approach, a series of characterisation experiments for different material systems was performed. The obtained results highlight a way forward in terms of rethinking experiments for materials used in manufacturing and beyond.

I would like to dedicate my thesis

to my beloved grandparents

PUBLICATIONS

Conference papers:

1. Koptelov, A., Belnoue, J.P.H., Georgilas, I., Hallett, S.R. and Ivanov, D.S., 2019, August. Machine-driven experimentation for solving challenging consolidation problems. In 22nd International Conference on Composite Materials, ICCM 2019.
2. Koptelov, A., Belnoue, J.P.H., Georgilas, I., Hallett, S.R. and Ivanov, D.S., 2019, August. Consolidation sensor for challenging material characterisation problems. In SAMPE conference Materials, 2019.

Journal papers:

The author would like to acknowledge that Abstract, Chapter 3, Chapter 4, Chapter 5 reuses work published in the paper below.

1. Koptelov, A., Belnoue, J.P.H., Georgilas, I., Hallett, S.R. and Ivanov, D.S., Revising testing of composite precursors – a new framework for data capture in complex multi-material systems, *Composites Part A*, vol. 152, 2022, doi: 10.1016/j.compositesa.2021.106697

Conferences:

1. 22nd International Conference on Composite Materials, Melbourne, Australia, 2019
2. SAMPE conference 2019, Nantes, 2019

Developed software:

The source code for parameters extraction framework (discussed in Chapter 4) is available at https://accis.github.io/DefGenParFit (access to the repository to be granted upon request).

ACKNOWLEDGEMENTS

I would like to express my sincere gratitude to my supervisors for accepting me as a student and for their extraordinary support. I am grateful to Dr. Dmitry Ivanov for his continuous guidance and mentorship throughout my PhD, and prompt and useful advice during my research; Dr. Jonathan Belnoue for his expertise with analytical modelling and experimentation; Prof. Stephen Hallett for monitoring my progress and for his insightful comments and suggestions on my journal paper and dissertation; Dr. Ioannis Georgilas for his technical support on my study.

I would like to thank Dr. Yusuf Mahadik whose expertise with the LabVIEW setup was irreplaceable. I am grateful to Mr. Guy Pearn and Mr. Peter Whereat for helping me with assembling and tuning my testing setup.

I express thanks to Dr. Iryna Tretiak for her expertise and assistance with performing compaction testing. I would like to acknowledge the assistance of Mr. Ian Chorley in preparation of my test samples.

I would also like to thank my dear friends from “the Coffee Crew”: Konstantina Kanari, Steven Grey, Jonathan Stacey and Josh Hoole who walked this journey with me.

Lastly, I would like to thank my parents, Sergey Koptelov and Tatyana Koptelova, whose support and love over the years provided me the strength and determination to keep going.

ACKNOWLEDGEMENTS

In Russian language

Я бы хотел выразить искреннюю благодарность моим научным руководителям за то, что они приняли меня в качестве студента, и за их исключительную поддержку. Я благодарен доктору Дмитрию Иванову за его руководство и наставничество на протяжении всей моей аспирантуры, а также за своевременную и полезную поддержку во время моей работы; доктору Джонатану Бельну за его опыт в аналитической и экспериментальной работе, профессору Стивену Халлетту за полезные предложение и комментарии по написанию моей статьи и диссертации; доктору Янису Георгилиасу за техническую поддержку в моих исследованиях.

Я бы хотел поблагодарить доктора Юсуфа Махадика, чей опыт работы с LabVIEW был незаменим. Я благодарен мистеру Гаю Пирну и мистеру Питеру Урайту за помощь в сборке и настройке экспериментальной установки.

Я выражаю благодарность доктору Ирине Третьяк за ее знания и помощь в осуществлении экспериментальной программы. Я также хотел отметить помощь мистера Иана Чорли в подготовке образцов для тестов.

Я бы хотел поблагодарить моих дорогих друзей из “Кофейной Команды”, которые прошли весь этот путь со мной: Константину Канари, Стивена Грея, Джонатана Стейси и Джоша Хула.

Наконец, я бы также хотел поблагодарить моих родителей – Сергея и Татьяну Коптеловых, чья поддержка и любовь придавала мне сил и решимости двигаться вперед на протяжении всех этих лет.

DECLARATION

I declare that the work in this dissertation was carried out in accordance with the requirements of the University's *Regulations and Code of Practice for Research Degree Programmes* and that it has not been submitted for any other academic award. Except where indicated by specific reference in the text, the work is the candidate's own work. Work done in collaboration with, or with the assistance of, others, is indicated as such. Any views expressed in the dissertation are those of the author.

SIGNED: ..... DATE 14 September 2021

CONTENTS

LIST OF TABLES

LIST OF FIGURES

LIST OF ABBREVIATIONS AND ACRONYMS

AFP	Automated Fiber Placement
ANN	Artificial Neural Network
CP	Cross-Ply
CPU	Central Processing Unit
CT	Computed Tomography
NaN	Not A Number
NCF	Non-Crimp Fabric
ODE	Ordinary Differential Equation
PC	Personal Computer
PDE	Partial Differential Equations
PID	Proportional Integral Derivative
PP	Polypropylene
RMSE	Root Mean Square Error
RTM	Resin Transfer Moulding
RTT	Real-Time Test
2D	Two-Dimensional
3D	Three-Dimensional

1 INTRODUCTION

The production of composites has its own challenges including a possible negative impact on the environment. The manufacture of a part made of carbon fibres requires 14 times more energy than its steel counterpart [1]. The existing methods for recycling of composites through the controlled pyrolysis process are energy demanding as well. To lower the energy consumption and make the manufacturing process more cost-efficient, it is important to reduce the number on unsuccessful manufacturing trials and defective composite parts.

Depending on the required size, geometry, and production rate of a composite structure, the manufacturing methods may be different: manual lay-up, automated fiber placement (AFP), resin transfer moulding (RTM), autoclave molding etc. The processing conditions for a chosen method must be selected with care to achieve target characteristics of a part within the specified tolerance. All these methods have a potential to introduce defects to a laminate structure if the specified manufacturing conditions are not optimal. To avoid such scenario, it is important to have an insight into material's behaviour under processing conditions.

Composites are complex material systems consisting of high strength fibrous network impregnated by a polymer matrix. The deformation mechanisms of composites are non-trivial due to mutual interactions between phases on different structural levels. To investigate these aspects of composites deformability, a characterisation of material behaviour under processing conditions must be performed. Due to the complexity of flow and deformation mechanisms, conventional approach requires a number of tests to

be conducted to gather enough data for a further material characterisation. However, manufacturing and testing is both expensive and time consuming.

A typical material's characterisation process involves a training of a chosen phenomenological model by fine-tuning its parameters. The goal is to achieve model's output similar to a material's actual behaviour. In order to estimate an obtained model's performance there is a need for a clear criterion of an efficient characterisation. Plain experimental program or low number of conducted tests could be insufficient for material's characterisation. Derived model might perform deceptively well within data provided for training but completely fail to adapt to changing processing conditions. The research question is how complex loading program should be and how many experiments is enough.

There is a vast variety of different physical models of resin flow occurring on macro and micro levels of the material. Normally, it is unclear for a researcher how material behaves during the compaction test. For this reason, the dominant deformation mechanism is assumed prior to the experiment and the testing program is designed in accordance with that assumption. Such approach introduces bias into the testing which might affect the validity of characterisation outcome within a different set of processing conditions.

There is no universal solution for the problem of characterisation of composites. The application of the machine learning techniques is more suitable for learning patterns of a studied system. The resulting models are not fully descriptive and do not provide an insight on the physics/nature of acting mechanisms. The development of analytical models of composites' deformation behaviour is very challenging. The studied mechanisms are often interconnected with each other and involve dozens of material parameters. Therefore, there is a need in a predictive tool capable of designing testing programs based on the material's viscoelastic behaviour, thus reducing the total number of experiments to a minimum.

To address the described technical challenges for characterisation of composite precursors, the aims of this research are specified as follows:

- Demonstrate the importance of sufficient experimental data for the robust material characterisation. Set the criteria for successful material model identification and the requirements for the characterisation testing approach.

- Develop the framework for the identification of material properties from experimental data. The system must be able to take advantage of the expanded datasets from several experiments and investigate the material models of choice specified by the researcher.
- Develop the autonomous unbiased testing system for the characterisation of composite precursors. The idea of the proposed approach is to build such a testing system, which will not be bound by any predefined assumptions about material's behaviour. Therefore, there will be no bias towards any supposed deformation mechanism. In that case a testing algorithm is not limited by a certain type of the material or researcher's previous experience.

2 LITERATURE REVIEW

The importance of the consolidation in composite manufacturing and its influence on the final quality of the composite part is discussed in the first part of this chapter. It is crucial to understand the underlying deformation mechanism in the laminate to avoid manufacturing defects and to achieve target dimensional tolerances.

Identification and characterisation of the predominant consolidation mode is not a trivial task. There is a vast variety of different mechanisms acting on different structural scales of the laminate (micro-, meso-, macro-). These mechanisms are often interconnected with each other, and it is hard to isolate a single phenomenon for studying. The review of some of these mechanisms is presented within Section 2.2 of this chapter.

Then, a review of conventional approaches for characterisation testing of composites is presented. There are a number of challenges arising on how to design an experimental programme. The conducted test should reveal the characteristic features of material behaviour for further analysis. There is no universal approach on how to perform testing and the choice of the test programme is often based on the experience of the researcher. It is also important to collect the sufficient amount of experimental data within minimum test trials.

Finally, different approaches to processing the obtained experimental data are discussed. Upon receiving the results of the test, it is necessary to develop a comprehensive material model which can adequately describe the behaviour of the composite. Advantages and limitations of different techniques and their applicability to the material characterisation problem are discussed within this chapter.

The proposed project is set to address the discussed challenges in material testing and to successfully characterise composite precursors under the processing conditions.

2.1 Consolidation of composite precursors as a central process of composite manufacture.

Consolidation in composite manufacturing is the process of plies engaging into contact and subsequent removal of volatiles and resin excess due to the application of processing conditions (temperature and pressure). The end goal of this process is to transform a stack of prepreg layers into a monolithic laminate [2]. Consolidation involves complex interactions between part geometry, tooling, pressure application programme, temperature, and fibre network/resin properties [3]. The diversity of factors involved makes the characterisation of the consolidation process a challenging task.

Consolidation of composite precursors is a quality-critical process in the manufacture of composites. It is essential in forming of thermoplastic components, debulking/autoclaving of prepregs, thermoforming of textile preforms prior to liquid moulding, etc. Consolidation-driven phenomena occurring during composite manufacture can lead to:

- The formation of internal wrinkles (non-visible out-of-plane fibre misalignment), external wrinkles (visible out-of-plane fibre misalignment), or in-plane waviness (in-plane fibre misalignment within a ply).
- Deviation from the target thickness of a laminate.
- The presence of voids in the laminate's structure.
- Shape distortions of a composite part (spring-in, warpage, fibre misalignment).

Understanding the underlying consolidation mechanisms is a key factor in achieving the designed characteristics of the laminate. The current section of the literature review covers the influence of the consolidation on the final quality of a composite part and the aspects of consolidation-driven defects formation.

2.1.1 The influence of consolidation on defects formation

Deformability of composite precursors defines their susceptibility to defects. Vast variety of composite manufacturing methods involves applying composite precursor layer by layer onto the surface of a tool/mould in manual or automatic manner. Then, the laminate is consolidated within the corresponding processing conditions (pressure and temperature) in order to remove entrapped air and to facilitate the required adhesion between neighbouring plies. As consolidation proceeds, composite layers are forced to comply with the geometry of a tool. In the case of component features, such as tapers,

corners, double curvature etc, this often leads to the generation of excess length that can be adapted through inter-ply shearing or, in the case of the absence of relative shear between plies, cause wrinkling or in-plane waviness [4]. Fibre wrinkle is a type of a through-thickness defect with an out-of-plane misalignment of fibres with local waviness [5]. If the bending-induced compressive stress resulting from the deformation is too high, the buckling of plies closer to the mould's surface (with larger excess length) is likely to occur causing the formation of out-of-plane wrinkles. Moreover, in-plane fibre waviness may occur due to the generated excess length of plies folding over each other [6].

The severity of this type of a defect can be characterised by its geometric parameters – amplitude, wavelength, and misalignment angle [7]. Depending on the geometry of the part, the through-thickness deformation of the laminate may lead to the formation of wrinkles or fibre crimp. Different research groups conducted studies to develop robust numerical and analytical consolidation models to predict wrinkles formation during composite manufacture [8], [9], [10].

Such defects can significantly impair the performance of the composite. Wrinkling disrupts the structure of fibre network, causing the build-up of extra bending stresses in fibres. It leads to a higher level of inter-laminar stress provoking delamination, resulting in premature failure of a composite part at significantly reduced loads [11]. Series of compression and tensile tests of flat coupons made of carbon fibre reinforced plastics were carried out by Nartey et al. [12] in order to estimate an impact of wrinkling of varying architectures (angles and amplitudes) on failure modes and overall strength knockdown of a composite. The results of the research indicated a significant drop in tensile and compressive strength of the part with the most severe wrinkling architecture by 21% and 37%, respectively. The impact of wrinkles on the premature failure of L shaped composite parts was investigated by Hu et al. [13]. It was shown that the introduction of wrinkles induces delamination due to the damage in the area of wrinkled plies. A significant strength knockdown of 30–40% was observed in both the numerical simulation and experimental results due to the local stress concentration in the damaged areas.

2.1.2 The influence of consolidation on achieving target thickness of a composite part

Understanding of the consolidation mechanism is crucial for achieving the target thickness of a composite part. The tolerance on thickness within the aerospace industry can be as tight as ±0.25 mm. As it was demonstrated by Matveev et al. [14], different processing conditions can lead to different levels of prepreg compaction. It was shown that the absence of the robust consolidation model can lead to significant thickness deviations even for simple-shape flat laminates.

The impact of ply thickness variation on mechanical properties of the laminate was investigated by Zhang et al. [15]. The research highlighted the influence of the ply thickness uncertainty on the probability of composite failure. Both fibre- and matrix-dominated thickness uncertainties were considered. It was demonstrated that thickness variability can cause a detrimental effect on laminate's failure. Additionally, it was noted that it is a non-trivial task to distinguish the dominating mechanism (fibre or matrix) as both may be present and interconnected with each other.

In order to ensure the compliance with dimensional tolerances, it is necessary to predict the compaction response of the material during consolidation process for chosen loading and temperature conditions. There is a number of studies aiming to develop comprehensive compaction models for a wide range of materials and manufacturing methods. The simulation of an autoclave process for thermoset matrix precursors was performed by Li et al. [16] as a two-dimensional consolidation problem. The numerical model developed within this study allows to describe the change of thickness profile and fibre volume fraction in the centre and edge regions of the laminate. Due to different consolidation rates in these regions (resin is able to flow out from the edge, hence, compaction runs quicker), the target thickness is achieved at the edges of the laminate first. The compaction continues in the centre until uniform thickness is established in all locations of the laminate. But if full consolidation is not achieved, the edge effect can cause thickness deviations in the part. It was shown by Hojjati et al. [17] that simply increasing operational pressure does not solve the problem of incomplete consolidation. Therefore, a proper compaction model is needed to select optimal processing conditions and to ensure the uniform final thickness of the composite structure.

There are different ways to estimate the achieved consolidation level of the part. It can be done in terms of fibre volume fraction, thickness, or void content. For instance, the

consolidation process in filament wound thermoplastic matrix composites was investigated experimentally by Roychowdhury et al. [18]. In that study the consolidation quality as a function of the applied load (tension in the filament) and winding speed was assessed in terms of the achieved void content and the average shear strength. It was demonstrated that the resin flow played the dominant role in determining consolidation quality. The results indicated that deviations from optimal load/temperature conditions can lead to a higher void content in the composite and impair part's performance.

2.1.3 The influence of consolidation on maintaining composite part's geometry

Composite parts with curved geometry may experience shape distortions as they are released from the tool. Deviations from the designed geometry results from the balancing of process induced residual stresses [19]. It can lead to part's dimensions falling out of the specified tolerance. The lack of reliable methods for predicting shape distortions of composite parts leads to an increase of development and manufacturing expenses due to the increased number of manufacturing trial attempts.

As shown by Wisnom et al. [20], there are four main mechanisms causing the build-up of residual stresses during manufacturing: thermal, chemical, tool-part interaction and consolidation-driven. Since the subject of this study is the characterisation of consolidation process, the first three mechanisms fall out of the scope of this research and are discussed briefly.

- The mismatch in thermal expansion properties between matrix and fibre phases leads to the build-up of residual stresses at the microscale level during the cooling stage. The 65% reduction of angled part's shape distortion by means of lowering resin's thermal expansion coefficient was reported by Shaker et al. [21]. The difference in thermal strains in fibre and transverse directions can lead to curvature or twisting in case of unbalanced laminates. Finally, laminates can experience deviations from the target curved geometry due to the difference in in-plane and through-thickness expansion coefficients [22].
- The chemical shrinkage of polymers occurs during cure stage, causing a substantial change in resin's volume. Similar to the thermal contraction case, it results in residual stresses at the microscale level or in-plane stresses in the laminate [23].

- Tool-part interaction can be the source of laminate's shape distortions. Metal tools are subjected to higher thermal strains than a composite due to the difference in thermal expansion coefficients. As the part released from the tool, non-uniform through-thickness in-plane stresses arise, causing the part to bend.
- The composite part can exhibit thinning or thickening in its curved regions due to the consolidation and resin flow. The flow of resin in angle laminates manufactured with the autoclave process under wide range of processing conditions was investigated by Hubert et al. [24]. It was demonstrated that the resin flow causes either corner thinning or corner thickening depending on the tool (convex or concave respectively). Substantial thickness variation (13% deviation from the baseline value) at radii of a 32 ply unidirectional carbon-epoxy curved beam was also reported by Wisnom et al. [25]. The corner thinning/thickening results in fibre volume fraction variations and resin rich regions which contributes to an increase of part's curvature. The phenomenon of geometry distortions due to acting residual stresses is commonly referred to as the spring-in effect.

Extensive experimental and analytical research has been conducted to study the spring-in effect in parts of different shapes (L-, V-, C- and U-shaped angled laminates) and its impact on composite part's geometry. The contribution of thermoelastic and non-thermoelastic factors to the developed spring-in for C-shaped cured preforms (Hexcel AS4/8552 thermosetting composite) was studied by Ersoy et al. [26]. It was shown, that thermoelastic effects account for only 50% of the developed spring-in angle, and the rest was considered to be driven by the consolidation mechanisms. Spring-in behaviour of L-shaped glass fibre parts during manufacturing was investigated by Causse et al. [27]. Due to the low processing temperature (slightly above room temperature) the consolidation was considered to be the main source of shape distortions. It was reported that consolidation stresses have a serious impact on composite part's residual deformations when concave tool was used. Moreover, as shown by Hubert et al. [24], the flow of resin during consolidation can have a significant effect on the final dimensions of curved parts. The influence of laminate's thickness and resin flow conditions on the resulting spring-in angle for L- and U-section geometries was studied by Çinar et al. [28]. The parts were manufactured of Hexcel AS4/8552 material in an autoclave. Both numerical and experimental results confirmed corner thickening effect due to the resin percolation. The resin bleeding was not uniform along the length of the

part and was more intense at the edges. A higher level of spring-in was reported for parts manufactured under bleeding conditions due to the through-thickness fibre volume fraction gradient.

Another source of dimensional distortions can be perturbations in the laminate structure, such as a layup angle misalignment or deviations in the fibre content. As it was shown by Kim et al. [29], even minor deviations from the designed microstructure may result in dimensional instabilities of a part such as warpage. It was concluded that the comprehensive material characterisation routine allows to estimate the dependence of dimensional tolerances of a part on microstructural parameters perturbations (layup angle and fibre content). The occurrence of warpage due to the through-thickness gradient in fibre content for V-shaped laminate was reported by Jerpdal et al. [30]. Warpage can occur even in flat unidirectional laminates due to through-thickness fibre volume fraction variations as shown by Radford et al. [31]. It was reported that non-uniform resin content is prone to arise in case when resin bleeds out during consolidation. It results in the difference in thermal expansion coefficient in laminate layers and subsequent shape distortions (convex bowing).

Therefore, consolidation, along with other mechanisms (thermomechanical effects, chemical shrinkage, tool-part interaction), is one of the key drivers causing shape distortions of the composite part during manufacturing. Relevant material compaction model is required to achieve specified geometry as it provides control of material and process parameters.

2.1.4 Summary

Thus, the challenge of consolidation characterisation is relevant for a wide range of manufacturing methods, parts' shapes/geometries, and materials. It is crucial to have a robust consolidation model for a chosen material. It allows the researcher to:

- determine optimal processing conditions for a chosen composite manufacturing method.
- achieve target fibre volume fraction and correct dimensional tolerances by predicting the compaction response of the material.
- maintain the desired geometry of the part and avoid shape distortions. Consolidation is one of the key factors causing spring-in effects and deviations from the target geometry.

- have a clear understanding of the problem of defects formation (wrinkling, voids etc.)
- The main goal of the characterisation of the consolidation process is to understand how material flows and deforms under processing conditions. There are variety of different deformation mechanisms taking place at different structural scales during consolidation process. An overview of these mechanisms is presented in the next section.

2.2 Deformation mechanisms

Material response in consolidation arises from a complex interaction of various deformation mechanisms (i.e. the internal or percolation flow of resin [32], flow of fibrous suspensions [33], densification of reinforcement [34], [35], relative movement of plies [36], and others). Different forms of these mechanisms take place at different structural scales and often occur in parallel or exhibit transition from one state to another.

Deformability of a composite is defined by the resin flow mode and/or the deformability of the reinforcement [37]. Several deformation modes of a composite precursor under processing conditions can be identified: shear flow of resin, percolation resin flow and the deformation of the reinforcement. The co-existence of different deformation phenomena and the transition from one mode to another was reported in a number of studies [38], [39]. For instance, as shown in Figure 2.1, characteristic features for both percolation (resin bleeding) and shear (ply distortion) flows were reported by Belnoue et al. [40].

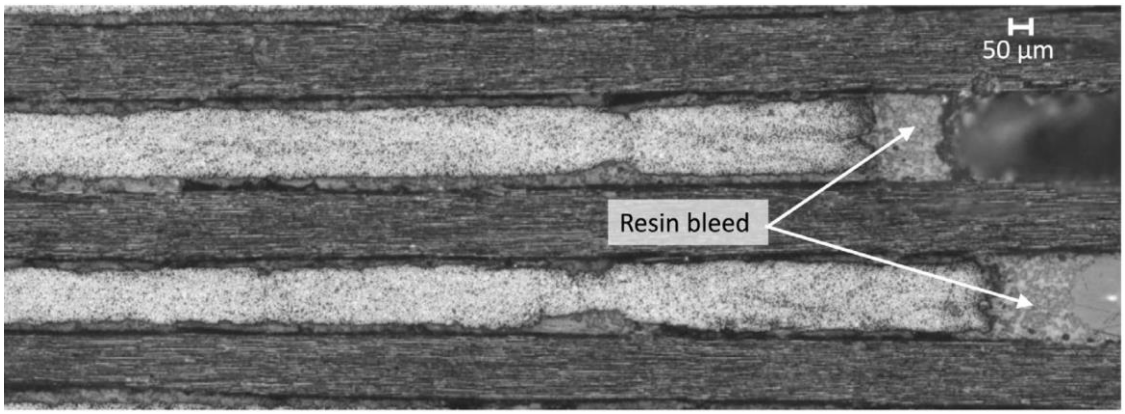

a

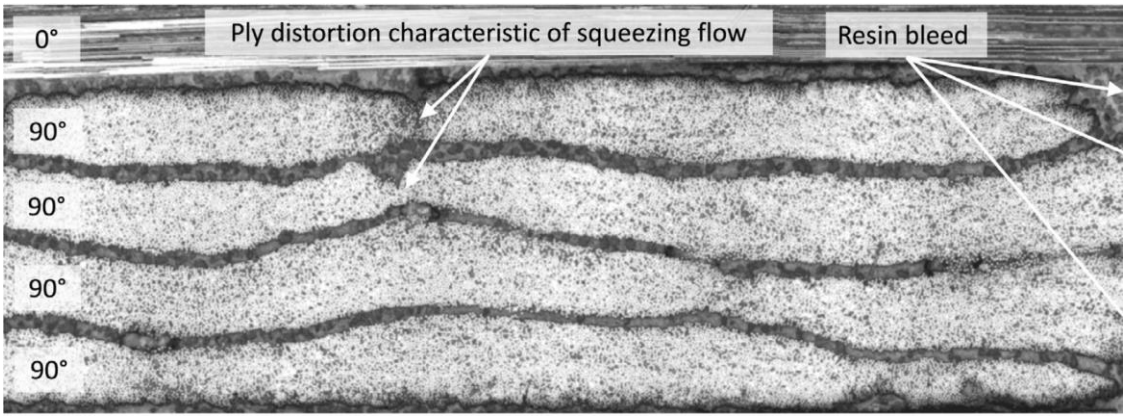

b

Figure 2.1: Different resin flow mechanisms [40]**; a) resin percolation, b) shear flow of resin.**

The purpose of this section is to demonstrate the vast variety of different deformation mechanisms occurring at different scale levels (micro, macro, meso) of the laminate during consolidation. Mathematical representations and derivations of governing equations for different resin flow modes are considered further in chapter 3.

2.2.1 Shear flow

For the shear flow in composite precursor matrix and reinforcement phases are considered to be moving together as a whole. For this type of resin flow the material is treated as a highly anisotropic viscous fluid. Key assumptions for the compaction model of shear resin flow include:

- The resin flow perpendicular to the fibre direction is prevalent. This effect is due to the very large value of extensional viscosity in the axial direction in comparison to transverse shear viscosity [41]. Therefore, the apparent dominant flow occurs across fibre orientation as resin follows the path of least resistance.
- The material is represented as a combination of inextensible fibres surrounded by incompressible viscous resin [42]. Due to that and the assumption that there is no resin percolation out of fibre bed (which imposes limitations on the viscosity of resin and entanglement of fibres [43]), the whole laminate is approximated as an incompressible anisotropic fluid.
- Normally, fibre tows are not ideally aligned prior to compaction and a slight twisting in orientation exists. As pressure gradient arises, twisting is further

developed trying to make inextensible fibre increase its length. Therefore, a twisted fibre acts as an effective brake on transverse resin flow. This mechanism was proven experimentally [44] after observing a distorted fibres in a specimen subjected to a transverse flow.

Shear flow is one of the key healing mechanisms at the stage of manufacturing of a composite part. Such an effect is achieved due to the squeeze resin flow in the direction perpendicular to fibres. Redistribution of matrix and reinforcement phases results in establishment of a bonding effect in laminate layers and elimination of voids and resin-dry regions [45]. Any composite manufacturing method requires an application of a sufficient consolidation pressure to ensure the suppression of voids in the laminate. However, an excessive consolidation pressure may induce a significant resin flow in the transverse direction and cause an irregularity in the composite structure such as fibre misalignment [46], which in turn affects the dimensions and mechanical properties of a composite part [47]. A robust analytical model of a shear resin flow allows to define optimum conditions of manufacturing process by predicting realistic deformation of a composite without causing undesirable defects in the fibre network.

Shear flow of an incompressible suspension can occur at the scale of resin bridges connecting isolated plies [48], of tapes deposited in automatic fibre deposition (AFP) processes [49], of individual yarns in dry fabric [50], of broad good prepreg plies [39], or even of entire component [44]. Different scales of acting deformation mechanisms within shear resin flow are shown in Figure 2.2.

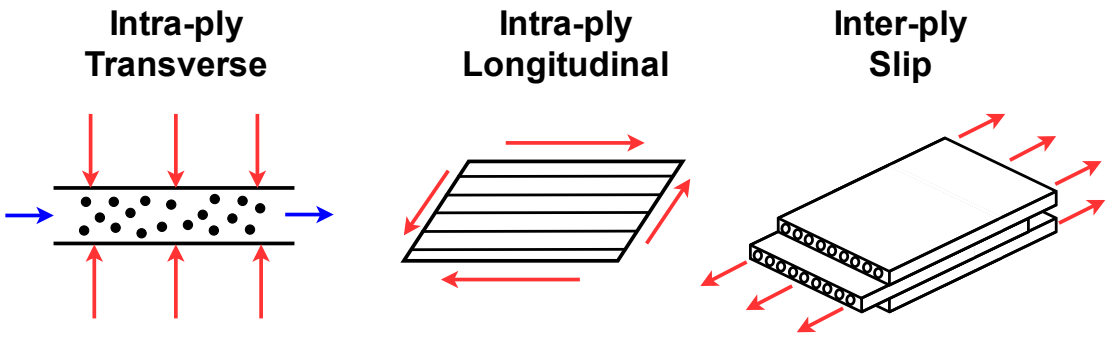

Figure 2.2: Shear flow mechanisms at different scales of the laminate.

There are two main deformation modes of shear resin flow acting on a ply level (intra-ply): across and along fibre direction as shown in Figure 2.2 (left and middle). Intra-ply shearing of individual fibres is an important mechanism in the formation of complex

curvature shaped composite parts. Due to the fibre inextensibility assumption, a flat sheet of composite precursor can only accommodate the curved shape of the tool through shearing, as fibres length must remain constant [51].

As shown by Hubert et al. [52], the estimated ratio between transverse and longitudinal intra-ply shearing viscosities varies significantly (0.77 to 2.0) within different research groups. It is not a trivial task to induce pure intra-ply shear in a test specimen without triggering inter-ply slip, which might be the source of discrepancies in viscosity measurements. The experimental characterisation of intra-ply shear behaviour of carbon fibre thermoplastic composite (APC-2) was conducted by Stanley et al. [53]. A custom-built apparatus for the steady-shear testing was introduced within the study to achieve pure intra-ply shear. The findings from this research indicate longitudinal to transverse viscosities ratio at 1.3.

- Shear flow can occur on the inter-ply scale (inter-ply slip). During the manufacturing of a composite part a resin-rich interface is formed between adjacent prepreg layers to achieve full consolidation and bonding between plies with different orientations [44]. Such resin rich region acts as a lubricant between adjacent plies and can facilitate shear deformations at the inter-ply level of the laminate [52] (as shown in Figure 2.2 on the right). Relative motion of two sliding prepreg layers can be a major source of manufacturing defects, including geometry distortions and out-of-plane wrinkling [54].
- An experimental investigation of this phenomenon was conducted by Vanclooster et al. [55]. Within that research, a series of ply pull-out tests was performed to study inter-ply shear behaviour of glass/PP fabric. An increase of yield stress was reported for lower values of the temperature and higher load application rate. Authors attributed this effect to the viscous nature of the inter-ply slip phenomenon. An increase of the applied pressure leads to the reduction of the resin-rich interlayer's thickness, which explains the increase of the yield stress for the higher values of the applied load. Another study on the influence of the processing conditions on the intra-/inter-ply shear behaviour of thermoplastic composite (Carbon/PP) was presented by Chen et al. [56]. The numerical and experimental trials were aimed to investigate the cohesive properties of the resin interlayer within a ply-pull testing for a range of operating temperatures. The numerical representation of inter-ply interaction was implemented through the three-dimensional cohesive element as opposed to the conventional approach,

where this phenomenon is modelled as contact between adjacent plies. The proposed approach allowed to predict different stages of the shear force evolution (fast increase – elastic response, peak – inter-ply slip, drop – relative motion of plies) within different processing conditions. The numerical results were then validated through a series of ply pull-out experiments where both inter-ply and intra-ply shear mechanisms were observed. Similarly to [55], the dependency of the yield stress on temperature and load application rate was reported.

2.2.2 Percolation flow

Percolation flow in composite manufacturing is a flow of resin through the network of fibres within the laminate [57]. The composite precursor is considered to behave as a permeable medium impregnated with a viscous fluid, where the reinforcement phase is represented as a network of elastic bending beams with multiple contact points [58]. There is a tendency for percolation flow to occur in materials with low viscosity matrices. The characteristic feature of such resin flow mode is the escape of resin from the laminate (resin bleeding) without shifting fibre network.

Percolation of resin under compaction pressure is one of the essential mechanisms in composite manufacturing. This flow mechanisms affects the degree of impregnation and plays an important role in bonding of adjacent plies in the laminate. By allowing resin to bleed through the reinforcement, a resin rich interface between the plies is formed, which directly contributes to the bonding of prepreg layers with different ply orientations [44].

Percolation consolidation model is described in the series of papers [59]–[61]. The proposed model is based on two main phenomena: resin flow through fibre network and elastic deformation of fibres. The detailed mathematical representation of the percolation resin flow is discussed in chapter 3.

Darcy's law is one of the most common modelling approaches to describe the flow through the porous medium. It describes the influence of the viscosity η and permeability K of a porous medium with the thickness h on the resin's velocity V induced by the pressure gradient ΔP_{res} [62], as follows:

$$\boldsymbol{V = -\frac{K}{\eta}\frac{\Delta P_{res}}{h}}. \qquad 2.1$$

The relation for flow motion (Darcy's law) is coupled with the deformation of porous medium through one of the fundamental assumptions in percolation flow under consolidation. The assumption about the balance between the pressure acting in resin and stresses caried by fibrous network was proposed by Terzaghi [63] (initially introduced for soil mechanics). It states the so-called additive superposition approach in which the applied pressure is counteracted by the sum of total pressure in resin and in fibre network. According to this assumption, the balance equation can be written as follows:

$$\boldsymbol{P_{applied}} = \boldsymbol{P_{res}} + \boldsymbol{P_{pre}} \qquad 2.2$$

where $P_{applied}$ is the applied pressure, P_{res} is the average resin pressure, P_{pre} is the fibre bed response. This assumption is widely used in mechanics of composite precursors, for instance [52], [57], [64], [65].

At the initial stage of the compaction the applied pressure is carried entirely by the resin phase and the fibre network remains unloaded. Nonetheless, due to the build-up of a pressure gradient resin starts to bleed out of the laminate. Consequently, fibre network compresses as well causing neighbouring fibres to come into contact and to carry a portion of a load which concurrently reduces resin pressure as shown in Figure 2.3 (σ_A represents the material spring constant influencing the fibre bed reaction, discussed in chapter 3). In the extreme case, when the resin is free to escape from the laminate, the applied load is balanced entirely by the fibre response and the resin pressure reduces to zero. Thus, final achievable thickness of the laminate is solely defined by the deformation characteristics of the fibre network.

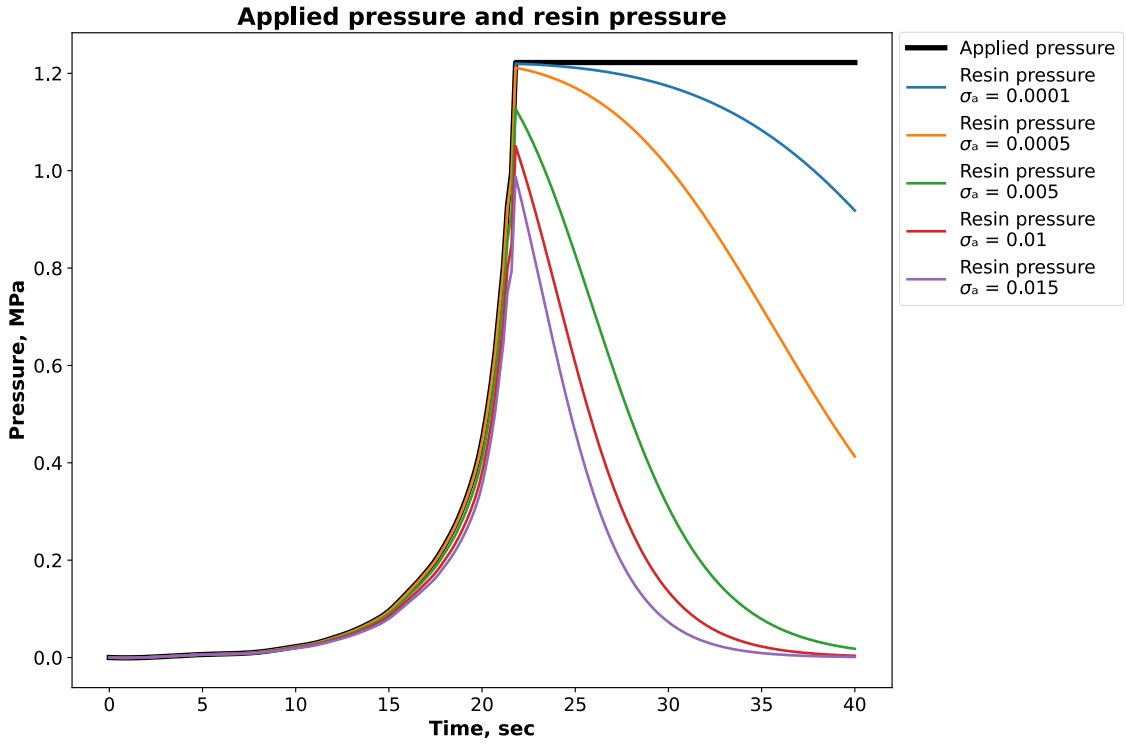

Figure 2.3: Applied pressure and resin pressure evolution during the compaction experiment.

The Terzaghi's assumption on the additive nature of the external pressure redistribution was originally developed for the characterisation of granular soils and is widely disputed within the research community. The original relation for stress formulation was extended by taking into account the degree of medium's saturation, the matric suction of dry regions, and the spatial distribution of the liquid phase [66], [67]. It illustrates the complexity of the balance equation problem for the saturated porous medium. Further discussion on the aspects of soil mechanics falls beyond the scope of this research.

Similar to other deformation mechanisms, percolation flow occurs at different scales of the composite precursor, including low-permeability gaps between fibres (intra-tow in the range of 10 µm, see Figure 2.4.a), high-permeability channels between tows (inter-tow in the range of 0.1 mm, see Figure 2.4.b) or through the thickness bleeding flow to an external bleeder [68]. The percolation flow mechanisms on intra-/ inter-tow scales are defined by acting capillary forces on the level of single fibres in the bundle (intra-tow) and viscous flow in the interspaces between fibre bundles (inter-tow). If the influence of the capillary effect is high, the inter-tow voids can appear in the space

between yarns. On the contrary, if the flow on the inter-tow scale is prevalent, then voids can be trapped in the micro-spaces between fibres [69].

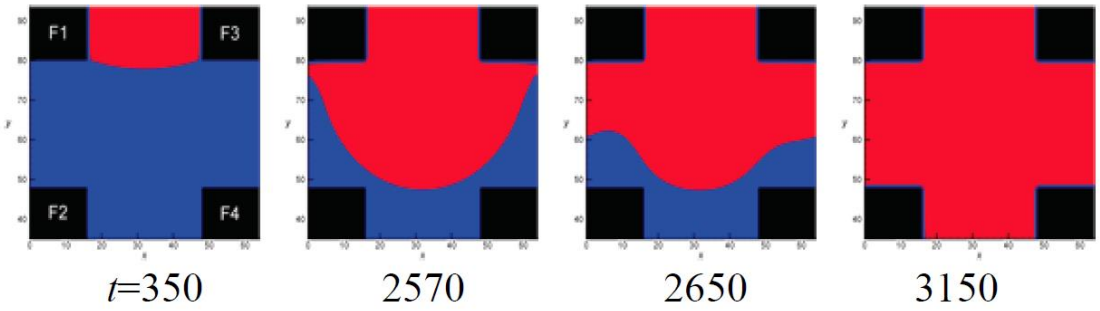

a

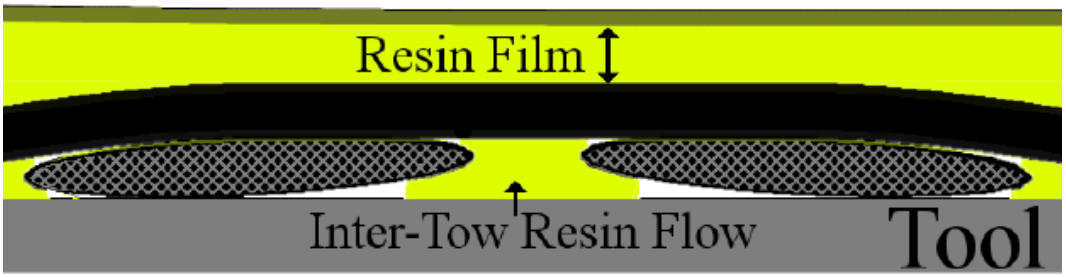

b

Figure 2.4: a. Intra-tow percolation flow [70]**. Black – fibres, blue -intra-tow gaps, red - resin; b. Inter-tow percolation flow** [71]**.**

The flow of resin on the scale of individual filaments was investigated by Inoue et al. [70]. The study was aimed at mathematical modelling of resin filling the gaps between fibres in the bundle on the microscale level. Two directions of resin flow were considered within the numerical simulation (as shown in Figure 2.4.a): the longitudinal-flow (main direction of the flow) and the transverse flow when the resin percolates into interspaces between filaments being driven by the capillary force. It was established, that the timescale for the transverse flow must be sufficient to release the entrapped air from the gaps. Authors concluded that microscale aspects of the intra-tow percolation resin flow directly influence voids generation.

An analysis of the inter-tow viscous flow of resin through the hexagonal array of fibre bundles was performed by Papathanasiou [72]. The dependence of the permeability of the medium on the inter-tow porosity and the arrangement of fibres within the bundle

(hex and square) was established within that study. Meso-scale percolation flow is relevant not only for the scale of fibre bundles but also for tapes deposition within automated fibre placement process. The effect of resin flowing into the gaps between neighbouring tapes was investigated by Li et al. [73]. Depending on the tooling (hard or soft), the regions of the composite with different levels of curing pressure caused resin to flow in the areas of gaps and overlaps. The study of this phenomenon allowed authors to build the robust numerical model of the process capable of predicting the influence of defect size on the strength knockdown of the specimen.

It is a challenging task to isolate the flow phenomenon at a single structural scale for studying, as inter- and intra-tow flow are interconnected and occur concurrently. The evolution of percolation flow at different scales was investigated by Cender et al. [71] within the study on resin impregnation of woven fabrics. Initially, the resin flow started with filling inter-tow gaps. As 35% of the total area was filled with resin, the initiation of the intra-tow flow was observed. As concluded by the authors, the transition between flow modes depends heavily on the applied pressure and temperature.

Percolation flow may occur on the macro scale of the laminate. If the composite precursor is processed under bleeding condition (bleeder is placed on top of the laminate), the resin pressure gradient is formed in in-plane and through-thickness directions. It provides the driving force for the resin to flow from the bottom to the top surface of the laminate, and to the bleeder. Such phenomenon results in different values of fibre volume fraction in the regions with different thickness, for instance in the tapered laminate as shown by Gu et al. [74]. The intensity of the through-thickness flow is significantly affected by bleeder's thickness as established by Ganapathi et al. [75]. A coupled cure-compaction numerical simulation of thick laminate's consolidation was performed within that study to predict resin's content and laminate's thickness in dependence of bleeder's parameters (thickness, permeability). The coupled nature of percolation flow was also reported by Thomas et al. [76]. Within that study, in-situ monitoring of through-thickness impregnation of one-layered fabric was performed. The authors observed the initiation of percolation flow at intra-tow scale after ~16 minutes from the start of the experiment.

2.2.3 Deformation of the reinforcement

Another group of material models is related to the deformation of the reinforcement. Many examples of reinforcement's deformability characterisation are available in the literature.

Visco-elastic model for compaction and relaxation of woven fabrics' reinforcement was proposed by Breard et al. [77]. The goal of the study was to distinguish the mechanical properties of the reinforcement from the resin flow properties. The proposed model (based on the generalised Kelvin-Voigt model for soils) was set to describe the rearrangement of fibre bundles caused by the effect of fluid pressure. This deformation mechanism can be characterised through the level of the porosity at micro- and macro-scales, as the fibre bundles were assumed to fill open spaces between the pores.

The need of taking into account permanent deformation of the reinforcement was addressed by Somashekar et al. [78]. In that study, a series of compaction tests for different types of glass fabric was performed. The results indicated three distinctive stages of dry material deformation: elastic spring-back, permanent (unrecovered) deformation, and recovery. These factors were influenced by the fibre volume fraction, layup, and load application rate.

The characterisation of reinforcement's deformability can be done at different structural scales of composite precursors. The numerical and experimental study on woven fabric's compaction (Hexcel G986) at the mesoscopic scale was performed by Nguyen et al. [79]. The object of the study was to determine the influence of the plies' relative orientation and the ply nesting on the compaction behaviour of the specimen. The fibre bed behaviour was assumed to follow rate (hypoelastic) constitutive law. It was established, that for different layups the compressive rigidity of the ply-stack may vary significantly due to the nesting effect. Another example of hypoelastic modelling approach was demonstrated by Badel et al. [80]. Within that study, the deformation of the reinforcement unit cell during the preforming stage was approximated with the continuum rate constitutive model. The proposed model accounts for meso- (change of the yarn cross-section shape) and macroscopic factors (fibre bed compaction and bundles rearrangement). The results of the simulations were in a good agreement with the actual evolution of the yarn's cross-section, as shown in Figure 2.5. As concluded by the authors, one of the possible developments of the considered approach is the implementation of coupling with resin flow simulation within deformed reinforcement.

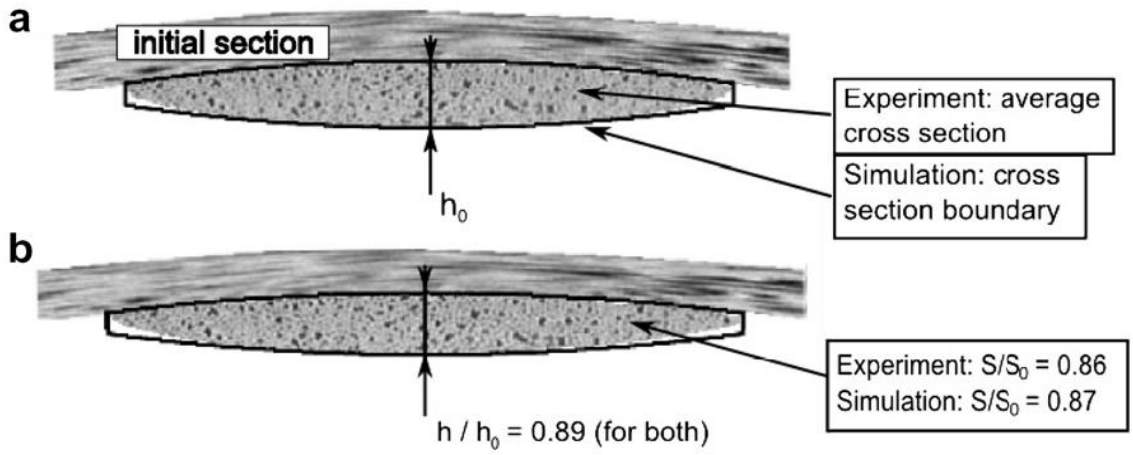

Figure 2.5: Reinforcement deformation under tension [80]**; a) initial state of the yarn cross section; b) deformed state of the yarn cross section.**

2.2.4 DefGen ProToCoL model of resin flow

The phenomenological hyper-viscoelastic consolidation the DefGen ProToCoL (Processing Tools for Composite Laminates) model [14], [38], [40], [81]–[84], [85] was developed to describe toughened prepregs systems with large range of viscosities at different temperatures. It has characteristic features of both shear and percolation flows. For example, it explicitly links the thickness evolution of a prepreg stack to the initial width and thickness of the constitutive plies within the stack (which is typical for shear flows) and, at the same time, converges to a compaction limit under compression (which is usually related to bleeding flows).

The results of the compaction testing (IM7/8552 and IMA/M21 prepregs) indicate significant variations in final thickness of specimens with different layup configurations [14], [39]. The plies' aspect ratio (thickness/width ratio) plays an important role in thickness evolution during compaction and the compaction limit of the layup. As shown by Belnoue et al. [40], the DefGen model is capable to describe the compaction behaviour of the material for different stacking sequences of a specimen, different aspect ratio of thickness to width, different processing conditions and strain rates. The examples of the considered layups within the study [39] are shown in Figure 2.6.

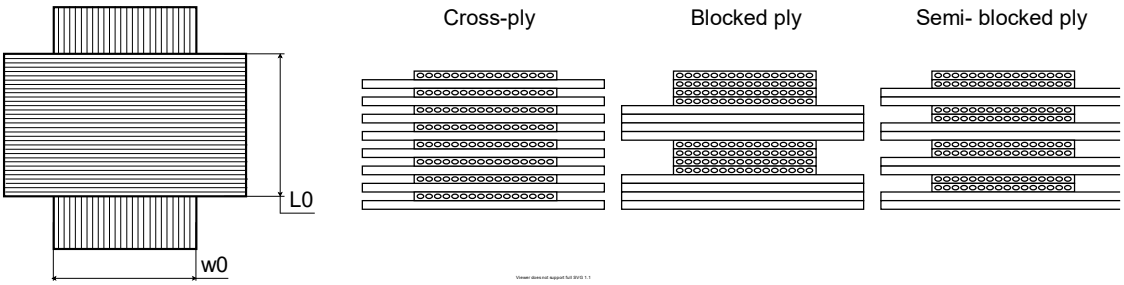

Figure 2.6: Schematic representation of the specimen layup options (CP $[90/0]_8$, BP $[90_4/0_4]_2$, SB $[90_2/0_2]_4$) with various thickness-to-width ratio.

The problem of the size effect of different layup configurations is addressed within the DefGen model by considering consecutive layers with the same orientation as a single layer of a larger thickness.

The important feature of this model is that both flow mechanisms co-exist, which agrees with the experimental results [38]. This is made possible through the implementation of a transition between flows described as an instant event. This transition from a squeezing to a bleeding flow is triggered when shear deformation at the ply edge reaches a critical value. During deformation, the upper fibre moves towards the fibre below, thus squeezing the resin in the transverse direction. Currently, when shear deformation reaches its critical value (deformation at locking) the flow direction changes. At this stage resin bleeds along the fibres, which is one of the key features of a percolation flow (mathematically described as squeezing flow along fibre direction).

The DefGen model is implemented in a way, that for a given temperature only three bespoke material parameters (*a*, *b*, and *k*) are required to fully characterise the compaction behaviour of the material. More thorough discussion on the model's parameters and mathematical implementation is presented in Chapter 3. In the initial formulation of the model, one of the limitations was that the proposed set of parameters was not linked with the known physical properties of the composite precursor (viscosity, fibre volume fraction, permeability) through an analytical expression. This problem was addressed in further developments of the DefGen model by Belnoue et al. [85]. Parameter *a* relates to the flow behaviour and defines whether the fluid is dilatant, Newtonian or shear-thinning. Parameter *b* represents an energy barrier controlling the ability of resin to flow through the fibre network. And lastly, parameter *k* is related to the size of a fibre in relation to the unit cell size (hence, can be represented as fibre volume fraction within one-dimensional formulation).

2.2.5 Summary

Multi-material systems exhibit complex behaviour under processing conditions. This is due to the existence of various deformation mechanisms of composite precursors. The diversity of deformation mechanisms results in a number of challenges for material characterisation:

- Different deformation mechanisms are based on the incompatible assumptions and are aimed to reflect different aspects of deformation (composite precursor is approximated as a reinforced fluid or resin flow through a porous medium; the existence of the compaction limit etc.).
- There are various flow modes occurring on micro-, meso-, macro scales of the composite precursors. These flow modes are coupled and occur concurrently. It is a challenging task to isolate the phenomenon at one structural scale to estimate its influence on the overall deformation behaviour of the composite precursor.
- The flow modes can co-exist within one deformation process. The transition from one mechanism to another was reported in a number of studies.

Successful characterisation of a composite precursor requires a comprehensive testing programme to reveal acting deformation phenomenon. Existing approaches to characterisation testing and arising challenges are addressed in the next section of this chapter.

2.3 Test methods for material characterisation

2.3.1 Material characterisation challenges

Material characterisation tests are drastically different depending on which mechanism is assumed to be prevailing. There is no standardised testing strategy that would be equally suitable for all the observed deformation/flow mechanisms.

In simple cases, isolated experiments with material components (e.g. compaction of dry reinforcement [86], rheological experiments on pure resin [87] or resin suspension [88]) can provide all the required input to describe the material behaviour. However, this is only the case when the model can precisely capture how individual components interact in the system. Often, reality suggests much more complex interaction mechanisms with no clear route to test constituents separately. For instance, the behaviour of dry

reinforcement and the same reinforcement in an impregnated preform will be different due to lubrication [89]. The apparent response of the tape exhibiting shear flow will be strongly affected by its interaction with the loading plate, which is often unknown or require separate testing programme, and not just material properties [90]. Uncertainty in properties, e.g. due to the high sensitivity of resin viscosity to environmental conditions and thermal history, also plays an important role [14], [91]. Other examples include transitional behaviours where different flow processes occur at different stages of the processes [39]. In these cases, the testing programmes require inverse property calculation procedures, and depend on the model and the initial hypothesis made by the experimenter.

The choice of the loading schedule and the temperature level for the characterisation test is defined by the researcher prior to the experimentation. Chosen processing parameters (load, load rate, temperature) drastically affect dominant deformation mechanisms and the flow of resin within a composite [92]. The main purpose of this section is to showcase the variety of testing approaches and the challenges arising at the experimentation planning stage. The testing programme's design can be influenced by:

- the material/specimen configuration (size effect, layup etc.);
- the studied phenomenon of the compaction behaviour (creep/recovery, relaxation, elastic and viscous response etc.);
- the pre-assumed consolidation mechanism/dominant resin flow mode;
- the need to simulate a specific manufacturing method;
- the previous experience in the corresponding field of study;

The acquired experimental data is then to be described by the chosen material model. Material constants can then be identified based on an optimisation procedure which attempts to minimise the deviation of the model predictions from the measured experimental data.

2.3.2 Examples of characterisation testing approaches

There are various examples of characterisation testing approaches available in the literature. A viscoelastic response of glass fibre continuous filament mats through the compression-relaxation load cycle was studied by Kelly [93]. A phenomenological form of a compaction model was suggested to reconcile the experimental observations. The

model was represented as a multiplicative decomposition of the compaction stress into functions of strain and strain-rate as follows:

$$\boldsymbol{\sigma}(\boldsymbol{\varepsilon}, \dot{\boldsymbol{\varepsilon}}) = \boldsymbol{f}_{\boldsymbol{\alpha}}(\dot{\boldsymbol{\varepsilon}})\boldsymbol{f}_{\boldsymbol{\beta}}(\boldsymbol{\varepsilon}) \quad 2.3$$

where σ is the compaction stress, $\dot{\varepsilon}$ is the strain-rate, ε is the strain.

A series of monotonic compression tests at various rates with the subsequent load relaxation were conducted as shown in Figure 2.7.a. As concluded by the author, four compaction-relaxation tests are enough to adequately determine material model's parameters. The tests must include "very slow" and "very fast" load application rates. The definition of "slow" and "fast" depends on the material and the predominant consolidation mechanism. Therefore, the final set of test programmes is driven by the studied material and assumptions on how the material flows and deforms. According to the testing methodology employed in Kelly's study, the completeness of the program (the number of tests, the explored load levels/application rates) also depends on the experience of the researcher.

Depending on the studied phenomenon characterisation approach may be different. The application of pressure is more relevant than application of displacement for composite processing. When put under constant loading, the multi-material system may exhibit complex behaviour such as creep. Creep is the tendency of materials to showcase an increase in deformation when subjected to unchanging processing conditions (load and temperature) [94]. Studies on the creep effect in composite precursors were conducted by different researchers, as shown below. The idea behind the characterisation testing in this case is to apply a constant load in order to observe elastic (initial deformation), viscoelastic (non-linear deformation) and viscous (deformation plateau) stages of the deformation as shown in Figure 2.7.b. Creep stage of the test is then followed by the recovery during which the load is removed. Upon instant load removal there are elastic and viscoelastic components of the recovery stage, resulting in a final deformation of a composite [95].

Creep behaviour of carbon fibre prepreg (Toray T700-12K-50C) was studied by Almeida et al. [96]. Three different unidirectional layup sets were explored within the study: $[0]_4$, $[30]_4$, $[60]_4$. The latch-based Weibull model [97] was employed to characterise the creep response of the material. To observe different strain levels, test programmes with two stress levels (2 and 5 MPa) at the constant temperature (30℃) were performed. The obtained model showcased the robust performance at higher stress

levels. The authors concluded that the stress level of 2 MPa was too low to observe sufficient material's compaction response due to the high stiffness of the specimens. A similar approach was taken by Monticeli et al. [95], where different levels of the applied pressure (1-5 MPa) and the temperature (50℃ – 190℃) were examined to study creep phenomenon. In both cases, the load programmes were designed to incorporate different elastic and viscoelastic deformation levels (higher stresses cause higher initial elastic deformation), but the actual load values and creep duration were specified by the experimenter.

Viscoplastic response of the carbon fibre material (Thornel T-300 12K) to short-term creep and load relaxation was investigated by Al-Haik et al. [98]. The material's behaviour was assumed to be compliant with the elastic/viscoplastic model proposed by Gates [99]. According to authors, the material's response was studied at three different temperatures (25℃, 40℃, 60℃). During the tensile experiment, test specimens were loaded to the level of 50% of the ultimate tensile stress for a given temperature. The results showed discrepancies between obtained model's prediction and experimental results for the higher temperature values and longer creep duration. The choice of the considered temperature levels was justified by the need to study the correlation of material parameters on the temperature in the range of room temperature to the glass transition temperature (T_g = 85℃). The choice of the load level was based on the experience of the researcher and was driven by the pre-assumed material's behaviour (the influence of the overstress on the creep phenomenon). There is no standard for the target load level within creep experimentation and the test programme may vary within different research groups. For instance, in the creep testing conducted by Guedes et al. [100] the target value of stress was chosen to be 69-72 % of the ultimate stress level (as opposed to 50% level in [98] case).

The description of composite precursor's compaction behaviour requires the characterisation of viscous and elastic response of the material (except for the case when shear flow is assumed). To study the contribution of each of these phenomena to the compaction response it is necessary to isolate them for characterisation. It must be done without modifying laminate's structure or altering fibre network arrangement. A testing method for separating viscous and elastic contributions of fibrous and resin components directly from carbon–epoxy prepregs (AS4/3501-6) was discussed by Hubert et al. [101]. The idea is to design the test programme in a displacement-controlled mode with load tracking. The applied displacement is increased

incrementally at each step of the test in a ramp-dwell manner. Every time the displacement is held at a constant value, the load starts relaxing due to the viscoelastic nature of the material. The duration of each displacement dwell increment is chosen to be sufficient for the load to relax to a stable value. Under assumption of the additive superposition of elastic and viscous components of stress response, the magnitude of the load at the relaxed state is directly related to the elastic fibre bed response for the corresponding strain level. The results show that the behaviour of the fibre bed response can be represented as a non-linear stiffening spring. The material is tested at different displacement levels in order to receive the data-rich compaction response of the material to fully characterise the elastic reaction of the prepreg. The processing conditions (temperature, applied displacement/displacement rate) were selected in a way to maximise experiment's duration before curing starts. The resulting displacement-controlled ramp-dwell loading programme is shown in Figure 2.7.c. The efficiency of the proposed approach was confirmed by validating the obtained load relaxation model against the load-displacement data obtained in the independent load-controlled compaction test.

The study on compaction behaviour of uncured toughened prepregs (IMA/M21 and IM7/8552) was conducted by Nixon-Pearson et al. [39]. The aim of the research was to characterises the compaction response of the material under processing conditions consistent with different types of composite manufacturing – automated fibre placement (low temperature/moderate pressure), autoclave consolidation (high temperature/high pressure), debulking (wide range of temperatures/low pressure). A wide range of load levels, load rates and temperatures (30℃ - 90℃) was explored. The experimentation was performed for different specimen's layup configurations to take into account size effects.

Two independent loading regimes were proposed to cover wider range of strain-rates. The first ramp-dwell loading programme comprised of several steps with high-rate incremental load increase followed by load dwell intervals. The second regime was a slow monotonic load raise where load was increased linearly through the whole test. The considered loading programmes are shown in Figure 2.7.d. The load levels/rates were chosen to be comparable to processing conditions seen in the abovementioned manufacturing methods.

Features relevant for both percolation (compaction limit, resin flow out of the fibre bed) and shear (inter-ply distortion) flow modes were observed. Moreover, the studied

material exhibited the transition between shear and percolation flow modes at temperatures around 60℃. It became possible to reveal these deformation mechanisms due to the comprehensive and extensive experimentation programme. The generated compaction data was then used for material characterisation by means of the hyper-viscoelastic model proposed by Belnoue et al. [40]. The proposed testing approach was employed to address the observed complex material behaviour and to identify/validate the material model [39].

Another example of characterisation experimentation influenced by the considered manufacturing method was presented by Govignon et al. [102]. In that study the aim was to model processing conditions arising during resin infusion. The pressure level was set at 1 bar as vacuum was simulated. The considered compaction programme is shown in Figure 2.7.e. The loading programme was divided into three distinctive stages: compaction of the dry preform, unloading during resin filling, re-compaction of the wet preform. Due to the fact that material is normally re-compacted from non-zero stress state, a series of tests with different compaction levels (shown with blue lines in Figure 2.7.e) were performed in order to acquire sufficient compaction response data.

Then, experimental data from each compaction stage was characterised within the material model proposed by Robitaille et al. [103], which provides the relationship between current fibre volume fraction and the compaction stress. The model predictions proved to be in good agreement with the validation set of experimental data.

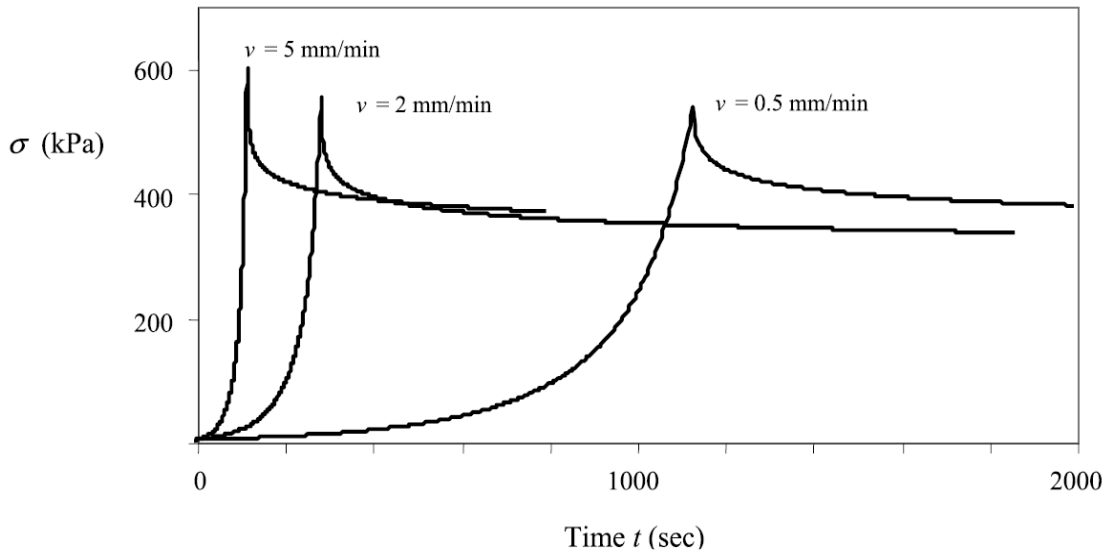

a

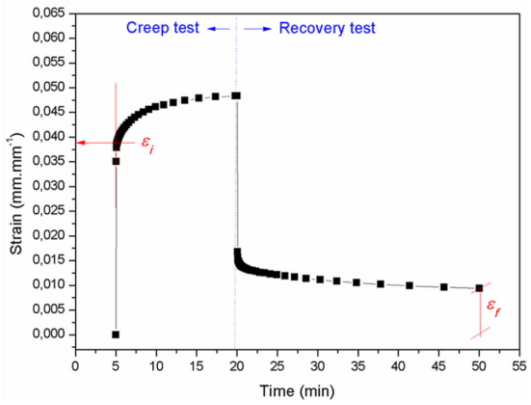

b

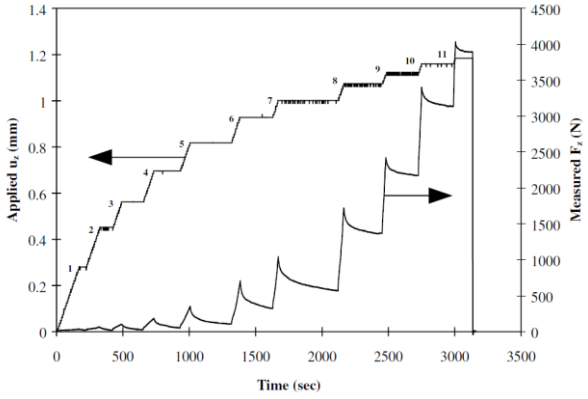

c

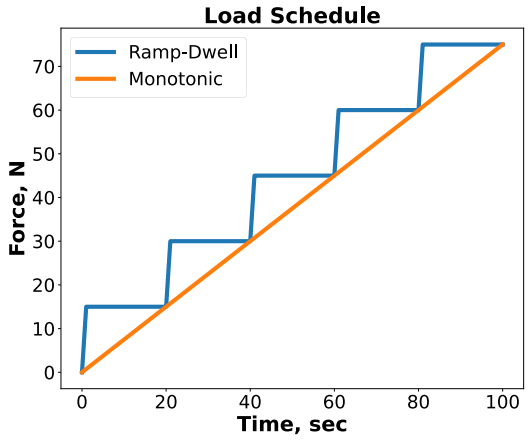

d

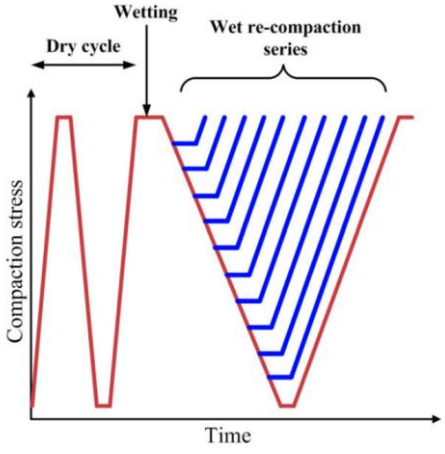

e

Figure 2.7: Test programmes for characterisation of composite precursors. a) compression testing at various rates [93]**; b) creep/recovery test** [95]**; c) ramp-dwell programme to separate viscous and elastic contributions of fibrous and resin**

components [101]**; d) ramp-dwell programme motivated by the need to cover wider range of strain-rates; e) compaction characterisation programme for modelling resin infusion process** [102]**;**

An overview of experimental techniques for shear flow was presented by Engmann et al. [104]. The commonly used methods include testing at a constant plate closure speed (which results in an increased strain rate), at a constant strain rate (the closure speed of the plate decreases exponentially with time), at stress relaxation conditions (stopping plates closure when target strain is reached to estimate the degree of elasticity of the material), at a constant stress (creep tests, discussed above). To observe various rheological behaviours, different test geometries can be facilitated by altering sample to plate size ratio (width and length):

- Constant area geometry – specimen's size is larger or equal than the plate's size, the specimen flows out. Such approach provides more control over the applied pressure, as the area remains constant during the test.
- Constant volume geometry – specimen's size is smaller than the plate's size, which results in the absence of material accumulation at the edges (as opposed to the constant area geometry). Therefore, there is no pressure build-up at the specimen's edges. Such approach is closer to industrial practice.
- Imperfect squeezing flow – the penetration of the compression plate into a volume of fluid
- Fully submerged plates – only applicable to the material with low viscosity

Depending on the plate's surface treatment (lubricated or roughened surface) no-slip or no-friction contact conditions can be facilitated. As concluded by the authors, obtaining rheological parameters from the experimental data is challenging. The examples of rheology measurements for shear flow were provided in the series of papers by Harrison et al. [105], [106]. The composite test samples (1 mm thickness) were placed in-between heated compression platens and squeezed to a gap of 0.8 mm. The corresponding shear rate was measured by the rheometer for a range of processing temperatures. The Carreau-Yasuda model for viscosity was then used to fit the obtained shear strain rate experimental data [105]. In another study [106] the rheometer was positioned in parallel within the custom built compression platens. The shear strain data was acquired as the shear stress and normal force were applied to the specimen. As concluded by the authors, using the rheometer is more effective in comparison with the

pull-though and pull-out testing. Nevertheless, one of the disadvantages of this approach is that the experimental loads are lower than the processing conditions employed within the industry.

Another group of studies reflects challenges arising within permeability estimation. Two benchmark exercises for permeability measurements were performed within different research groups [107], [108] to establish guidelines for standardised measurement approach. The flow of resin-imitating test fluid (to exclude cure reaction) through fabric test sample placed in-between two mold surfaces (as for a standard Resin Transfer Molding setup) was analysed within the study. In the second exercise [108], the level of permeability data dispersion below 25% was achieved. The main source of results discrepancies was concluded to be human factors (experience, specimen preparation, raw experimental data processing).

Characterisation of dry materials may provide relevant data about fibre network's response to loading. Shear behaviour of dry woven composite material was analysed in a series of tests by Sharma et al. [109]. Employed test methods included uniaxial bias extension, biaxial, and picture frame tests. The displacement application rate for all test was fixed at 60 mm/min. The variety of testing approaches allowed to investigate the development of in-plane shear stresses, the effect on shear resistance, tows rearrangement, and lock-up behaviour the material.

The lack of standard guidelines for material parameters measurements impedes researchers from comparing resulting data obtained within different experimental setups. Differences in experimental and data processing approaches, different testing apparatus, human factors may lead to scatter in the results.

2.3.3 Summary

Designing an extensive characterisation test programme is not a trivial task. To reveal the underlying deformation mechanism the material must be trialled against a wide range of loading conditions to receive sufficient compaction response. There is no universal approach for characterisation testing of composites. The choice of experiment's loading schedule is often based on the assumed dominant consolidation mechanism, studied phenomenon or the need to replicate processing conditions specific to a certain manufacturing method.

The next step after characterisation testing is to use the acquired experimental data for building a comprehensive material model capable of capturing the compaction behaviour of a composite precursor. An overview of different approaches for defining physical models of system's behaviour from data is provided in the next section of this chapter.

2.4 Retrieving physical models from experimental data.

There are different methods on how to approach the processing of experimental data for building physical models of the studied system's behaviour. The problem of retrieving governing equations from data is not specific to the field of composite materials only and is relevant in other fields of study as well.

There are several important factors which influence the choice of the approach for model identification:

- Assumed models of the studied system's behaviour. In this case the parameterised governing equation is available, and the aim is to identify the values of the model's parameters.
- Time constraints and computational resources. The requirements on algorithm's promptitude and the availability of the computational power may put limitations on the usage of more sophisticated methods.
- Sufficient or scarce set of experimental data. Certain methods are more sensitive to scarce datasets and require a diverse input to capture the studied features of system's behaviour, which lead to more experimental work to obtain the required data.

An overview of different approaches for building physical models from experimental data is presented below.

2.4.1 Regression analysis

If the governing equation for the selected flow mode is available (meaning that the assumption about the dominant deformation mechanism has been made), then the main objective is to find an optimum set of material parameters to match model's prediction with the experimental data. It is done through conducting nonlinear regression analysis. The essence of the regression process is to minimise the difference between model's prediction $f_{prediction}$ and the actual experimental data $f_{experimental}$ by varying the

values of material parameters. The cumulative difference in prediction over the span of input data is called the residual function $f_{residual}$ [110]:

$$\boldsymbol{f_{residual}} = \sum_{\substack{\boldsymbol{all\ data}\\ \boldsymbol{points}}} \left(\boldsymbol{f_{experimental}} - \boldsymbol{f_{prediction}}\right)^{\boldsymbol{2}}. \qquad 2.4$$

The residual function is minimised within an optimisation method of choice such as Least Squares, Nelder Mead, etc.

The general form of the governing equation describing the compressibility of the viscoelastic material is defined as a differential equation as follows (mathematical representation of various flow modes will be discussed more thoroughly in Chapter 3):

$$\frac{\boldsymbol{dh}}{\boldsymbol{dt}} = \boldsymbol{F(t,h)} \cdot \boldsymbol{Q(h)} \qquad 2.5$$

where *F(t, h)* is a function containing the history of the evolution of the applied pressure, *h* is the thickness, $\frac{dh}{dt}$ is the thickness rate, and *Q(h)* is a function of thickness which contains the material parameters. The experimental data represents a set of measured thickness values $h(t)_{experimental}$ evolving during the experiment.

There are two ways to formulate a residual function when the target governing equation is represented in a form of ODE.

- To solve ODE within the residual function.
  To compare the measured thickness response with the model's prediction $h_{prediction}(t)$, the corresponding ODE must be solved. In this case the residual function is formulated as follows:

$$\boldsymbol{f_{residual}} = \sum_{\substack{\boldsymbol{all\ data}\\ \boldsymbol{points}}} \left(\boldsymbol{h(t)_{experimental}} - \boldsymbol{SolveODE}\left(\frac{\boldsymbol{dh_{prediction}}}{\boldsymbol{dt}}\right)\right)^{\boldsymbol{2}}. \qquad 2.6$$

- The main advantage of this approach is that it is possible to use "raw" noisy experimental data $h(t)_{experimental}$ without pre-processing (denoising, filtering etc.). Therefore, the experimental data will not undergo any modifications and will be submitted in its pure form. On the other hand, the need to solve a differential equation every time there is a request for the residual function's value significantly slows down the process of regression analysis.

- To differentiate the experimental data to obtain derivatives $\frac{dh_{experimental}}{dt}$. Composite's thickness values are measured directly within the experiment. After calculating the thickness rate $\frac{dh_{experimental}}{dt}$, the residual function is represented as follows:

$$\boldsymbol{f_{residual}} = \sum_{\substack{\boldsymbol{all\ data} \\ \boldsymbol{points}}} \left(\frac{\boldsymbol{dh_{experimental}}}{\boldsymbol{dt}} - \frac{\boldsymbol{dh_{prediction}}}{\boldsymbol{dt}} \right)^{\boldsymbol{2}}. \qquad 2.7$$

This approach is considerably faster rather than solving ODE within the residual function. The experimental data contains noise component. It results in the main pitfall of this method: the derivatives can only be found for a "smooth" data. The source of that noise may be different: equipment's compliance, data acquisition algorithm's imperfections, faulty sensor etc. It becomes necessary to filter the noisy thickness data in order to conduct differentiation on a smooth $h(t)$ curve. There are various techniques for finding derivatives of noisy data, including polynomial regression (fitting high order polynomials) [111], Fourier filtering (decomposing the initial signal and excluding high-frequency noise components) [112] or non-parametric spline regression [113]. The key challenge for a noise smoothing algorithm is not to introduce any bias to the initial pure data.

2.4.2 Data-driven approach for identifying governing equations.

There are ways to identify fully parameterised system from experimental measurements without prior knowledge of the governing equations (hence, without prior assumptions on system's behaviour). Data-driven method for extracting governing equations from experimental data was explored by Brunton et al. [114], Rudy et al. [115].

The idea of the method is to use sparse regression to determine only the fewest relevant terms in the governing equations to adequately describe the data. The terms are selected from a large pool of user defined high-dimensional nonlinear functions. The selection process is based on the assumption that only a few important terms define system's behaviour (hence, sparse regression).

The proposed approach was applied to the well-studied fluid dynamics problem of fluid flow and vortex shedding behind a cylinder. The visual representation of the problem is shown in Figure 2.8. In that example the studied system was represented as a system of differential equations $\dot{x}(t), \dot{y}(t), \dot{z}(t)$ (denoted as $\dot{X}$ in a matrix form). To capture the

transient nature of the studied system, an additional *z* axis was introduced which represented the transition from the unstable steady state to the vortex state. The experimental data was modelled based on the Navier-Stokes equations at a range of different flow conditions.

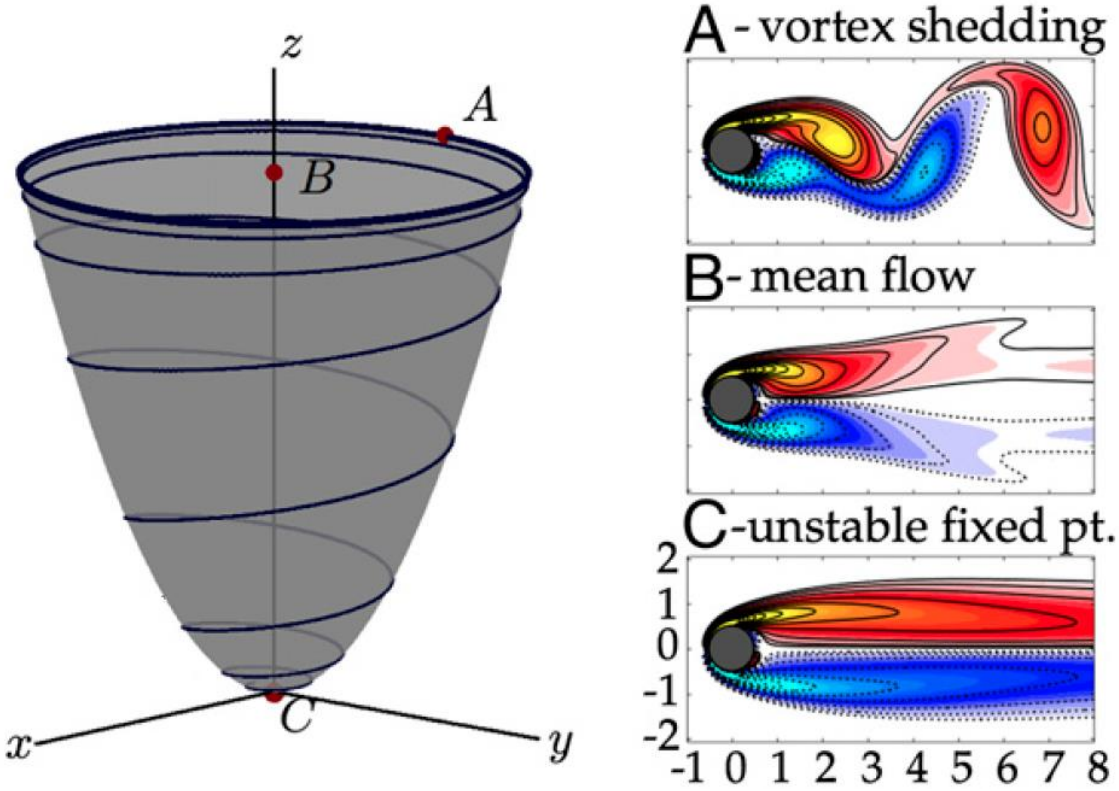

Figure 2.8: The problem of fluid flow and vortex shedding behind a cylinder [114]**. Left – three-dimensional representation of the problem, where Z axis represents the transition between states of the process. Right –two-dimensional flow behind the cylinder at different states.**

The problem of sparse regression was formulated as follows:

$$\dot{\boldsymbol{X}} = \boldsymbol{\Theta}(\boldsymbol{X})\,\boldsymbol{\Xi} \tag{2.8}$$

where $\Theta(X)$ is a library of candidate non- linear functions. In the considered example it was represented as a fifth order polynomial as follows:

$$\boldsymbol{\Theta}(\boldsymbol{X}) = [\boldsymbol{x}(\boldsymbol{t}) \quad \boldsymbol{y}(\boldsymbol{t}) \quad \boldsymbol{z}(\boldsymbol{t}) \quad \boldsymbol{x}(\boldsymbol{t})^{\boldsymbol{2}} \quad \boldsymbol{x}(\boldsymbol{t})\,\boldsymbol{y}(\boldsymbol{t}) \quad \cdots \quad \boldsymbol{z}(\boldsymbol{t})^{\boldsymbol{5}}]. \tag{2.9}$$

As stated by the authors, other functions (*sin, cos, log*) as well as polynomials of higher order could also be considered. Basic knowledge of the studied system's physics may

significantly simplify the regression process as non-relevant candidate functions would be excluded from the considered $\Theta(X)$.

Ξ represents sparse vectors ξ_i of coefficients, which determine what terms are active in $\Theta(X)$ for a given differential equation in $\dot{X}$ as follows:

$$\boldsymbol{\Xi = [\xi_1 \quad \xi_2 \quad \cdots \quad \xi_n].} \tag{2.10}$$

If a term in ξ_i is 0, the corresponding candidate function in the polynomial set $\Theta(X)$ is not relevant and can be dropped. Non-zero value in ξ_i not only activates the term in the governing equation, but also defines the value of a corresponding model parameter. The comprehensive visual representation of the considered sparse regression problem is provided in [114] (Figure 1).

Thus, upon conducting sparse regression and identifying relevant terms in the governing equations, the fully parameterised dynamic system was discovered for a range of sampled parameters values. The identified model matches the Navier-Stokes equations, even though no initial assumptions were put forward (meaning no governing equations were available prior to the analysis)

There are limitations to this approach. The method's performance highly depends on the fortunate choice of candidate functions $\Theta(X)$ and chosen coordinate system (as shown in Figure 2.8). Moreover, noise filtering or data-curve smoothing is required to compute derivates $\dot{X}$ from the experimental data X. The application of the sparse regression method in a high-dimensional space requires considerable computational resources in order to converge to the optimum set of governing terms/model parameters.

2.4.3 Data approximation with artificial neural networks

The approximation/learning of the experimental data by means of artificial neural networks (ANN) is becoming more relevant in many different disciplines. The major advantage of this approach is that no prior knowledge or assumptions about the studied system's behaviour is required.

ANN is a mathematical representation of groups of elements called neurons which are organised in a layered structure. An example of neural network's architecture [116] is shown in Figure 2.9. In that work the influence of the reinforcement particles on the compressibility of Al–SiC composite powders was investigated. The proposed neural network used the content of the reinforcement particles (SiC-Vol %), the particle size

ratio (PSR), and the compacting pressure (P) as input parameters. Based on the input data ANN output the predicted density of the compacted Al–SiC batches.

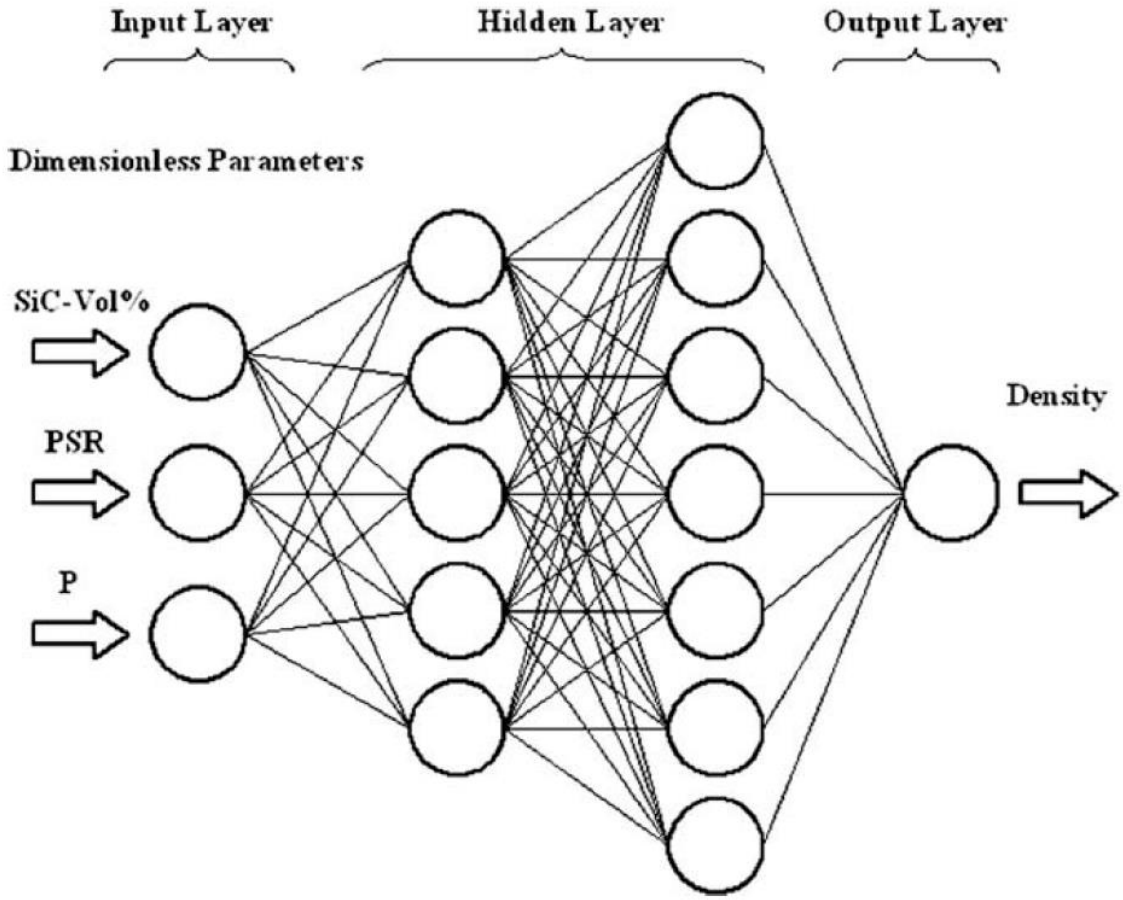

Figure 2.9: Neural network's architecture [116]**. Input layer contains three neurons as three inputs are submitted. Output layer consists of one neuron since only one property of the system (density) is studied. The number of hidden layers and their size is defined by the researcher.**

Regardless of the application, different ANNs follow the same principle. The first input layer receives an external data from the environment as an input and passes it further to the next layers. The last layer outputs network's prediction which is to be compared with the experimental data. The first and the last layers are connected through several hidden layers, where the information is processed. Every layer may contain different number of neurons. Basic representation of a neuron is shown in Figure 2.10.

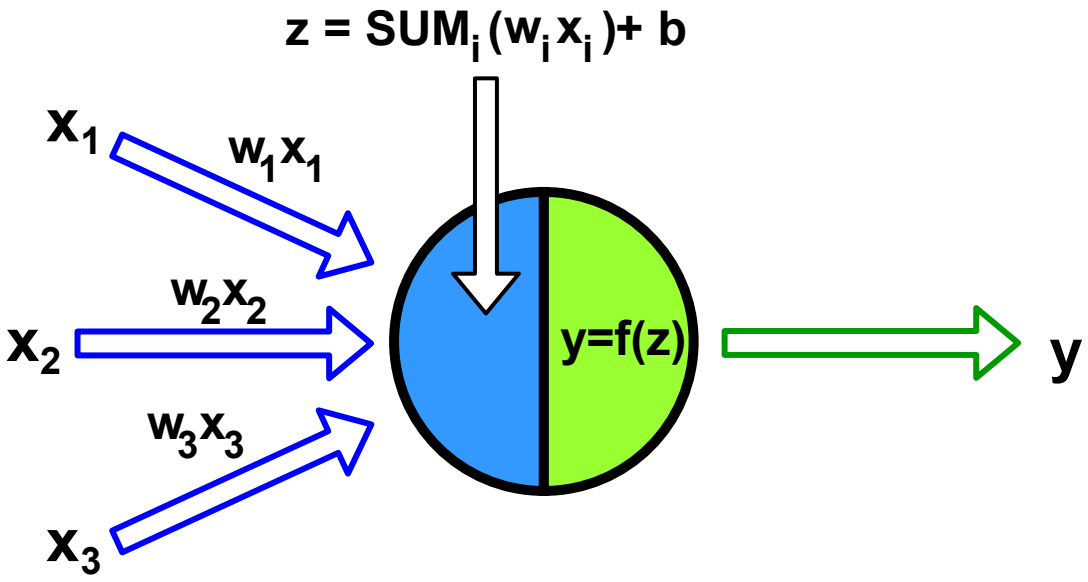

Figure 2.10: The structure of a neuron. Inputs and output.

Neurons in different layers are linked with each other (see Figure 2.9). Therefore, each neuron has several inputs and one output. Each link has an assigned weight coefficient to it. A neuron's output y is formed by conducting a series of mathematical operations – weighted inputs $w_i x_i$ and bias b are summed up and transformed through the user-defined activation function *f()* (see Figure 2.10) as follows:

$$y = f\left(\sum_i (w_i x_i) + b\right). \qquad 2.11$$

Thus, the neuron's output can be adjusted by tweaking the weights of connecting links and neuron's bias coefficient. Then, neuron's output is passed further to the next neuron as in input. The process of adjusting weights and biases of all neurons in the network until the resulting output matches known experimental data is called training. The training continues until the errors between prediction and results are sufficiently small. Upon the completion of training, ANN is able to simulate the response of the studied system and output model's predictions for new batches of the input data [117].

The ANNs are widely used to simulate the behaviour of composites under processing conditions by approximating the studied phenomena [118]. Such approach does not require computation of derivates from the experimental data, hence no data pre-processing (noise filtering or curve-smoothing) is needed [119]. There are various examples of neural network's application available in the literature. The usage of neural networks to predict manufacture-induced disturbances and resin flow inconsistencies

was explored by González et al. [120]. The non-linear response of ionic polymer-metal composite actuators was approximated with ANN within the study by Díaz Lantada et al. [121]. The compressive and impact strength of fibre reinforced concrete in dependence on the content and the structure of the reinforcement was approximated through ANN by Sangeetha et al. [122]. In all cases fully trained neural network could predict the target behavioural feature based on the supplied material parameters and processing conditions.

The usage of ANNs has its limitations. The input data has to be diverse in order for the network to capture the behaviour of the studied system. Scarce input dataset is not sufficient to approximate system's response to changing processing conditions. There is also a requirement for a powerful GPU hardware in order to train the network within reasonable time.

One of the major drawbacks of ANNs is that it is not possible to implement a physical model of the system based on the trained network. A neural network represents a black box which can approximate a function (governing equation), but it will not provide an insight on the structure of learned relationships. Moreover, there can be two networks with the same topology but different weights and biases which produce the same result.

One of the major developments in this field is the introduction of physics-driven neural networks [123]. A new concept of neural ordinary differential equations was described by Chen et al. [124]. The idea of the proposed method is to parameterise the dynamics within hidden layers according to a specified ordinary differential equation (ODE). In this case the input layer $h(0)$ and output layer $h(T)$ are defined to be a solution to the defined ODE at the corresponding time moment (0 or T). The solution of an ODE is done by the black-box solver within the network. More thorough mathematical implementation of this method can be found in [124]. This approach seems to be promising for tackling the abovementioned "black box implementation problem" of the conventional ANNs. It has found its application in different disciplines including the field of composite materials. For instance, the simulation of the thermochemical curing process within the physics-informed neural network was performed by Niaki et al. [125]. The network was designed to follow the solution of the system of governing differential equations describing exothermic heat transfer and resin reaction. As reported by the authors, the developed network was able to predict the resulting temperature field and the degree of cure in the composite-tool system.

2.4.4 Summary

Processing experimental data aims to reveal physical processes undergoing during the test. Different methods for extracting physical models from the data were discussed within this section. The considered approaches include nonlinear regression of the target model, sparse regression using a set of candidate terms for the governing equation, neural network approach aimed to reveal characteristic patterns in the dataset.

A processing method has to be chosen with care. The considered approaches may or may not be suitable for certain applications due to the inherent limitations (the availability of the assumed behaviour model, execution time constraints, required computational resources, sensitivity to the scarcity of the experimental dataset).

2.5 Problem statement

There are a number of existing gaps in the conventional methods for consolidation characterisation. One of the main challenges is that the available experimental data are often limited as material testing is both complicated and time consuming. Hence, the information obtained in these tests may appear to be deficient and may not reveal all the underlying processes. In this case, property identification may provide a seemingly good match with the experimental data irrespective of which mechanisms is presumed to happen. However, it does not mean that such model represents the physical reality, and it can often fail to adequately represent a wider set of experimental data. This sets a fundamental dilemma, as the material behaviour (i.e., the model selected) needs to be decided prior to conducting the tests, which introduces a strong subjective element. If the developed loading schedule (load values, application rates, steps duration) is based on the pre-assumed dominant deformation mechanism, the obtained material's response might be insufficient as the material was not exposed to various processing conditions. Additionally, the proposed testing programme often relies on previously adopted practices or the experience of the researcher. Another challenge is the choice of the robust material model identification technique. Employing unsuitable model retrieval method even within the comprehensive dataset may lead to the misleading physical model of the consolidation (incorrectly defined set of material parameters).

There is a need in a new testing methodology that is capable to identify the deformation mechanisms as well as the relevant material properties. This methodology should be able to check different hypothesis on the deformation mechanisms and autonomously design a testing program based on the measured behaviour of the material. This

methodology should also lead to reduced number of experiments while making sure that the obtained data is representative and sufficiently captures all the main features of the material behaviour. Another benefit of the proposed approach is that apart from the macro-response, the retrieved physical model of the flow is able to provide an important insight on what is happening inside the material – e.g. filling the AFP gaps with resin or fibre suspension.

The current research is organised in a following structure:

- The current Chapter 2 presents an overview of different aspects of the consolidation characterisation. The review outlines the importance of the consolidation process in composite manufacturing and the complexity of the revealing the underlying consolidation mechanisms. Different methods of characterisation testing and experimental data processing are discussed. Existing gaps in the conventional approaches are addressed and the aims of the current project are established.
- Chapter 3. The concept of the consolidation library is introduced. This library contains the most representative models of the resin flow. The chapter includes mathematical representations, used assumptions and boundary conditions of the considered resin flow models. The importance of the robust characterisation method is demonstrated within two examples of flawed characterisation.
- Chapter 4. The definition of a data-rich testing programme is discussed within this chapter. The main requirements for the robust material parameters definition are established, and the parameters extraction framework is introduced. To demonstrate the advantages of the diverse testing programme for material characterisation, the developed framework is applied to the compaction data received within a series of compaction tests.
- Chapter 5. The challenges of defining unbiased (flow assumptions free) data-rich characterisation test programme are addressed within this chapter. The conceptual design of the real-time adaptive consolidation sensor framework is introduced. The proposed framework's functionality is estimated within the set of virtual exercises.
- Chapter 6. The application of the developed adaptive testing framework within the real experimental setup is explored within this chapter. The framework is connected to the testing apparatus through the specially developed setup. Arising

technical challenges (processing time delay, noisy input/output data, safety issues, PID control etc.) and the ways of tackling them are discussed. The consolidation framework is then tested within the characterisation trials for a range of different materials.

- The conclusions chapter presents an overview of the conducted work and the achieved results. The discussion of the effectiveness of the proposed approach and the fulfillment of the established goals is presented. Finally, the scope for possible developments of the proposed approach is set.

3 PHYSICAL MODEL OF RESIN FLOW IN CONSOLIDATION

The mechanics of flow and deformation in composite precursors can solve many practical problems. This chapter explores a number of consolidation models which are relevant in application to the flow of resin in fibre-reinforced thermosetting prepregs containing thermoplastic tougheners. The concept of the consolidation library is introduced in the current chapter. The pre-coded library contains mathematical representations of all considered models. The library is used in conjunction with the developed autonomous testing framework which is described in further chapters.

Although the models considered below do not capture all possible aspects of the material's compaction behaviour, they cover arguably most dominant mechanisms of resin flow which was shown experimentally in various studies. The selection of models is limited by those than can be explicitly integrated to obtain ordinary differential equations (ODEs) relating pressure/load, thickness, and thickness rate. Such integration requires simplifying assumptions regarding the behaviour of the material and its interaction with loading system (e.g. the models of shear/percolation flow shown in [17], [89], [126]). Not all the problems can be integrated like that – some can be condensed to partial differential equations (PDE) (e.g. the problem of consolidation with the bleeder [16], [75]), some contain constitutive equation that are too complicated for analytical derivations (e.g. Carreau shear flow [127], [128]). Most of the problems that are written for large deformations cannot be integrated. The class of non-integrable problems is intentionally omitted at this stage (a) for simplicity of implementation and (b) since many relevant problems can be described using the integrable models. A further extension of the library is possible but at the expense of some loss in computational efficiency (case of PDE) or constructing phenomenological model as synthesis of structural models (Carreau [16], [75] or DefGen [85] case).

Finally, this chapter illustrates the importance of a robust testing programme and data extraction technique for the successful material characterisation. The demonstrated examples pose a question on the testing rationales and on how data-rich programmes

should be designed. These lessons build the ground for the autonomous testing concept presented in the next chapters.

3.1 Material model identification

All composite manufacturing methods require an application of an external pressure to achieve the required thickness of a part and to prevent defect formation. In many cases, the description of these processes can be approximated by the compression of a composite precursor between two rigid plates. Under this simplification, the contact surface remains flat, and the area of pressure application is either constant or evolves with the flow of material. The relation between the applied pressure / pressure rate and the resultant thickness / thickness rate is dependent on flow mode, material properties and interaction with the loading plates. The resultant relationships can often facilitate the optimisation of manufacturing method.

When a composite precursor is compacted between two rigid parallel plates, the application of external pressure leads to reactive pressure and pressure gradients build-up within the material. This, in turns, induces a resin flow and the deformation of the reinforcement. Simplifying assumptions and explicit integration of the mass balance, the constitutive and the equilibrium equations, as shown further in section 3.2, leads to the general form which can be written as:

$$\frac{\boldsymbol{dh}}{\boldsymbol{dt}} = \boldsymbol{F}(\boldsymbol{t}, \boldsymbol{h}) \cdot \boldsymbol{Q}(\boldsymbol{h}) \tag{3.1}$$

where *F(t, h)* is a function containing the history of the evolution of applied compression force with time *F(t)*, *h* is the thickness, $\frac{dh}{dt}$ is the thickness rate, and *Q(h)* is a function of thickness which contains the material parameters. This equation form covers the incompressible shear flow of Newtonian and non-Newtonian suspensions under different (tool-material) boundary conditions and the percolation (also refer to as bleeding) flow of impregnated fibrous network, as well as some synthetic models.

Figure 3.1 introduces initial dimensions of a specimen and the coordinate system used in the description of a resin flow process. This figure shows a general representation of a composite in between rigid plates and does not describe any particular flow mode. Its purpose is to set up a common ground for further introduction of different consolidation models. The current distance between plates, hence the thickness of a composite

precursor, is denoted by h and the initial width/length by w_0/L_0 correspondingly. The compression force applied to the top squeeze plate is specified as F.

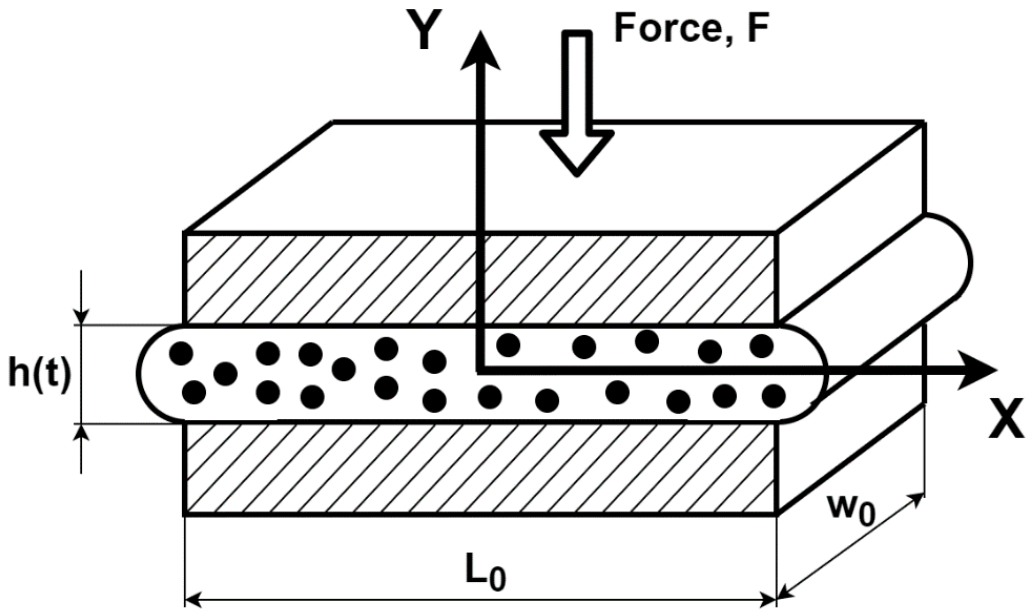

Figure 3.1: Schematic representation of a composite precursor within parallel squeeze plates.

3.2 Consolidation models library

3.2.1 Model unification.

Various consolidation models were derived within the studies conducted by different researchers. All these models use different notation, variables (defined through strain/strain rate or thickness/thickness rate), specimen geometry representation, baseline reference system, etc. This Chapter unifies notations and aligns them with Figure 3.1. An overview of consolidation models used in this research project as well as models' key assumptions, mathematical representation, and theoretical background is presented below. Additionally, every model's compaction response to material parameters variation is explored, as it is important for further characterisation to have an insight into model's behaviour.

The models of squeezing or percolation flow are initially formulated for a point in three-dimensional space. The corresponding governing equations are integrated under simplifying assumptions to get one-dimensional pressure-thickness-thickness rate response. The properties of the laminate are defined by the flow and deformation characteristics of the individual plies. The considered models are used to deduce the

properties of a unidirectional ply and not the effective properties of the laminate. It is essential to emphasize that the considered models assume a certain preferential direction of the resin flow. This assumption is valid as it applies to the ply and not to effective/average sample properties. For instance, the shear flow model suggests that the flow in compaction occurs only in the transverse direction, whereas the flow in the longitudinal direction can be neglected. The percolation model assumes that permeability in one direction is much greater than permeability in the other direction and hence the flow in the other direction can be neglected. The simplifying assumptions allow in some cases to condense the full 3D formulation to 2D problem without compromising the physical meaning of the studied flow mechanism. Once such response is identified all the considered models can be restored to predict full 3D state – including transverse deformations or amount of resin bled through the fibre network [40], [129]. This is fundamentally important when trying to assess the process occurring at local scales. All these different models not only predict the difference in how, for instance, an impregnated material tape would react to an applied load but also would indicate very different outcome in terms of the width change of the tape, fibre volume fraction, resin pressure distribution, and the uniformity of the deformations within the tape. Consequently, this may lead to very different outcomes in terms of closure of gaps between AFP deposited tapes with suspension or pure resin and follow-up wrinkle occurrence [130]. Investigating the mechanisms occurring at mm-scale would require deep insight on structural deformations such as high-resolution microscopy, CT examinations. On the other hand, it seems plausible that these features may be determined by the difference in mechanical response.

The material constants used in the models' formulation include the viscosity of resin and resin suspensions, the constants describing the evolution of viscosity as the functions of shear rate, material constants for the permeability of the fibre network and their dependence on fibre volume fraction, and the constants needed to describe the elastic fibre bed response. As a result, the differential equations contain several material constants that need to be determined holistically to match available experimental data.

Shear flow models

Governing equations.

The relation between stress and applied pressure for an incompressible viscous fluid at low Reynolds numbers is described by Stokes flow constitutive equation. The extension

of the original formulation for an isotropic Newtonian fluid to the shear flow in a fibre reinforced fluid was proposed by Rogers [90]. The presence of fibres affects the response of the fluid. In this case the stress depends on fibre orientation. Therefore, according to Rogers stress - strain rate relationship in Cartesian coordinates can be written as follows:

$$\boldsymbol{\sigma_{ij} = -p\delta_{ij} + Ta_i a_j + 2\eta_T d_{ij} + 2(\eta_L - \eta_T)\left(a_i a_k d_{kj} + a_j a_k d_{ki}\right)} \qquad 3.2$$

$$\boldsymbol{d_{ii} = 0,\ (i,j = 1,2,3)}$$

where σ – stress, d – rate of strain, p – hydrostatic pressure, δ_{ij} – Kronecker delta, η_T – transverse shear viscosity of the fluid, η_L – longitudinal shear viscosity of the fluid, T – arbitrary stress reaction in the fibre direction, a – unit vector, representing orientation of the fibre.

Additionally, the condition of inextensibility in the direction of a unit vectors for the fibre reinforced material is:

$$\boldsymbol{a_i a_j d_{ij} = 0,\ a_i a_i = 1} \qquad 3.3$$

and time derivative of a is given by Spencer [131]:

$$\boldsymbol{\dot{a}_i = \left(\delta_{ij} - a_i a_j\right) a_k \left.\partial v_j\right/_{\partial x_k} = a_k \left.\partial v_i\right/_{\partial x_k}} \qquad 3.4$$

where v_i – velocity of the material point. The constitutive equations are complemented with mass balance:

Mass balance equation (incompressibility condition, assuming that no flow occurs in the fibre direction):

$$\boldsymbol{v_z = 0,\ \frac{\partial v_x}{\partial x} + \frac{\partial v_y}{\partial y} = 0} \qquad 3.5$$

where z axis is in the fibre direction (according to Figure 3.1), hence $v_z = 0$ due to the inextensibility in the fibre direction.

Global equilibrium equation:

$$\boldsymbol{\frac{\partial \sigma_{yx}}{\partial x} + \frac{\partial \sigma_{yy}}{\partial y} = 0 \quad \frac{\partial \sigma_{xx}}{\partial x} + \frac{\partial \sigma_{xy}}{\partial y} = 0\,.} \qquad 3.6$$

It was noted that boundary conditions interaction between composite and compression platens can radically affect the resin flow. It may represent smooth or rough tool surface or the presence of lubricating agent in the contact region which in turn eliminates shear

traction in the interface. Boundary conditions have a significant influence on a through-thickness resin velocity distribution and an overall flow behaviour. According to [90], no-slip and no-friction boundary conditions were considered.

When there is no slip between the composite and the tool, the velocity field at the interface equals zero. Therefore, the boundary condition can be written as:

$$\boldsymbol{v_x}\big|_{\boldsymbol{y=h/2}} = \mathbf{0}\,. \tag{3.7}$$

For the case of no friction platens are free from shear traction, meaning:

$$\boldsymbol{\sigma_{xy}}\big|_{\boldsymbol{y=h/2}} = \mathbf{0}\,. \tag{3.8}$$

Additionally, the possible change of a contact surface area was taken into account by considering constant $L(t)=L_0$ and varying $L(t)>L_0$ contact region's length correspondingly.

These equations form the set of constitutive equations for a fibre- reinforced linear viscous fluid. Then, these equations (together with boundary conditions, mass balance, and global equilibrium equations) were condensed to 2D relation between applied pressure and thickness for different boundary conditions at the prepreg-tool contact surface. To do that, two-dimensional problem of a shear flow in a fibre reinforced Newtonian fluid squeezed in between two rigid platens was considered.

As described previously in section 2.3.2, different sample to compression platen size ratio (width and length) can be employed to facilitate various rheological behaviours of the material. In this regard Rogers considers cases of constant and various contact regions between the specimen and the tool. Once integrated, the resulting equations for shear flow according to [90] can be written as:

No friction interface, constant contact region boundary condition:

$$\frac{\boldsymbol{dh}}{\boldsymbol{dt}} = \frac{\boldsymbol{P_{applied}}}{\boldsymbol{4\,\eta}}\boldsymbol{h}. \tag{3.9}$$

No friction interface, varying contact region boundary condition:

$$\frac{\boldsymbol{dh}}{\boldsymbol{dt}} = \frac{\boldsymbol{P_{applied}}}{\boldsymbol{4\,\eta\,h_0}}\boldsymbol{h^2}. \tag{3.10}$$

No slip interface, constant contact region boundary condition:

$$\frac{dh}{dt} = \frac{P_{applied}}{\eta h_0 (w^2 + 3h^2)} h^4 . \quad 3.11$$

No slip interface, varying contact region boundary condition:

$$\frac{dh}{dt} = \frac{P_{applied}}{\eta\, h_0 \left(w_0^2 h_0^2 + 3h^4\right)} h^6 \quad 3.12$$

where h_0 – initial thickness, t – time, $P_{applied}$ – pressure applied to the top surface of a composite precursor, η – Newtonian viscosity.

The abovementioned governing equations are derived for the reinforced Newtonian fluid, where the viscosity is independent of the shear rate of the material. Which means that strain-rate effects are not taken into account within such models. However, there are a lot of evidences that the behaviour of viscous polymer suspension is often non-Newtonian [127], [45]. In order to make model more adaptive to changing processing conditions, it is worth considering strain-rate effects on the fluid's viscosity. Such study has been undertaken by a number of different researchers [49], [127], [132], [133].

For Newtonian fluid [134], the relation between shear stress and shear rate for 2D case (Figure 3.1) can be written as:

$$\tau_{XY} = -\eta_T \dot{\gamma}_{XY} \quad 3.113$$

where τ_{XY} is a shear stress, η_T – transverse viscosity, $\dot{\gamma}_{XY}$ – shear rate.

In this relation viscosity remains constant for a given temperature and pressure.

After modifying Newton's law, the viscosity becomes a function of a shear rate $\dot{\gamma}$:

$$\tau_{XY} = -\eta_T(\dot{\gamma}_{XY})\, \dot{\gamma}_{XY}. \quad 3.14$$

The power-law model for viscosity function is:

$$\eta_T(\dot{\gamma}) = m\, \dot{\gamma}_{XY}^{n-1} \quad 3.15$$

where m and n denote consistency index of the fluid and power-law exponent, respectively.

Consistency index in turn is represented through time constant λ and zero-shear-rate viscosity η_0:

$$m = \eta_0 \lambda^{n-1}. \quad 3.16$$

Therefore, the resulting function for shear-rate dependent viscosity is defined as follows:

$$\boldsymbol{\eta_T(\dot{\gamma}_{XY}) = \eta_0\,(\lambda\dot{\gamma}_{XY})^{n-1}.} \tag{3.17}$$

To connect an expression for viscosity with existing governing equations for shear flow, shear rate term is redefined through platen closure rate $\frac{dh}{dt}$ and sample thickness h at the instant time:

$$\dot{\gamma}_{XY} = \left.\frac{dh}{dt}\right/_{h}. \tag{3.18}$$

Thus, the final expression for viscosity is described by an expression below:

$$\boldsymbol{\eta_T(\dot{\gamma}_{XY}) = \eta_0 \left(\lambda \left.\frac{dh}{dt}\right/_{h}\right)^{n-1}}. \tag{3.19}$$

After examining an expression for power-law viscosity, it is evident, that the Newtonian model is recovered for a power law exponent n = 1, while 0 < n < 1 shows that a fluid is shear thinning.

The extension of the existing models for shear flow (according to Rogers) was inspired by the structural approach used for the solution of Carreau fluids governing equation, where the obtained ODEs are not integrable (the solution is split as a combination of Newtonian and power-law fluids) [45], [133]. Structural approach is also used for problems with large deformations, where the solution is divided in a sequence of steps where deformations are small, hence the assumptions for small deformations problem are valid. After substituting shear-rate-dependent viscosity in place of Newtonian viscosity and isolating platen closure rate $\frac{dh}{dt}$ term, the resulting governing equation for shear flow in the transverse direction with power law shear thinning is defined as following:

No friction constant contact region boundary condition:

$$\frac{\boldsymbol{dh}}{\boldsymbol{dt}} = \frac{\boldsymbol{P_{applied}}}{\boldsymbol{4\,\eta_0 \left(\lambda/_{h}\right)^{n-1} \frac{dh^{n-1}}{dt}}}\boldsymbol{h}$$

$$\frac{\boldsymbol{dh^n}}{\boldsymbol{dt}} = \frac{\boldsymbol{P_{applied}}}{\boldsymbol{4\,\eta_0\,\lambda^{n-1}}}\boldsymbol{h^n} \tag{3.20}$$

$$\frac{dh}{dt} = \sqrt[n]{\frac{P_{applied}}{4\,\eta_0\,\lambda^{n-1}}}\,h.$$

The same mathematical routine is repeated for other governing equations for shear flow:

No friction varying contact region boundary condition:

$$\frac{dh}{dt} = \frac{P_{applied}}{4\,\eta_0\left(\lambda/h\right)^{n-1}\frac{dh}{dt}^{n-1}\;h_0}h^2$$

$$\frac{dh}{dt}^{n} = \frac{P_{applied}}{4\,\eta_0\,\lambda^{n-1}\;h_0}h^{n+1} \qquad 3.21$$

$$\frac{dh}{dt} = \sqrt[n]{\frac{P_{applied}}{4\,\eta_0\,\lambda^{n-1}\;h_0}}h^{\frac{n+1}{n}}.$$

No slip constant contact region boundary condition:

$$\frac{dh}{dt} = \frac{P_{applied}}{\eta_0\left(\lambda/h\right)^{n-1}\frac{dh}{dt}^{n-1}\;h_0(w^2+3h^2)}h^4$$

$$\frac{dh}{dt}^{n} = \frac{P_{applied}}{\eta_0\,\lambda^{n-1}\,h_0(w^2+3h^2)}h^{n+3} \qquad 3.22$$

$$\frac{dh}{dt} = \sqrt[n]{\frac{P_{applied}}{\eta_0\,\lambda^{n-1}\,h_0(w^2+3h^2)}}h^{\frac{n+3}{n}}.$$

No slip varying contact region boundary condition:

$$\frac{dh}{dt} = \frac{P_{applied}}{\eta_0\left(\lambda/h\right)^{n-1}\frac{dh}{dt}^{n-1}\;h_0\left(w_0^2h_0^2+3h^4\right)}h^6$$

$$\frac{dh}{dt}^{n} = \frac{P_{applied}}{\eta_0\,\lambda^{n-1}\;h_0\left(w_0^2h_0^2+3h^4\right)}h^{n+5} \qquad 3.23$$

$$\frac{dh}{dt} = \sqrt[n]{\frac{P_{applied}}{\eta_0\lambda^{n-1}\,h_0\left(w_0^2h_0^2+3h^4\right)}}h^{\frac{n+5}{n}}.$$

The influence of material parameters on the shear models' thickness prediction.

Newtonian suspension and power law fluid models' compaction response to parameter variation is presented in Figure 3.2 and Figure 3.3 respectively.

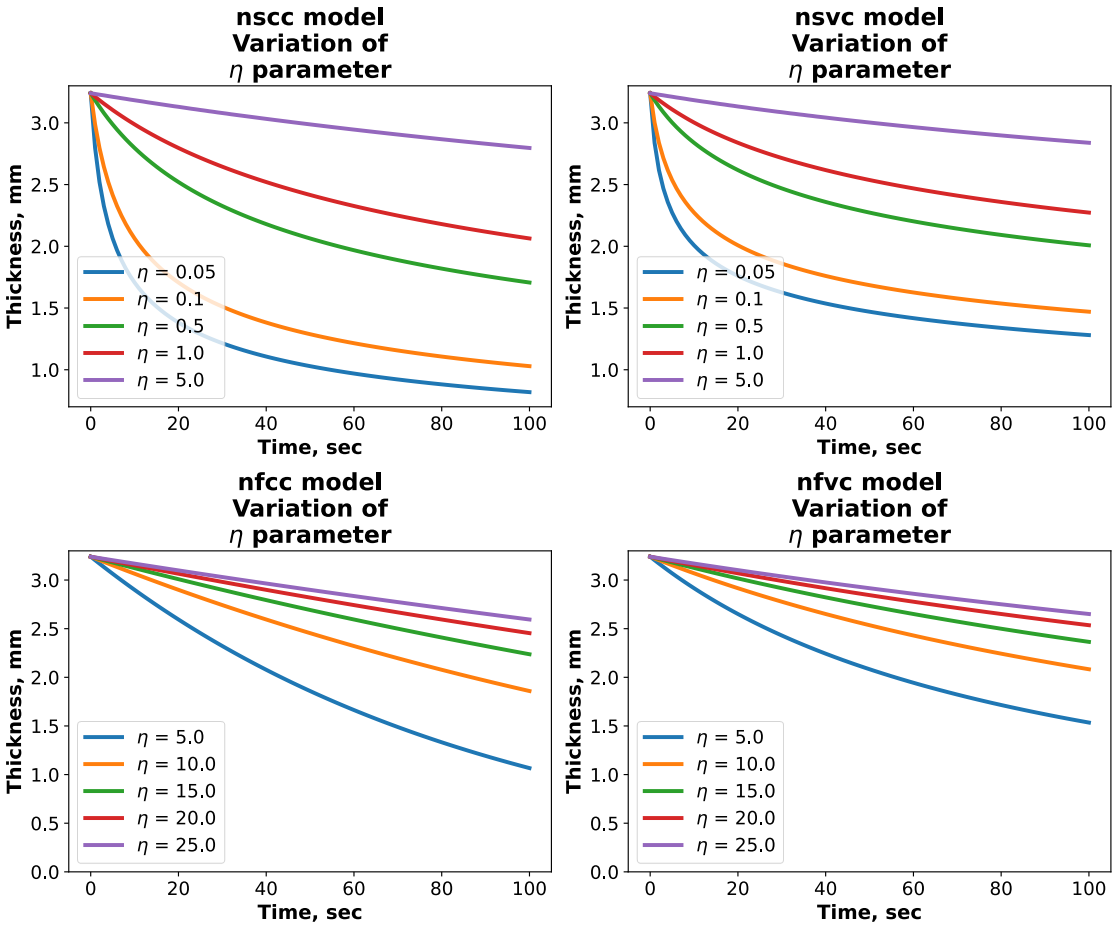

Figure 3.2: Incompressible shear flow of Newtonian suspension model's compaction response to parameter variation. Newtonian suspension models' abbreviations: zero friction with tool and constant/evolving tool-material contact – nfcc/nfvc; no-slip conditions and constant/evolving tool-material contact – nscc/nsvc.

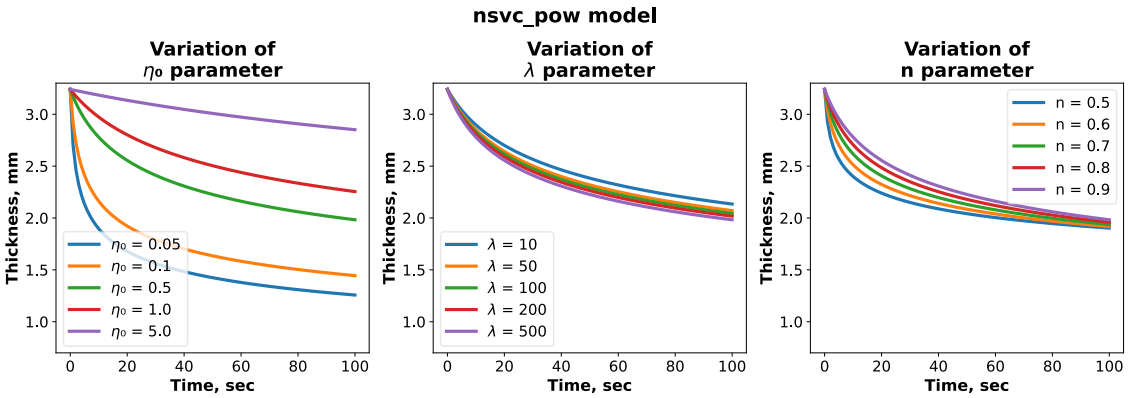

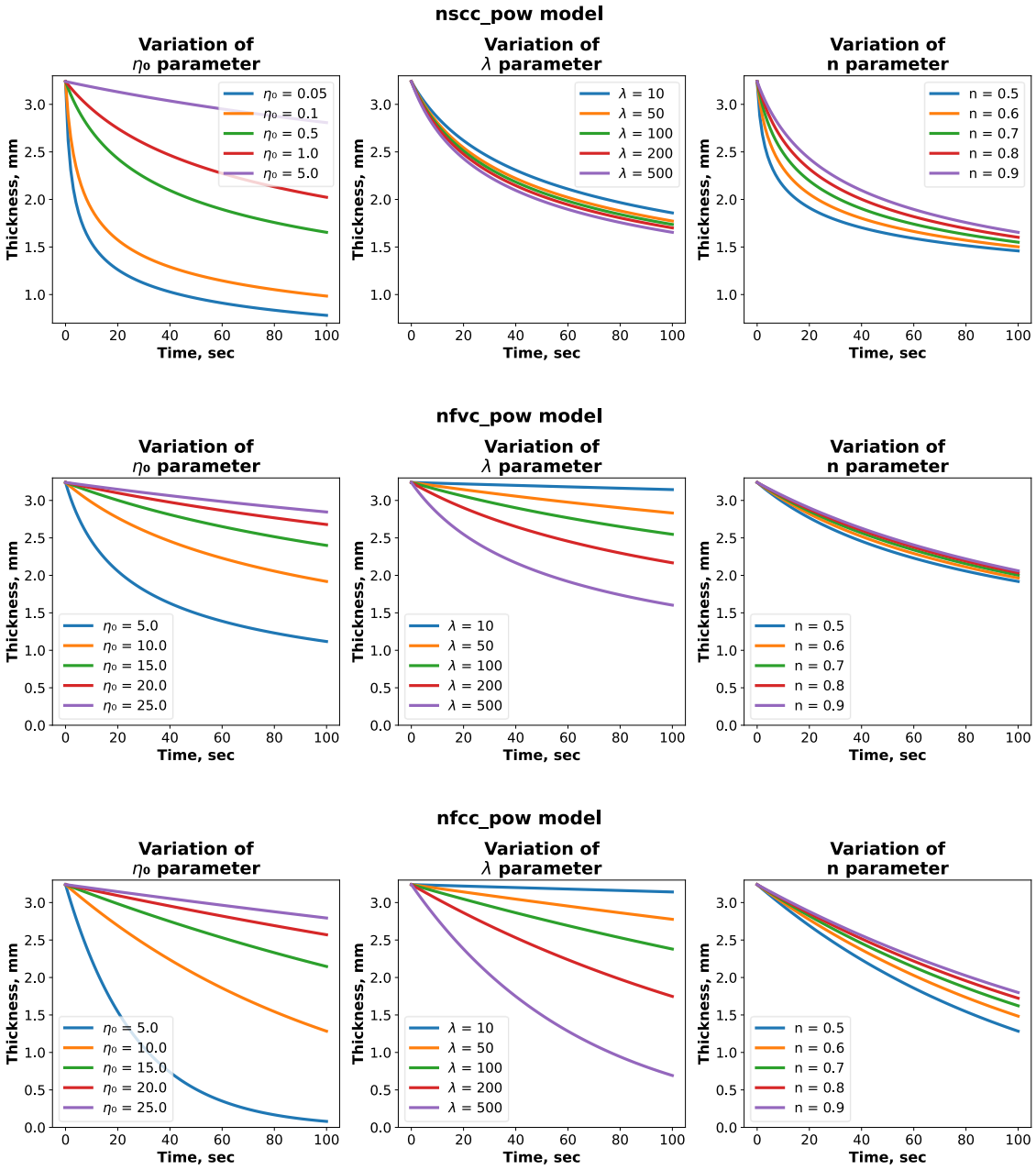

Figure 3.3: Incompressible shear flow with power law shear thinning model's compaction response to parameter variation. Power law shear thinning models' abbreviations: zero friction with tool and constant/evolving tool-material contact – nfcc_pow/nfvc_pow; no-slip conditions and constant/evolving tool-material contact – nscc_pow/nsvc_pow.

The point of these graphs is to showcase how the variation in material parameters propagates to an error in model's thickness prediction. The scatter of parameters values may be the result of the uncertainty in measurements of material parameters, possible experimental errors, or the sensitivity to processing conditions (T). For instance, the range of viscosities up to 6 orders of magnitude was observed during curing process for

the relevant material systems [135]. The variation of time constant λ and power law exponent n parameters was specified according to Bird et al. [134].

As expected, Newtonian model for shear flow demonstrate significant increase in thickness rate with the decrease in viscosity value (as shown in Figure 3.2). Shear-rate dependant models demonstrate a similar to Newtonian model's response to the viscosity variation. There are more material parameters (λ and n) affecting the predicted thickness output, hence the model showcases more complex compaction behaviour (change of thickness rate, final thickness, see Figure 3.3).

3.2.2 Percolation models

Governing equations

Percolation flow describes the resin's movement through (percolation) or out (bleeding out from the edge of the laminate) of the composite. Generally, the resin flows relatively to the fibres of the laminate during the compaction and is assumed to behave as an incompressible Newtonian fluid (although there are non-Newtonian Darcy models, they are not considered here). The deformation of reinforcement and the flow of resin can occur in different directions and/or at different rates. Therefore, the resulting governing equations for the percolation flow model should cover the behaviour of both matrix and reinforcement phases of the composite.

The governing relation between the applied pressure and the thickness evolution for percolation flow is derived for a two-dimensional problem of a composite precursor squeezed between two parallel plates. Different processes occurring during manufacturing can be represented in this way. For instance, such problem statement is relevant for description of the bleeding closure of the gap between two tapes within AFP manufacturing process. The schematic representation of the problem is shown in Figure 3.4.

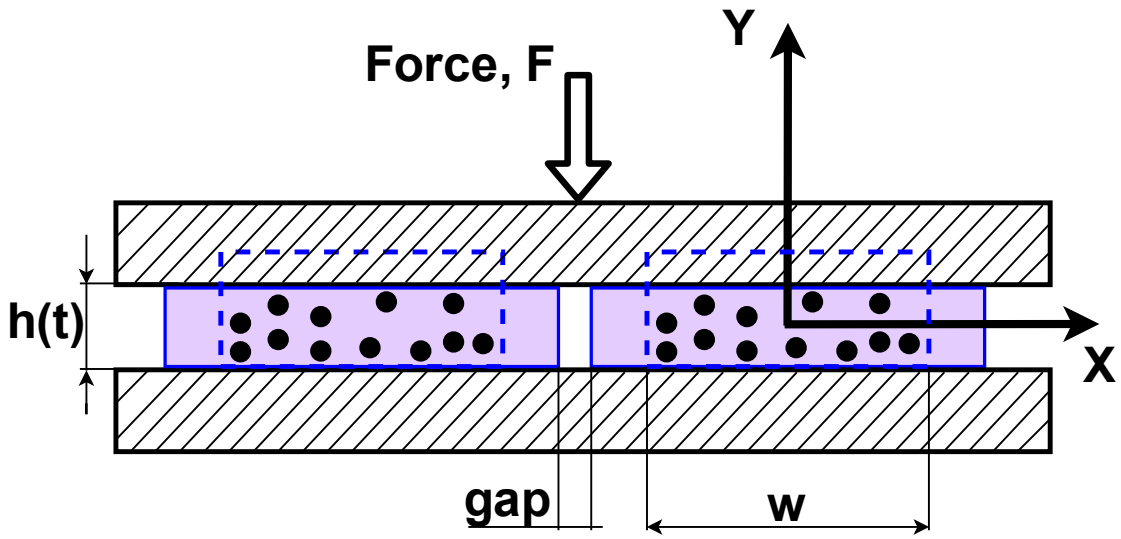

Figure 3.4: Bleeding closure of the gap. Purple – bleeding resin, black dots – fibres, dashed line – initial contour of the tape.

Assumptions used for the formulation of percolation flow governing equations include:

- The assumption on load sharing between the resin and the fibrous phases (discussed within the literature review in section 2.2.2).
- Resin acts as an incompressible Newtonian fluid.
- Assumptions on the suspension velocity V_x and V_y:

$$\boldsymbol{V_x = 0,\ \ V_y = V_y(y).} \tag{3.24}$$

- Resin velocities v_x and v_y are functions of *x* and *y* correspondingly:

$$\boldsymbol{v_x = v_x(x),\ \ v_y = \frac{1}{1-f} V_y(y).} \tag{3.25}$$

- The chosen model for permeability (Kozeny-Carman equation).
- The model for the elastic response of the fibrous phase (model of Gutowski).

Saturated slow motion of a fluid through yarns or fabrics can be characterised by Darcy's law equation:

$$\boldsymbol{\overrightarrow{v_D} = -\frac{K}{\eta} \nabla P} \tag{3.26}$$

where $\overrightarrow{v_D}$ is the phase average velocity vector, $\overrightarrow{v_D} = (1-f)\vec{v}$, $\vec{v}$, is the actual pore velocity vector, *K* is the saturated permeability, η is the viscosity, ∇P is the pressure gradient, f is the fibre volume fraction.

For the two-dimensional problem (described above) Darcy's law can be written as follows:

$$\boldsymbol{v_x = -\frac{K}{\eta(1-f)}\frac{\partial P_{res}}{\partial x}} \qquad 3.27$$

where P_{res} is average resin pressure, η is the viscosity of resin, K is the permeability in the flow direction, f is the current fibre volume fraction, v_x, v_y – resin velocity.

To describe the relationship for the velocity gradients of resin/suspension, the equations of mass balance for the incompressible resin and the compressible suspension are formulated as follows:

Mass balance for incompressible resin equation:

$$\boldsymbol{\nabla \vec{v} = 0}$$
$$\boldsymbol{\frac{\partial v_x}{\partial x} + \frac{\partial v_y}{\partial y} = 0,\ \ v_z = 0.} \qquad 3.28$$

Mass balance for compressible suspension equation:

$$\boldsymbol{\nabla(\rho\vec{V}) = -\frac{d\rho}{dt}}$$
$$\boldsymbol{\frac{\partial(\rho V_x)}{\partial x} + \frac{\partial(\rho V_y)}{\partial y} = -\frac{d\rho}{dt}} \qquad 3.29$$

where ρ is the density of the suspension, V_x, V_y is the velocity of compressible suspension in the corresponding directions (v_x, v_y is the velocity of resin).

To integrate mass balance equation, the relation for suspension's density and boundary conditions are required. The assumption on the incompressibility of resin can be represented in terms of fibre volume fracture *f*:

$$\boldsymbol{\rho = \rho_f f + \rho_r(1-f)}$$
$$\boldsymbol{\rho = (\rho_f - \rho_r)f + \rho_r} \qquad 3.30$$

where ρ_f, ρ_r is the density of the fibres/resin.

The considered boundary condition at the tool's surface is:

$$\boldsymbol{V_y\left(y = -h/2\right) = 0.} \qquad 3.31$$

Integrating mass balance equation along with the boundary conditions and the relation for suspension's density provides an expression for suspension's velocity V_y:

$$\boldsymbol{V_y = -\left(y + h/2\right)\frac{1}{f}\frac{df}{dt}}. \quad 3.32$$

Using this expression together with resin's mass balance equation and the assumption on resin's velocity results in:

$$\boldsymbol{\frac{\partial v_x}{\partial x} = \frac{1}{f(1-f)}\frac{df}{dt}}. \quad 3.33$$

Following integration with boundary condition $v_x(x = 0) = 0$ results in the expression for resin's velocity:

$$\boldsymbol{v_x = x\frac{1}{f(1-f)}\frac{df}{dt}}. \quad 3.34$$

After substituting the obtained equations for the resin velocity v_x into Darcy's law and following integration (boundary condition $P_{res}\left(x = {}^{w}/_{2}\right) = 0$), an expression for resin pressure can be written as:

$$\boldsymbol{P_{res} = \left(\frac{\eta}{K}\frac{w^2}{3}\right)\frac{1}{f}\frac{df}{dt}}. \quad 3.35$$

Permeability of a fibrous material is inversely proportional to the resistance of a porous medium to the resin flow induced by pressure gradient. In general, the resistance of the reinforcement phase increases with the raise in fibre volume fraction within composite's compaction. The time required for a full impregnation of a composite part with a higher fibre content becomes longer proportionally to the square of flow length as the space between the fibres is reduced.

A vast variety of studies have been conducted to predict and measure the evolution of the composite precursor's permeability [136]–[139] within different manufacturing methods. As shown in section 2.3.2, experimental estimation of the permeability is a challenging task [107], [108]. Normally, the relation for permeability represents a function connecting the evolution of fibre volume fraction and the fibre arrangement structure (quadratic, hexagonal etc).

One of the most used permeability models is Kozeny-Carman equation [140] which takes into account the permeability of the channels between fibres. It was originally developed to estimate the permeability of granular solids [141]:

$$\boldsymbol{K(f) = K_A \frac{(1-f)^3}{f^2}} \tag{3.36}$$

where K_A is a function of fibre network geometry and fibre radius, *f* is the current fibre volume fraction.

Extensive research has been conducted to develop a permeability model specific to a certain fibre arrangement structure. Gebart's model [142], [143] describes permeability for quadratic and hexagonal fibre arrangement for the resin flow in both transverse and along the fibre direction:

$$\boldsymbol{K_1 = \frac{8 r_f^2}{c} \frac{(1-f)^3}{f^2}; \qquad K_2 = C_1 \left(\sqrt{\frac{f_{lim}}{f}} - 1 \right)^{5/2} r_f^2} \tag{3.37}$$

where K_1 is the permeability along the fibre direction, K_2 is the permeability perpendicular to the fibre direction, r_f is the fibre radius, *c* is the shape factor depending on fibre arrangement (quadratic and hexagonal), C_1 – material constant, f_{lim} is the maximum achievable fibre volume fraction. These expressions were derived considering Stokes flow through an idealised unidirectional reinforcement for both longitudinal and transverse flows.

As discussed previously in section 2.2.2 of the literature review, one of the major assumptions in percolation flow reflects the idea of sharing the pressure applied to the laminate by resin and fibrous phases of the composite:

$$\boldsymbol{P_{applied} = P_{res} + P_{pre}} \tag{3.38}$$

where $P_{applied}$ is the applied pressure, P_{pre} is the fibre bed response, P_{res} is the resin pressure.

To fully define every term in the balance equation above, the model for the reaction of the fibrous phase has to be proposed. The rate independent fibre bed response component reflects the non-linear stiffness behaviour of the fibre network under compression. One of the most popular expressions which governs such a response was derived and confirmed experimentally by Gutowski [61] [144]. The proposed equation for the fibre bed response was developed by approximating fibres as bending beams between multiple points of contact. Such beam's length is proportional to the composite's thickness. As compaction of the laminate progresses, additional contacts

between fibres are established. By analysing the proposed equation for fibre bed response, it can be clearly seen, that fibre network carries only a small portion of a load when laminate deformation is low, due to the low fibre volume fraction value. Nonetheless, with the change of thickness fibre volume fraction increases causing rapid increase of the composite's elastic response. The resulting relation can be written as follows:

$$\boldsymbol{P_{pre}(f) = \sigma_A \frac{\sqrt{f/f_0} - 1}{\left(\sqrt{f_{lim}/f} - 1\right)^4}} \quad 3.39$$

where σ_A is the material spring constant, f is the current fibre volume fraction, f_0 is the initial fibre volume fraction, f_{lim} is the maximum achievable fibre volume fraction.

All considered flow models are represented within thickness – thickness rate terms. The current thickness value can be calculated through the fibre volume fraction. The total number of fibres is not changing during the compaction process (meaning constant areal density of the reinforcement). Hence, the relation between fibre volume fraction and thickness can be expressed as:

$$\boldsymbol{f = \frac{1}{h}\frac{A_\rho}{\rho_f}} \quad 3.40$$

where A_ρ is the areal density of the precursor, ρ_f, is the density of fibres.

Finally, after substituting an expression for resin pressure into balance equation and isolating thickness rate $\frac{dh}{dt}$ term, the governing equation for percolation consolidation model (for the considered two-dimensional problem) can be written as follows:

$$\boldsymbol{\frac{dh}{dt} = -\frac{3K(h)}{\eta w^2}\left(P_{applied} - P_{pre}(h)\right)h} \quad 3.41$$

The influence of material parameters on the percolation model's thickness prediction.

Percolation models' compaction response to material parameters variation is presented in Figure 3.5. Experimental determination of the material parameters is not a trivial task. The lack of standardisation for the material parameters measurements leads researchers to investigate the required parameters within different test setups, which can lead to significant discrepancies in the results. For instance, an extensive research was carried out to determine the in-plane permeability of a carbon fabric within different research groups [107], [108]. The obtained permeability values were scattered up to one

order of magnitude between different experimental procedures. As concluded by the authors, the reason for such dispersion of the results could be experimental uncertainties, variability of the specimens and human factors. The discrepancies in material parameters values can greatly contribute to the propagation of error in model's thickness prediction. That is why it is important to have an insight on model's response to the change in parameters values. The range of values for parameters variation was specified according to Gutowski [61] [144], Gebart [142], [143], permeability benchmark exercises [107], [108].

The thickness rate $\frac{dh}{dt}$ is inversely proportional to the viscosity η and directly proportional to the permeability K_A. The compaction of the impregnated preform occurs faster if resin faces less resistance from the reinforcement phase as it flows (hence, higher permeability) or if the resin's viscous response is lower (lower viscosity).

Model's response to the compression clearly showcases the existence of the limit for the maximum achievable thickness, which is explained by the presence of the elastic response of the fibre network. As shown in Figure 3.5, the material spring constant σ_A. affects how fast the compaction limit is reached. If the stiffness of the fibre network is high, the time required for the elastic reaction of the fibres to take the higher fraction of the external load decreases. Finally, the load is carried entirely by the fibres and the composite cannot be compressed any further.

Technically, the compaction response is also affected by the values of the initial f_0 and final f_{lim} fibre volume fractions. The current implementation of the model suggests that these parameters are defined by the researcher (treated as constants), as experimentally determined values are available in the literature (e.g. [40]). Therefore, the variation of these parameters is not presented within the model's compaction response study.

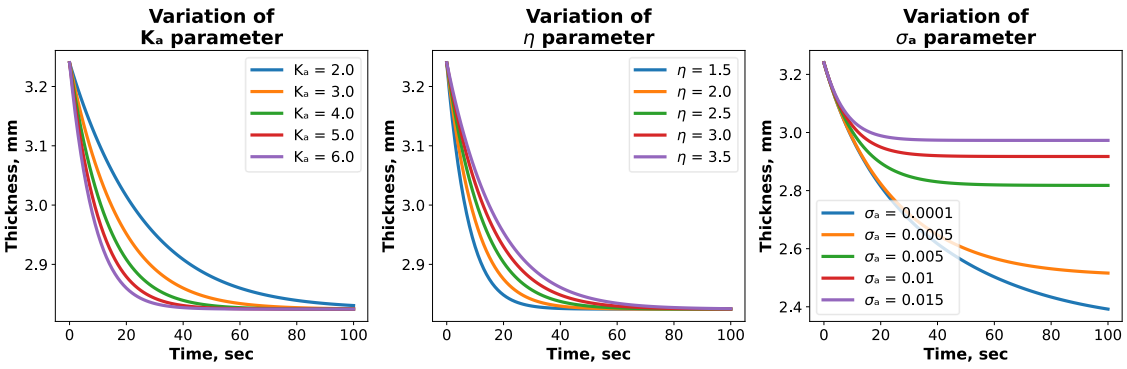

Figure 3.5: Percolation model's compaction response to parameter variation.

An important feature of the considered flow model is its response to unloading. Different manufacturing methods require the application and subsequent removal of the external pressure (e.g. AFP). In regard to this research, the model's ability to capture the material's behaviour at the unloading stage will become relevant, when the concept of the autonomous testing framework is introduced (chapter 5).

To address this effect more thoroughly, two different load cases are considered (see Figure 3.6). The first load case is a conventional ramp-dwell loading programme, where the load remains at a constant level upon reaching a defined level (0.2 MPa). The second load case follows the same pattern until the moment when pressure drops to a lower value and then dwells again.

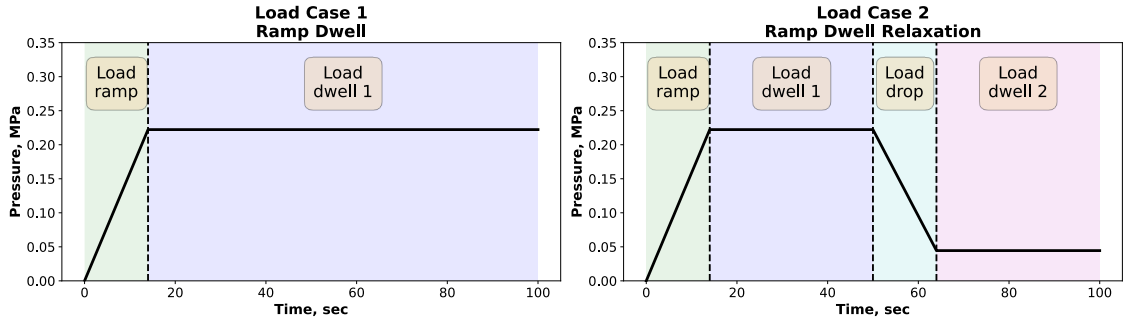

Figure 3.6: a – load case 1, pressure drop load schedule, b – load case 2, conventional ramp-dwell loading schedule.

The compaction response for both load cases is presented in Figure 3.7. Graphs on the left illustrate thickness evolution curve as a result of the applied external pressure within the corresponding load case. Graph on the right depicts fibre bed response evolution relative to the applied external pressure (shown as black curve). The model's feedback during load relaxation stage is defined by the non-linear stiffness reaction of the fibre network. For that reason, model's response curves are presented for different values of the material spring constant σ_A.

After the rapid external load relaxation, the stiffness reaction of fibres relaxes as well, but at a much slower pace. Therefore, the difference between the external pressure and the fibre bed response $\left(P_{applied} - P_{pre}(h)\right)$ becomes negative. Which in turn results in the sign change of the thickness rate $\frac{dh}{dt}$ term. As a result, the thickness evolution changes its trend at the unloading stage from the compaction to the spring back as shown in Figure 3.7.

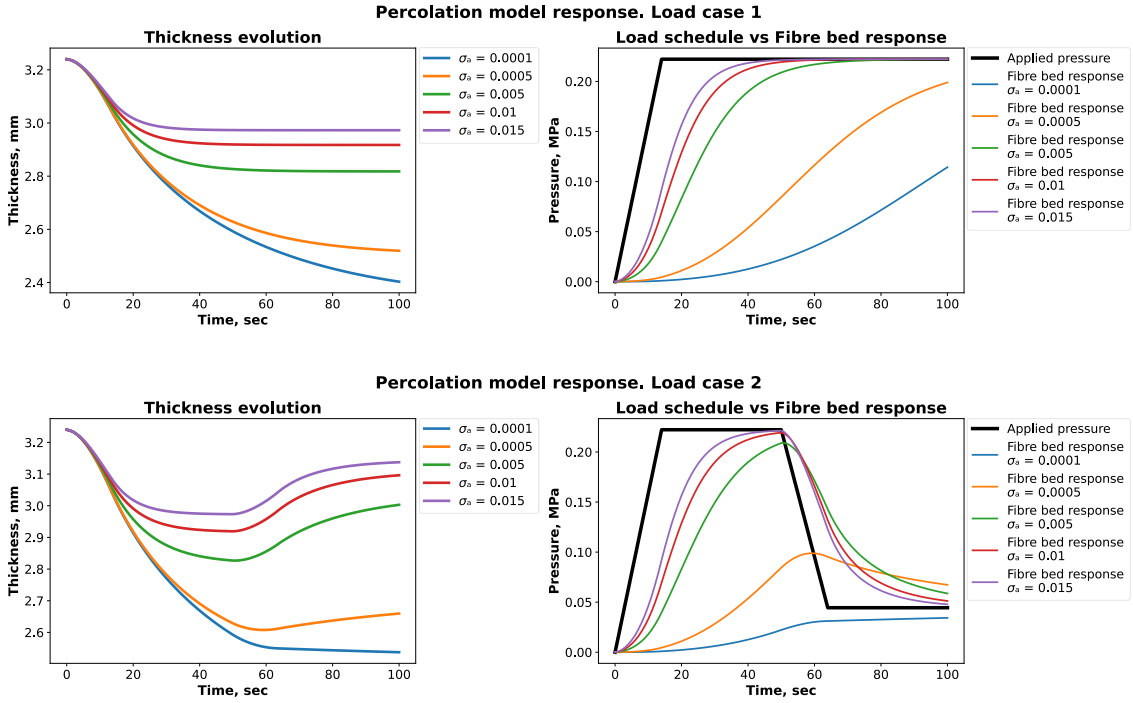

Figure 3.7:Percolation model's feedback to unloading and the corresponding fibre bed response.

All considered models (including the current one) suggest that there is no separation between the surface of the composite precursor and the top compression platen. From perspective of the physics of the process, non-separation condition means that the test specimen is under tension during unloading stage. That explains the change of the sign of the $\left(P_{applied} - P_{pre}(h)\right)$ term, as shown above: if $\left(P_{applied} - P_{pre}(h)\right) < 0$, then $\frac{dh}{dt} > 0$ (which corresponds to tension), otherwise $\frac{dh}{dt} < 0$ (which corresponds to compression).

Upon analysing the expression for the elastic reaction, it becomes clear that the fibre-bed response can only become zero when $\sqrt{f/f_0} - 1 = 0$, meaning that $f = f_0$. Therefore, if the external load is removed completely, the model predicts that the composite specimen fully restores its thickness due to the active nonlinear elastic response (until the moment when $f = f_0$). Experimental results of the compaction-relaxation tests do not confirm such material behaviour. The compaction response of an actual material (e.g. e-glass preforms) showcases that only a fraction of specimen's thickness is restored due to the spring-back effect of the fibre network [145], [146].

The explanation of such phenomenon is that the model of Gutowski for fibrous reaction was designed for an active load only. The actual behaviour of fabric in compaction-

unloading cycle exhibits substantial hysteresis, as demonstrated by Lomov et al.[147]. Therefore, the proposed model provides controversial thickness prediction upon unloading. The proposed exercises demonstrate that the unloading regime requires a more sophisticated material model for fibre bed response and more careful consideration of the material/tool interaction.

3.2.3 DefGen ProToCoL (**Pro**cessing **To**ols for **Co**mposite **L**aminates)

The discussion on the phenomenological DefGen material model and the assumptions behind it was presented earlier in the section 2.2.4 of the literature review.

Governing equations

The synthetic phenomenological DefGen ProToCoL model is represented as a multiplicative decomposition of a strain and a strain rate dependent term. The strain dependent term is in turn a product of terms accounting for deformation at ply (macro) and micro levels.

$$\boldsymbol{P_{applied} = \eta_{micro}(\varepsilon)\eta_{ply}(\varepsilon)\eta_{rate}(\dot{\varepsilon})\dot{\varepsilon}} \tag{3.42}$$

where $\eta_{micro}(\varepsilon)$ is the micro level strain dependent term, $\eta_{ply}(\varepsilon)$ is the ply level strain dependent term, $\eta_{rate}(\dot{\varepsilon})$ is the strain rate term, $\varepsilon = ln(^{h}/_{h_0})$ is the Hencky measure of strain. Thorough description of these terms can be found in [40].

According to the DefGen formulation, the rate dependant term $\eta_{rate}(\dot{\varepsilon})$ is assumed to follow a standard power law function:

$$\boldsymbol{\eta_{rate}(\dot{\varepsilon}) = exp(\bar{b}) \cdot (-\dot{\varepsilon})^{a}} \tag{3.43}$$

where $b = \bar{b} + ln(\eta_{res})$, *a*, *b*, *k* – DefGen ProToCoL material parameters [40].

To join shear and percolation formulations within a single model, the bleeding flow is represented as the shear flow along the fibre direction. Therefore, the micro level term $\eta_{micro}(\varepsilon)$ formulation is based on analytical expression for squeezing flow of a Newton fluid [90] of viscosity η_{res} between two neighbouring fibres:

$$\boldsymbol{\eta_{micro}(\varepsilon) = \eta_{res} \cdot 2 \cdot \sqrt{\chi_l} \cdot exp(\varepsilon) \cdot k \cdot \left(\left(\frac{k}{\sqrt{\chi_f} exp(\varepsilon) - k}\right)^{2} + 3\right)} \tag{3.44}$$

where η_{res} – the viscosity of a resin, χ_f, χ_l - the aspect ratios of a unit cell at the compaction limit and locking stage, respectively.

Initially the shear flow of resin is incompressible, meaning that deformation in the compaction direction is equal to the deformation in the transverse direction. After reaching the critical strain, the flow becomes fully compressible. It results in the absence of the transverse deformation due to the resin loss through bleeding flow. Prior and post locking transverse behaviour of the material is described by the macro $\eta_{ply}(\varepsilon)$ term given below:

$$\boldsymbol{\eta_{ply}(\varepsilon)} = \begin{cases} \boldsymbol{2\left(\frac{w_0}{h_0}\right)^2 exp(-4\varepsilon),} & \boldsymbol{\varepsilon \leq \varepsilon_l} \\ \boldsymbol{2\left(\frac{w_0}{h_0}\right)^2 exp\left(-2(\varepsilon+\varepsilon_l)\right),} & \boldsymbol{\varepsilon > \varepsilon_l} \end{cases} \qquad 3.45$$

where ε_l - the strain level at the moment of flow locking.

Therefore, there are only 3 required material parameters *a*, *b*, *k* for a given processing temperature, which have to be determined experimentally. The parameters *a* and *b* characterise the behaviour of the resin with respect to the strain rate. The parameter *a* can be viewed as a power law exponent, while the parameter $exp(\bar{b})$ serves as a consistency index in the power law formulation for resin's viscosity. The parameter *k* reflects the size effect of the channels between neighbouring fibres within the unit cell at the micro-scale. It explicitly affects the critical deformation, as the flow transition occurs when fibres come into contact and lock the shear driven flow.

Since all of the previously considered models are represented in terms of thickness rate instead of deformation, the previous equation is reformulated as follows:

$$\boldsymbol{\frac{dh}{dt} = -\sqrt[a+1]{\frac{P_{applied}}{\overline{\eta_{micro}} \cdot \eta_{ply} \cdot \overline{\eta_{rate}}}} \cdot h} \qquad 3.46$$

where $\overline{\eta_{micro}} = \frac{\eta_{micro}}{\eta_{resin}}$, $\overline{\eta_{rate}} = e^b$.

The influence of material parameters on the DefGen model's thickness prediction.

The illustration of DefGen model's transitional behaviour is demonstrated in Figure 3.8. It can be clearly seen that the thickness compaction curve changes its rate upon reaching the critical deformation level (deformation at locking). At this moment, the transition between different stages of the flow occurs instantaneously.

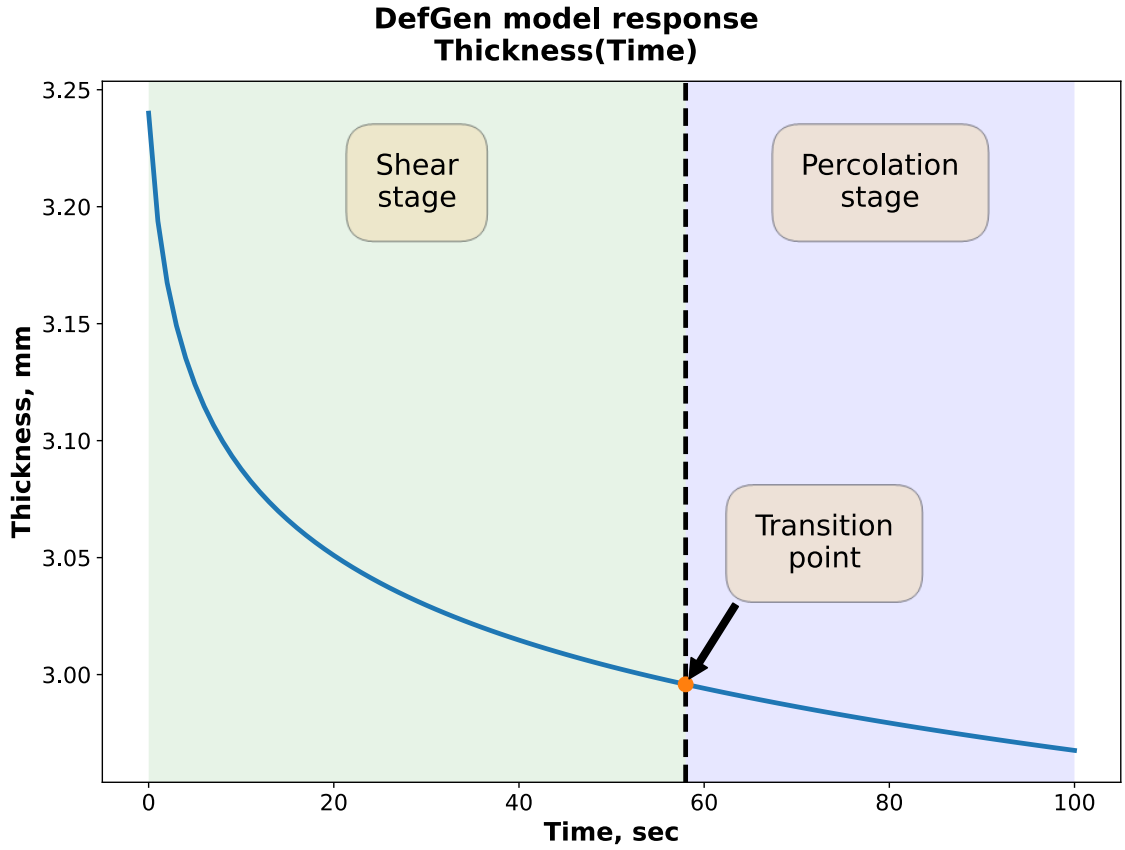

Figure 3.8: DefGen ProToCoL model's transitional behaviour.

Figure 3.9 depicts DefGen models' compaction response to parameter variation. The range of *a*, *b*, *k* parameters values were specified according to [14], [40], [82], where these values were determined experimentally for IMA/M21 and IM7/8552 prepregs.

Parameters *a* and *b* have a similar effect on the model's compaction response as λ and *n* in shear rate dependant models, as they are inspired by the power law. The variation of these parameters does not affect the transition point between flow modes. As parameter *k* reflects the stiffness of the fibre network, lower value of this parameter results in lesser compaction of the material. The level of critical locking deformation is affected by the change of parameter *k* only, as it is related to the fibre structure of the ply.

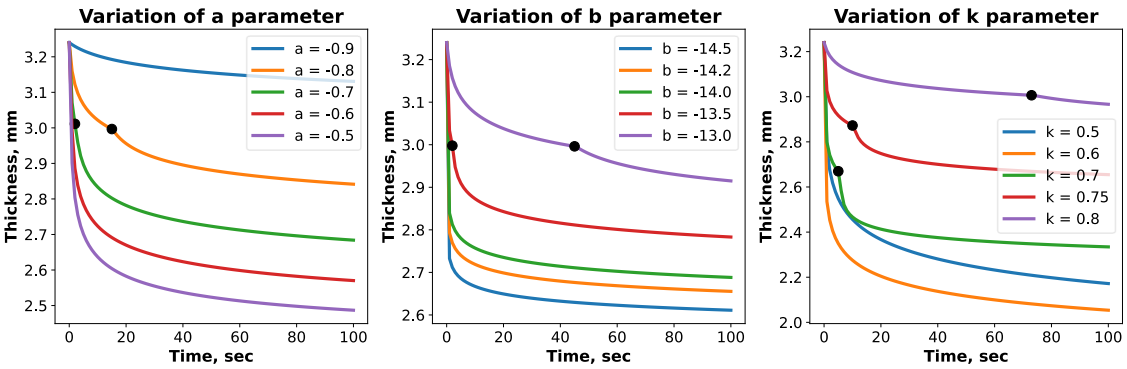

Figure 3.9: DefGen ProToCoL model's compaction response to parameter variation.

3.2.4 Consolidation library. The summary of the considered models

All models considered in this section are stored within the consolidation library. This library represents a pre-coded implementation of the discussed governing ODEs and is used further in this research. The library is implemented in Python programming language environment [148]. Each model has its own input set of material parameters and the assigned abbreviation (id). The library is used in the following order:

- Request the chosen consolidation model by its id.
- Specify the values of the material parameters.
- Input load/time history to receive thickness output.

The summary of all considered models, assigned abbreviations and the required model parameters is presented in

Table 3.1 below. The application of the consolidation library will be shown in further chapters.

Table 3.1: Summary of selected flow models for unidirectional fibre-resin suspensions.

Flow mode type (id)	F(t, h)	Q(h)	Material parameters
Incompressible shear flow of Newtonian suspension in the transverse direction [90]			
Zero friction with tool and constant tool-material contact (nfcc)	$P_{applied}$	$\frac{h}{4\,\eta}$	η
Zero friction with tool and evolving tool-material contact (nfvc)	$P_{applied}$	$\frac{h^2}{4\,\eta h_0}$	η
No-slip conditions and constant tool-material contact (nscc)	$P_{applied}$	$\frac{h^4}{\eta h_0(w^2+3h^2)}$	η
No-slip conditions, evolving tool-material contact (nsvc)	$P_{applied}$	$\frac{h^6}{\eta h_0(w_0^2 h_0^2+3h^4)}$	η
Incompressible shear flow in the transverse direction with power law shear thinning [127], [132], [133]			
Zero friction with tool and constant tool-material contact (nfcc_pow)	$\sqrt[n]{P_{applied}}$	$\sqrt[n]{\frac{1}{4\eta_0\,\lambda^{n-1}}}h$	η_0 λ n

Flow mode type (id)	**F(t, h)**	**Q(h)**	**Material parameters**
Zero friction with tool and evolving tool-material contact (nfvc_pow)	$\sqrt[n]{P_{applied}}$	$\sqrt[n]{\frac{1}{4\,\eta_0\lambda^{n-1}\ h_0}}\,h^{\frac{n+1}{n}}$	η_0 λ n
No-slip conditions and constant tool-material contact (nscc_pow)	$\sqrt[n]{P_{applied}}$	$\sqrt[n]{\frac{1}{\lambda^{n-1}\,\eta_0 h_0(w^2+3h^2)}}\,h^{\frac{n+3}{n}}$	η_0 λ n
No-slip conditions, evolving tool-material contact (nsvc_pow)	$\sqrt[n]{P_{applied}}$	$\sqrt[n]{\frac{1}{\lambda^{n-1}\,\eta_0 h_0(w_0^2 h_0^2+3h^4)}}\,h^{\frac{n+5}{n}}$	η_0 λ n
Percolation flow of compressible tape under additive superposition of resin pressure and fibre bed response [59]–[61]			
Flow in the longitudinal direction (bgc)	$P_{applied}$ $-P_{pre}(h)$	$-\frac{3K(h)}{\tilde{\eta}{w_0}^2}h$	$\tilde{\eta}$ K_A σ_A
Empirical model for transition behaviour of toughened prepreg with features of shear and percolation flows [40]			
DefGen model (defgen)	$\sqrt[a+1]{P_{applied}}$	$-\sqrt[a+1]{\frac{1}{\overline{\eta_{micro}}\cdot\eta_{ply}\cdot\overline{\eta_{rate}}}}\cdot h$	a b k

where h_0 – initial thickness, t - time, $P_{applied}$ – pressure applied to the top surface of a composite precursor, η –viscosity of incompressible Newtonian suspension, η_0 – zero-shear-rate viscosity, $\tilde{\eta}$ – the viscosity of resin, f - current fibre volume fraction, $K(f) = K_A\frac{(1-f)^3}{f^2}$ – permeability function [142], $P_{pre}(h) = \sigma_A\frac{\sqrt{f/f_0}-1}{(\sqrt{f_{lim}/f}-1)^4}$ – fibre bed response, where σ_A is the material spring constant, f_0 is the initial fibre volume fraction,

f_{lim} is the maximum achievable fibre volume fraction, w_0 – width of a specimen, n – power-law exponent, *a, b, k* – DefGen material parameters [40]

3.3 Criteria for model performance

The property identification problem is equivalent to the data regression in the space of thickness rate, thickness, and pressure. The model and property identification procedure can be assessed by examining (a) the quality of the fit for a training set, i.e., the experimental data used to identify material constants and (b) the quality of the fit for an independent validation set of experiments.

Low value of the regression error between model's prediction and an experimental data used for training is not enough to safely assume that characterisation was carried out successfully [149]. The discrepancy between the fit in training and validation sets may point at either the deficiency of the training set, the inability of fitting procedure to find global maximum in the space of material parameters, or inadequacy of examined model.

In case a validation step is omitted, it is not guaranteed that a derived model fits data well and is able to adapt to changing processing conditions. To illustrate it more thoroughly, two different cases of a flawed characterisation are provided below.

Both considered case studies are conducted in a form of a virtual exercise. The "experimental data", as referred to further in this section, is simulated based on one of the models from the library with an added noise. Therefore, the simulated material's behaviour is characterised solely by the fully defined target flow model. The experimental data are calculated in response to applied pressure schedule. The main advantage of such approach is that the target material model and its parameters are known, therefore it is possible to draw a conclusion about the validity of the developed material models with an absolute certainty.

A set of candidate models from the library, labelled as models A, B and C, are initialised for material characterisation within training "experimental data" in a training loading set. Upon full material properties identification, these models are trialled against another batch of "experimental data" within a validation set.

As shown in Figure 3.10, there are two different load schedules considered for model's training and validation. The training schedule is relatively simple and consists of one pressure ramp followed up by dwell at a constant pressure level. The validation test program is more complex and consists of several ramp-dwell stages. The parameters of

the validation load schedule (load rate/magnitude, number and duration of dwell stages etc.) were not selected to reproduce any specific set of processing conditions. The goal was to subject the defined candidate material models to a more complex (in comparison with the training stage) loading regime. The characterisation is considered successful if a trained model is able to adapt to a changing load input and to describe the validation batch of "experimental data".

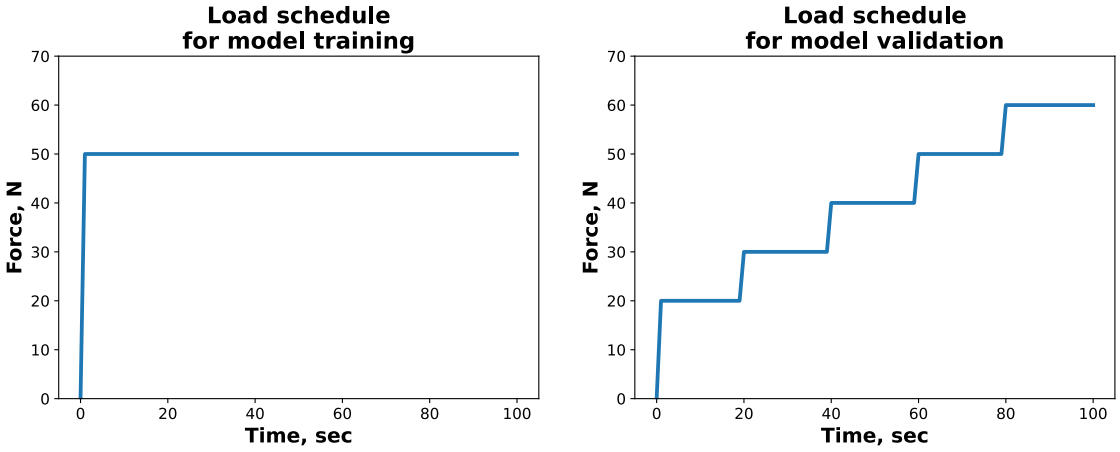

a b

Figure 3.10: a – load schedule for model training; b – load schedule for model validation

In the first identification problem, two different candidate models (model A = DefGen ProToCoL model (defgen 1.1), model B = squeezing non-Newtonian flow (nvfs_pow)), drawn as green and red curves respectively in Figure 3.11.a, are fitted against a training data set. Both models exhibit a very similar agreement with the "experimental data". The simulator of experimental data is based on the DefGen ProToCoL model with added noise, which is the same as one of the candidate models.

As illustrated in Figure 3.11.b, after being exposed to a more complex validation loading program, the model B completely fails to output a feasible prediction of the material's behaviour. However, at the training stage, this same model B (that is different from the model used to simulate an experiment) was able to better fit the simulated experimental response. This perfectly illustrates the importance of a validation check.

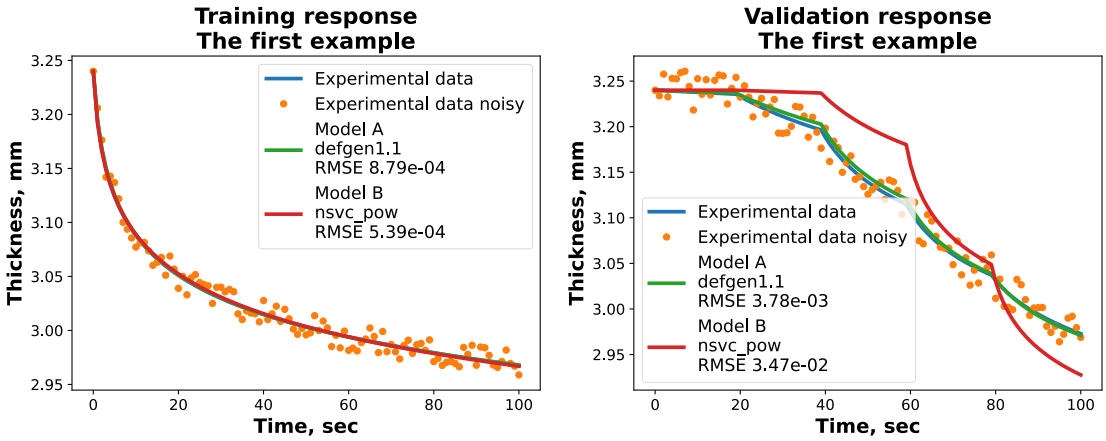

a b

Figure 3.11: Case study 1. Model's overfit, where RMSE is root mean square error.

This is a typical example of model's overfitting and that was reported by numbers of researchers in various fields [150], [151].

Governing equations of high-performance consolidation models may contain complex over-parameterised terms and are able to fit any given data set [143], which may lead to overfitting of the training input sets [152]. In such a case, the underlying patterns and relationships of the experimental data are not captured by the algorithm. Instead, dependencies only specific to the training case are taken into account, which are not relevant for the whole range of possible load cases. Consequently, a model is likely to provide a wrong prediction for a different history of pressure evolution [153].

Another possible challenge is an encounter of a local minimum of an objective function. If a chosen consolidation model is a strong non-convex function, it may exhibit multiple local minima. In this case the result of a characterisation largely depends on a starting vector of material parameters [154]. Several local minima of a target function result in a more than one set of parameter values which fit the training data equally well [155]. Therefore, if a starting vector is next to a local minimum of an objective function, an optimiser will not converge to the correct material parameters [156]. This will cause a disrupted model's prediction for an input different from training data.

An illustration of that scenario is shown in Figure 3.12. Here the exact same model C is used twice, but with different sets of initial values for parameters definition. The experimental data is an instance of the same model C. Yet again, both are shown to find the good match with training set (see Figure 3.12.a.). However, only the model with a

more appropriate set of initial parameters converges to a global optimum. Therefore, it is able to adapt to a changing load program and to adequately predict material's response (see Figure 3.12.b.).

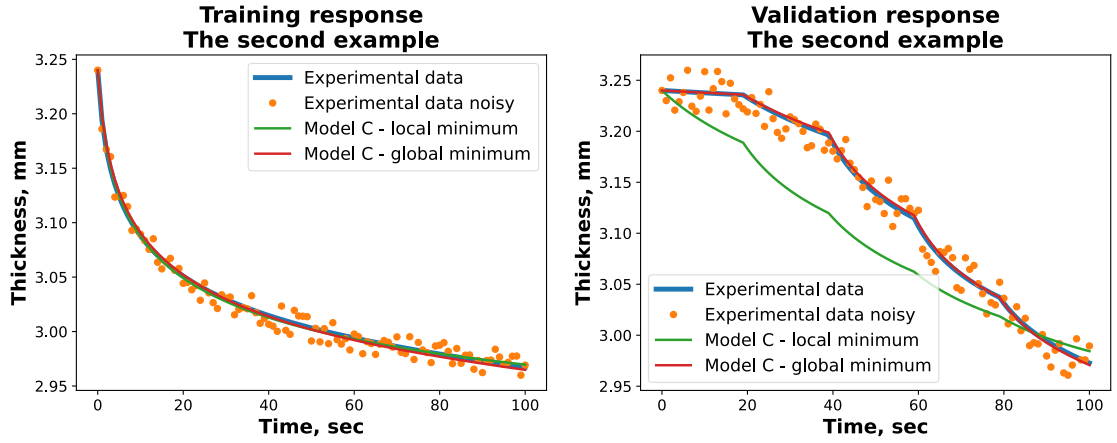

a b

Figure 3.12: Case study 2. Local minimum encounter.

The variation in the defined values of material parameters and the subsequent implications on the candidate models' performance are illustrated in Figure 3.13. To showcase all material parameters within the same scale (for the sake of comparison), the corresponding values are represented in the normalised form (see Figure 3.13.a). As stated before, the candidate model with the local set of parameters reveals its flaw only at the validation stage (see Figure 3.13.b, where cumulative error in prediction is much higher at the validation stage for one of the models).

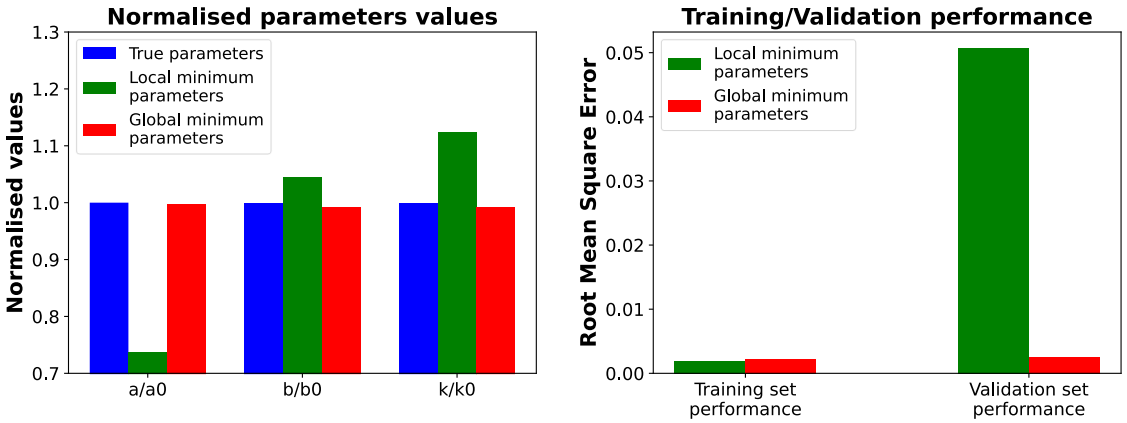

a b

Figure 3.13: a – normalised parameters' values; b – candidate models' performance at training and validation stages.

Completeness of both the training and validation experiments needs to be carefully examined. Tests that lack structural information may lead to misleading outcomes in prediction of the correct flow mechanism. An optimum programme for both may appear to be dependent on the material behaviour. Therefore, there is a clear need in a more sophisticated testing algorithm or a more thorough testing programme (considered in the Chapter 4 of this research).

3.4 Conclusions

The concept of the consolidation library was introduced within this chapter. This library contains unified mathematical representations (in a form of ODEs) of the main flow mechanisms occurring in toughened prepregs during compaction. Each material model was accommodated for one dimensional problem of composite precursor's compaction between parallel compression plates. The library can be complemented with additional models depending on suspected mechanisms that may occur.

Two case studies with flawed model identification process were presented to demonstrate possible sources of errors during material characterisation – non-optimal set of retrieved material parameters and insufficient compaction data from the experiment. The results clearly showcased the need for the comprehensive material model identification mechanism. It should include the robust material parameters extraction routine and the identification of the data-rich testing programme.

In the following, the data-rich testing programme means that the provided compaction response is sufficient to capture characteristic features of a material's behaviour. Such programme may include several tests with different load levels and load application rates. It is beneficial for a rational testing programme to minimise the volume of tests without the loss of gain in obtaining information. In this regard, it is interesting to deduce the optimum data-rich testing programmes for the training sets. The next Chapter addresses this problem in application to a material that was extensively characterised in past and for which the models in the consolidation library were found to be efficient.

4 EXPERIMENTAL DATA-RICH TEST PROGRAMME

The fourth chapter of the research addresses the testing regimes in application to well-studied toughened prepreg IMA/M21 [14], [39], [157] known to exhibit complex transitional behaviour. The main purpose of this revision is to establish an optimum loading schedule for material characterisation. In the following, “optimum” is defined in the sense of minimum number of tests containing enough information to define the material properties accurately. This testing explores what are the most data-rich testing programmes for some of the characteristic flow mechanisms.

4.1 Problem statement.

In this section, the importance of a comprehensive test programme for robust material characterisation is demonstrated. A series of experiments with different loading programmes were carried out to explore the compaction behaviour of fibre-reinforced thermosetting prepregs containing thermoplastic tougheners.

Experimental programmes were designed in a way to incorporate a wide variety of pressure levels, pressure rates in various loading modes – slow monotonic and ramp-dwell regimes. Some programmes were conventional ramp-dwell schedules as used in the literature [39]. Another batch of programmes were inspired by the adaptive testing approach outcomes, which will be discussed in the next chapter of this research. In this case load slowly reaches an intermediate level, dwells, and then keeps raising again. The set of all considered load schedules is presented in Figure 4.1.

An ideal characterisation programme should cover maximum range in the space of load/load rate/strain, so the material is exposed to various loading regimes at different stages of deformation (elastic, viscoelastic, viscous). The range of load values is sensible to the achieved compaction level of the test specimen. The dwell regime allows to recover the creep behaviour of the material but the load level at which sample dwells can be selected differently.

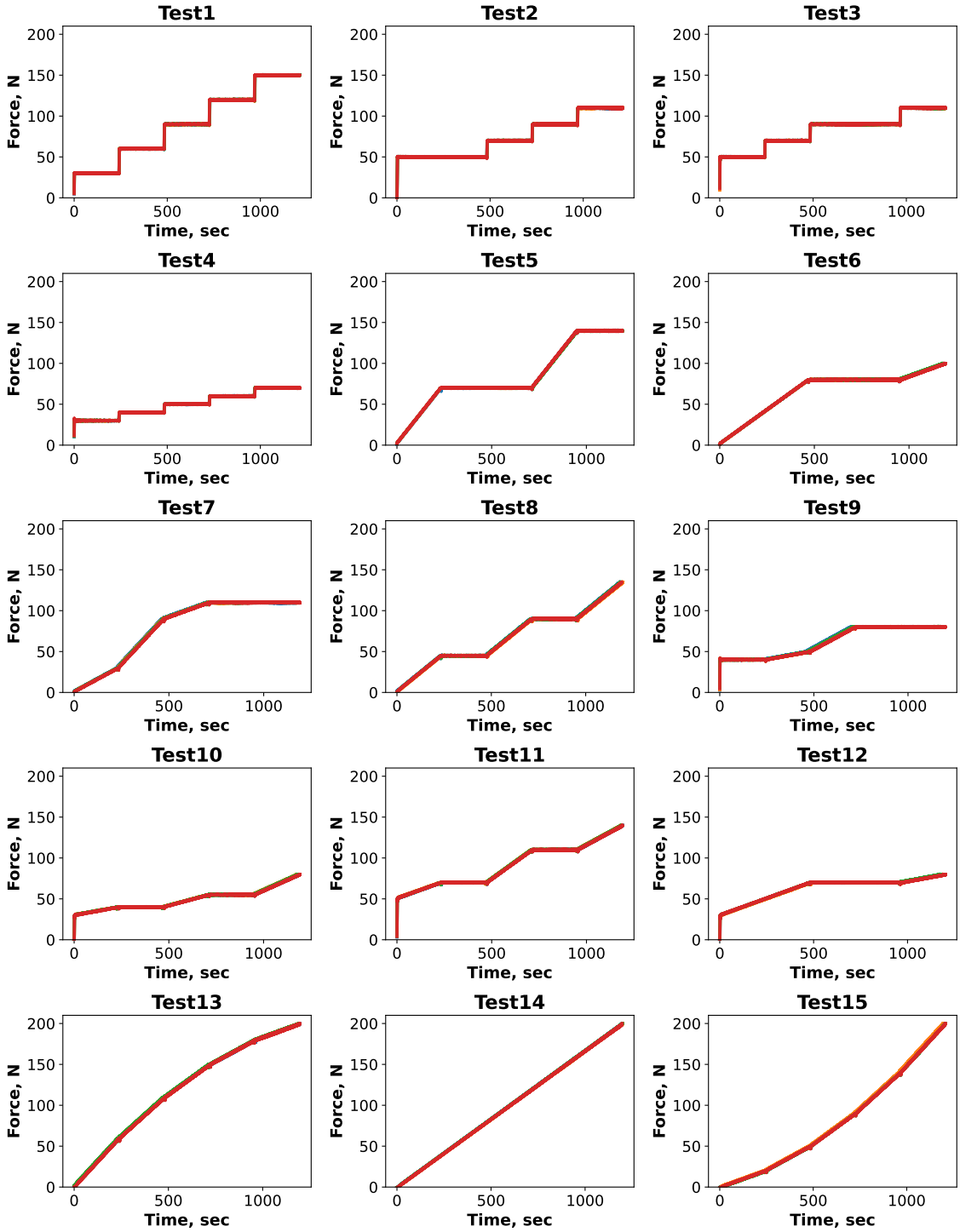

Figure 4.1: Load programmes for the conducted tests.

The test programmes considered were not aimed to reproduce any particular processing conditions specific to existent manufacturing methods. The end goal was to showcase the advantage of certain loading schedules over the other ones as well as the necessity of multiple experiments to get a data-rich compaction response of the material.

Several different loading regimes were considered within this study: load ramp-dwell (Tests 1 - 4), monotonic load raise – dwell (Tests 5 - 8), monotonic load raise only

(Tests 13 - 15), and the combined mode (Tests 9 - 12), which included all of the abovementioned regimes.

Every loading schedule was comprised of five load steps of 240 s each. For a ramp-dwell regime the fastest load application rate was 0.1 MPa/s and was followed by dwell intervals of different duration. In case of a monotonic regime load rate varied between 1.8e-4 and 1.3e-3 MPa/s. An incremental compression force within one load step was specified in a range from 10 N to 70 N. It is not possible to replicate every loading scenario specific to different manufacturing methods within the considered set of loading programmes (Figure 4.1). The range of load values/rates, load steps numbers/duration was inspired by previously conducted work for DefGen model characterisation [14], [39], [40], [129]. Each specimen was tested at a constant temperature of 60℃ throughout the experiment. This temperature was chosen as it is a characteristic temperature at which the transition between flow mechanisms occurs particularly explicitly [38].

4.2 Test specimen. Material and geometry specification.

The prepreg material used in this research was IMA/M21 with a nominal cured ply thickness of 0.184 mm and 59.2% fibre volume fraction [158].

It was necessary to ensure steady contact between neighbouring plies during compression. Material tends to spread transversely as the plies are squeezed from underneath the area under compression. For that reason, following test specimens were laid up in a cruciform configuration to allow plies to remain in contact as shown in Figure 4.2. The baseline area under compression is 15 mm x 15 mm.

The test specimens were manufactured in a clean room following standard lay-up guidelines. All specimens were laid-up in a 16 plies cross-ply (CP) configuration $[90/0]_8$ with a total thickness of ~3.3 mm. During lay-up at room temperature ten-minute debulking routine was carried out for every four plies. Upon manufacturing, specimens' dimensions were measured by digital Vernier callipers.

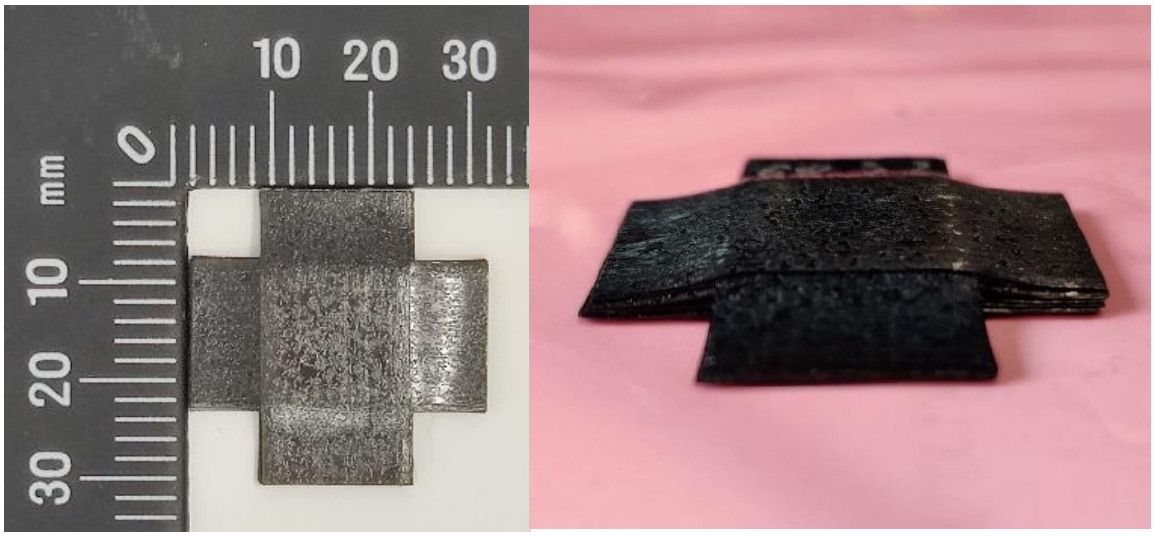

Figure 4.2: Test specimen of a crucifix shape. The area under compression is 15 x 15 mm.

4.3 Testing apparatus.

The experimental testing was carried out using Instron 5969 [159], [160]. It is an electromechanical universal testing machine with a 50 kN load cell.

The machine was operated in the load control mode since all test programmes were defined as the change of the compression force over time. It means that the test machine defines the position of the crosshead at every moment of time based on equilibrium between the defined value of the force and the value measured by the load cell.

The value of the compression load throughout the experiment is relatively low in comparison with the load cell's capacity (maximum value of the applied force does not exceed 200 N). The main concern was if the resolution of the load cell is sufficient to execute the load schedule, as the test programme operates within 0.5% of the load cell's capacity.

Due to the well-tuned PID (proportional integral derivative) controller, the resultant load curves do not deviate from the user-defined schedule and do not contain any considerable noise component (see Figure 4.1). It is important to say, that a different type of test sample or material might require additional tuning of the feedback controller due to changes in overall stiffness of the studied system.

Prior to an experiment, a test sample covered in a release film was placed in between custom-built temperature-controlled compression platens as shown in Figure 4.3. A control thermocouple and a thick film conduction heater were attached to each platen to

ensure that specified temperature conditions are met. The testing apparatus allows to transfer controlled load to the specimen within an isothermal programme and to measure corresponding compaction response of the material.

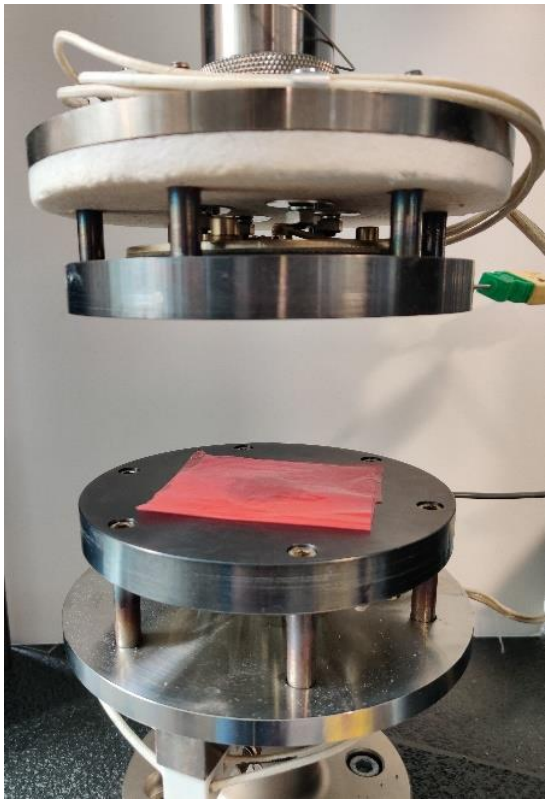

Figure 4.3: Temperature-controlled compression platens, test specimen in a release film.

4.4 Pressure application uniformity. Contact surface mapping.

In order to obtain consistent and reliable experimental data, it is crucial to ensure uniform stress distribution on a composite's contact area throughout the whole duration of a test. If top and bottom platens' surfaces are not parallel to each other, the pressure will be applied only to a part of a specimen at the start of the test as shown in Figure 4.4.

The flow models from the consolidation library require operating pressure values as an input. The load schedule for the compression machine is defined through the compression force. Given that the effective loaded area is known, the compression load (N) is redefined through the external pressure (Pa). Thus, inconsistent contact area throughout the experiment leads to the discrepancy between the computed and actually applied pressure. As a result, a candidate model from the library is trained on the mismatched input data and its prediction capability is impaired. Additionally, non-

uniform pressure application would lead to the off-set compaction of the composite, which is not covered by any of the considered consolidation models.

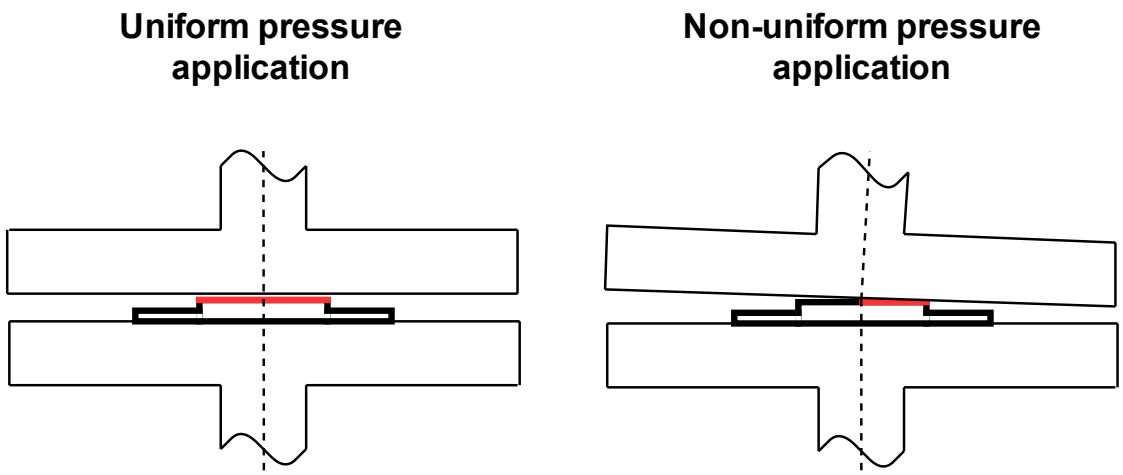

Figure 4.4: The influence of the compression platens misalignment. Red region represents the contact area between the specimen and the platen.

One way to accomplish the top and bottom platens' surfaces alignment is to use spherically seated compression platen [161]. It can accommodate platen's angular displacement with reference to a universal testing machine's loading axis. The current testing rig shown in Figure 4.3 was implemented without spherical seat, thus, it does not provide self-aligning action. It is mounted to the crosshead of the machine through the cylinder push rod and fixed by quick release clevis pins. It is not possible to level the platens against each other within such setup.

Therefore, it is necessary to ensure uniform pressure application on the specimen's surface. To do that a separate compression test with the pressure mat in between of the specimen and top platen is conducted, as shown in Figure 4.5.a. The matrix-based pressure sensor is composed of two thin polyester sheets with electrically conductive stripes. Upon force application, the electrical resistance of the sensing elements changes proportionately to the applied force. The sensor is connected to the data capture device (Tekscan T-Scan Evolution Handle [162], see Figure 4.5.b), which in turn is connected to the computer through USB port. Such setup allows to view the pressure map and to track any inconsistencies arising during the test.

a b

Figure 4.5: Pressure mapping setup, a – pressure sensor on top of the specimen, b – Tekscan data capture device

In order to review the evolution of the contact surface, the compression force was gradually increased from 30 N to 6000 N, although the maximum load within all test programmes (see Figure 4.1) does not exceed 200 N. Figure 4.6 shows the gradient pressure map for different values of the load. Green contour represents the original shape of the test specimen's contact area. Each figure is represented within its own scale, the pink colour depicts the areas with the highest pressure applied. The effect of the compression platens misalignment is more evident for larger samples, especially if the sample is placed closer to the edge of the platen. For illustration purpose, the example of a non-uniform pressure application to a larger size specimen (30x30 mm as opposed to 15x15 mm used in this study) is shown in Figure 4.6.a. It can be clearly seen that the pressure is applied to the lower half (as represented in the figure) of the specimen first creating significant inconsistency in the loading scheme. A smaller size specimen placed correctly in the centre of the compression platen does not produce such discrepancies. The pressure map for a 15x15 mm specimen used in this research is shown in Figure 4.6.b. Given the absence of irregularities in the contact area's pressure

map, the pressure is applied to the surface uniformly through all stages of the compression force raise. Therefore, the platens provide sufficient alignment for further testing.

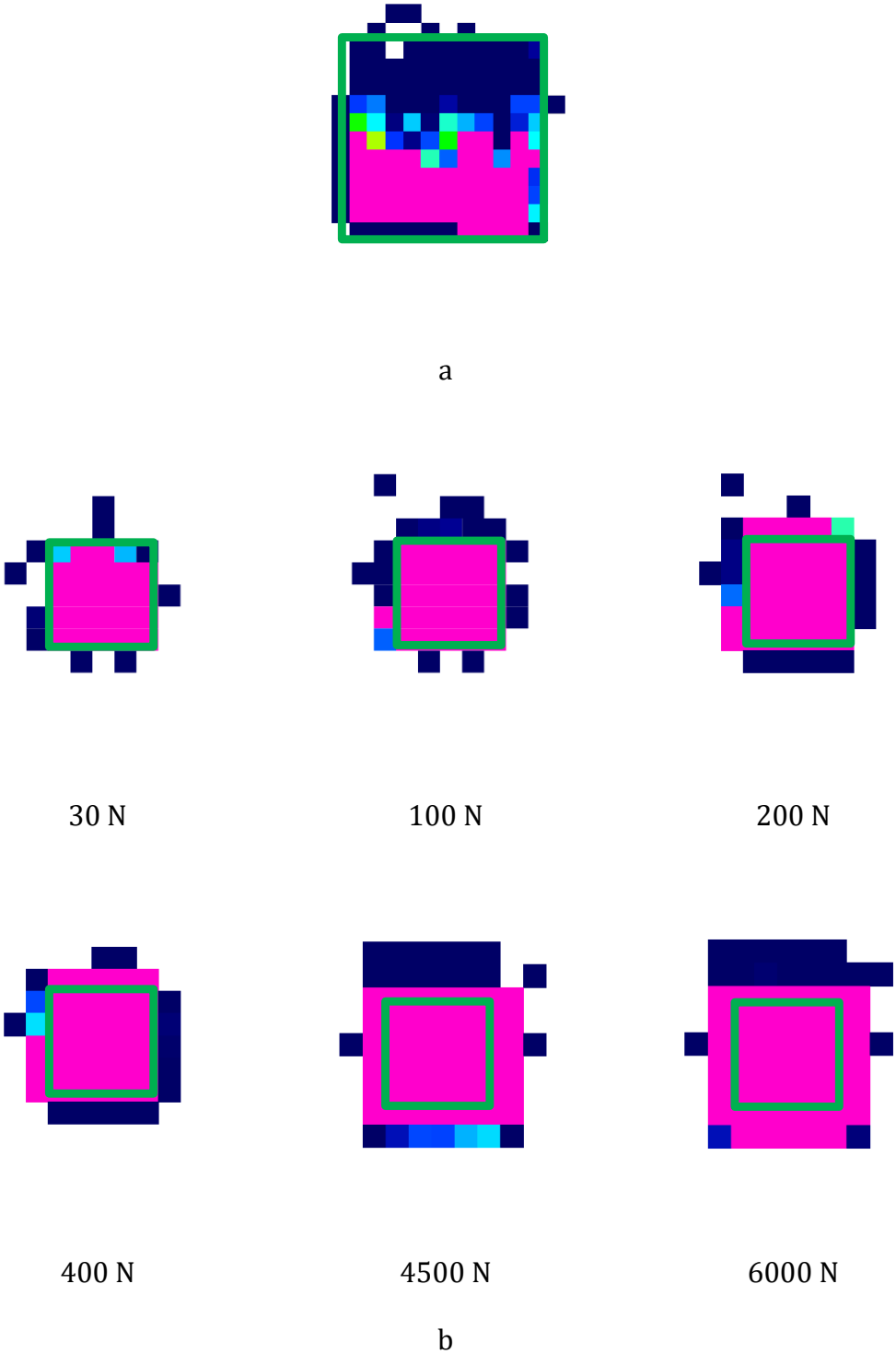

Figure 4.6: Green contour represents the original shape of the test specimen's contact area. a – The example of non-uniform pressure application for 30x30 mm

specimen; b - Pressure distribution on the contact surface for a range of compression force values.

4.5 The compaction response of the material.

Given the effective loaded area of the tested samples was 15 mm x 15 mm and the maximum compression load was 200 N (Test 13 – 14), maximum applied nominal pressure did not exceed 0.9 MPa.

An insignificantly small compression force of 0.1 N was applied to a test specimen prior to the main loading programme in order to establish sufficient contact between the specimen's top surface and the compression platen. Additional dummy tests within the same loading programme but without a specimen were carried out in order to take into account compression rig's compliance. Then, the top platen's displacement as function of time was subtracted from the resulting displacement curve for each sample.

The final thickness of the specimen was measured independently immediately after the experiment. In line with the previous work [13], [38], [39], it is assumed that at the moment the experiment is over the spring-back effect is not developed yet. To obtain a resulting thickness evolution curve of a specimen, the platen displacement curves were shifted to comply with the resulting thickness value. Such approach eliminates the uncertainty in the initial thickness of a sample. Each test programme was conducted for four samples to ensure repeatability and data consistency. The obtained compaction curves are shown in Figure 4.7. Each test batch showcases a significant reduction in thickness at the first stage of compaction followed by the approach of the compaction limit. Compaction curves demonstrate high consistency in terms of the intermediate and final thickness values with little scatter between different batches within one loading programme.

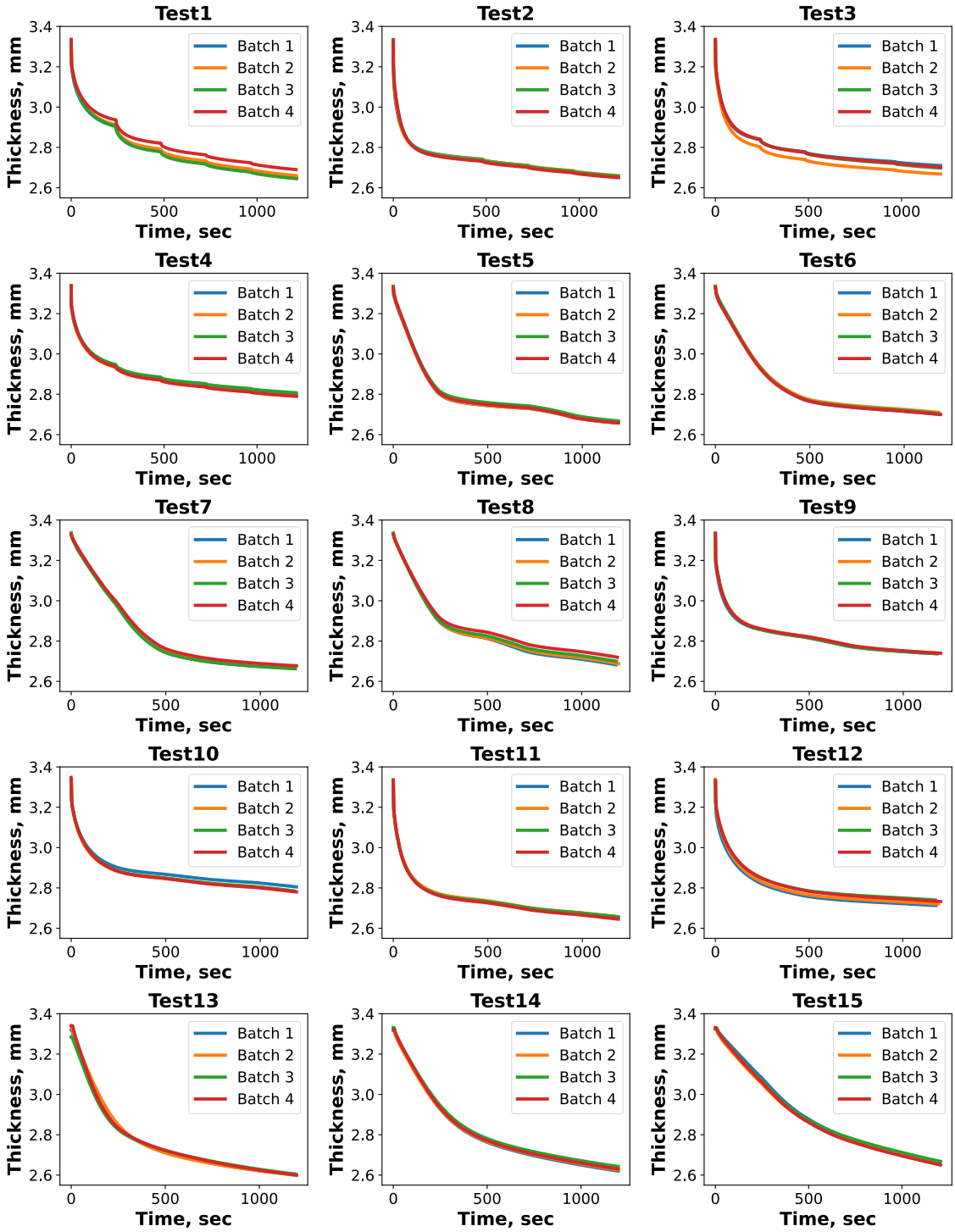

Figure 4.7: Material's compaction response.

4.6 Analysis of the results. Training and validation of candidate models.

To identify the data-rich testing programme from which the maximum information can be collected whilst performing the smallest amount of experiments, compaction results

from different loading programmes were arbitrarily split into complementary subsets called training and validation sets.

The following convention is used further to describe the characterisation process:

- Candidate model is a flow model selected from the consolidation library. Each candidate model is trained on an input dataset comprised of the experimental compaction data. The goal of training is to find the best combination of material parameters that allows a candidate model to fit experimental data as accurately as possible. Then, a fully defined model is verified within a different validation dataset to estimate its overall performance. The metric for performance estimation is a cumulative error between the model's prediction and the actual data (root mean square error, hereinafter referred to as RMSE). The process of training and validation of a candidate model is demonstrated previously in the section 3.3. Upon challenging every model from the library, all candidate models are ranked in accordance with its' performance.

- Training set is a group of tests used for the training of candidate models. These tests are chosen from a general pool of tests as shown in Figure 4.8 (experimental data framed in red colour). Since one of the goals is to reduce an involvement of material and experimental efforts to a minimum, the size of the training set was capped to a maximum of three tests.

- Training combination is an actual dataset used as an input for the training of a candidate model. To demonstrate the effect of a data-rich test programme, all possible combinations of loading schedules within a training set were explored at the stage of model definition as shown in Figure 4.8 (framed in green colour). In the presented example (Figure 4.8) training combinations are built within (1, 4, 7) training set (number in parentheses represents test number).
  The candidate model can be trained separately on the data from a single test (1,), (4,) or (7,). Another option is to expand the input datasets by joining data from two tests (1, 4,), (1, 7) or (4, 7). The last scenario is to use every test in the training set (1, 4, 7) as a single input dataset. Given the size of a training set, there are seven possible training combinations within a training set. A separate analysis for every training combination was carried out, meaning that a characterisation routine for each model from the consolidation library was performed to fit corresponding compaction curves.

- Validation set is used to verify candidate models' ability to adapt to changing input data. The models were put to the test against each batch of data in the validation set and the cumulative error in prediction served as a performance measure. The validation set is comprised of tests which were not included in the training set. Given the total number of tests conducted and the maximum training set size, the size of the validation set was fixed at the size of twelve programmes. As shown in Figure 4.8, validation set remains constant for every training combination within the same training set, providing consistency in performance estimation.
- The process of forming training sets/combinations and validation sets out of the experimental data is illustrated in Figure 4.8.

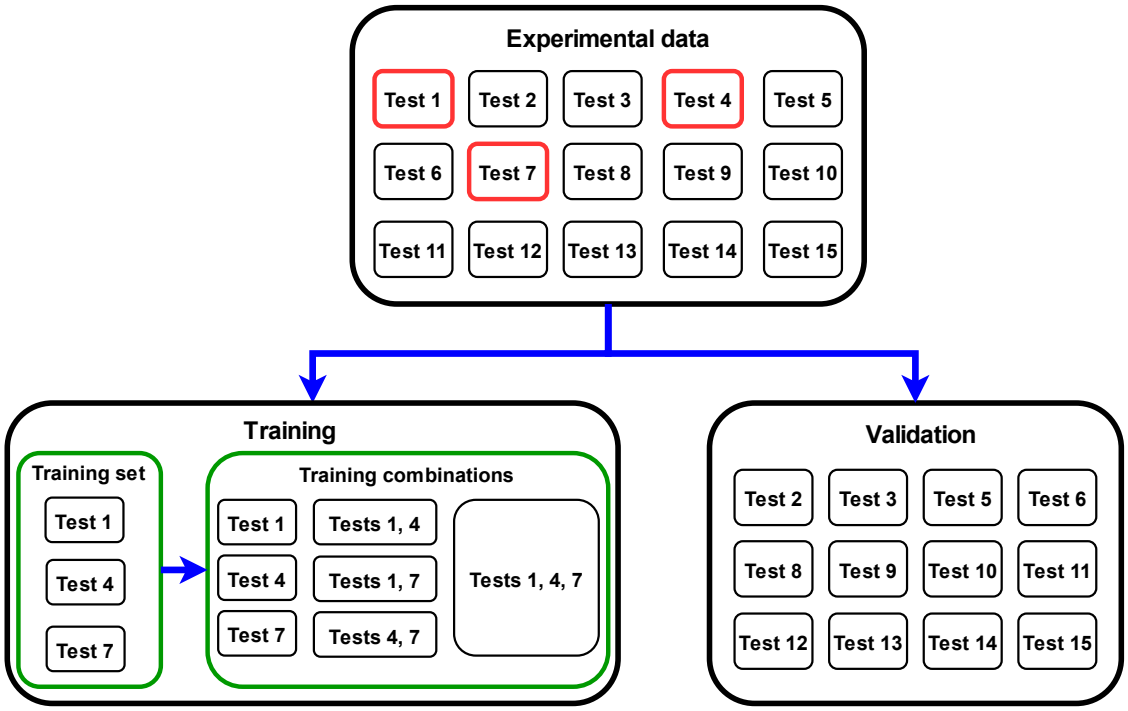

Figure 4.8: Building training and validation sets from the experimental data.

In order to explore more training scenarios within the limited number of experiments, different training / validation split options are considered. The visual representation of data organisation for different split options is shown in Figure 4.9. Characterisation routines within each split are independent of each other and are performed only to explore more training input options.

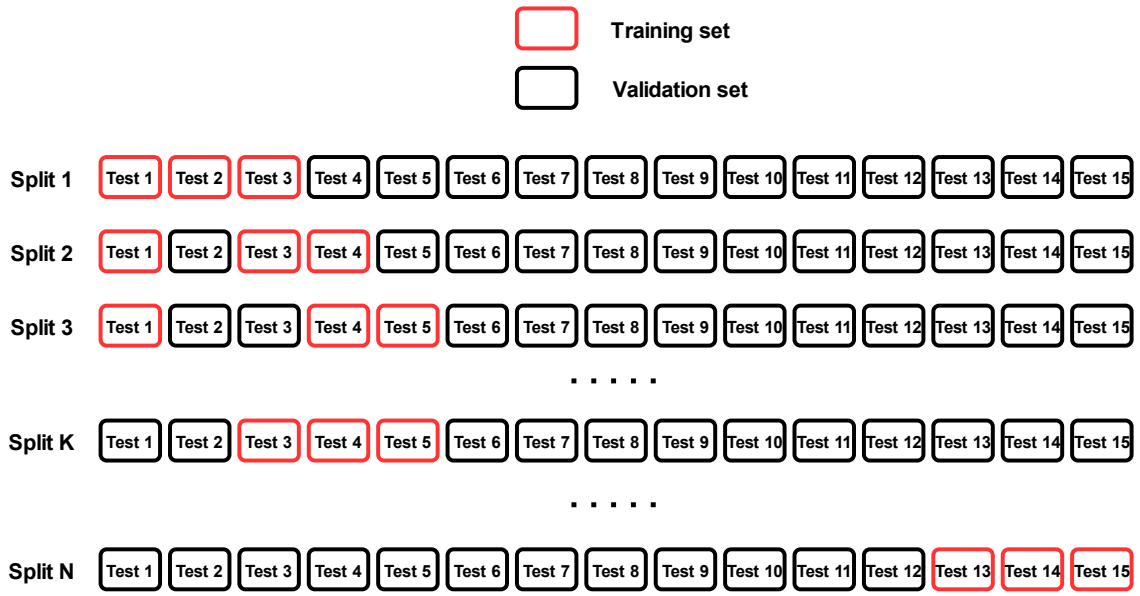

Figure 4.9: Splitting experimental data into training / validation sets.

An overview of training and verification sets' structure is presented in Table 4.1.

Table 4.1: Training and verification sets. Training combinations. Numbers in parentheses represent test numbers.

Training set	Training combination	Verification set
(1, 2, 3)	(1,)	(4, 5, 6, 7, 8, 9, 10, 11, 12, 13, 14, 15)
(1, 2, 3)	(2,)	(4, 5, 6, 7, 8, 9, 10, 11, 12, 13, 14, 15)
(1, 2, 3)	(3,)	(4, 5, 6, 7, 8, 9, 10, 11, 12, 13, 14, 15)
(1, 2, 3)	(1, 2)	(4, 5, 6, 7, 8, 9, 10, 11, 12, 13, 14, 15)
(1, 2, 3)	(1, 3)	(4, 5, 6, 7, 8, 9, 10, 11, 12, 13, 14, 15)
(1, 2, 3)	(2, 3)	(4, 5, 6, 7, 8, 9, 10, 11, 12, 13, 14, 15)
(1, 2, 3)	(1, 2, 3)	(4, 5, 6, 7, 8, 9, 10, 11, 12, 13, 14, 15)

(2, 3, 4)	(2,)	(1, 5, 6, 7, 8, 9, 10, 11, 12, 13, 14, 15)
(2, 3, 4)	(3,)	(1, 5, 6, 7, 8, 9, 10, 11, 12, 13, 14, 15)
...		
(13, 14, 15)	(14, 15)	(1, 2, 3, 4, 5, 6, 7, 8, 9, 10, 11, 12)
(13, 14, 15)	(13, 14, 15)	(1, 2, 3, 4, 5, 6, 7, 8, 9, 10, 11, 12)

4.7 Characterisation routine

Processing compaction data requires the analysis of flow models from the consolidation library. As stated previously in Section 3.3, there are two main challenges arising at the characterisation stage: identifying a data-rich test programme and avoidance of the local minima at the stage of material parameter identification. The first problem is addressed at the stage of the test programme design. In order to deal with the second problem, a robust parameter extraction tool is required. It must retrieve true values of material parameters for a chosen candidate model with high confidence. The proposed tool consists of two main parts:

- The parameter extraction routine. Material parameters identification is done by conducting a nonlinear regression analysis of a chosen candidate model.
- Joining datasets. The proposed tool must be able to process joined batches of data from different tests for a chosen training combination to take advantage of a more diverse dataset.

The described routines are organised as a sole standalone parameter extraction module for processing compaction data. The complete description of this module and the detailed application example are given below.

The proposed module can be used either separately, as demonstrated further in this Chapter, or can be embedded into a larger-scale project as one of its functional parts. Such development is addressed further in Chapter 5.

The parameter extraction module was implemented in Python programming language environment [148] using nonlinear optimisation package *lmfit* [163]. The source code, created by the author of this dissertation, is available at https://accis.github.io/DefGenParFit (access to the repository to be granted upon request). It is widely used within the local research community and proven its efficiency in the variety of tasks.

4.7.1 Parameter Extraction Routine

A comprehensive parameters extraction procedure is required to retrieve true values (i.e., global minimum) of the identified material parameters for a chosen model.

The essence of the nonlinear regression process is to minimise a residual function by varying its parameters. A residual function is the cumulative difference between experimental compaction data and the thickness prediction of the candidate model.

One of the main challenges for a regression algorithm is to avoid stacking in a local minimum (as demonstrated in Section 3.3). Hence, it is of the utmost importance to pick reasonable initial values for material constants in optimisation and do it without sacrificing computational speed. For this reason, a two-stage optimisation procedure is utilised within the proposed framework.

The flowchart of this procedure is presented in Figure 4.10. At the initial stage, the objective function is minimised over a given range of parameter values by an exhaustive search method, hereinafter referred to as a brute force method. The primary goal is to establish a feasible set of initial values for material constants which are then used for further minimisation. To achieve that, an objective function is evaluated at each point of a multidimensional grid of possible parameter values.

The parameter extraction tool provides an option for the researcher to omit the first (brute force) stage, in case when initial values for material parameters are defined manually.

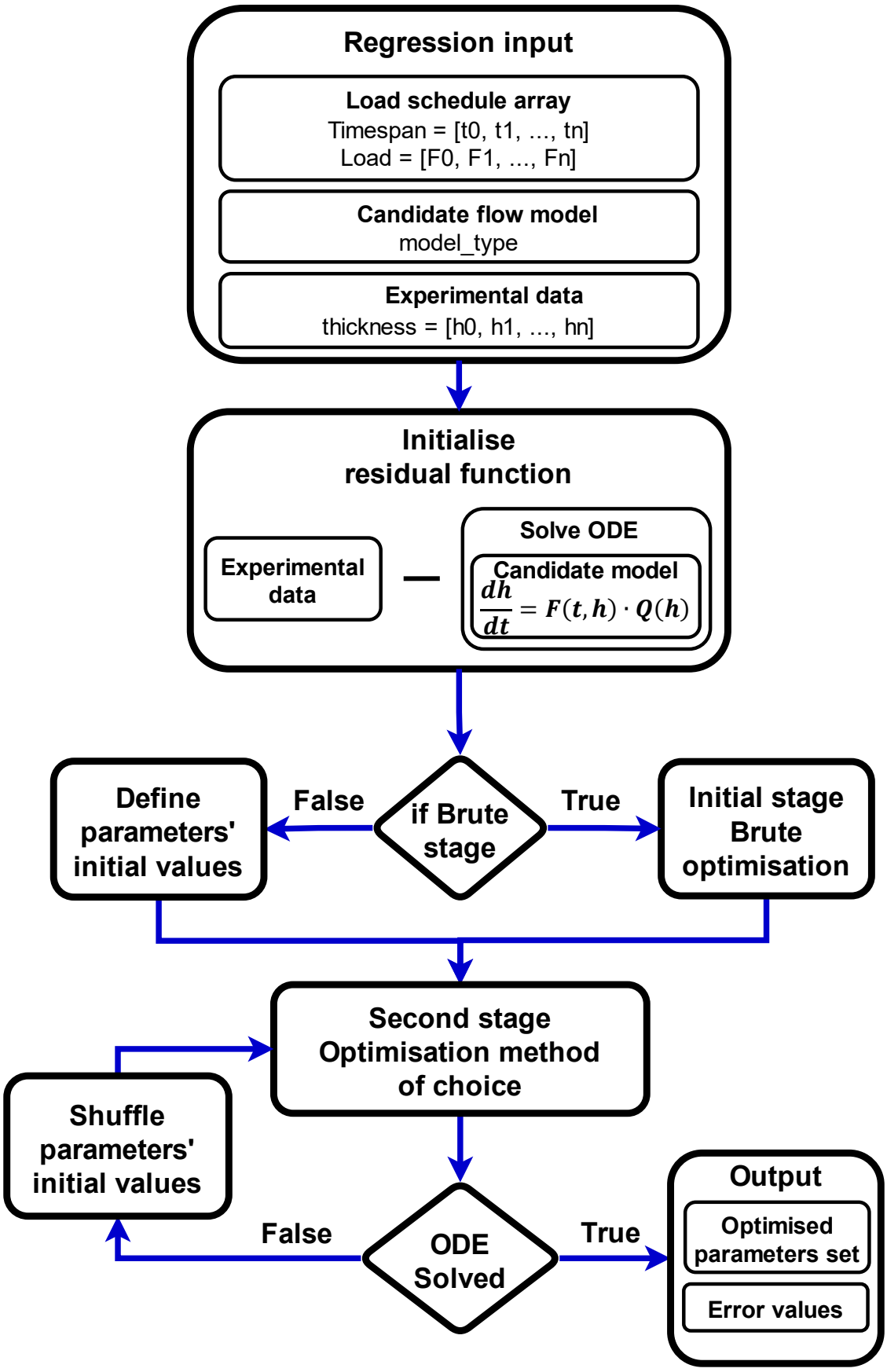

Figure 4.10: Optimisation routine flow chart.

In general, brute force method is inefficient and takes a long time to execute. The total number of the objective function's evaluations equals n^d, where *n* is the number of parameters and *d* is the density of the grid. Therefore, finding a global minimum for complex models with three or more material parameters would require an unreasonable amount of computational time and would significantly slow down the characterisation process. Hence, an objective function is minimised over a grid with a coarse spacing.

The best result is then used as a starting point at the second stage of the parameter extraction where it is possible to select a nonlinear optimisation method of choice. The two main approaches used are the Nelder-Mead [164] and the nonlinear least squares [165] methods. Upon completion of the routine, an optimal parameter set for each candidate model is retrieved.

There is a number of global optimisation approaches, which, by definition, are independent of parameters' initial values and always converge to a global minimum e.g. Basin-hopping method [166], differential evolution [167]. However, due to the high computational cost they are not applicable in this project. As stated previously, the parameter extraction tool can be used as a functional part of a larger scale framework, where execution time plays an important role. For this reason, the proposed tool is designed to be computationally efficient. The issue of the algorithm's promptitude and possible time constraints is covered in the Chapter 5.

4.7.2 Differential equation solver

As stated in the previous section, parameter extraction is performed through the minimisation of a residual function (which represented as a difference between experimental data and the thickness prediction of a corresponding candidate model). Since the consolidation models in the library are represented in a form of differential equations, the framework has to solve a chosen differential equation to retrieve thickness over time data. Solving an equation requires an input of a timespan array $[t_0 \quad t_1 \quad \cdots \quad t_n]$ along with the corresponding array of force values $[F_0 \quad F_1 \quad \cdots \quad F_n]$. Additionally, a set of material parameters for a selected consolidation model must be provided. After successful integration on a defined time interval, a resulting thickness array $[h_0 \quad h_1 \quad \cdots \quad h_n]$ is output.

Most of the manufacturing methods for composites deploy pressure instead of displacement as means of the consolidation (except for certain methods e.g. the rigid tool RTM, forming etc.). Hence, the model's governing equation involves a function

$F(t, h)$, which represents an applied compression load. It is a time-dependent function. Such a term in ODE is called a forcing term [168]. It models external effects acting on the system, which can be changed or withdrawn 'instantaneously' at any moment of time.

This term introduces additional complexity for the solver. Due to the time-dependent component, it is, now, not possible to integrate the whole timespan of the test using standard solver tools. The standard solver cannot handle sudden "jumps" or "discontinuities" in function's behaviour caused by the rapid (or instant) change of the external forcing function. Such problem was encountered by a number of researchers [169], [170].

Hence, the framework solves the differential equation in a step-by-step mode by sequentially integrating data on the $[t_{i-1} \;\; t_i]$ intervals. A solution on an interval $[t_{i-1} \;\; t_i]$ satisfies the prescribed boundary condition $h(t_{i-1}) = h_{i-1}$. The thickness value h_{i-1} is recovered from a previous interval $[t_{i-2} \;\; t_{i-1}]$ integration and updated at each step. The value of a forcing function on an interval $[t_{i-1} \;\; t_i]$ is treated as constant. Thus, it is possible to take into the account time-dependant force function by updating its value at each time interval.

4.7.3 Joining data sets.

If a training combination contains more than one test, the input dataset must be expanded by considering joined compaction data from several experiments. It allows more testing schedules with different load levels and load rates to be explored within a single parameter extraction iteration. In this case the candidate model takes into account experimental programmes with various loading history and is trained directly on the corresponding material's feedback.

Generally, time, load and thickness data from several experiments is structured in a following way:

$$\text{Timespan} = \begin{bmatrix} \begin{bmatrix} t_0 \\ t_1 \\ \vdots \\ t_n \end{bmatrix} & \begin{bmatrix} t_0 \\ t_1 \\ \vdots \\ t_m \end{bmatrix} & \begin{bmatrix} t_0 \\ t_1 \\ \vdots \\ t_k \end{bmatrix} \end{bmatrix}$$

$$\text{Load} = \begin{bmatrix} \begin{bmatrix} F_0 \\ F_1 \\ \vdots \\ F_n \end{bmatrix} & \begin{bmatrix} F_0 \\ F_1 \\ \vdots \\ F_m \end{bmatrix} & \begin{bmatrix} F_0 \\ F_1 \\ \vdots \\ F_k \end{bmatrix} \end{bmatrix} \qquad 4.1$$

$$\text{Thickness} = \left[\begin{bmatrix} h_0 \\ h_1 \\ \vdots \\ h_n \end{bmatrix} \quad \begin{bmatrix} h_0 \\ h_1 \\ \vdots \\ h_m \end{bmatrix} \quad \begin{bmatrix} h_0 \\ h_1 \\ \vdots \\ h_k \end{bmatrix}\right].$$

It should be noted that abovementioned data structures for the timespan, the load and the thickness evolution are not standard two-dimensional arrays. Each test may and most probably will contain different number of datapoints. For this reason, separate one-dimensional arrays cannot be united in a form of a matrix due to different length, which is reflected by different endpoint notation *n, m, k*. Hence, different one-dimensional arrays are united in a form of a *list*. It is a standard data type in Python which allows different size of its elements.

To take advantage of an increased dataset, it is necessary to flatten list data structure and to present it in a one-dimensional form before submitting it to the parameter extraction module as follows:

$$\begin{aligned} \text{Timespan} &= [t_0 \quad t_1 \quad \cdots \quad t_n \quad t_0 \quad t_1 \quad \cdots \quad t_m \quad t_0 \quad t_1 \quad \cdots \quad t_k]^T \\ \text{Load} &= [F_0 \quad F_1 \quad \cdots \quad F_n \quad F_0 \quad F_1 \quad \cdots \quad F_m \quad F_0 \quad F_1 \quad \cdots \quad F_k]^T \\ \text{Thickness} &= [h_0 \quad h_1 \quad \cdots \quad h_n \quad h_0 \quad h_1 \quad \cdots \quad h_m \quad h_0 \quad h_1 \quad \cdots \quad h_k]^T. \end{aligned} \tag{4.2}$$

Upon data structure reshape, the regression is conducted for 2d flattened curve. The example for the (1, 4, 7) training combination (presented in Figure 4.11) demonstrates the transition from fitting separate compaction curves in 3D space to 2d regression. Every time solver comes across t_0 time point in the timespan array, the initial conditions for thickness are reset back to h_0 value. By implementing this feature, it is now possible to feed a joint dataset composed of several tests to the solver module for the further parameter extraction.

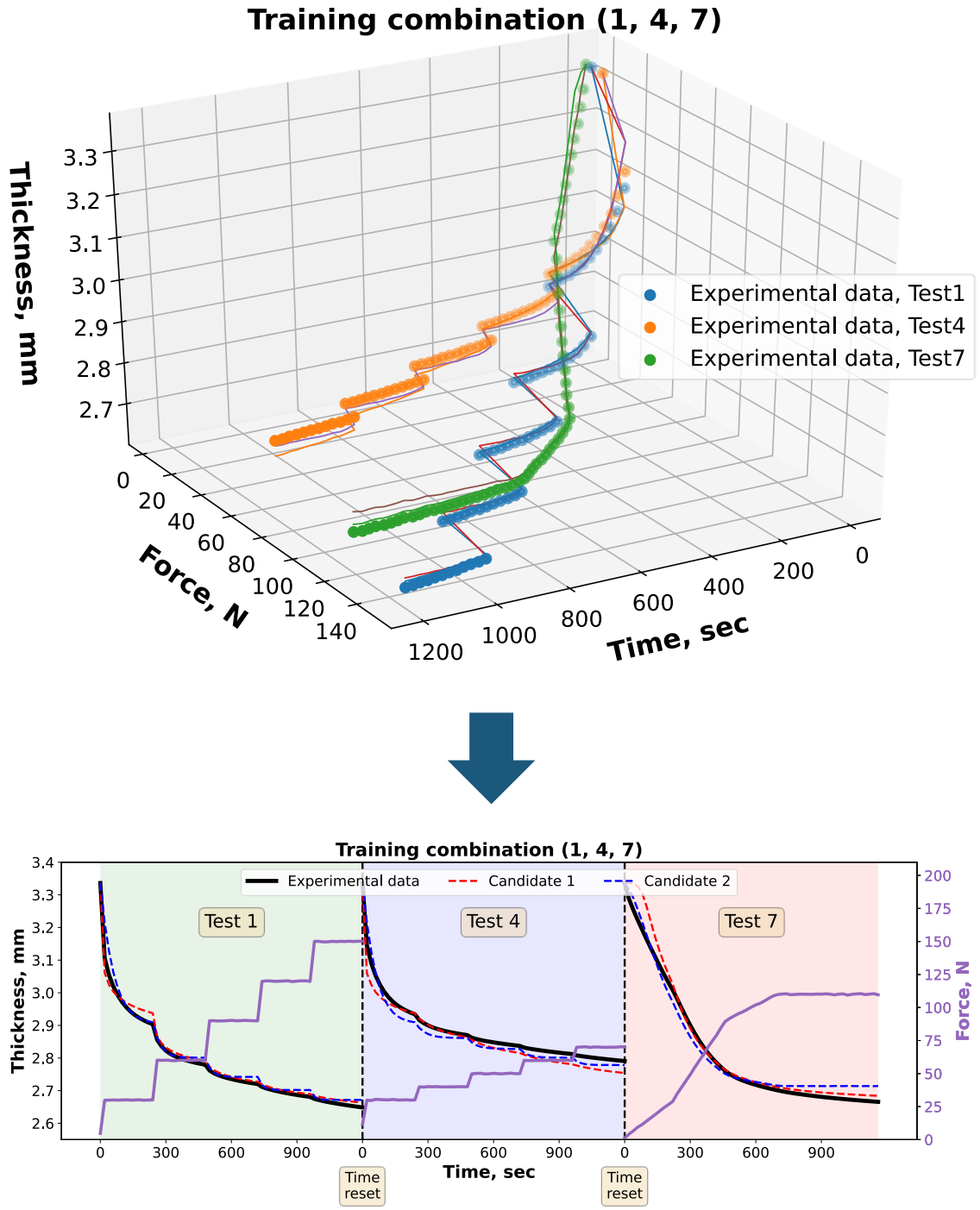

Figure 4.11: The transition from fitting separate curves in 3D space to 2d flattened curve regression.

4.7.4 Solver's numerical instability error handling

A possible pitfall of the ODE's solution process is an occurrence of the numerical instability. It is possible to define such set of material parameters which leads to a rapid variation in the solution's output. In order to get the reliable output and to keep the solution curve smooth, the solver reduces integration step below the smallest value

allowed [171], [172]. Differential equations for which numerical methods fail to converge to a solution are called stiff ODEs [173].

In case when a governing equation for a chosen candidate model becomes stiff due to unacceptable initial parameters' values, the standard ODE solver results in error (in Python environment the solution evaluates to *NaN* value, meaning that the integration step size is below the allowed value). To tackle this problem, the additional error checker is implemented within the solver module. Its sole purpose is to trace the solver's output for errors (*NaN* values). If the checker is triggered, the solver returns to the initial stage of the solution, but the material parameters' initial values are shuffled randomly within the defined limits.

This functionality is especially relevant at the stage of model's parameter extraction when the initial values of material parameters are unknown and may be defined manually.

4.8 Results and discussion

Because of the sheer volume of obtained data, only two characteristic examples are shown in this section. The parameters extraction procedure results for the training set comprised of tests (1, 4, 7) are presented below.

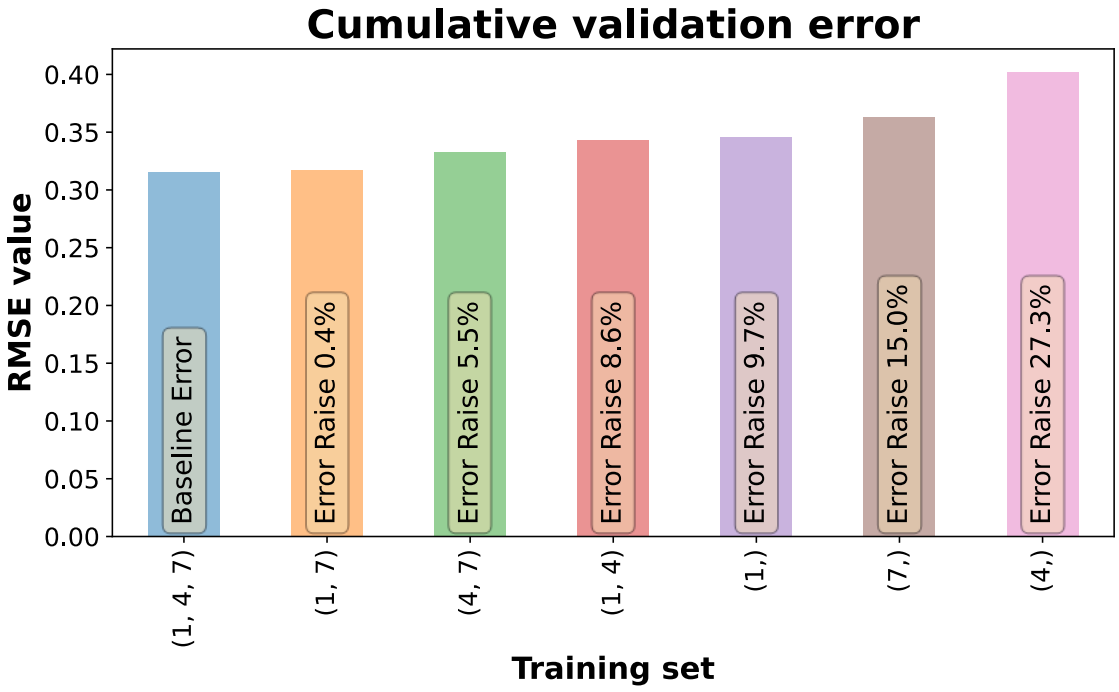

Figure 4.12: Training set (1, 4, 7). Training combinations performance comparative bar chart

Figure 4.12 presents a ranking bar chart for all seven possible training combinations within the selected training set. Several conclusions can be made upon examination of the results.

The general trend of experimental outcomes follows the theoretical predictions with regard to the importance of data-rich compaction response of the material. The findings confirm that the input sets comprised of more diverse loading programmes demonstrate a superior performance on a validation data set. Models trained on fully populated training combination (1, 4, 7) (Figure 4.13.a) are more capable of predicting material compaction response within the validation loading schedules as illustrated in Figure 4.13.b.

On the contrary, models based on the training combination (4,) demonstrate a significant drop in accuracy as shown in Figure 4.14.b. As expected, formulated models are able to fit the single input set from test 4 at the training stage with high level of accuracy (Figure 4.14.a).

However, there is a substantial offset between experimental compaction curves and model's output at the validation phase (Figure 4.14.b). It results in a 27.3 % error raise compared to the baseline value. Such outcome is a clear indication of an insufficient input training data. Candidate models were not exposed to a variety of loading schedules at the formulation phase and did not capture the material's response to changing processing conditions. Consequently, they are worse at predicting thickness evolution for experimental programmes with different load amplitudes and load application rates. The resulting candidate models and parameters within both training combinations are presented in Table 4.2.

Table 4.2: Candidate models within different training combinations.

	Model type	Parameter 1	Parameter 2	Parameter 3
Training combination (1, 4, 7)				
Candidate model 1	DefGen	a: -0.8283	b: -13.87	k: 0.8124
Candidate model 2	Percolation (bgc)	$K_A/\tilde{\eta}$: 0.6015	σ_A: 0.0031	
Training combination (4,)				
Candidate model 1	DefGen	a: -0.5122	b: -12.41	k: 0.8560
Candidate model 2	Percolation (bgc)	$K_A/\tilde{\eta}$: 0.6410	σ_A: 0.0036	

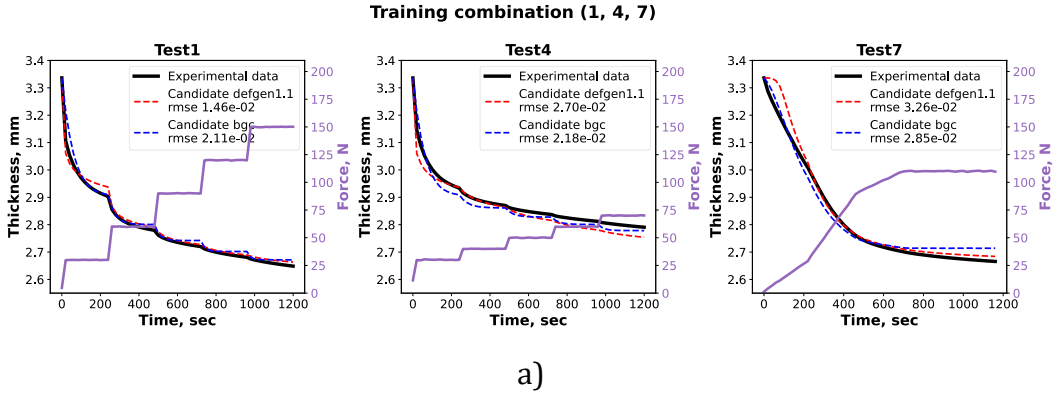

a)

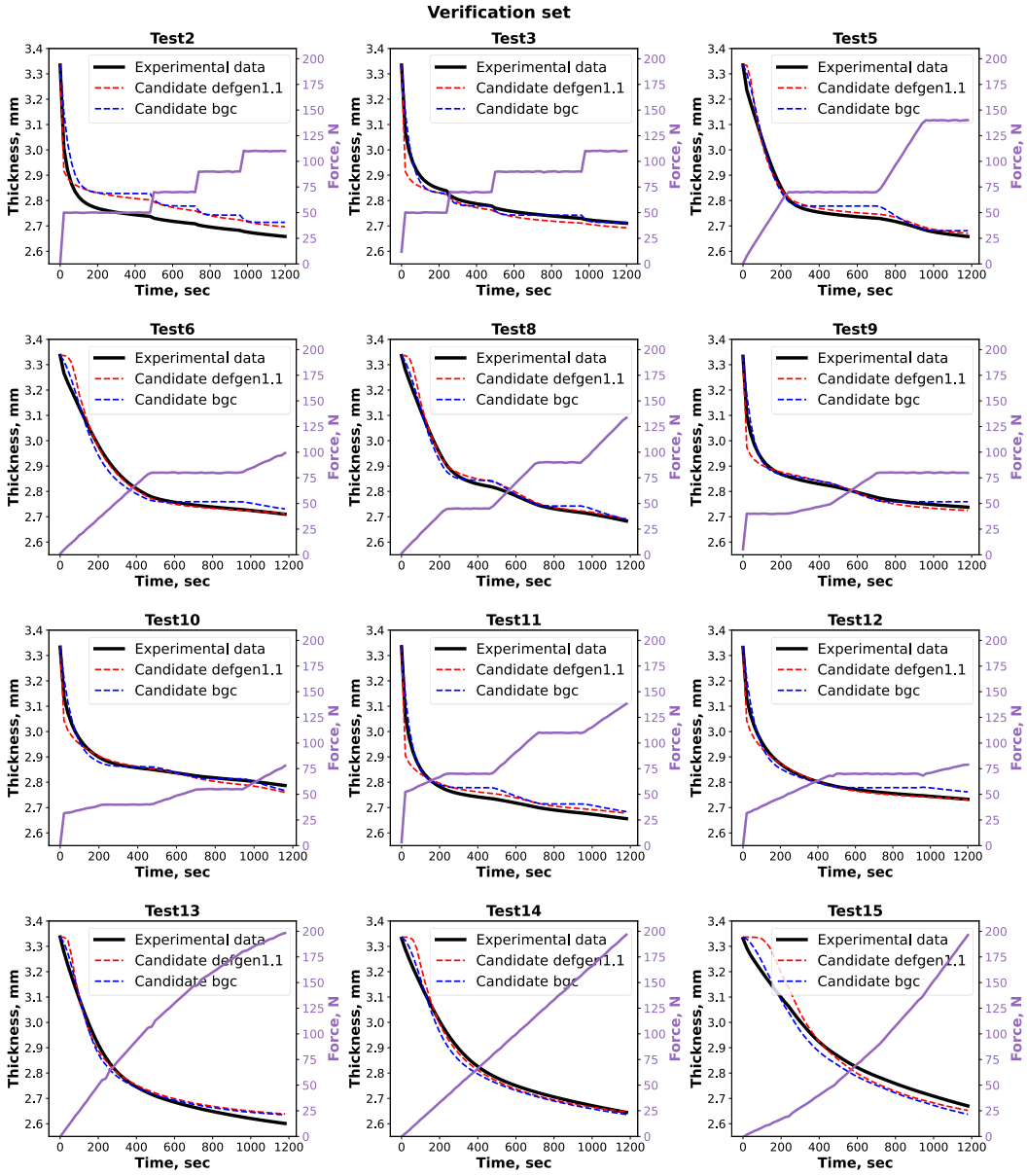

b)

Figure 4.13: a – two best performing candidate models fit experimental data for (1, 4, 7) training set, b – validation of two best performing candidate models based on (1, 4, 7) training set.

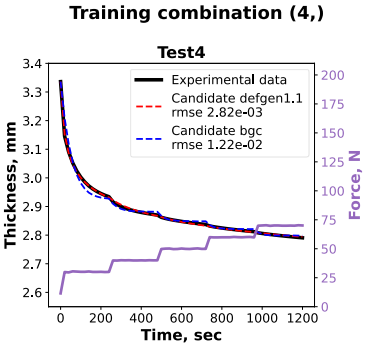

a)

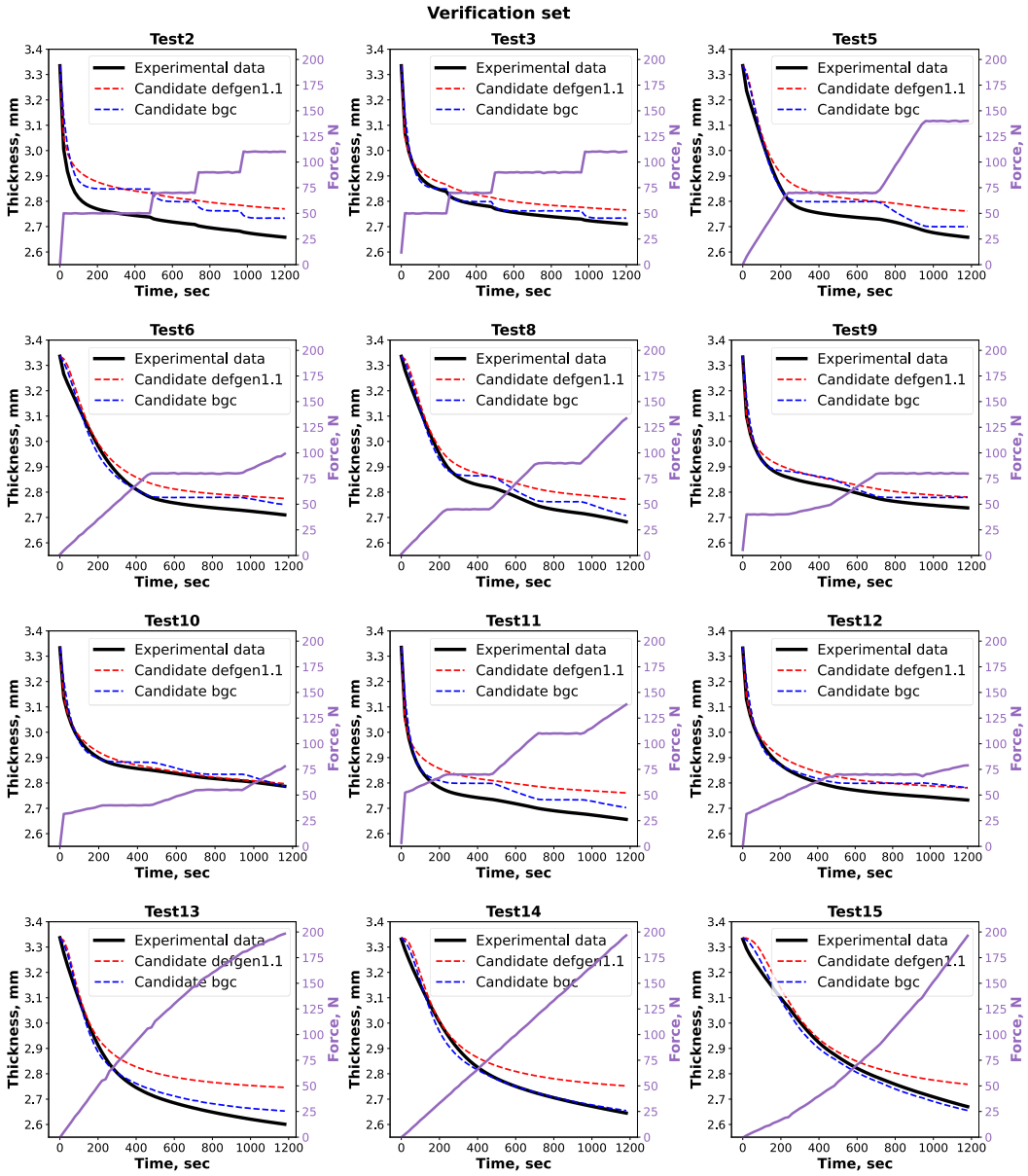

b)

Figure 4.14: a – two best performing candidate models fit experimental data for (4,) training set, b – validation of two best performing candidate models based on (4,) training set

The results shown in Figure 4.12 indicate that there is no substantial advantage of the full training set over the second-best training combination (1, 7). The difference in total error in thickness prediction between these input options is 0.4%. That is to say, conducting characterisation test 1 does not bring a considerable value to the training combination (1, 7) and can be omitted. The same accuracy can be obtained with a smaller number of tests, meaning lesser amount of time and material required for a complete experimentation.

Additionally, for certain training sets there is a possible occurrence of an outlying phenomenon which stands out from the observed trend. To illustrate that, a ranking bar chart for the training set (1, 7, 10) is shown in Figure 4.15. The fourth-best training combination (10,) is advantageous in comparison to (1, 10). It means that adding test 1 to an input training combination (1,) impairs the final result. The most likely explanation of such phenomenon is that the validation set is underpopulated.

It is important to note that every candidate model from the library has its own limitations and might not be able to reflect the material behaviour for a certain load set within specified processing conditions. A more diverse validation set would require conducting more characterisation tests. From the outcome of these experiments, it is possible to conclude that the current number of tests for validation is sufficient.

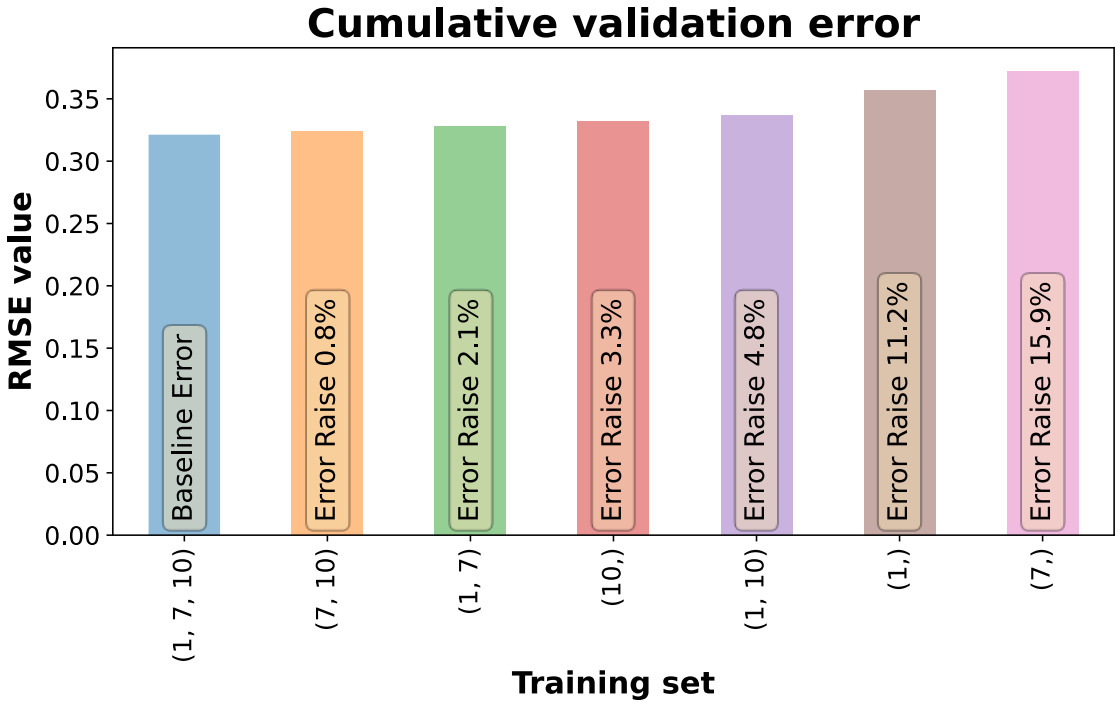

Figure 4.15: Outliers within training set (1, 7, 10). Training combinations performance comparative bar chart.

4.9 Conclusions

Upon review of the experimental results presented in this chapter, the question arises as to how to build an appropriate /rational /data-rich testing programme. It is fundamentally important for modelling composite manufacturing processes. It was clearly illustrated that deficient and insufficient testing may lead to fundamentally wrong predictions of material states and completely mislead the results of process optimisation procedure.

The robust material parameters extraction tool for processing experimental data is introduced in this chapter. It is able to retrieve true values of material parameters for a chosen candidate from the compaction data. The tool can be used standalone or be embedded as a functional part of a larger scale project.

The problem of testing rationales and subjectivity in material testing is addressed in the next chapter. The new adaptive consolidation sensor framework that enables flexible autonomous steering of a testing programme is introduced. The framework does not rely on any initial hypothesis or prior knowledge regarding the deformation modes. It focuses on the identification of the underlying physical mechanisms rather than material properties identification in a rightly or wrongly assumed flow mode.

5 ADAPTIVE CONSOLIDATION SENSOR FRAMEWORK

In many cases the underlying physical mechanisms are difficult to know in advance and wrong subjective assumption about the flow modes will lead to conceptual mistake in understanding materials' behaviour. In the current environment when materials become multi-functional and contain a lot of additives to enhance their performances, it becomes increasingly difficult to know the right flow mode in advance. Moreover, as has been established previously [39], [40] the same material may exhibit different deformation responses when temperature varies within a relatively small range.

As demonstrated in the previous chapter and in section 3.3, the testing programme plays a crucial role for the robust characterisation of a composite. Insufficient experimental compaction data may lead to the distorted results due to the lack of information for candidate model training.

To challenge this problem, the adaptive consolidation sensor framework is introduced in this chapter. It is designed to build a testing programme in real time in a reactive manner based only on the compaction response of the material. The proposed approach removes a subjective judgement about the material behaviour. The detailed description of the proposed consolidation sensor framework and its constituent modules is presented below.

The main focus of this chapter is on the example of the virtual real-time experimentation and the examination of the framework's overall performance. In the proposed virtual exercise, the suggested framework is set to identify the right mechanisms and extract parameters of a material model hidden in the pre-coded module "BlackBox". Upon the completion of the test, the analysis of the framework's capability to identify the underlying flow mechanisms is carried out. Finally, the discussion on the test's initial settings/constraints and its' influence on the framework's outcome is presented within this chapter.

5.1 Implementation of the Framework

5.1.1 Conceptual Design

The adaptable testing framework suggested below aims at identifying flow mechanism as a result of a continuous material's compaction response and at an analysis of the obtained data in real time. The primary driver for such an algorithm is not to determine the material properties per se (though this is also achieved as a by-product of the process), but to select the right flow mode.

For a start, it is assumed that the compacted material can be adequately described by one of the consolidation models from a pre-defined library (described in section 3.2), but there is no prior knowledge about what model should be chosen. As stated previously, the library contains models of resin flow in the form of ordinary differential equations (such as shown in

Table 3.1).

There are several requirements for the proposed consolidation sensor framework:

- The proposed system must enable a "conversation with the material". It means that the decision about further steps of the testing programme is based on the real-time compaction response of the material.
- There must be no bias towards any of the consolidation models. For that reason, every model from the library must be trialed against each other. Thus, the framework is only limited by the diversity of the candidate models in the consolidation library. Moreover, the library can be expanded by adding new compaction models in case a new material is considered.
- The designed loading programme must be aimed towards accommodating the framework to distinguish between best performing candidate models most efficiently (here the performance is defined in the same way as in the previous chapters – cumulative error in thickness prediction).
- An extra level of complexity is added due to the real-time nature of the experimentation. Interim results analysis takes place while a characterisation test is still running. For this reason, the framework's execution time must be reduced to a minimum, as opposed to standard postprocessing procedures where computational promptness is less critical.

5.1.2 Detailed algorithm of the consolidation sensor

The detailed algorithm of the framework is illustrated in Figure 5.1. The framework was implemented in Python programming language environment [148].

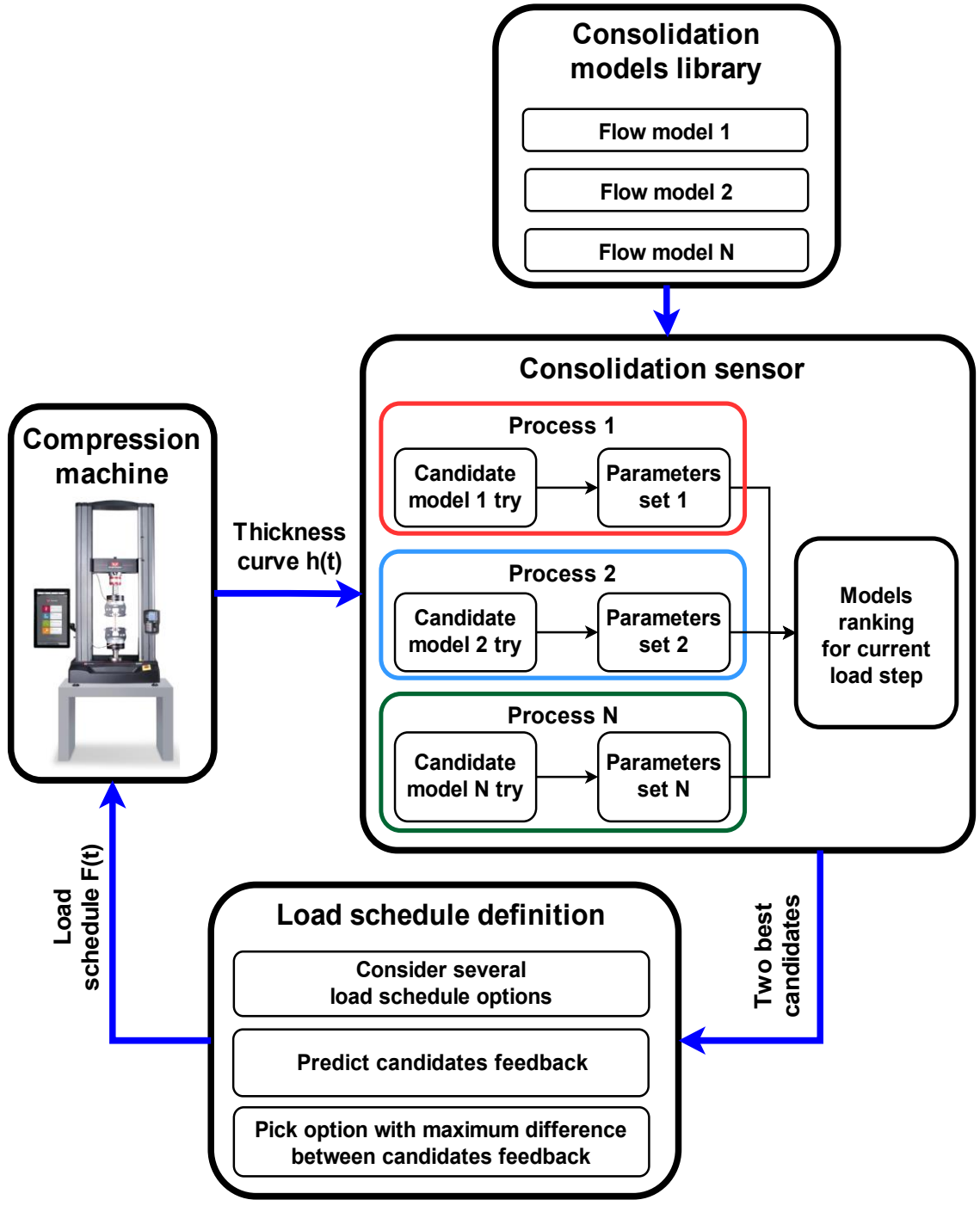

Figure 5.1: Detailed algorithm of the consolidation sensor

The pressure-controlled loading programme is arranged as a sequence of steps. There is a fixed time defined for each of these steps. At the end of each step the load can be ramped (faster, slower or in ramp-dwell fashion), or the material may be let to creep under constant load as shown in Figure 5.2.

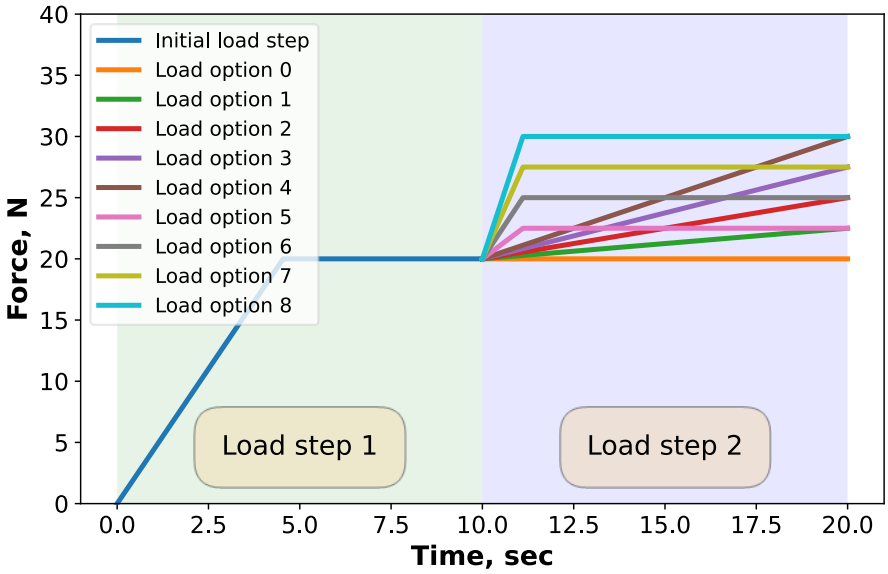

Figure 5.2: Possible load schedule options in a real-time testing

The consolidation framework allows to design a load schedule not only within the scheme presented in Figure 5.2, but also with respect to load relaxation (see Figure 5.3).

As shown previously in section 2.2.2, the models in the consolidation library are not designed to model unloading and cannot reliably predict the laminate's thickness evolution at such stage. Therefore, no unloading is considered at this stage of the framework's application, though this may be an interesting development particularly when models with plastic response are added to the consolidation library.

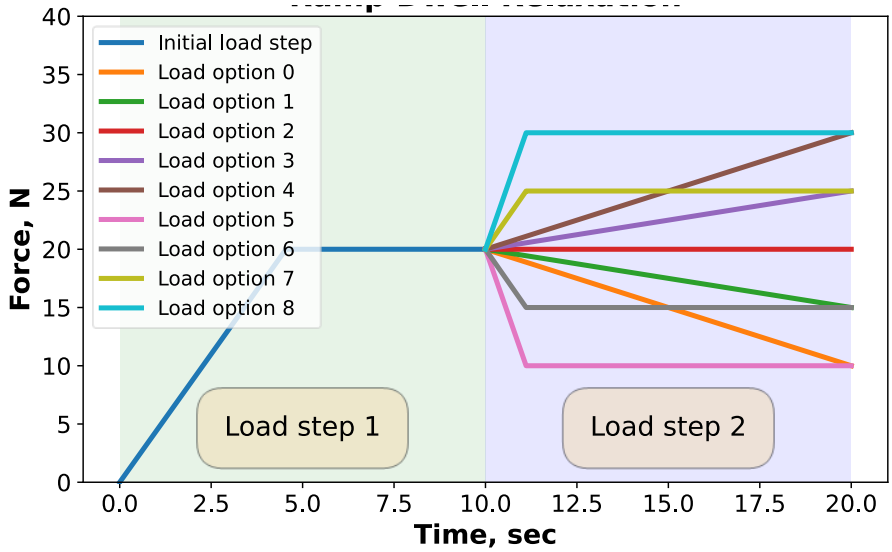

Figure 5.3: Possible load schedule options in a real-time testing, including load relaxation.

The decision of what needs to be done for a particular load stage is dictated by the framework for all the stages except the very initial step. At the start of the loading a predefined compression load is applied since there have not been any experimental data received yet.

The output of this testing is an evolution of the sample thickness throughout all loading stages. At each stage of an experiment the consolidation sensor starts challenging every model from the library to determine its ability to characterise the material. This is done by conducting a two-step nonlinear regression analysis of a chosen candidate model. The process is automated and is implemented as the custom-built standalone parameter extraction tool, as described in section 4.7. In this case it is used as a functional part of the consolidation sensor framework. Therefore, after reviewing the consolidation library, a set of material parameters corresponding to a particular flow model is retrieved.

The parameter extraction routine is repeated at each load step of the test. It is possible to use a parameter set from a previous load step as a starting point for the current one. In this case, the brute force stage can be omitted which speeds up the whole process. Since optimisation methods at the second stage are not global, there is still a possibility of converging to a local minimum. In that case the density of the grid used at the brute force stage can be increased to provide a more propitious starting parameters set.

It is now possible to predict material's feedback to a possible load schedule change in further load steps of the test in accordance with a chosen consolidation model. Moreover, fit quality provides some preliminary ranking of the models. After reviewing the results from the current stage of the test, the two most capable candidate models are selected. The selection is driven by the need to identify the best candidate out of two best performing models. Hence, two candidates are then passed to the load schedule definition module. Possible load schedule scenarios are selected by picking the load option which maximises the difference in prediction between two best candidate models as shown in Figure 5.4. In this example the load option 6 (highlighted in red colour) produces the largest difference in compaction response of candidate models.

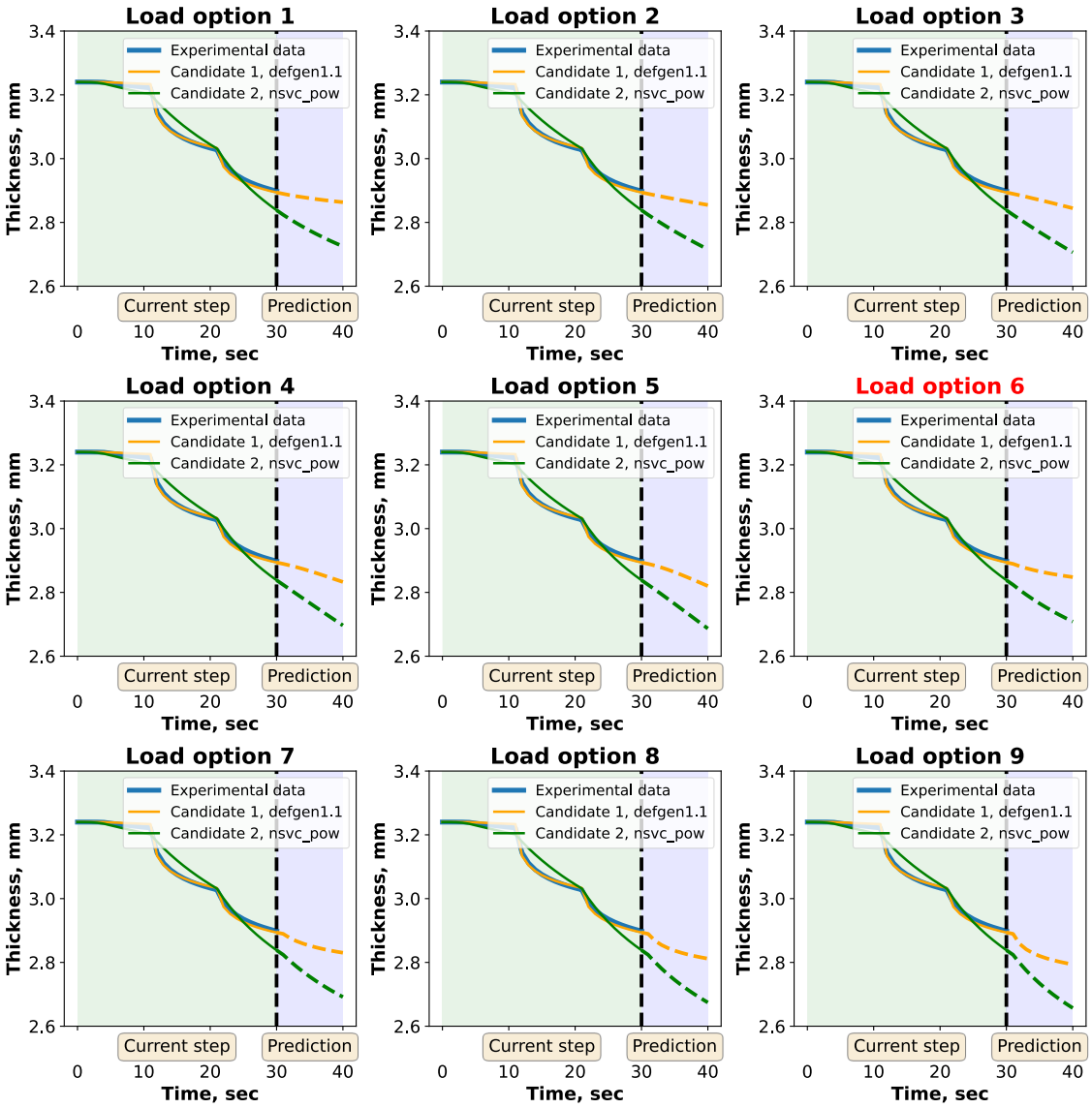

Figure 5.4: Best candidates models' predictions to different load options. Load option 6 (shown in red colour) is chosen for the next load step.

Therefore, the resulting testing program is designed in a way, which allows to distinguish between best performing consolidation models most efficiently and to reduce the uncertainty on the material's deformation mechanism. Upon completion of data processing, a newly designed load schedule is sent to the compression machine for the execution within the next load step. The whole process is then repeated until the testing is over.

5.1.3 Accounting for the previously processed data

The developed framework analyses incoming data from the testing setup in the real-time mode. It means, that within each load step of the test the input data from the compression machine comes in batches after the corresponding loading programme is

conducted. Upon the completion of a load step, the framework receives the new batch of data for further analysis.

For this reason, there is a constant need of processing the new input with regard to the already received data from the previous load steps. When the solver receives the new data batch, it now uses the last computed thickness value from the previous iteration as an initial condition for the current step. Therefore, the initial condition for the current load step is $h(t_N) = h_N$, where t_N is the last time value of the previous load step, as opposed to $h(t_0) = h_0$ at the start of the test.

5.1.4 Multiprocessing

As stated previously in section 5.1.1, the framework's processing speed is of prime importance. An important factor of processing the results is that the analysis of each candidate model is independent of each other. On this account, it becomes possible to significantly speed up the overall parameters extraction routine by processing each candidate model from the consolidation library in a concurrent manner. By leveraging all available CPU cores, tasks for execution can be submitted as separate processes [174] as shown in Figure 5.1. The framework automatically manages a pool of candidates to be processed and assigns available cores to perform the parameters extraction.

Therefore, if the number of CPU cores (including virtual cores) in the machine is more or equal to the number of models in the library, the total execution time is limited by the most complex and slowest candidate model.

5.1.5 Virtual Testing

It is essential to ensure correct functioning of the framework before conducting tests on a real material. To validate the predictive capacity of the suggested framework, virtual tests have been performed. The material behaviour is simulated by an instance of one of the models in the library with added noise representing uncertainty of the experiments. The simulated material response is produced by a virtual module hereinafter referred to as 'BlackBox'. Before the start of the experiment, one target model from the library is selected and fully defined by specifying all required parameters. Then, it is placed inside the BlackBox module. The consolidation framework is unaware of what model is hidden inside the BlackBox. The main goal here is to investigate predefined flow

mechanism and its parameters by challenging candidates from the library as in a real experiment. The example of such virtual exercise is given in the section 5.2.

Similarly to a universal test machine, the proposed module receives a load program as an input. After the load schedule input is submitted to the BlackBox, a differential equation corresponding to a hidden target model is solved and outputs the evolution of the sample's thickness over time. Then, a noise component is added to the resulting thickness output to introduce an extra challenge for the framework. The BlackBox module's routine is presented in Figure 5.5.

The main advantage of virtual testing is that the correct material formulation is known; therefore, the framework's performance can be directly assessed by comparing the target model in the BlackBox and the model defined by the testing framework. The success of the current batch of the models is when each of them can be properly detected from live interaction with the "material".

Moreover, it is possible to put a test on pause for debugging purposes. It is important for adjusting and fine-tuning consolidation models as well as improving algorithm's overall promptitude. The real materials testing does not offer such flexibility.

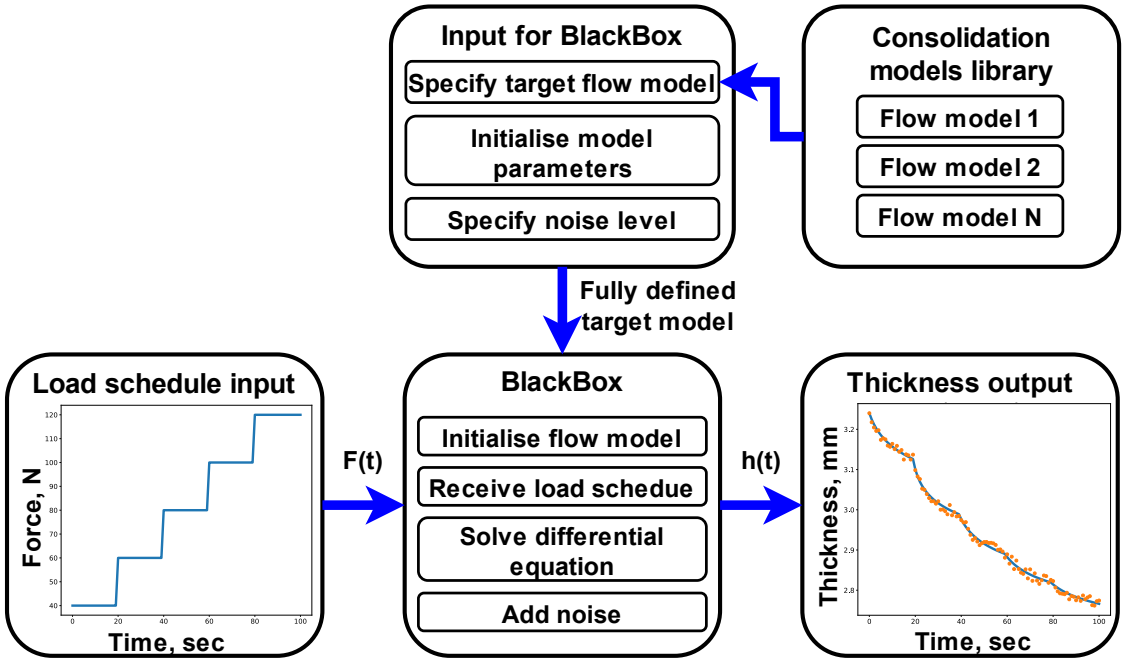

Figure 5.5: BlackBox module's algorithm.

5.2 Virtual experimentation

5.2.1 Virtual experimentation case study

The following example of virtual testing shows a fully defined DefGen ProToCoL model initialised inside the BlackBox module using parameters of Table 5.1. The test consisted of ten load steps with a duration of 10 seconds per step. Initial ramp-dwell schedule with a maximum amplitude of 30 N was conducted at the start of the test. The maximum possible load change within one load step was set at 30 N. Every model from the library, including the DefGen model, was challenged to fit the BlackBox's output at each load step of the test. Prior to the experiment, initial values of model parameters for the candidate models were set up randomly within defined limits. These were set based on maximum/minimum achievable values of material parameters within a chosen consolidation model.

A visual representation of a virtual testing process is illustrated on Figure 5.6. Each load step figure consists of three separate graphs. The BlackBox's thickness evolution curve and two best performing candidate models' feedback curves are depicted on the left. There is also an area of the candidates' predicted output for a chosen load within the next load step, which maximises the difference in thickness evolution between them. There is also a noisy output of the BlackBox similar to the example presented in Figure 5.5. For the sake of clarity, it is not shown on the graph.

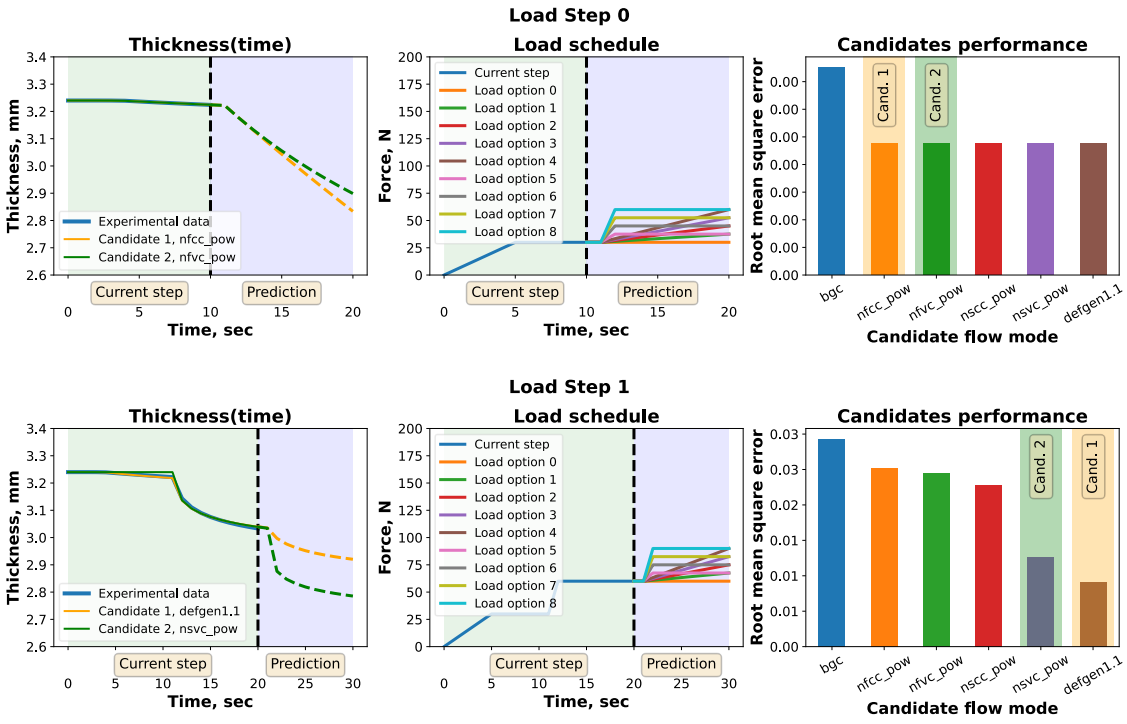

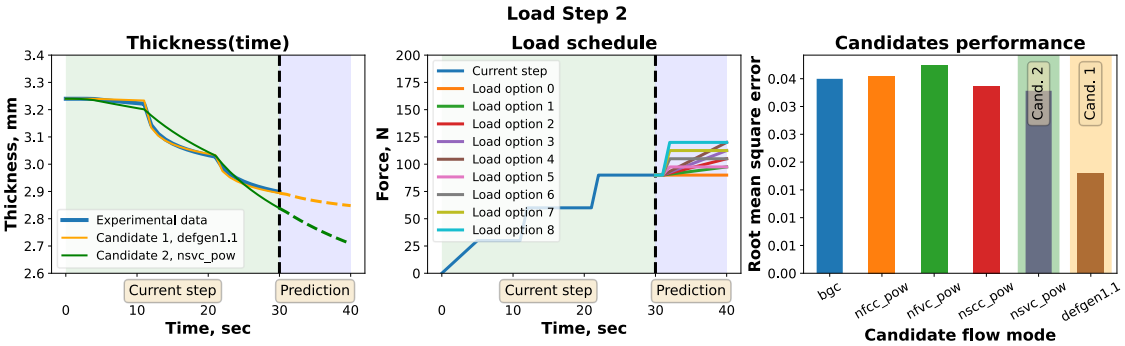
Load Step 2
Thickness(time)
Thickness, mm
Experimental data
Candidate 1, defgen1.1
Candidate 2, nsvc_pow
Current step
Prediction
Time, sec
Load schedule
Force, N
Current step
Load option 0
Load option 1
Load option 2
Load option 3
Load option 4
Load option 5
Load option 6
Load option 7
Load option 8
Time, sec
Candidates performance
Root mean square error
Cand. 2
Cand. 1
bgc
nfcc_pow
nfvc_pow
nscc_pow
nsvc_pow
defgen1.1
Candidate flow mode

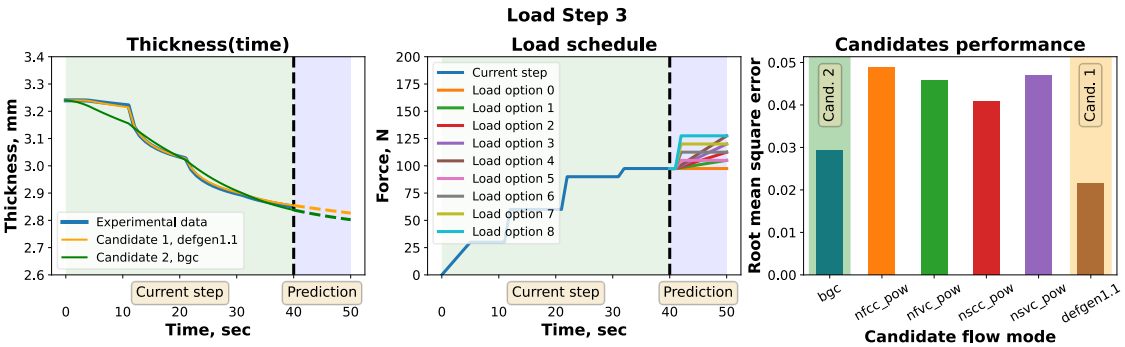
Load Step 3
Thickness(time)
Thickness, mm
Experimental data
Candidate 1, defgen1.1
Candidate 2, bgc
Current step
Prediction
Time, sec
Load schedule
Force, N
Current step
Load option 0
Load option 1
Load option 2
Load option 3
Load option 4
Load option 5
Load option 6
Load option 7
Load option 8
Time, sec
Candidates performance
Root mean square error
Cand. 2
Cand. 1
bgc
nfcc_pow
nfvc_pow
nscc_pow
nsvc_pow
defgen1.1
Candidate flow mode

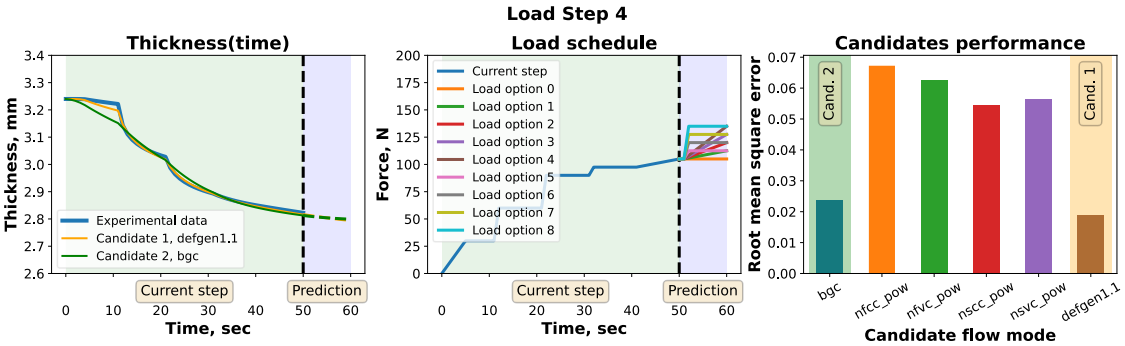
Load Step 4
Thickness(time)
Thickness, mm
Experimental data
Candidate 1, defgen1.1
Candidate 2, bgc
Current step
Prediction
Time, sec
Load schedule
Force, N
Current step
Load option 0
Load option 1
Load option 2
Load option 3
Load option 4
Load option 5
Load option 6
Load option 7
Load option 8
Time, sec
Candidates performance
Root mean square error
Cand. 2
Cand. 1
bgc
nfcc_pow
nfvc_pow
nscc_pow
nsvc_pow
defgen1.1
Candidate flow mode

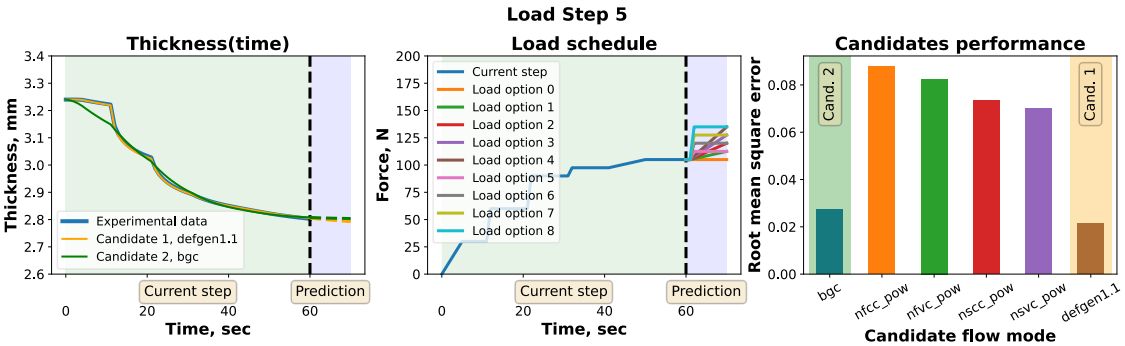
Load Step 5
Thickness(time)
Thickness, mm
Experimental data
Candidate 1, defgen1.1
Candidate 2, bgc
Current step
Prediction
Time, sec
Load schedule
Force, N
Current step
Load option 0
Load option 1
Load option 2
Load option 3
Load option 4
Load option 5
Load option 6
Load option 7
Load option 8
Time, sec
Candidates performance
Root mean square error
Cand. 2
Cand. 1
bgc
nfcc_pow
nfvc_pow
nscc_pow
nsvc_pow
defgen1.1
Candidate flow mode

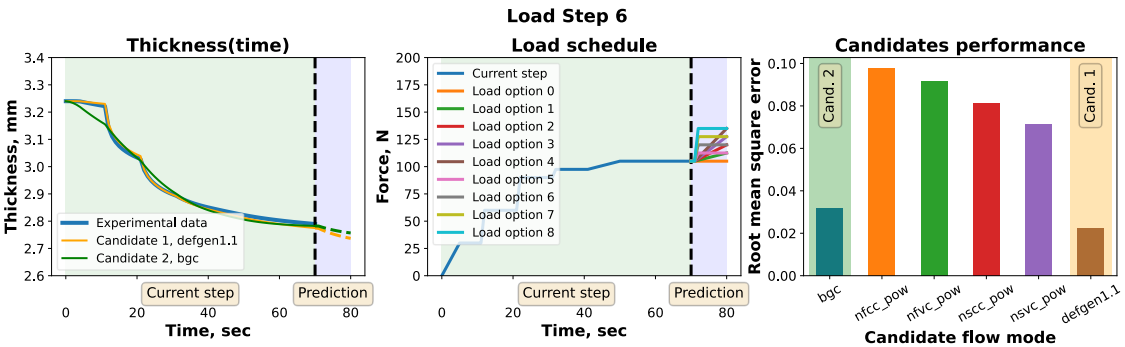
Load Step 6
Thickness(time)
Thickness, mm
Experimental data
Candidate 1, defgen1.1
Candidate 2, bgc
Current step
Prediction
Time, sec
Load schedule
Force, N
Current step
Load option 0
Load option 1
Load option 2
Load option 3
Load option 4
Load option 5
Load option 6
Load option 7
Load option 8
Time, sec
Candidates performance
Root mean square error
Cand. 2
Cand. 1
bgc
nfcc_pow
nfvc_pow
nscc_pow
nsvc_pow
defgen1.1
Candidate flow mode

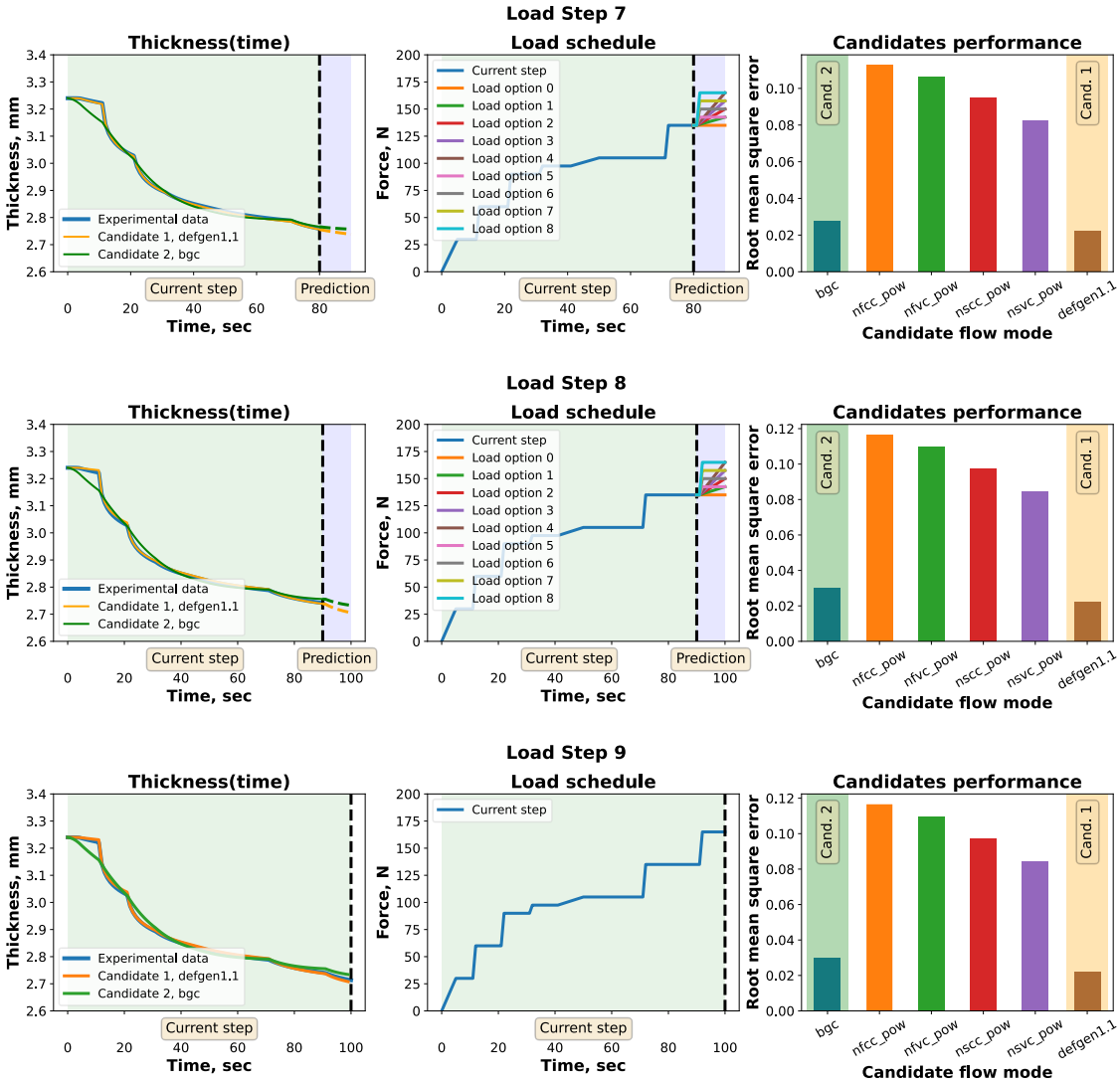

Figure 5.6: Virtual testing step by step routine.

The current load schedule and possible options for the following load step are presented in the middle graph. The bar chart on the right showcases each model's performance in terms of the corresponding values of root mean square error within the current load step. It outlines the competition between candidates and the change of a trend in dominating deformation mechanism as test goes on. The results of the test indicate that the framework successfully worked as a consolidation sensor. It correctly identified the target model inside the BlackBox along with its material parameters. Table 5.1 summarises the outcome of the target and two best candidate models.

Maximum discrepancy in the parameters values does not exceed 4.5%. This discrepancy was caused by the excessive noise level in the BlackBox output, which often is much smaller in a real compaction testing (as shown later in Chapter 4).

Table 5.1: Virtual experimentation outcomes

	Model type	**Parameter 1, a**	**Parameter 2, b**	**Parameter 3, k**
Target model inside Blackbox	DefGen	a: -0.8378	b: -12.96	k: 0.7953
Candidate model 1	DefGen	a: -0.8015	b: -12.81	k: 0.7991
Candidate model 2	Percolation (bgc)	$K_A/\tilde{\eta}$: 0.9143	σ_A: 0.0080	-

It is interesting to examine the resultant load schedule and check whether it displays any characteristic pattern. Typically, these curves are rather complicated, but a few features can be distinguished. For example, on the curve presented in Figure 5.6, the resulting load schedule demonstrates that the compaction force raises up to 100 N, followed by a dwell stage for 50 seconds. At the last 30 seconds of the test load starts increasing again in a ramp-dwell manner. The resultant load comprises a very wide range of loading rates and a considerable dwell stage at intermediate load.

At the early stage of the deformation, the consolidation sensor concludes that the most likely candidates are various forms of incompressible shear flow model along with the correct DefGen candidate. This shows that the initial loading does not provide sufficient data to make a reliable conclusion and a comprehensive test programme for the material characterisation is needed.

The favourable models evolve throughout the test. Upon completion of the test, the second-best candidate was defined as a percolation flow model. The second-best ranking was not constant through the test and for the first three load steps sensor defined the second-best candidate as a shear flow model. As the load schedule became more sophisticated, the accuracy of the shear model decreased significantly, and the percolation model's performance became more robust.

The visualisation of the two-step parameters extraction of one of the candidate models is presented below. The process is repeated for every candidate model at each load step through the test. To showcase the initial brute force step, a scatter plot matrix visualising bivariate relationships between the model parameters is depicted in Figure

5.7. It allows revealing the influence of material parameters on the objective function and to gain an insight into possible pitfalls of an optimisation process for a chosen model, such as areas of local minima. There are several areas of local minima visible in Figure 5.7. The actual global minimum and the brute stage result for a given grid density are depicted with red and purple dashed lines correspondingly.

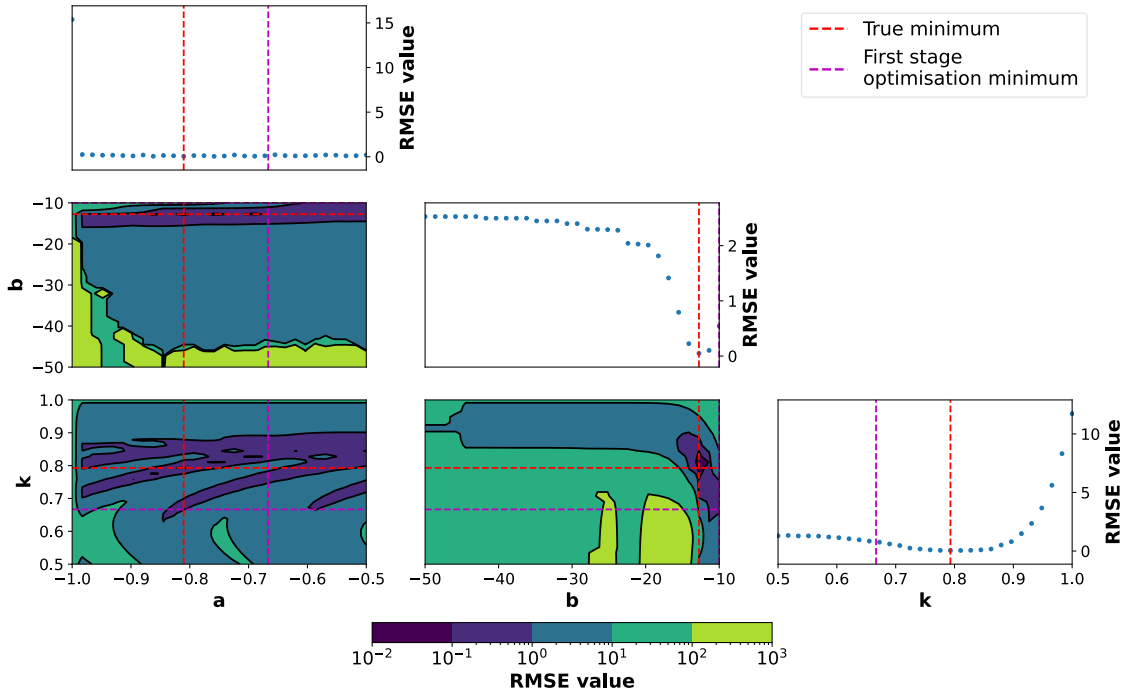

Figure 5.7: Parameter extraction visualisation. Initial stage brute force optimisation heatmap.

As expected, there is a gap between the outcome of the brute optimisation and the target value. It is to be eliminated in the secondary optimisation stage.

Since every consolidation model from the library has three parameters to vary, the optimisation is carried out in four-dimensional space. To illustrate the secondary optimisation process, the residual function is plotted as a three-dimensional grid, where each axis represents one of the material parameters. The value of the residual function is reflected by the size and the colour of a marker. To make the areas of interest more visible, the lower values are depicted with larger marker size and darker colour. This way, local minimum “branches” are clearly seen as illustrated in Figure 5.8. The figure shows how the optimiser avoids getting trapped in the areas of local minimum and converges to the global minimum. As stated in the previous section, the starting point for parameters values is the end result of the initial brute force stage.

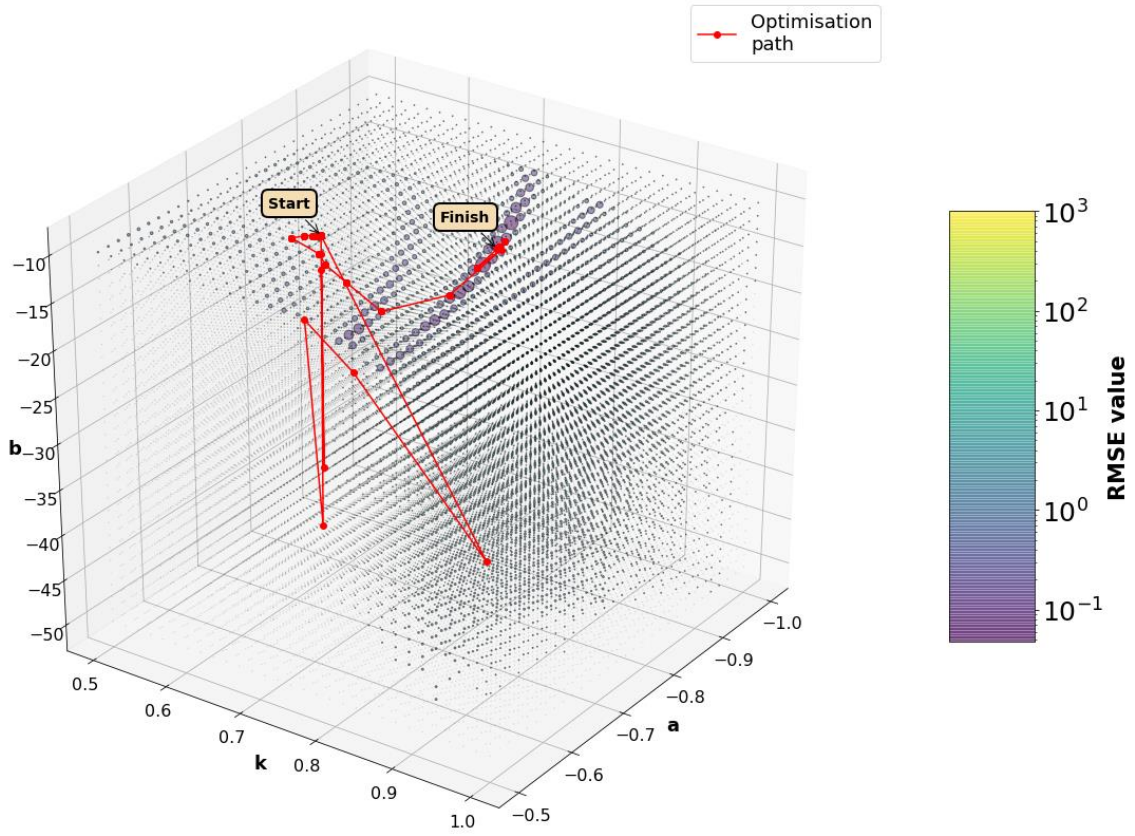

Figure 5.8: Parameter extraction visualisation. Secondary stage optimisation path within an objective function's mesh grid.

5.2.2 Validation of candidate models

The obtained candidate models were then verified against a different input load schedule. As shown in Figure 5.6, there is no substantial advantage in terms of the prediction error of the first best DefGen candidate compared to the second-best percolation one within a single characterisation test. Despite the fact that the target model is predefined and the correct answer is known, the verification stage is still relevant.

Figure 5.9 illustrated the validation process. A conventional ramp-dwell load programme used in previous studies [39] served as an input for the models. As expected, the best candidate selected by the framework (the DefGen model) adapts to the changed input successfully, whereas the second-best percolation one demonstrates a significant offset in prediction, despite an adequate performance at the characterisation stage.

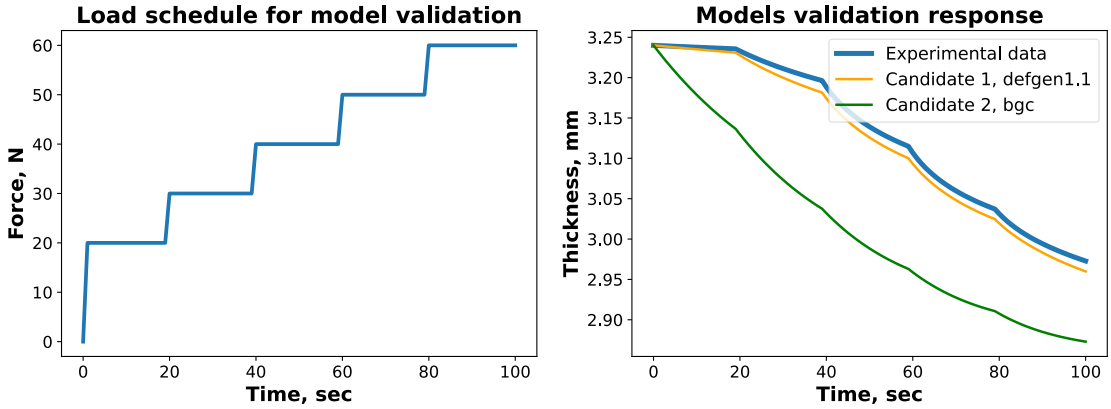

Figure 5.9: Candidate models validation

5.2.3 Different target models

The framework is designed to steer the load schedule based on the material's compaction feedback. As a consequence of that, the algorithm produces different resulting experimental programmes for different materials. In order to explore this effect more thoroughly, the same virtual exercise was conducted for different target models inside the BlackBox module, including percolation and power-law shear flow models. The resulting compaction curves and load schedules are presented in Figure 5.10.

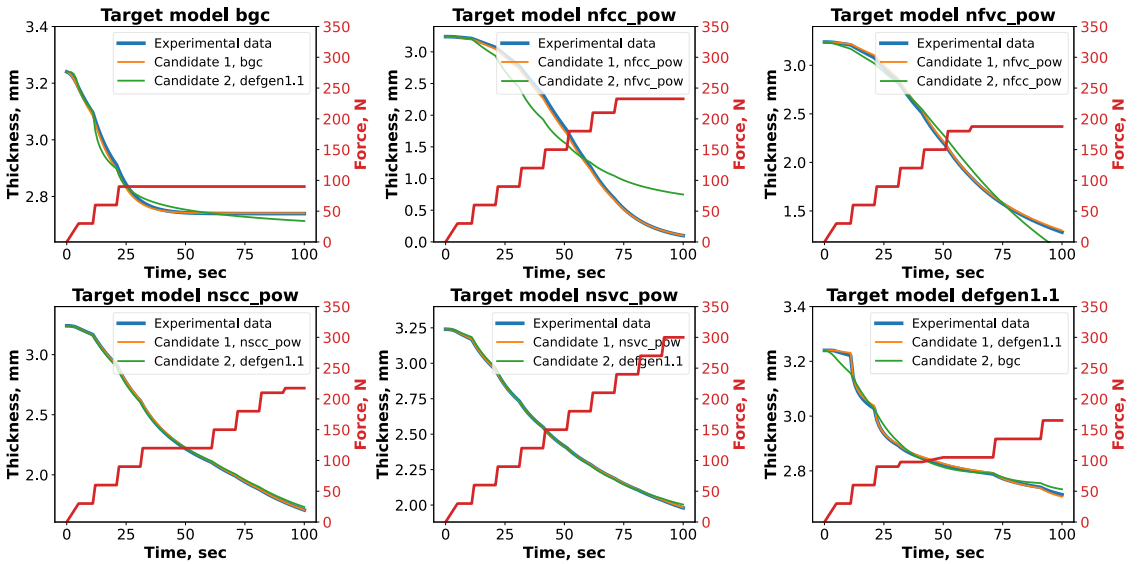

Figure 5.10: Framework's outcome for different target models inside the BlackBox module.

The first example illustrates the framework's output in case the percolation flow model (*bgc*) is used as a target model. Initially, the load raises to a certain value within first three load steps. Then, it starts to dwell at a constant level until the experiment is over. On the contrary, load schedules within the examples with shear target models

(*nfcc_pow*, *nfvc_pow*, *nscc_pow*, *nsvc_pow*) demonstrate consistent load increase throughout the whole experiment.

Whenever at least one of two best performing candidate models has no compaction limit and is very sensitive to the load rate change (like shear models from the library), the most likely scenario for the algorithm is to raise the load. Such model is more prone to produce higher thickness rate in response to the external pressure and is not bound by the compaction limit. Therefore, the difference between candidates' prediction will be higher as the external load grows. As stated in the previous chapter, the framework designs load schedule for the next load step based on the maximum difference between candidates. Hence, the algorithm tends to increase the pressure within the described examples.

The fifth case study with the shear target model (*nsvc_pow*) is particularly interesting in terms of the maximum achievable compression load throughout the experiment. The resultant load schedule is comprised of the consistent load ramps only. Such result means that the framework took the decision to maximise the load at every step of the experiment. It is particularly important in terms of the safety of the equipment when it comes to conducting tests on a real material. If the load value exceeds the capacity of a load cell on a compression machine, it may cause the irreversible damage of the expensive equipment. The problem of equipment's safety is addressed more deeply in the Chapter 6, where the interactive testing of real materials is considered.

In a conventional experimentation the test programme is defined explicitly by a researcher. It is straightforward to operate within the equipment's safety limits. In case of the interactive real time testing, the compression load is not known in advance. Therefore, one should always be aware of the maximum achievable load prior to the experiment. It is simply the product of the total number of load steps and the maximum load amplitude allowed within each step. Depending on the initial settings of the test these values may vary.

It is important to make clear, that the demonstrated loading programmes for different target models are not ultimate. There are two main factors that can affect the test. The first one is the completeness of the consolidation models library. If a library is complemented by a model more suitable for the studied material, the framework will design the test programme differently, as the pool of candidates change.

Moreover, the resulting programme is affected by a number of test settings and constraints. The final result within the same material under the test may vary depending on the specified options. This problem is addressed in the next section of this Chapter.

5.2.4 The impact of test settings on the result

There are several test settings, which have to be specified prior to the experiment:

- The initial load step must be defined in advance because the framework does not have any feedback from the material to operate with at the start of the test. There are two settings that have to be specified – load amplitude at the end of the initial step and the type of the load schedule (linear or ramp-dwell load raise).
- The maximum load amplitude specifies how far the algorithm can alter the current load value within one step.
- The number of the considered load options defines the density of the design space for the framework (see Figure 5.2). Each schedule option is constructed by populating $[F_i \quad F_{i+1} \quad \cdots \quad F_n]$ compression force array either in a linear (interpolation) or ramp-dwell manner (where F_i.and F_n are the start and the end values respectively). Load options are equally spaced between the dwell variant and the option with maximum load value at the end of the step. It is possible to put a constraint on the load schedule by considering either linear or ramp-dwell options only.

Technically, it is possible to set the maximum load amplitude at a high value and to specify a large number of the considered load options to increase the design space for the framework. But such approach would significantly increase the required computational time for the algorithm. The problem of the data processing speed is covered in the next section of this chapter. Besides, it is necessary to limit the load rate for the sake of equipment safety.

The virtual exercise described in the Section 5.2.1 was conducted within various setup configurations to demonstrate the impact on the resulting test programme. Several test settings were varied within each case study – initial load step (amplitude, linear or ramp-dwell), load schedule (liner and ramp-dwell or linear only) and load amplitude within one step. The resulting compaction curves and test programme are presented in Figure 5.11.

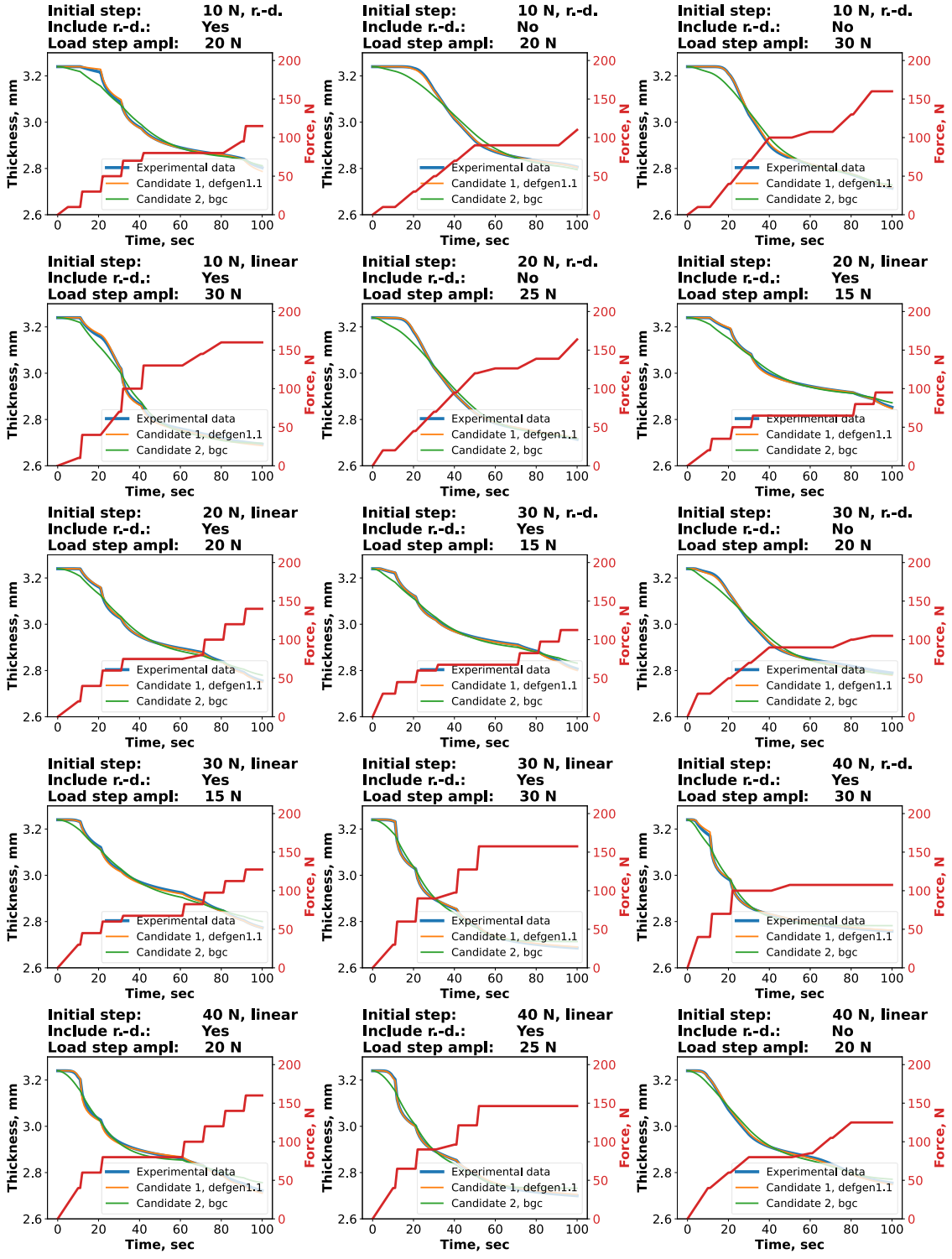

Figure 5.11: Load schedules for different test settings configurations, where r.d. – ramp-dwell.

In most cases the framework repeats the trend demonstrated within the baseline example. The compaction load raises up to a certain value, followed by a dwell stage and then starts increasing again. The set of the best candidates remains constant for every test.

5.2.5 The promptitude of data processing

The time required for data processing and decision making is not crucial at the stage of virtual experimentation. The BlackBox is simply put on pause while “waiting” for the framework to execute tasks in the queue (candidate models analysis, load schedule design etc). The computational promptitude of the framework starts playing an important role at the stage of experimentation with a real compression machine. In this case the test runs without pauses including the time when the framework processes the data. The impact of the time delay required for data processing on the overall result and the way of tackling this problem is covered in more detail in the real-time experimentation part of this research in Chapter 6. Nevertheless, it is useful to tune optimiser’s settings accordingly to achieve faster processing time within the virtual exercise prior to the actual testing.

As it was mentioned earlier in the section 5.1.4, all candidate models from the library are processed concurrently in the multiprocessing mode. To illustrate the significant impact of this approach on framework’s promptitude, the virtual test was conducted in both single- and multiprocessing modes. The comparative bar chart is presented in Figure 5.12. The execution time within single- and multiprocessing regimes for each load step of the test are represented with orange and blue bars correspondingly.

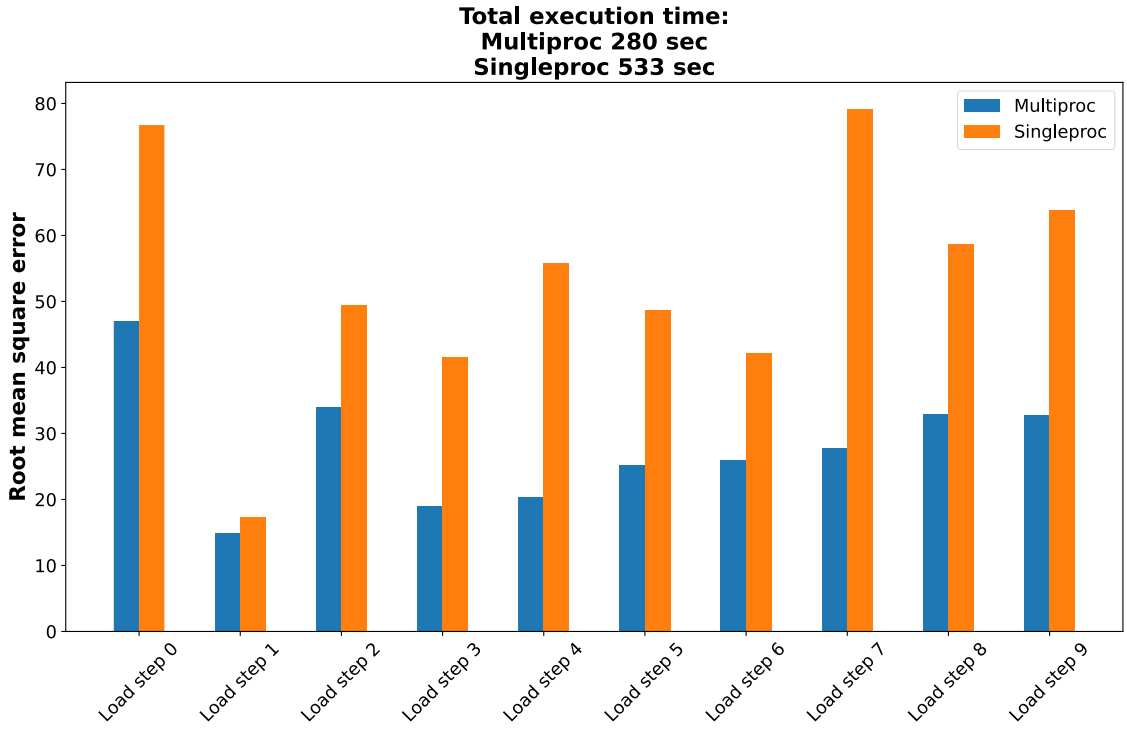

Figure 5.12: Consolidation framework promptness within each step of the test in single- and multiprocessing modes.

It takes significantly more time to process the initial load step than the rest, because two step parameter extraction is conducted at this point only. For the following steps, the framework uses the parameter values for candidate models retrieved from the step before as a starting point. Therefore, the subsequent steps require less time as only the second stage of the parameter extraction is employed (no brute force stage, see Section 4.7.1).

Starting from the second load step there is a gradual increase of the processing time for every subsequent step because the data set size expands as the test goes on. In certain cases (e.g. load step 2) the framework struggles to find an optimum set of parameters and it takes longer to output the result.

Employing the multiprocessing mode provides a large 47,5% advantage in terms of the computational time comparing to the sequential single processing mode (280 sec versus 533 sec respectively). Although, these values will vary for different hardware setups (current setup: CPU Intel Core i7-7700HQ 2.80 GHz, RAM 16 GB 2400 MHz), the predominance of the concurrent data processing approach is clear.

5.3 Conclusions

The concept of the adaptive consolidation sensor framework is introduced in this chapter. The proposed tool is set to operate in conjunction with the compression testing machine. Its main purpose is to steer loading programme based on the incoming real-time compaction data from the material. The framework's efficiency was tested in a virtual exercise.

The virtual trials successfully confirmed correct functioning of the framework. For the considered models, the framework manages to reveal a model type inside the BlackBox along with material parameters after two, sometimes three load steps with high fidelity. One characterisation test always appeared to be sufficient. The experiment's outcomes showcased candidate models' evolution in a step-by-step process and proved the consolidation sensor's capability to investigate material models.

The computational efficiency of the framework also appears to be quite promising and suitable for testing in a real environment. The approach presented here shows the potential to be implemented in real-time, in a reactive manner.

Even though the significant noise level was added to the target model's output, the framework always managed to distinguish the correct model from the library. When

testing actual materials, the deformation pattern may be significantly more complicated and show multiple deformation modes. The application of the adaptive framework to real materials is explored in the next Chapter. Finally, newly designed data acquisition system and the connection interface between the framework and the testing machine are introduced.

6 Real-Time Experimentation

The application of the proposed adaptive consolidation sensor framework for the characterisation of a real material is considered within this chapter. The chapter starts with the presentation of the testing setup's conceptual design. Since the framework has to operate in conjunction with the standard testing equipment (such as hydraulic Instron testing machine), the data transfer/acquisition hardware setup is developed. To manage the data exchange between the framework and the testing rig, the specially developed controlling software is proposed. The challenges for the data input/output, processing time delay, safety etc. and the ways to tackle them are discussed.

Finally, the adaptive testing framework is put to the test within several characterisation exercises for three different material systems. The output of the proposed testing method – model and materials properties for the tested materials – is compared with the results of more conventional characterisation tests with the predefined load schedule.

6.1 Real-time framework's conceptual design

6.1.1 Technical challenges

The experimentation with closed-loop feedback on real materials imposes a number of technical challenges which have to be addressed:

- The adaptive consolidation sensor must provide a continuous data exchange between the framework and the compression machine. The applied loading programme must be defined by the framework and supplied to the compression machine prior to every load step. The compaction data from the experiment must be received by the consolidation sensor at the end of each load step for post-processing and load programme definition. The required input for the framework should include time, applied load and specimen's thickness.
- The acquisition of the experimental data from the testing rig should not be interrupted at any point of the test. It means that the experiment cannot be

stopped or put on pause while the framework processes the compaction results, despite the fact that the load command for the next step is not formulated yet. For that reason, data processing time must be minimised to reduce the time delay between receiving the input and defining the load trajectory for next step.

- Equipment safety presents a serious concern when it comes to the real-time load control experimentation. The load schedule is not defined explicitly by a researcher and is built on the go. Therefore, the maximum load value may exceed safety limits for the compression setup. To avoid such scenario, safety protocols on software and hardware levels must be implemented.

6.1.2 An overview of the setup for the real-time experimentation

The conceptional design of the autonomous characterisation testing setup is presented in Figure 6.1. There are four major parts in the system including:

- A compression machine with the installed heater platens (similar to the setup described in chapter 4). The characterisation tests are to be conducted in the load-controlled mode. The main requirement for the machine is the presence of the analog input and output ports, as the machine must be able to receive commands from the framework and to send back the compaction data in a reactive manner.
- The adaptive consolidation sensor framework – discussed in the previous chapter 5. The framework is located on the external host (PC/laptop).
- A data acquisition system. The PC/laptop is connected to the compression test machine through the National Instruments data acquisition hardware. Its main purpose is to send and receive the data to/from the test rig. To do that, the input/output data is converted to a voltage signal (discussed below in this chapter). This signal is then transmitted/received through the hardware's analog ports. The signal is decoded back to the actual load schedule or the experimental compaction data by the compression machine/external host (PC/laptop).
- A data managing framework. The National Instruments hardware is managed by the custom developed framework implemented in the LabVIEW environment [175]. This framework is located on the same PC/laptop as the adaptive consolidation sensor. Data exchange between the Python and LabVIEW frameworks is implemented through the exchange of csv (comma separated

value) files. The Python framework outputs the commanding loading schedule for the next load step in the specially designated csv file. The LabVIEW framework detects the appearance of this file and reads it. The load is then converted to a voltage signal and transferred to the compression machine at a specified pace. Simultaneously, the compaction data from the machine is received by the LabVIEW framework and saved in another csv file by the end of each load step for the Python framework to process.

The data conversion to a voltage signal is conducted by the framework. The maximum output voltage of the hardware is 10 Volts. Maximum voltage corresponds to the maximum value of the transferred parameter. For instance, if it is expected, that the load value will not exceed 300 N, then the conversion coefficient will be 30 N/V. The displacement is encoded in a similar manner. It is important to note, that if the actual load exceeds the specified value (300 N), the hardware will not be able to output more than 10 Volts. Hence, the system will consider the load to be 300 N (for the described example), which would cause an inconsistency in the test programme. To prevent it from happening, it is possible to either raise the maximum possible load value (higher than 300 N for the described example) or lower the number of load steps/possible amplitude change within a single load step (the discussion on test settings was given in section 5.2.4 of this thesis), so the final load value will not exceed the limit.

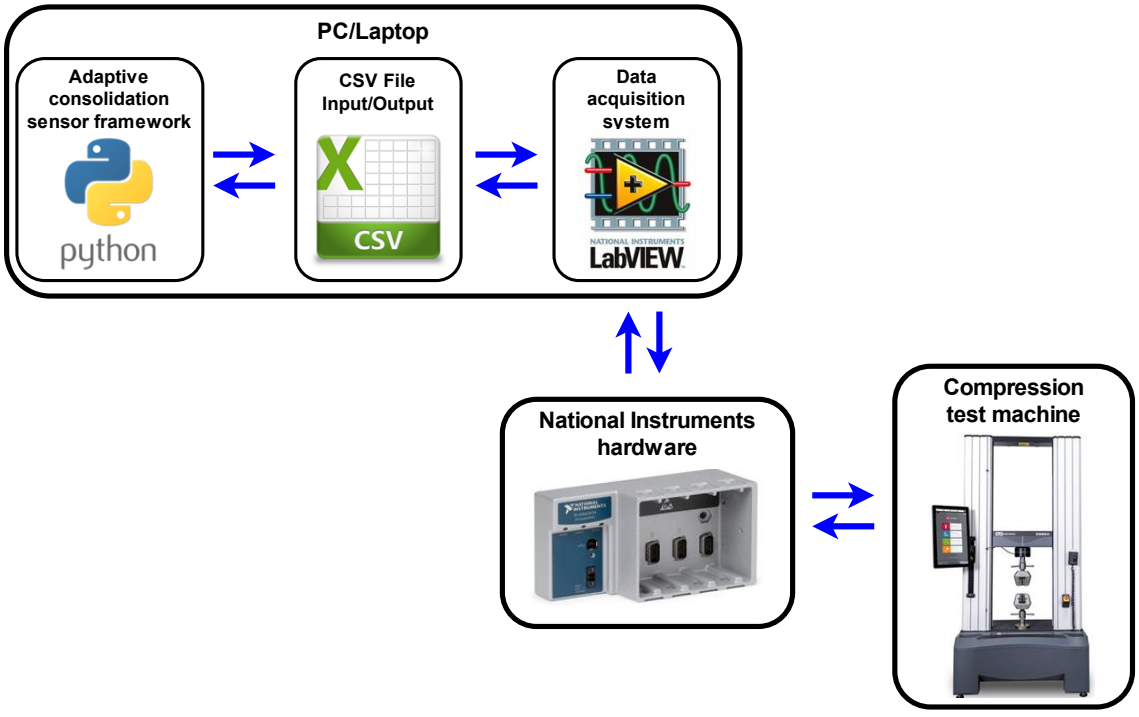

Figure 6.1: Autonomous real-time testing setup overview.

It is important to emphasise, that only load and displacement values (encoded as voltage) are transmitted and received. The corresponding time values are not defined explicitly. The time value is calculated by specifying the update rate (e.g. load value is updated every 0.2 seconds, data from Instron is received every 0.2 seconds). Care should be taken as the minimum possible value of this parameter may vary for different equipment setups. Less advanced versions of universal testing machines may not be able to update the commands at the specified pace which would cause a disruption in data transfer.

Another challenge for building a robust adaptive experimentation system is the occurrence of the noise in the input/output signal. Although, as described in chapter 4, the framework can process the noisy data, it is necessary to ensure, that there are no external factors causing data contamination with systematic errors. Besides equipment malfunction, there are two main sources of the noise in the signal within the current setup:

1) Incorrectly defined conversion coefficients (mm/V for the displacement or N/V for the load). As stated above, the maximum output voltage of the data acquisition setup is 10 Volts. Improperly defined conversion coefficient may lead to a case when only a fraction of the voltage signal's capacity is used. For instance, if the displacement conversion coefficient is defined as 100 mm/V, and the actual displacement of the specimen is ~1 mm, then the output voltage level would be less than 0.1% of the hardware's capacity. Figure 6.2.a illustrates several examples of the resulting displacement curves for different values of the displacement conversion coefficients within the exact same experimental setup. It can be seen that properly performed displacement-to-voltage conversion drastically improves the smoothness of the compaction curves. The same approach applies to the transmission of the load data.
2) Low resolution of the load cell. Based on the required pressure for the chosen size of the specimen (15 mm x 15 mm), the maximum compression force does not exceed 300 N within the current experimentation. If the load cell is designed for high values of acting loads, it will operate at a small fraction of its capacity within the current setup. In this case the compression machine's PID control may not be able to operate with precision in the load control mode, as the controlling sensor's (load cell) resolution is too low. As shown in Figure 6.2.b (the image from the LabVIEW framework), the difference between the

defined/applied load for 10 kN and 1 kN load cells is significant. For both cases the load does not exceed 100 N. In case of the 10 kN load cell, the compression machine struggles to adjust the applied load (represented as red curve) according to the submitted load schedule (represented as a white curve). For the 1kN load cell this problem was not observed.

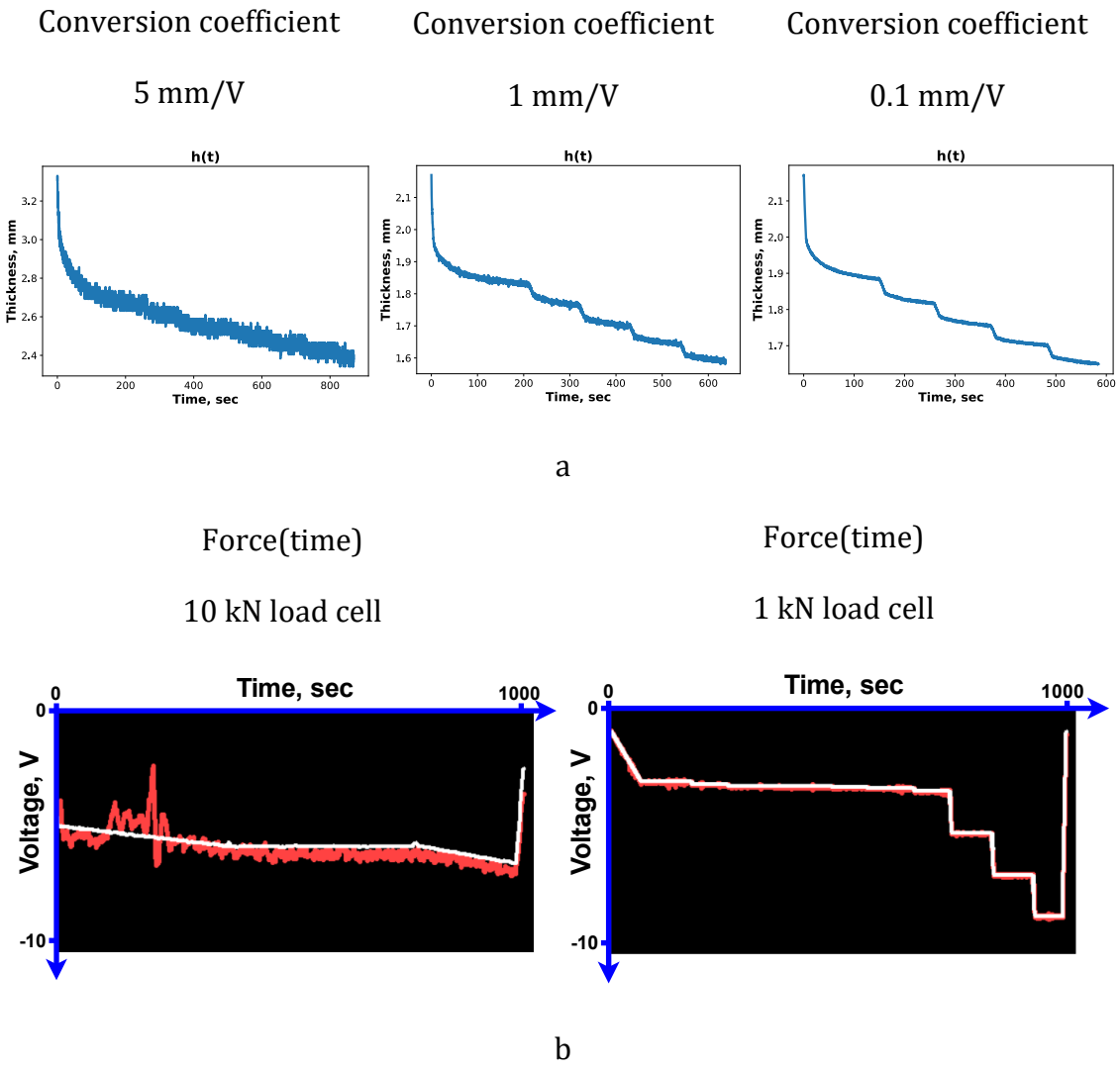

Figure 6.2: Examples of clean and noisy signals. a) compaction curves obtained for different values of the conversion coefficients, b) loading curves for different load cells (1 kN and 10 kN) setups. White curve – what was sent. Red curve – what was applied by the compression machine.

6.1.3 Minimisation of time delay.

When consolidation framework was trialled within a virtual exercise (chapter 5), the transition between load steps was performed instantly without any delay, as shown in Figure 6.3.a. In that case it was possible to put the test "on pause" while waiting for the

framework to process the data and to output the command for the next load step. In case of a real experimentation, such scenario is not possible, as the test must continue during the processing of information from the previous step. Therefore, there is a need for a adding an inter-step waiting time while the framework analyses the compaction response of the material and deciding what should happen with the applied load during this period.

The chosen approach is to keep the load at the steady level as shown in Figure 6.3.b (pink "dwell" region). Changing the load level during processing stage may pose a safety threat, as the data analysis may take more time as expected. This scenario can lead to overloading above the acceptable level and possible equipment damage.

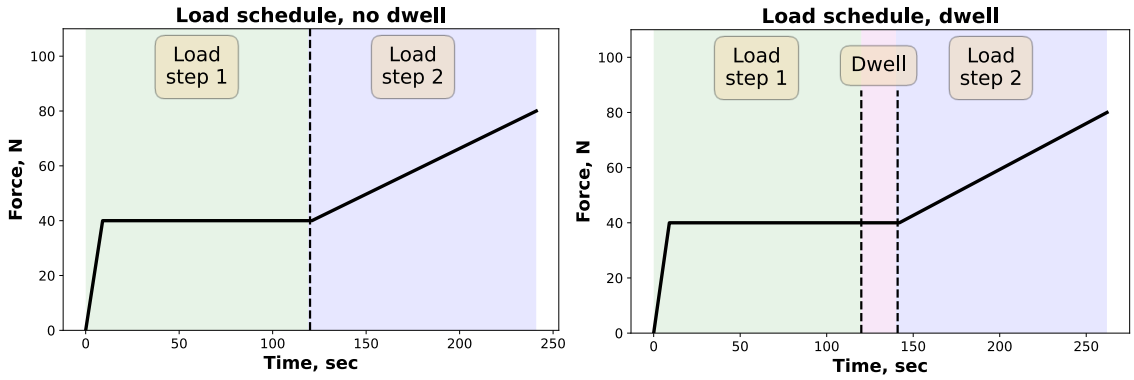

a b

Figure 6.3: a) instant transition from load step 1 to load step 2; b) dwell stage between load steps required for data processing

Although the "dwell stage" compaction data is still received by the framework and used in further analysis, it is necessary to minimise the time delay. The reason for that is that the employed load schedule at this stage is not designed to distinguish between candidate models (as opposed to the "controlled" load schedule at the other stages of the test). The time delay between load steps is present purely for computational purposes. The excessive duration of such "dwell stages" in the resulting load schedule defeats the purpose of a material-driven experimental programme. In such case, the compaction history data used for the load step definition would contain regions which were not aimed for the efficient material characterisation. Moreover, introduction of dwell stages may affect the resulting path of the load curve, because the framework's algorithm might find a different set of favourable candidate models for the provided compaction dataset (as demonstrated in the example in section 3.3). Therefore, measures must be taken to make the transition between load steps as quick as possible.

The duration of the time delay for the load dwell stage reflects the processing speed of the consolidation framework and depends on several factors:

- The complexity of the candidate models (the number of model parameters the complexity of data fitting related to model's non-linearity).
- The number of the candidate models in the library. If the number of candidate models is greater than the number of CPU cores, the framework will not be able to process all models concurrently (as discussed in section 5.1.4).
- The chosen methods for optimisation (the density of the brute stage grid, secondary optimisation method as discussed in section 4.7.1).
- The available hardware for running the framework (PC/laptop).
- The number of data points in the set of the experimental data.

The first four factors were discussed in the previous chapters. The main route to increase the processing speed at this stage of the research is to reduce the number of datapoints in the experimental "raw" dataset. Depending on the model, the compression testing machine yields around 60000 measurements within a 20 min test. Such a dataset's size is excessive for the parameter extraction framework. Before submitting the compaction data to the framework, the "raw" dataset is reduced in size by keeping only every *nth* point (the rest are removed). To find the feasible reduction ratio *nth* (the indication of how many points to save from the original set), a comparative parameter extraction study for different sizes of the dataset was performed.

The baseline "raw" dataset (60000 entries) was reduced to the size of 70, 100, 140 and 200 entries. Time delays for every load step were investigated for each reduced dataset. The comparative timeframe graphs are presented below in Figure 6.4 (the processing time is represented in blue). For all cases the first load step took the longest to process (due to the two-step optimisation, as discussed in the previous chapter). It can be seen from the graphs that starting from the dataset size of 140 points it takes ~30% more time to process the data, while there is no significant difference between 70 and 100 sizes.

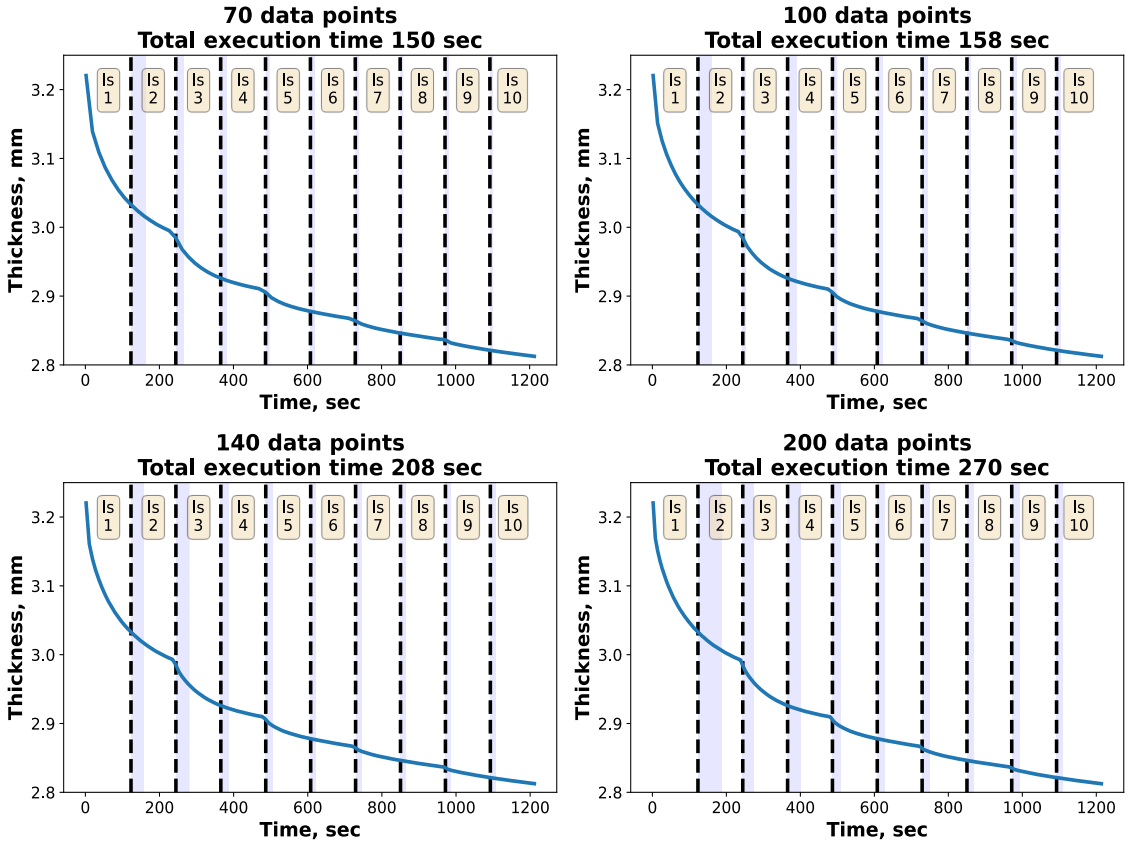

Figure 6.4: Time delay for different dataset sizes. Blue region represents the time required for data processing. Black dashed line is the separation between load steps.

The size of the dataset must be sufficient for the consistent parameters' extraction. If the number of datapoints is too low, some of the characteristic features of the compaction response (which are present in the "raw" data) might be lost. For instance, the stage of the material's elastic response (significant reduction in thickness at the initial stage) occurs within the first moments of the test. Reducing the dataset's size may leave just a few datapoints in this region of the compaction curve (such effect can be seen for 70 points dataset in Figure 6.4, where the curve is not smooth in this region). For this project the size of the dataset was limited to 100 points. It proved to be sufficient for the consistent parameter extraction within acceptable processing time.

It must be emphasized, that the small-sized input dataset may not be the only reason for inconsistencies in the model identification study. As shown in the examples of flawed material characterisation (section 3.3), another reason for the misleading results can be a poorly designed testing load schedule.

6.1.4 Experimental data acquisition setup

The connecting interface of the National Instruments hardware is shown in Figure 6.5. The main parts of the setup include:

- A compact data acquisition chassis cDAQ-9174 which serves to create portable sensor measurement systems. The chassis has four slots for inserting measuring input/output modules. It controls the synchronisation, timing, and data transfer between measuring modules and an external host (PC/laptop). The chassis has 9-30 V power supply port and USB port for connection with the PC/laptop.
- A voltage output module NI 9263. The module is attached to the port №3 of the chassis. Its purpose is to transmit a voltage signal to the compression machine. The signal is transmitted through one channel only, as only the load value is sent. The connection with the testing machine is implemented through the BNC cable.
- A voltage input module NI 9201. The module is attached to the port №1 of the chassis. This module receives a voltage signal from the compression machine. There are two channels employed, as both load and displacement data are received from the compression machine. Similar to the output module, the connection is performed through the BNC cable (2 cables as there are 2 channels).

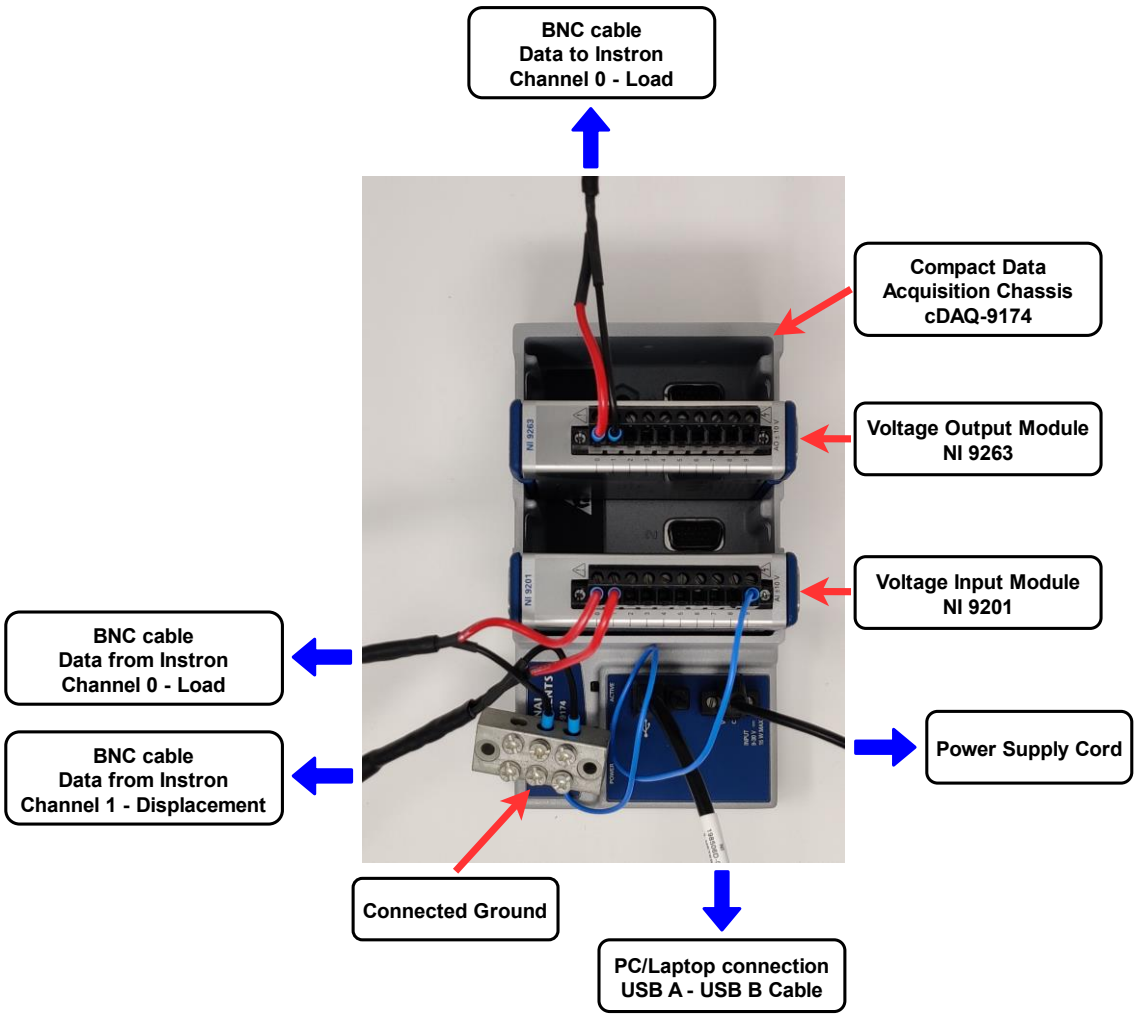

Figure 6.5: National Instruments cDAQ-9174 chassis. Input/output modules.

6.1.5 LabView state machine

The LabVIEW data managing framework is implemented in the form of a state machine. A state machine is a type of program architecture which allows to implement a complex decision-making behaviour. Employing this approach allows the system to adequately respond to the changing input from the experiment.

The core idea is that the framework's operation is represented as a set of different states. Each state has its own designated function. For instance, it could be sending data to the compression machine, writing results file, finishing the test etc. The switch between states is performed when the trigger event happens. A trigger event could be a manual command (pressing the "Start" button) or a condition fulfilment (the designated time for load step is over, the command csv file is detected etc.).

The principal scheme of consolidation framework (Python) – LabVIEW state machine – Instron universal testing machine is shown in Figure 6.6.

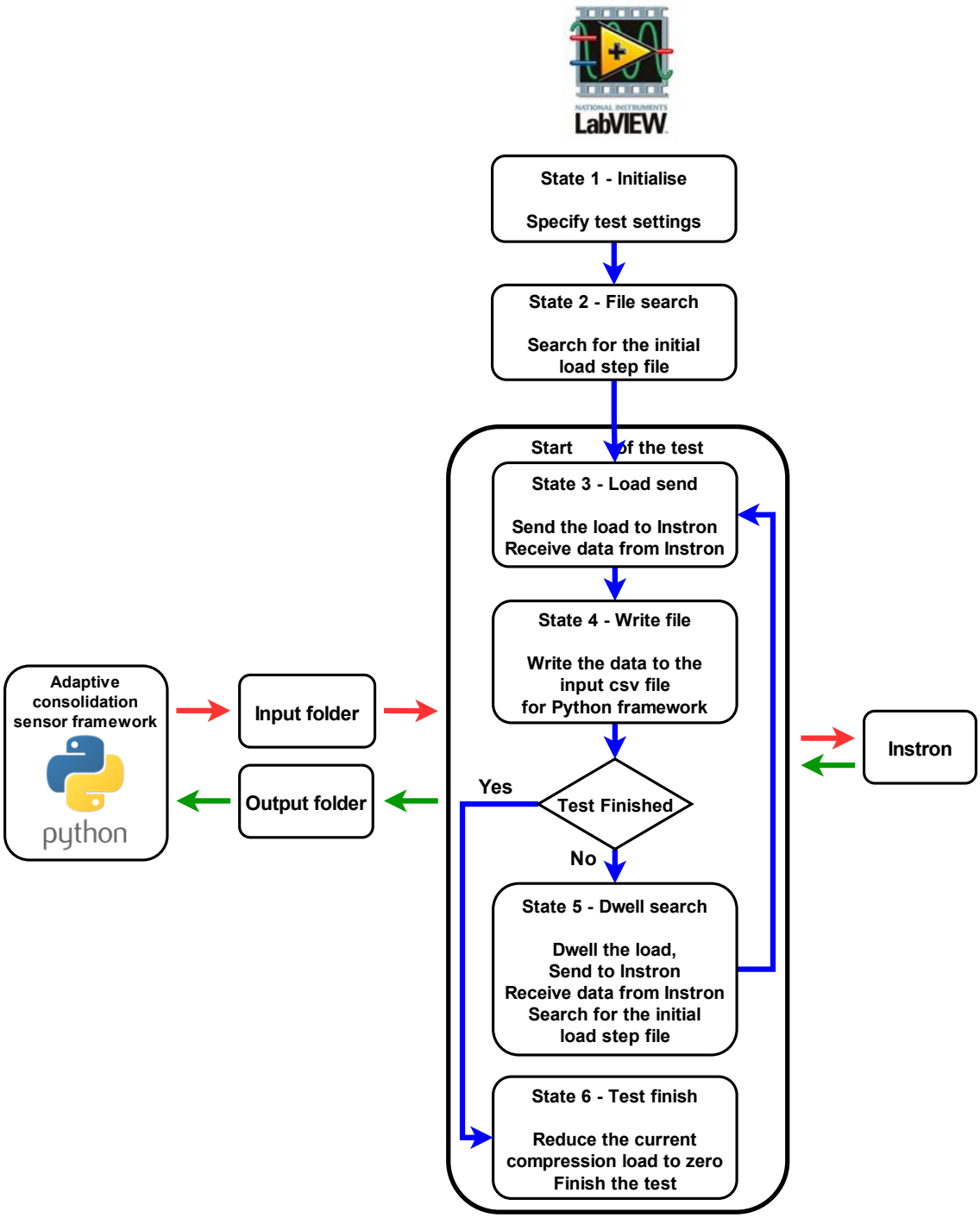

Figure 6.6: LabView state machine overview.

The detailed explanation of each state is presented below:

- State 1. Initialise.

  This state is executed prior to the experiment. The purpose of it is to specify the initial settings for the test, including:

  - The number of load steps.
  - Data update rate (discussed above).

- Force-to-voltage conversion coefficient, V/N.
- Unloading time – this parameter indicates how fast the compression force will be reduced to zero upon the completion of the testing.
- Specifying input/output channels on the NI data acquisition hardware.

After all settings are initialised, the system switches to the next state.

- State 2. File search.
  At this state the LabView framework is searching for the csv file with the commands for the initial load step. The file is generated by the Python framework. As soon as the file is detected in the designated location, the characterisation test is commenced. The rest of the test is conducted entirely in autonomous mode. The detection of the command file serves as a trigger to switch to the State 3.

- State 3. Load sending.
  The load values (converted to a voltage signal) are sent to the compression machine with the specified update rate. Concurrently, the machine's feedback with the compaction data (time/displacement/load) is received. The framework transfers to the next State 4 as soon as the last load command from the csv file is performed (meaning that the current load step is over)
  During State 3 the Python framework (not a state machine) is constantly searching for the csv output file with the experimental data to process.

- State 4. Write file.
  This state is always executed in the end of each load step. The LabVIEW framework creates an output csv file with the experimental data at the designated location. This file serves as an unput for the adaptive consolidation sensor framework (Python).
  After creating a results file, the framework checks the condition if there are any more load steps left to execute. If so, the system transfers to the next "State 5 Dwell search". Otherwise, the system moves to "State 6 Test finish", as the experiment is completed.

- State 5. Dwell search.
  The main objective of this state is to allow the adaptive consolidation framework (Python) to process the incoming experimental data and output the command for

the next load step. While the data is processed, the load on the compression machine is kept steady at the last recorded load level (hence, dwell).
When the LabVIEW framework detects the command csv file, the state machine is switched to “State 3 Load sending” again, as the next load step begins.

- State 6. Test finish.
  When the last load step is performed, the system automatically unloads the specimen. The unload rate is specified by the researcher at the Initialise state (State 1). Upon the unloading completion, the software ceases its operation.
  For the sake of safety, this state can be triggered manually at any point of the test by pressing the “Stop” button in the framework’s interface. Additionally, the test can be stopped physically by activating the red “Stop” switch on the compression machine.

6.2 Experimentation

6.2.1 Testing apparatus

The universal testing machine used in the previous experimentation for exploring data-rich loading programmes (chapter 4) does not have a functionality to receive an input control signal due to the absence of an analog input port. For that reason, the autonomous real-time experimentation was performed on the servohydraulic Instron 8872 machine. It imposes changes on all parts of the testing rig as the fixtures are not compatible between different versions of testing machines. The setup used for autonomous testing is discussed below (shown in Figure 6.7).

The lower heater platen was attached to the external cantilever beam load cell (1 kN capacity) which was installed on the angle plate. The default 25 kN load cell does not provide the required resolution for the load control experimentation due to the PID controller’s limitations (see the example of noisy load control above in Figure 6.2.b). The upper platen was placed on a lower one before locking into the hydraulic grip to avoid platens misalignment (unlike the setup described in chapter 4 where the platens were mounted on extension rods). Controlling thermocouples were attached to both platens. The data acquisition hardware (not shown in Figure 6.7) was connected to the analog input/output ports of the Instron’s data logger.

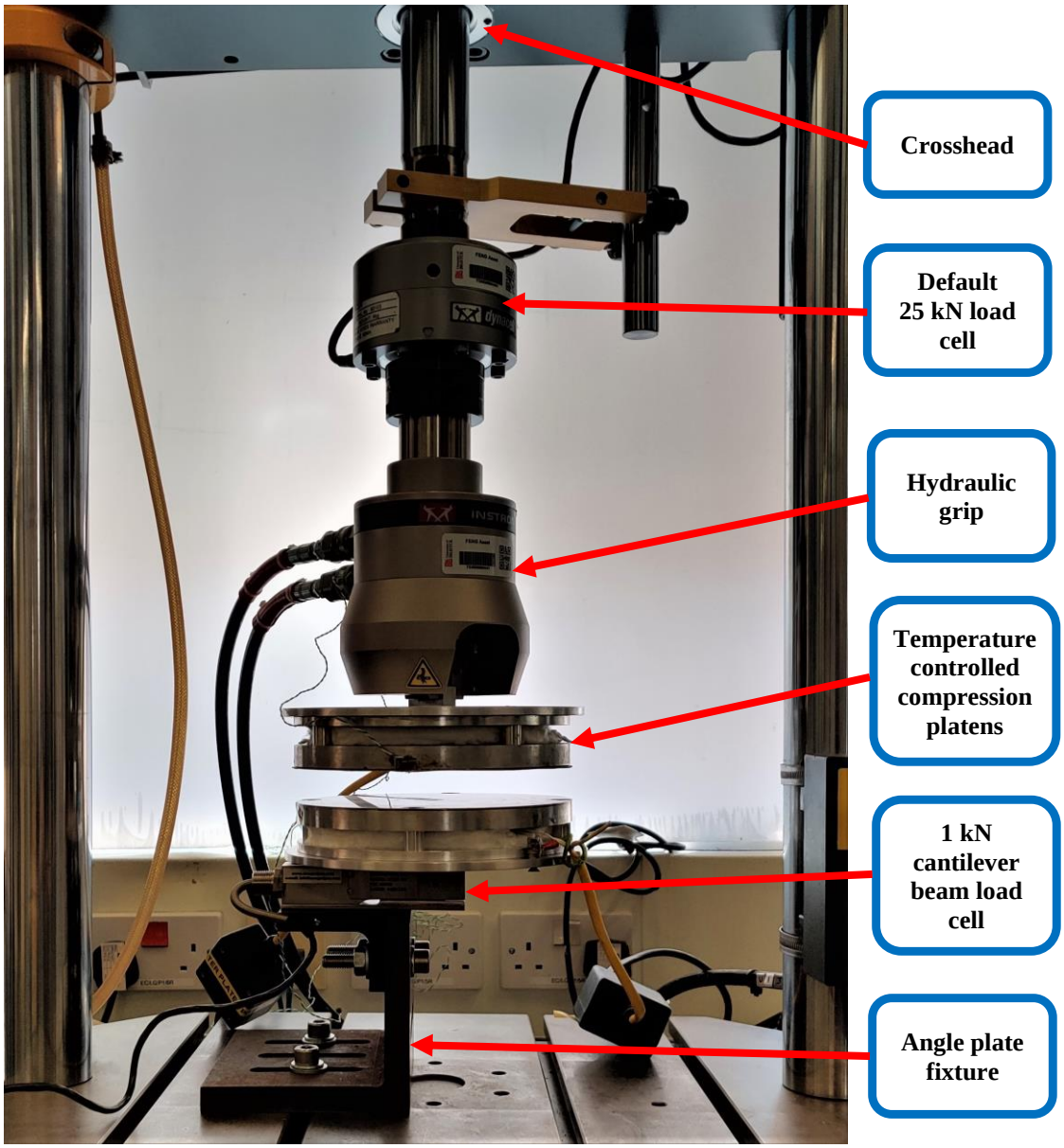

Figure 6.7: Compression heater platens, cantilever load cell, fixture.

Due to different actuation mechanism, the hydraulic compression machine operation differs from the electromechanical one. The machine can be used in low (for adjusting position) or high (for applying force) pressure modes. This switch between position and load control modes must be performed explicitly on the control pad.

The used model of Instron (hydraulic 8872) does not allow to set the relative value of the crosshead's displacement to zero (like most modern versions) and always operates in absolute values. For that reason, the level of Instron's crosshead must be adjusted prior to the experiment to achieve the initial value of the displacement as close to zero as possible. This requirement is due to the displacement-to-voltage conversion. As shown in the example above (see the example in Figure 6.2.a), the encoded value of the

measured parameter should lie between 0 and 10 V. If, due to the crosshead's position, the initial displacement value is high (in comparison with the specimen's displacement), the encoded value of the measured displacement will take a fraction of a voltage signal's amplitude. The following example illustrates this problem in more detail. For instance, the initial displacement of the crosshead is set to 50 mm and the specimen's displacement is 1 mm. If we assume that the initial displacement corresponds to 1 V signal, then the combined specimen's and initial displacement (51 mm) would correspond to 1.02 V signal. The whole data transfer takes 0.02 V amplitude instead of 10 V. Therefore, to avoid the contamination of data with noise (as shown in Figure 6.2.a), the initial displacement should be comparable (or less) with the displacement of a specimen.

Since the experimentation is performed in a real-time load-controlled mode, it is necessary to ensure that the applied load follows the designed schedule. It is done through tuning of the machine's PID controller. Depending on the specimen's stiffness (hence, different reaction to compression), properties of the PID controller may vary. The compression machine allows to run an auto-tuning routine to find the best set of the required PID parameters for a given type of a tested specimen.

6.2.2 Testing methodology

There is a number of compulsory procedures that must be carried out prior to experimentation:

- Setting the target temperature of the heater platens. In line with previous work (chapter 4) each specimen was tested at a constant temperature of 60℃. Normally, the heater controller overshoots the target value of the temperature by ~5℃. For that reason, it is necessary to let the temperature balance to establish.
- Due to the high sensitivity of the employed load cell, it is necessary to balance it (set to zero) to compensate the weight of the lower compression platen.
- Launch Python and LabVIEW frameworks on the laptop/PC.
- Specifying the required settings in the LabVIEW framework (State 1, described above).
- Setting Instron's safety limit for the compression load (500 N for the current experimentation). If the actual load exceeds the safety value for any reason

(operator's error, error in PID load control causing the system to lose balance etc.), the test will be automatically stopped.

The abovementioned procedures are executed only once at the preparation stage. The step-by-step sequence of actions during experimentation is presented below:

- Then, the test batch is covered in the release film (same as described in chapter 4) and installed inside the compression plates. It is important to place the specimen in the centre of the platen. An offset in placement causes the appearance of an eccentric force (hence, bending moment). High sensitivity of the load cell may cause inconsistency in load control and trigger safety limits.
- While in position control mode, the location of the upper platen is adjusted to be closer to the specimen's surface.
- Then, the compression machine is switched to the load control mode. A precompression load (0.1 N) is applied to establish the initial contact between the specimen's surface and the top platen.
- The Instron is set into "the listening mode". In this mode the machine follows the commands received through the specified source (in case of the current project it is the analog port).
- The adaptive consolidation sensor framework (Python) generates the csv file with load schedule commands for the first load step. The LabVIEW framework detects it, and the test continues in automatic mode after this point.
- After the test is finished (the last load step is executed) and the unloading sequence is performed, the specimen is retrieved from the compression platens and its final thickness is measured.

6.2.3 Studied materials

The real-time experimentation was performed for three different material systems:

- IMA/M21 toughened prepreg. This material was used for the identification of the data-rich testing programme in chapter 4. The shape and the layup of the cross-ply specimen remained unchanged. Manufacturing details and the rationale for the crucifix shape are discussed in chapter 4. The test sample is shown in Figure 4.2.

- IM7/8552 prepreg [176]. The test sample is shown in Figure 6.8.a. The prepreg material has a nominal cured ply thickness of 0.131 mm and 57.7% fibre volume fraction. Like IMA/M21 test batches, all specimens were laid-up in 16 plies cross-ply (CP) configuration $[90/0]_8$ with a total thickness of ~2.17 mm.
- Dry fibre material. This type of the material was chosen to trial the consolidation framework within the material which is not represented in the consolidation library. There were two material systems trialed:
    - ampliTex 5040 flax fibre twill weaved fabric [177] with a ply thickness of 0.48 mm. The specimens were laid-up in 8 plies cross-ply (CP) configuration $[90/0]_4$. The specimen is demonstrated in Figure 6.8.b.
    - Carbon fibre non-crimp fabric (NCF) with a ply thickness of 0.86 mm. The specimens were laid-up in 6 plies cross-ply (CP) configuration $[90/0]_3$. The specimen is demonstrated in Figure 6.8.c.

  Due to the absence of resin, plies did not stick to each other. Hence, it was not possible to prepare samples in advance (like samples made of IMA/M21 and IM7/8552 materials). For that reason, dry samples were laid up right on the surface of the lower compression platen prior to the experiment. Such approach to samples preparation, as well as the absence of resin, introduced a variability in the specimens' structure – the plies were not perfectly aligned. This problem is addressed in the experimentation section of this chapter. It is important to emphasise, that due to the absence of resin phase there was no particular reason to manufacture dry specimens in a crucifix shape (the rationale for this shape is discussed in chapter 4). Nevertheless, it is done for the sake of consistency with the previous experimentation.

The compaction area of the crucifix specimens for all types of material was chosen to be 15 x 15 mm to be consistent with the previous work.

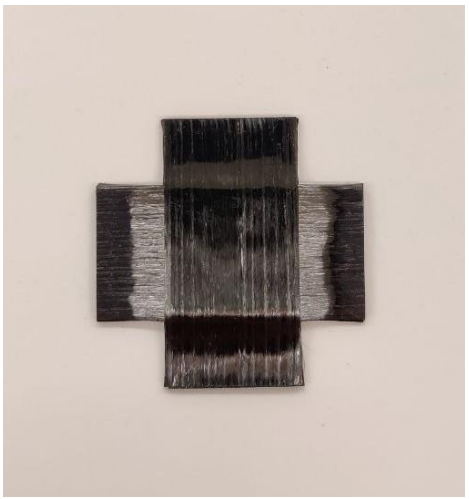

a

b

c

Figure 6.8: a - IM7 test sample; b - ampliTex 5040 flax fibre twill weaved fabric; c – carbon fibre NCF test sample

6.2.4 Material testing. Results and discussion

There are several framework settings which can affect the load routing of the resulting testing programme:

- The form (monotonic or ramp-dwell), amplitude, and duration of the initial load step.
- Load step parameters: the number of the considered load step options (see Figure 5.2), the duration of a single load step, the maximum possible load amplitude within one load step, the total number of load steps.
- Optimiser's parameters (brute optimisation grid density, secondary optimisation method). These settings affect the processing time, hence the duration of the load dwell stage (see section 6.1.4).

Different test settings were explored within the experimentation on three types of materials. The goal was to investigate the framework's output (resulting loading programme) and candidate models ranking in dependence on the different load/strain rates and reached compaction level of the studied material. A more thorough discussion on the specified parameters of the tests for each case can be found below.

In line with the previous work conducted within this research, the temperature for the experimentation for all specimens was set at 60℃ (temperature where both shear and percolation flows may occur explicitly). The experimental results for three different material systems are presented below.

Testing of IMA/M21 material samples.

Both monotonic and ramp-dwell initial load step options with the load amplitude variation between 40 N and 50 N were explored for testing of IMA/M21 material samples. The load amplitude within following steps was varied between 20 N and 50 N. The duration of a single step was specified in range 30 - 80 sec. The framework had a choice of 5 different load options at the end of each load step (dwell option, 2 ramp-dwell options, 2 monotonic options – see Figure 5.2). The summary of all performed tests is presented in Table 6.1. The resulting real-time test programmes along with the corresponding compaction response of the material are presented in Figure 6.9.

Table 6.1: Explored test settings for the real-time testing of IMA/M21 material. RTT stands for real-time test.

Test id	Initial load step		Further load steps		
	Load amplitude, N	Loading regime	Maximum load amplitude, N	Step duration, sec	Number of load options
RTT_M21 1	40	Ramp-dwell	20	60	5
RTT_M21 2	40	Ramp-dwell	50	30	9
RTT_M21 3	50	Monotonic	40	80	5
RTT_M21 4	50	Ramp-dwell	20	60	5

All resulting test programmes for IMA/M21 material demonstrated a similar trend. The load reached a certain level (~50 N for tests RTT_M21 1, 3 and ~100 N for tests RTT_M21 2, 4) in 1-3 steps and held steady. Within the last 3-4 load steps the load started to raise again. This phenomenon had an interesting implication for the candidate models ranking, as it will be shown below in the step-by-step parameter extraction breakdown.

Closer to the end of the test RTT_M21 2 (at ~1000 sec of the test) a local spike in the load feedback can be observed. Such effect is the result of the instability in the load PID control. As it can be seen from the compaction curve (black curve), the amplitude of the load spike was not significant enough to affect the thickness feedback. Due to the high-resolution of the load cell and properly adjusted load-voltage conversion (see section 6.1.2) such phenomenon is rare and does not cause a detrimental effect on the experimental results (as shown in Figure 6.2.b).

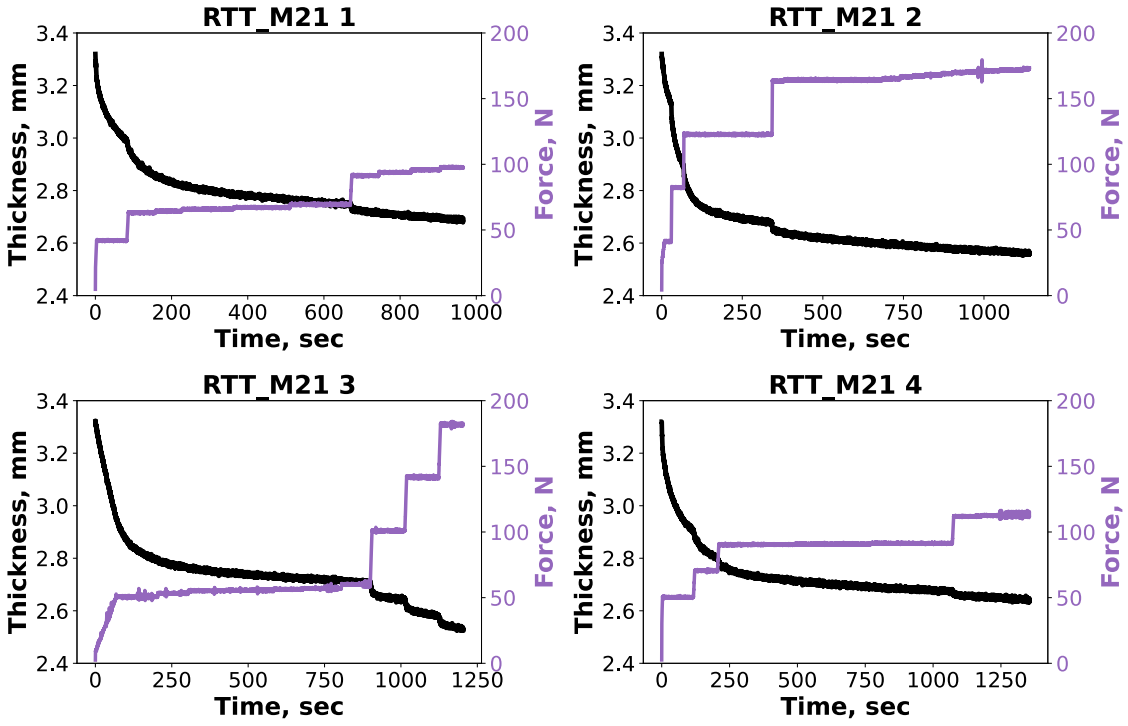

Figure 6.9: IMA/M21 material testing. Resulting loading programmes and compaction curves.

Similarly to the characterisation exercise in a virtual space (chapter 5), the sequence of the parameter extraction steps for a chosen test (RTT_M21 3) is shown in Figure 6.10. Each graph is complemented with the preliminary candidate models ranking and the processing time required by the framework.

Upon the completion of the initial step, the framework defined the shear and the percolation models as top two candidates. The shear model was successfully reflecting the material's compaction response up to the second stage of the load ramp within the last three load steps (red curve, load step 7). After the change in the load pattern, the shear model struggled to output a robust prediction and showed a significant deviation from the material's thickness evolution curve.

An interesting observation is that the framework defined a non-optimal set of material parameters for the DefGen model (purple compaction curve) after the first load step. The model demonstrated a significant offset from the experimental data and was ranked fourth. The model's parameters set was corrected within further load steps and two best candidates (DefGen and percolation) were defined in the end of the test. Such effect shows the advantage of the employed approach, when the model definition is refined at each load step with regard to the previously obtained results.

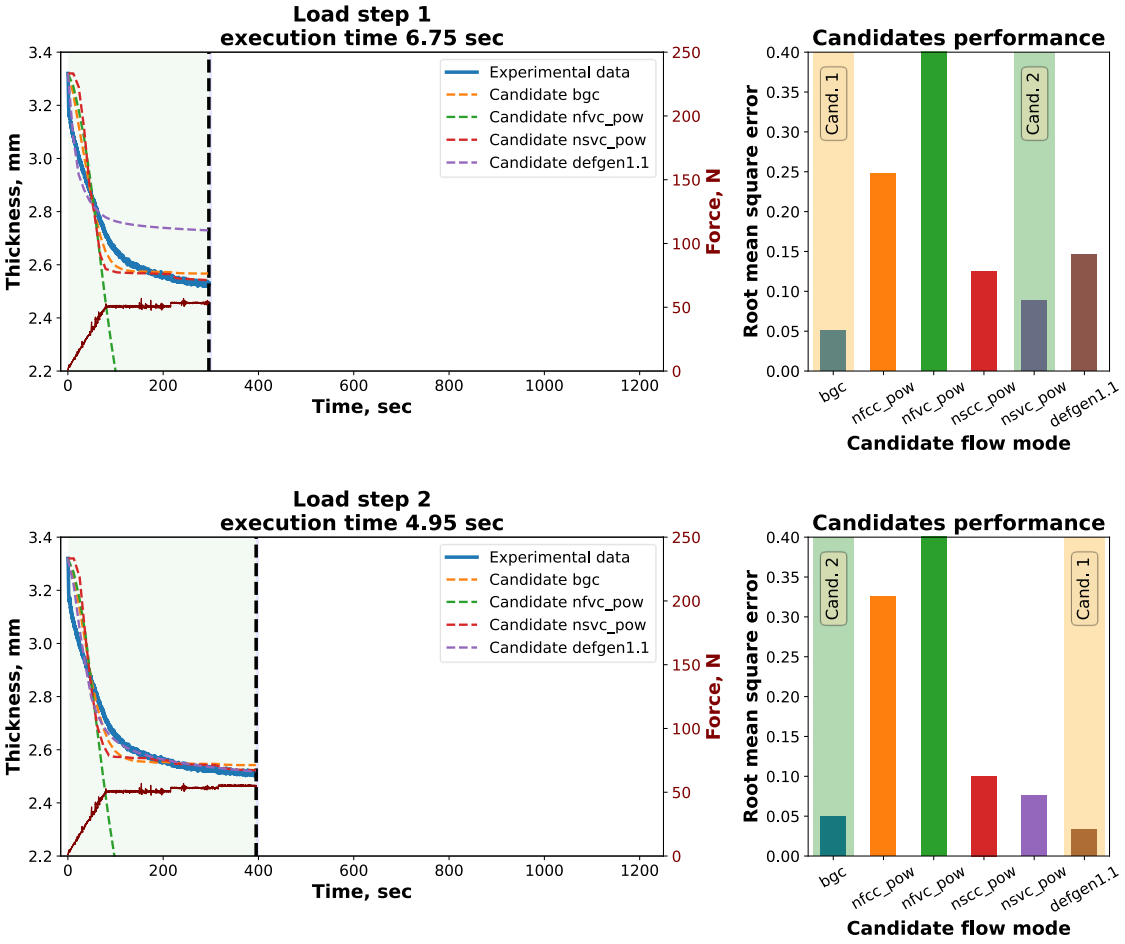

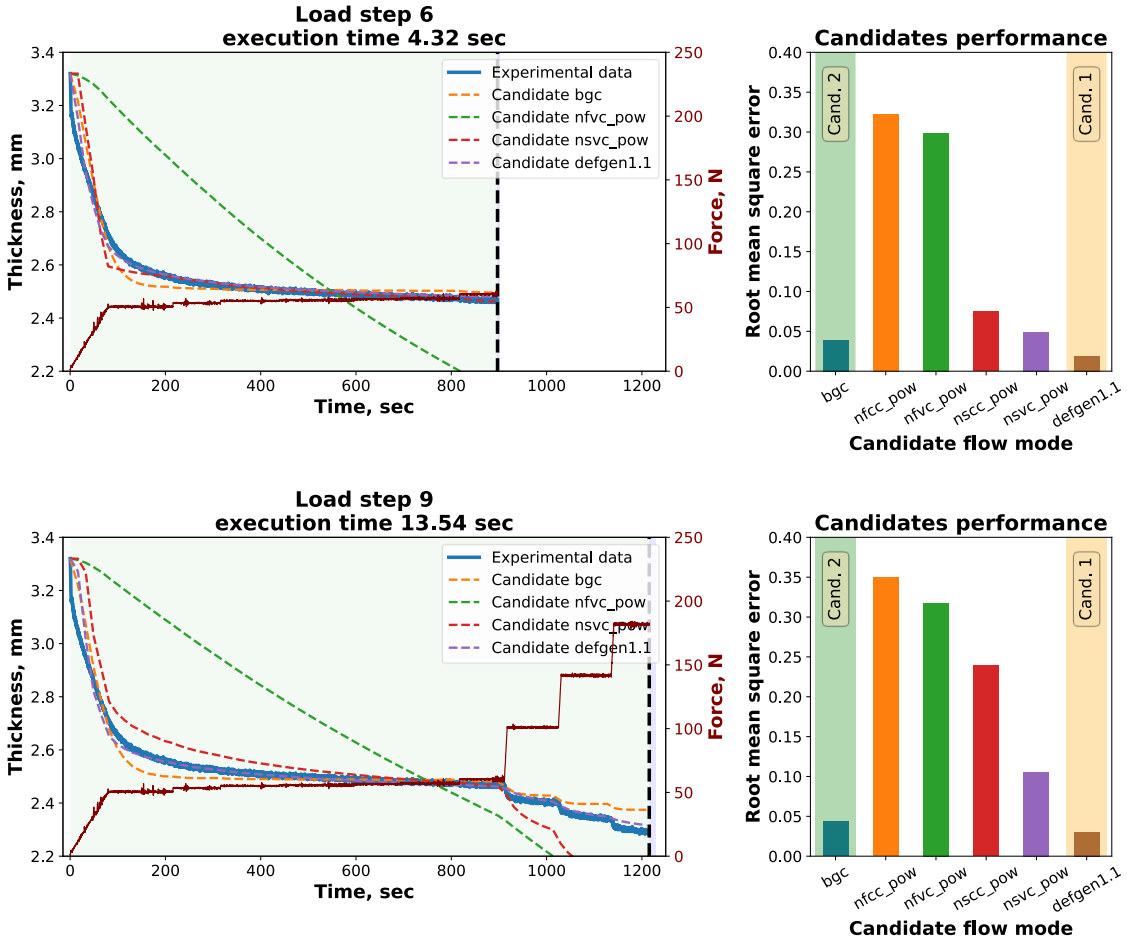

Figure 6.10: IMA/M21 experimentation. Step by step routine. Green region – all previously received data. Blue region (on the right from the vertical black dashed line) – required processing time.

The results of the models' training for all four tests are presented in Figure 6.11. For the sake of clarity, only four candidates are shown (along with the experimental data) on the graphs. It can be seen that the second-best candidate (percolation, "bgc") showcased a very close output in comparison with the DefGen model with a slight deviation in the value of the final thickness. The shear model ("nscc") also demonstrated a good fit until the point of the load trend changed in the second half of the test (as discussed earlier).

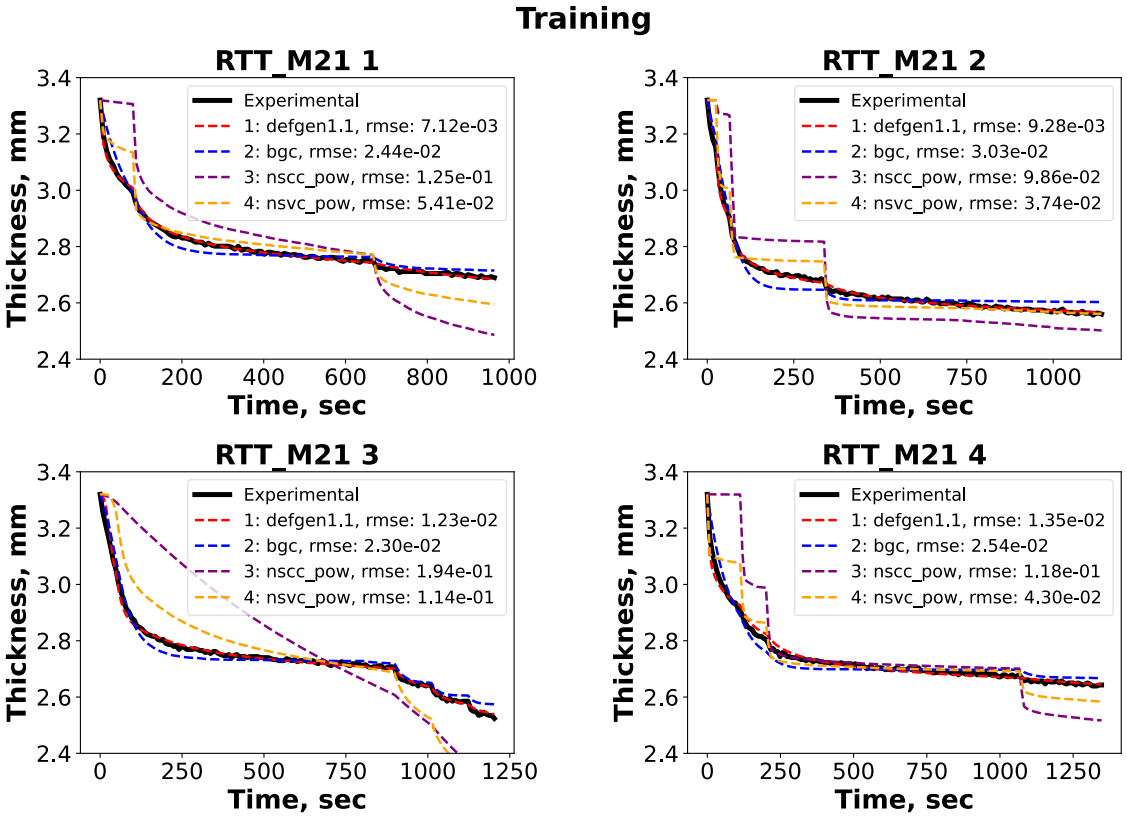

Figure 6.11: IMA/M21 material testing. Training results.

Previously in this thesis (see chapter 4), the IMA/M21 material was subjected to 15 characterisation tests with predefined loading programmes. Three tests (1, 4, 7) were selected to train the candidate models and the rest of the tests were used for model's validation. To estimate the effectiveness of the proposed adaptive testing approach, the derived material models within each real-time testing programme (RTT_M21 1-4) were trialled on a validation set of data obtained for the exploring data-rich testing programmes (chapter 4). The validation results of these models were compared with the model for the predefined training combination (1, 4, 7). Only fully populated training combination (1, 4, 7) was used for comparison, as it was better for predicting material's response than less diverse sets (1, 4), (1, 7), (4, 7) etc. The ranking bar chart of the real-time test programmes and predefined tests combination (1, 4, 7) is shown in Figure 6.12.

It is shown that the model based on fully populated training combination (1, 4, 7) performs better on the validation data set than models obtained within the real-time approach. However, the second- and the third-best real-time tests (RTT_M21 2 and RTT_M21 1) demonstrated better data fit than two-test (1, 4), (1, 7), (4, 7) training combinations (not showed in the bar chart in Figure 6.12, can be found in Figure 4.12).

As discussed in chapter 4, the maximum error raise for double-test combinations (1, 4), (1, 7), (4, 7) was 8.6% which is higher than 5.5% and 6.5% for tests RTT_M21 2 and RTT_M21 1 respectively. The worst result for deterministic tests ((4,) training combination as per Figure 4.12) was 27.3% which is more than twice higher than the least effective result for the real-time test RTT_M21 4 (error raise 13.3%). It is possible to conclude, that within the conducted experimentation for IMA/M21 material the real-time tests were more effective than the majority of double- and single-test deterministic alternatives. Nevertheless, the fully populated dataset (1, 4, 7) still yielded a better result than the rest of the tests.

It is important to emphasise, that for this material system the tests with predetermined and real-time programmes were performed on different equipment setups (as discussed in section 6.2.1). The change of the equipment may introduce systematic discrepancies in the results. For instance, as discussed in the previous chapters of this thesis, the permeability measurements between different research groups showcased deviations from each other [107], [108]. If the equipment introduces any bias (platens misalignment, load cell or temperature control measurement error etc.), the candidate model will reflect it in its behaviour upon the completion of the training process. Consequently, the model will not perform well on the validation dataset obtained on a different equipment setup. Both adaptive and deterministic testing of the next material system IM7/8552 was performed on the same equipment setup. The findings indicated a different trend in the results, which will be discussed later in this chapter.

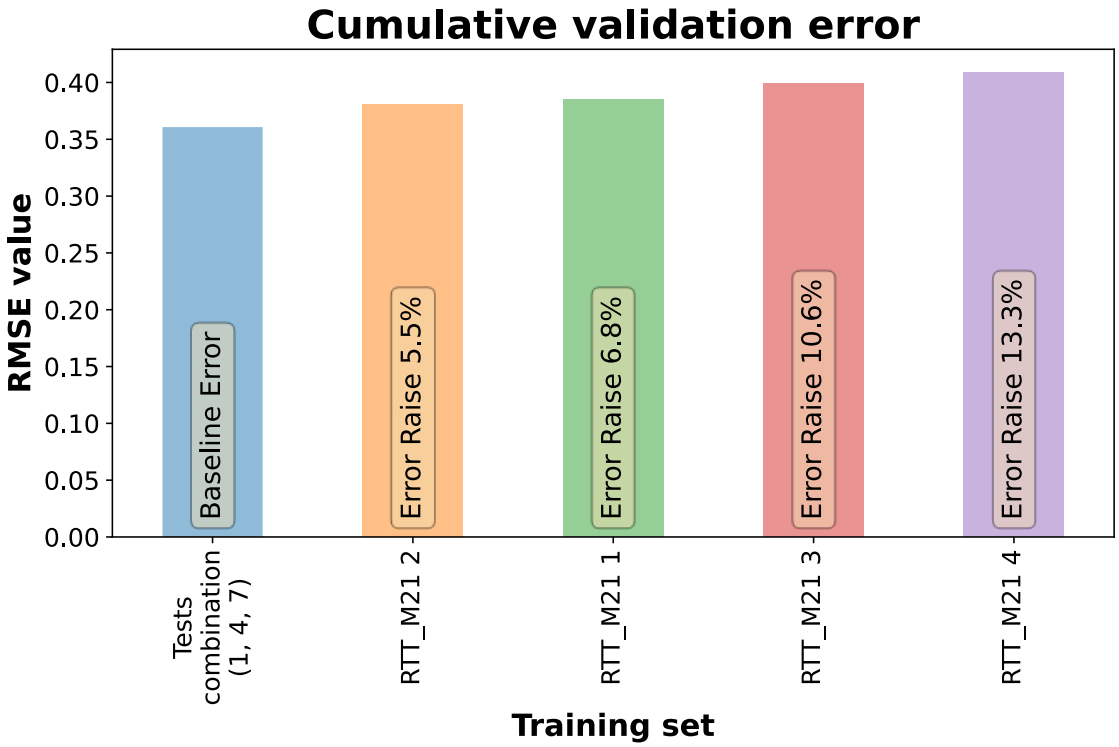

Figure 6.12: IMA/M21 material testing. Candidate models' ranking for different test programmes.

The resulting thickness predictions for all derived models within the validation set are shown in Figure 6.13. It can be seen on the graphs that for certain validation tests the real-time candidate models were less effective in producing a realistic prediction (tests 3, 6, 9, 10, 12) and produced an offset from the experimental data. The validation for these tests made the most contribution to the cumulative error of the real-time models reflected in the bar chart above. For the validation tests 5, 8, 11, 14, 15 the prediction capability of the real-time models was on the same level as for the fully populated deterministic model (1, 4, 7) – the compaction curves overlapped with the experimental data. For the tests 2, 11, 13 the prediction of the real-time models was more accurate and showed no deviations from the material's response in comparison with the deterministic model.

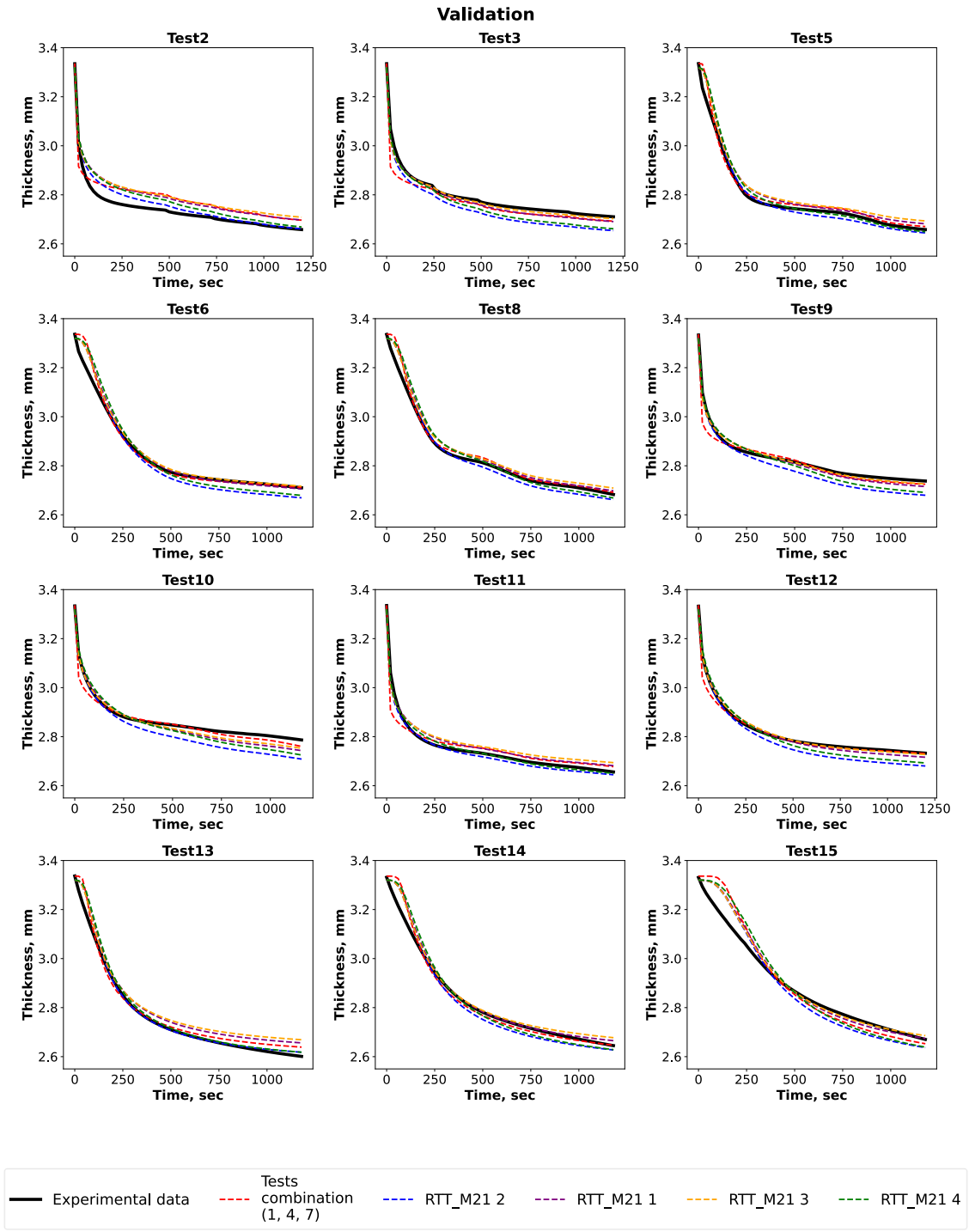

Figure 6.13: IMA/M21 material testing. Candidate model's validation.

The resulting sets of material parameters for all models are presented in Table 6.2 below. For all testing programmes the framework consistently identified the DefGen model as the most relevant model to represent the material behaviour. The material parameters' values for the real-time candidate models were consistent with a maximum deviation of 6.6%, 1.1%, and 2.0%, for the parameters *a*, *b*, and *k* respectively. On the other hand, the maximum difference between real-time and deterministic models' parameters was 34.7%, 12.2%, and 2.4% (for *a*, *b*, and *k*). The largest discrepancy in

parameters was registered for the material parameter *a*. The possible reason for this is the existence of the optimal parameter's value for the considered model and the input dataset. As it was shown in the residual function's correlation graph in Figure 5.7, the correlation between the value of parameter *a* and the residual function (the minimised value of the error in thickness prediction) is a flat curve (meaning that the parameter *a* does not have a significant impact on the solution). For the framework's optimiser it means that there is no well-pronounced global/local minimum (in comparison with *b* and *k* parameters on the same graph Figure 5.7, where the global minimum is well established). For that reason, it becomes challenging for the framework to define the optimal value of this parameter. The shape of the correlation function depends on the employed material model (its mathematical representation) and the input dataset for the model's training. Another possible reason for the difference in material parameters between deterministic and real-time models could be the influence of the equipment change (as discussed earlier). This problem is addressed in the testing of the next material system, where the testing rig remained the same throughout the experimentation.

Table 6.2: Candidate models' parameters for deterministic and real-time characterisation programmes. Studied material system – IMA/M21.

	Model type	Parameter 1	Parameter 2	Parameter 3
Tests combination (1, 4, 7)	DefGen	a: -0.8283	b: -13.87	k: 0.8124
RTT_M21 2	DefGen	a: -0.6026	b: -12.28	k: 0.8211
RTT_M21 1	DefGen	a: -0.6091	b: -12.42	k: 0.8297
RTT_M21 3	DefGen	a: -0.6277	b: -12.66	k: 0.8329
RTT_M21 4	DefGen	a: -0.6453	b: -12.39	k: 0.8168

Testing of IM7/8552 material samples

The testing procedure of IM7/8552 material followed the same pattern as the characterisation of the previous material system. At first, a series of real-time tests with different framework's settings were conducted, and the candidate material models were trained. The obtained results were then trialled against the conventional testing approach with predefined loading programmes. Both real-time and deterministic tests were performed on the same equipment setup. Similarly to the previous exercise, both monotonic and ramp-dwell initial load step options with the load amplitude variation between 40 N and 80 N were explored. For further load steps the load amplitude was varied between 20 N and 50 N for the duration of 70 sec and 100 sec. The number of possible load options remained the same (5 options) as in the previous testing for IMA/M21 material. The summary of all performed tests is presented in Table 6.3. Four resulting real-time programmes and the corresponding compaction response of the material samples are presented in Figure 6.14.

Table 6.3: Explored test settings for the real-time testing of IM7/8552 material. RTT stands for real-time test.

Test id	Initial load step		Further load steps		
	Load amplitude, N	Loading regime	Maximum load amplitude, N	Step duration, sec	Number of load options
RTT_IM7 1	60	Ramp-dwell	20	70	5
RTT_IM7 2	40	Monotonic	40	100	5
RTT_IM7 3	40	Monotonic	50	100	5
RTT_IM7 4	80	Monotonic	50	100	5

The shape of the resulting loading programme was shown to be consistent for all performed tests. Upon reaching a certain level (120 N for tests RTT_IM7 2, 4 and ~160-170 N for tests RTT_IM7 1, 3), the load held steady until the end of the experiment. As before, the shape of the loading schedule had a direct implication for candidate models ranking, which will be discussed below. An interesting observation is that the framework proposed both monotonic and ramp-dwell load step options (for the

steps following the initial one) for the test RTT_IM7 3, which was not observed in the previous experimentation.

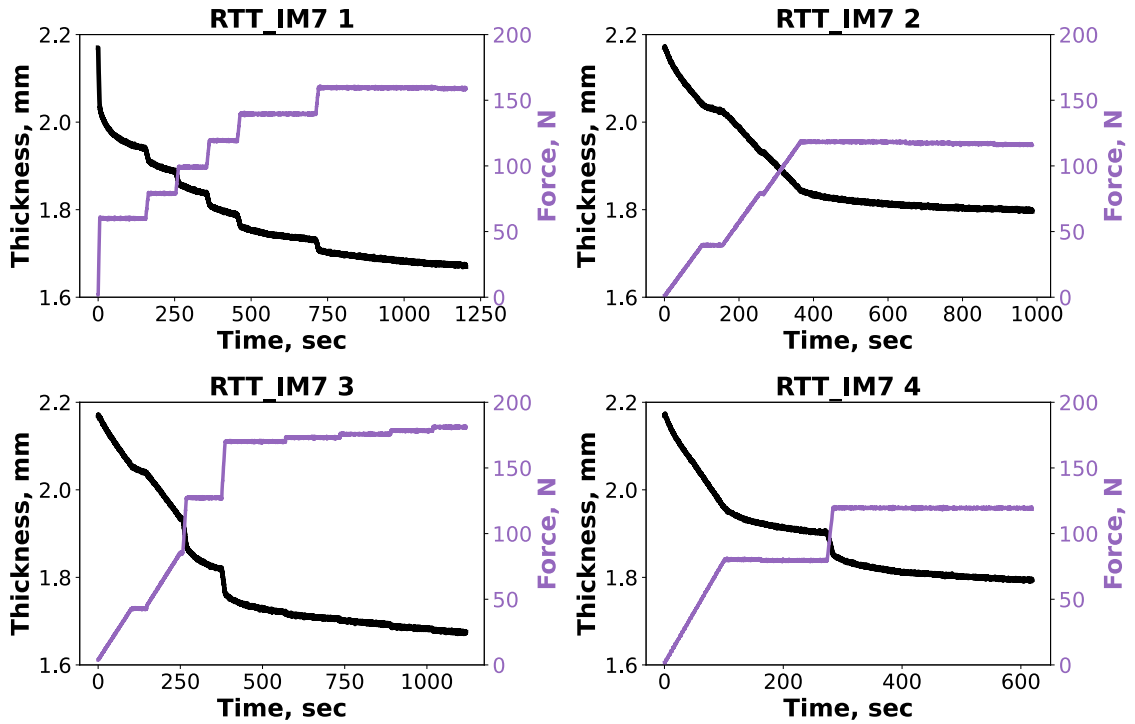

Figure 6.14: IM7/8552 material testing. Resulting loading programmes and compaction curves.

The step-by-step parameters extraction routine breakdown for the test RTT_IM7 3 for IM7/8552 material samples is shown in Figure 6.15. The framework identified two-best candidates as percolation and DefGen models. During the first four steps where the load level was raising, the percolation model showcased a more accurate fit and was selected as the first candidate (see the models ranking bar chart in Figure 6.15). Shear models were also able to reflect the changing compaction response for the first two load steps, before the test programme became too complex. But, as the programme evolved to the load hold (second half of the test), the DefGen model managed to output a more accurate prediction for the material's behaviour. As a result, it was chosen as the first candidate in the end of the test. It must be emphasised, that the second-best percolation model candidate's performance was close with 3.2% error raise from the best candidate. As it will be shown later in this section, the framework chose percolation model as the best candidate after processing the validation data for one of the real-time tests (test RTT_IM7 4).

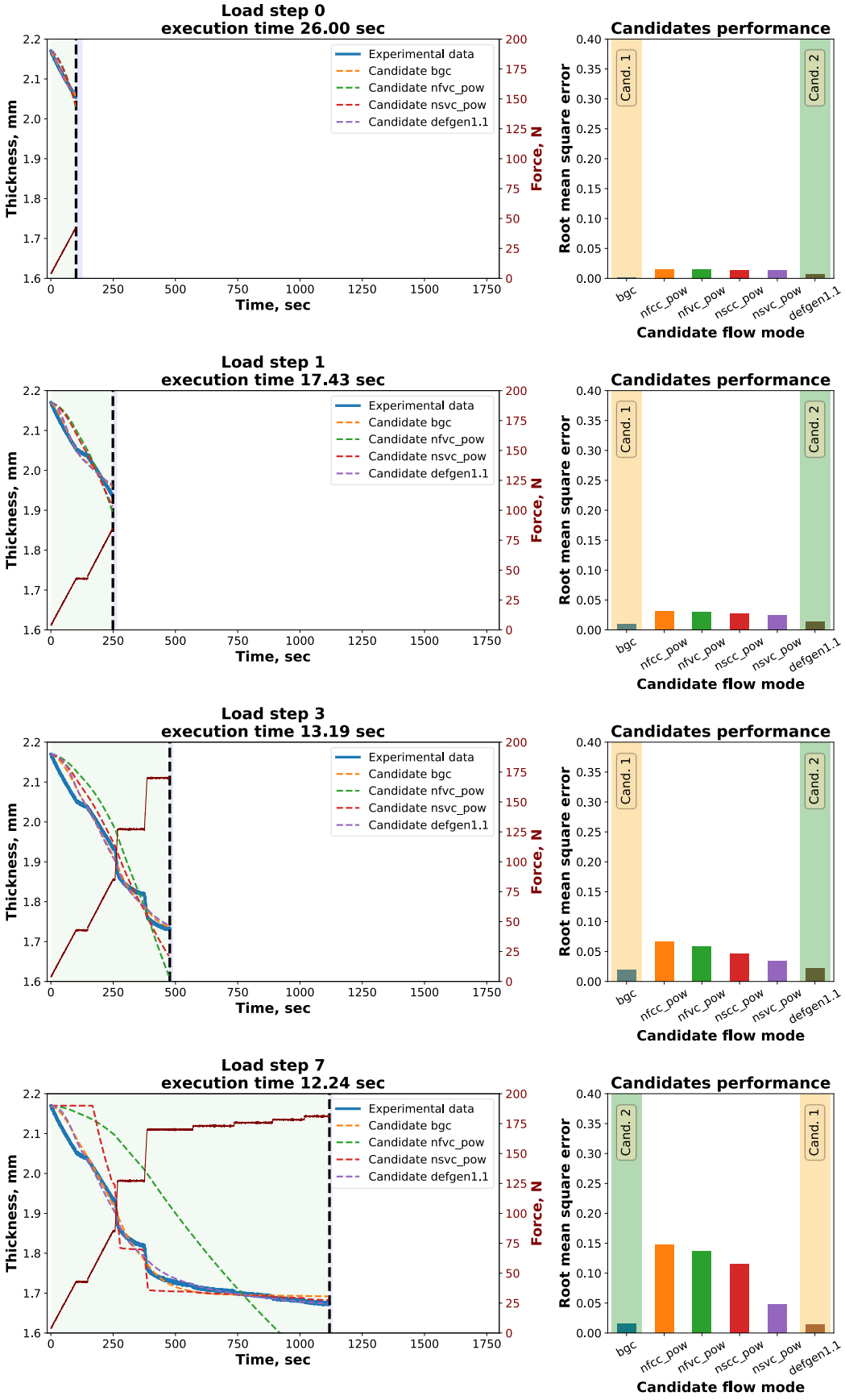

Figure 6.15: IM7/8552 experimentation. Step by step routine. Green region – all previously received data. Blue region (on the right from the vertical black dashed line) – required processing time.

The results of the models' training for all four tests are presented in Figure 6.16 (only four candidates are shown for each test). The second-best candidate was also able to capture the material's behaviour (especially for tests RTT_IM7 2 and RTT_IM7 3) with the error raising by 3.2% and 16.5% in comparison with the best candidate DefGen. The resulting shear models produced a visible offset from the experimental data.

Since the pool of candidate models remained the same for all experiments performed within this research, it is interesting to compare the training results between IMA/M21 and IM7/8552 material systems. The training results for IM7/8552 were less accurate on average by 27%. As it can be seen from Figure 6.16, the main contribution to the training error was introduced from the experiment stages with monotonic load increase, where top candidate models failed to fit the compaction feedback accurately. For the IMA/M21 material such phenomenon was not observed. This is an indication of the material models' limitations to reflect the considered material's behaviour for the specific processing conditions (monotonic load change within the chosen temperature conditions).

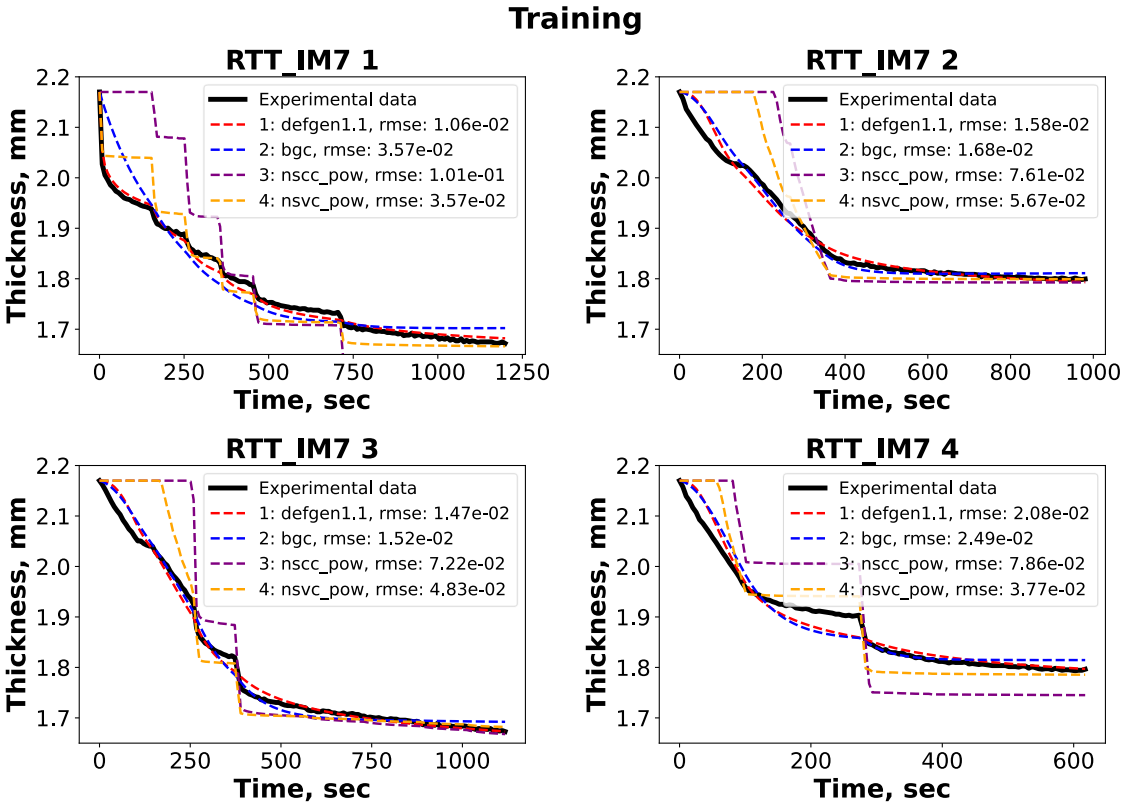

Figure 6.16: IM7/8552 material testing. Training

To validate the obtained results and to compare the effectiveness of the proposed (reactive testing) and the conventional (testing within predefined programmes)

characterisation approaches, the set of 8 deterministic tests was performed for IM7/8552 material. For the sake of consistency, the loading programmes were chosen in line with the deterministic tests conducted for IMA/M21 material (the rationale for the load schedules was discussed in chapter 4).

The loading programmes and material's compaction response is shown in Figure 6.17.

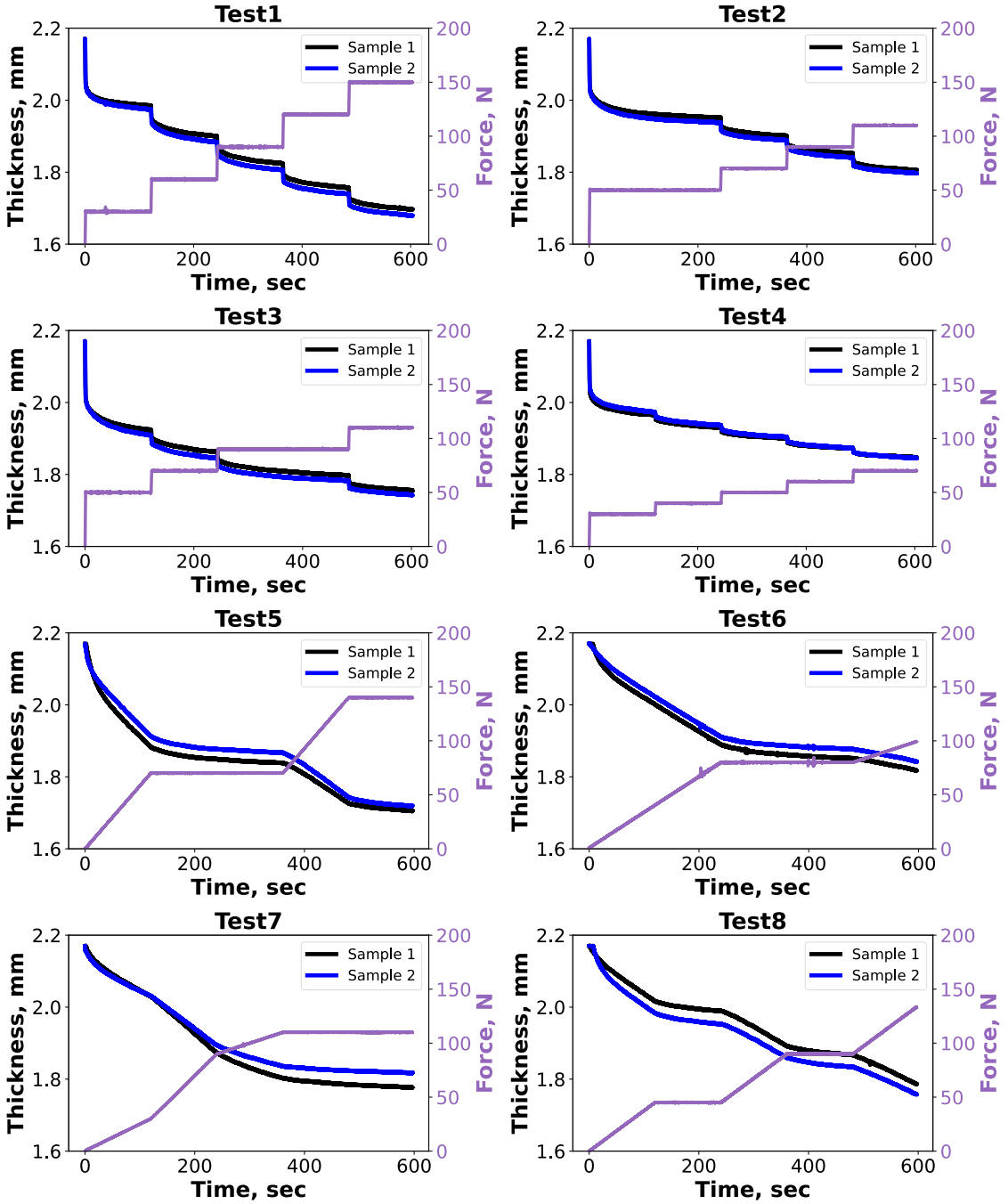

Figure 6.17: IM7/8552 material testing. Deterministic tests

The validation process followed the same pattern as for the previous material system. To form a fully populated training combination, three tests were selected from the

predefined set shown in Figure 6.17. Due to the sheer number of possible training combinations, one group of tests (1, 5, 7) was used as an example (in this case test indices (1, 5, 7) correspond to Figure 6.17 for the predefined training combinations). Then, the expanded compaction dataset was submitted to the parameter extraction framework for material model definition in the same way it had been done within chapter 4. The obtained deterministic models, along with the resulting models from the real-time testing, were trialled against the validation set, which was formed from 5 remaining tests in the deterministic programme. The comparative ranking bar chart for all training tests is presented in Figure 6.18.

The expanded deterministic dataset was ranked fourth with an error increase of 5.3% in comparison with the highest-ranked real-time test RTT_IM7 3. Tests RTT_IM7 2 and RTT_IM7 1 showcased a similar performance with an error raise of 3.4% and 3.8% respectively. The increase in prediction error for the last-ranked characterisation programme RTT_IM7 4 was registered at 7.4%. Therefore, three out of four real-time programmes outperformed the fully populated (hence, more labour intensive) training combination of deterministic tests. This is an important conclusion, as it means that less experimental trials were required for the successful material characterisation.

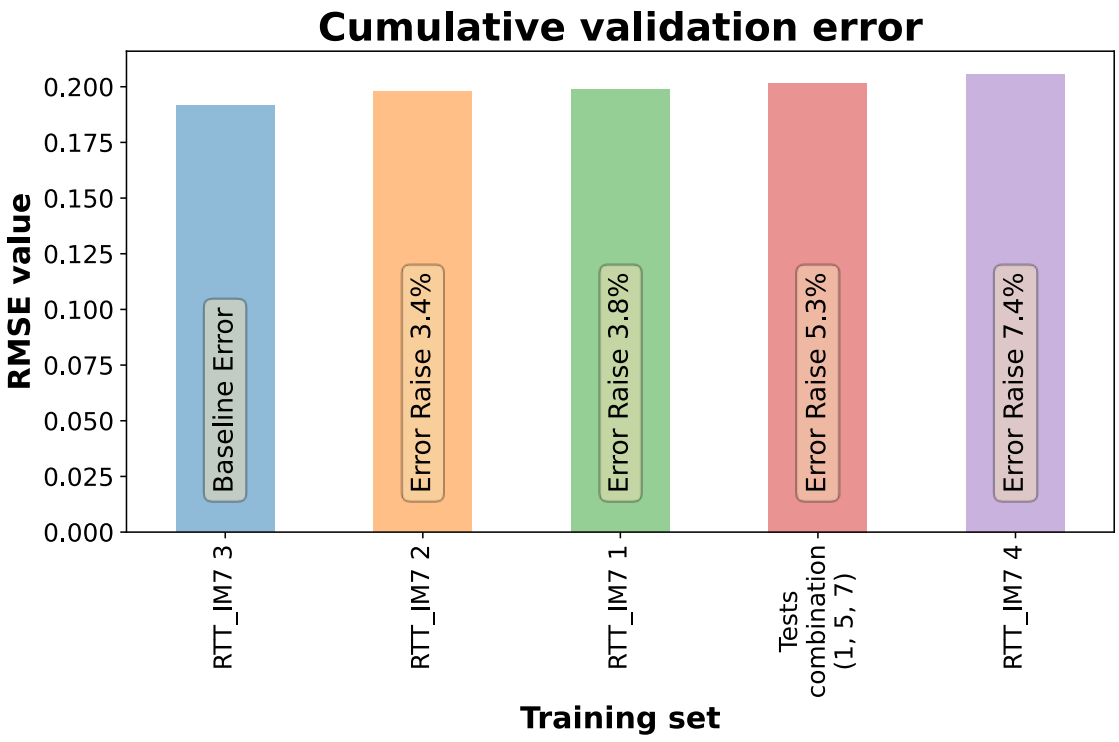

Figure 6.18: IM7/8552 material testing. Candidate models' ranking for different test programmes.

The models' thickness predictions within each test in the validation set are presented in Figure 6.19. As it was concluded before, the candidate models demonstrated a higher value of fitting error in comparison with the previous material system. The same trend can be observed at the validation stage as well. All models struggled to fit the monotonic stages (Test 6, Test 8) of compaction. The highest level of the prediction offset was registered for the validation Test 4. However, the maximum deviation in the value of the final thickness within all validation tests did not exceed 4.4%.

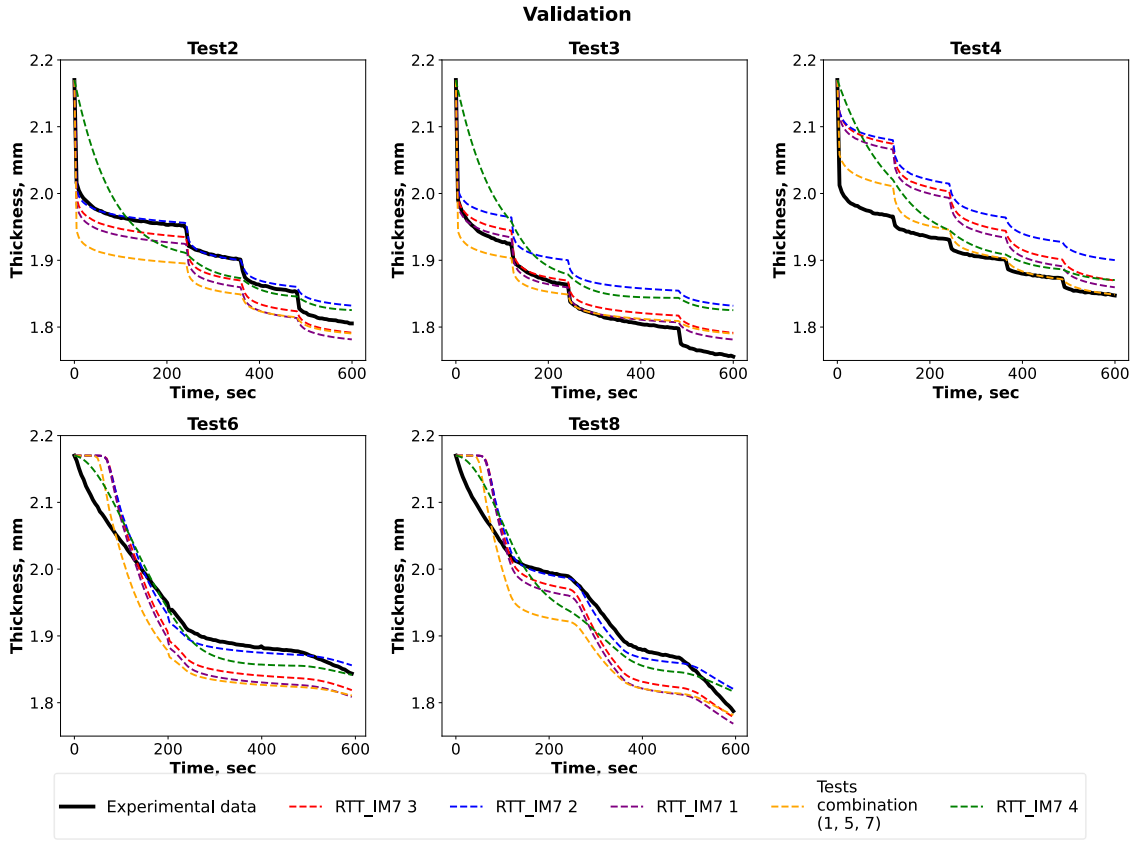

Figure 6.19: IM7/8552 material testing. Candidate model's validation.

The corresponding material parameters for the best candidate models for each characterisation test are presented in Table 6.4. The deviation in the values of material parameters *a*, *b*, and *k* was registered at the level 1.0%, 3.1%, 3.2% respectively.

It should be noted, that for the real-time test RTT_IM7 4 the percolation model was defined as more accurate (less value of the cumulative error) during the validation. This model was ranked second during the training stage with a lag behind the DefGen model (12.5% error raise). In comparison with other characterisation programmes, test RTT_IM7 4 was ranked fifth during the validation stage.

Table 6.4: Candidate models' parameters for deterministic and real-time characterisation programmes. Studied material system – IM7/8552.

	Model type	Parameter 1	Parameter 2	Parameter 3
RTT_IM7 3	DefGen	a: -0.9429	b: -14.50	k: 0.7647
RTT_IM7 2	DefGen	a: -0.9427	b: -14.75	k: 0.7860
RTT_IM7 1	DefGen	a: -0.9429	b: -14.51	k: 0.7619
Tests combination (1, 5, 7)	DefGen	a: -0.9342	b: -14.95	k: 0.7838
RTT_IM7 4	Percolation (bgc)	$K_A/\tilde{\eta}$: 0.2580	σ_A: 0.0058	

Testing of dry material samples

The purpose of this exercise was to put the autonomous testing framework in challenging conditions, when the candidate material models in the consolidation library are not designed for the studied material system specifically. The idea was to demonstrate the existing limitations of the proposed approach. As the definition of a loading programme is based on the difference between two best performing candidate models, there is a compulsory requirement for the presence of at least two comprehensive models in the library relevant to the studied material. All considered models (chapter 3) are formulated for two-phase materials (e.g. shear thinning flow of the reinforced fluid, resin's percolation through the fibrous network, the transition between squeezing and bleeding flow modes). It is possible to assume why the current set of material models in the library could potentially reflect the behaviour of a dry fibre material:

- Air represents a fluid in the material system. In this case, the range of viscosities would be significantly different in comparison with the conventional two-phase

material system (e.g. prepregs IMA/21, IM7/8552 etc.). Such development presents a potential challenge for the framework to derive the optimal set of material parameters.

- There are certain aspects of the considered candidate models which could reflect characteristic features of dry material's behaviour. For instance, the set of material parameters can be defined in a way, which makes resin's contribution negligible. For percolation model it would mean that only elastic reaction of fibrous network contributes to the compaction response. For shear models it could be the distortion of fibre network's structure (widening of yarns) during compaction.

To explore different loading scenarios, the initial and following load steps' amplitudes were varied in ranges 40 - 80N and 30 - 50N respectively. The summary of al performed tests is presented in Table 6.5. The resulting test programmes and samples' compaction feedback for flax and NCF samples are shown in Figure 6.20.a and Figure 6.20.b respectively.

Table 6.5: Explored test settings for the real-time testing of dry material. RTT stands for real-time test.

		Initial load step		Further load steps		
Test id	**Material**	**Load amplitude, N**	**Loading regime**	**Max. load amplitude, N**	**Step duration, sec**	**Number of load options**
RTT_DRY 1	Flax	40	Ramp-dwell	30	100	5
RTT_DRY 2	Flax	80	Ramp-dwell	50	100	5
RTT_DRY 3	NCF	80	Ramp-dwell	50	100	5
RTT_DRY 4	NCF	40	Ramp-dwell	30	100	5

Both material systems demonstrated a significant drop in thickness within the first seconds of the test. Loading programmes for flax samples showed a trend for a constant increase of the load level up to 250 N with several dwell stages (RTT_DRY 2). The programmes for NCF samples demonstrated a different trend. The load reached a plateau (100 N for the test RTT_DRY 4 and 200 N for the test RTT_DRY 3) and held

steady up until the end of the experimentation. Similar to the real-time test RTT_IM7 3 for IM7/8552, the framework selected both monotonic and ramp-dwell loading options for the test RTT_DRY 4.

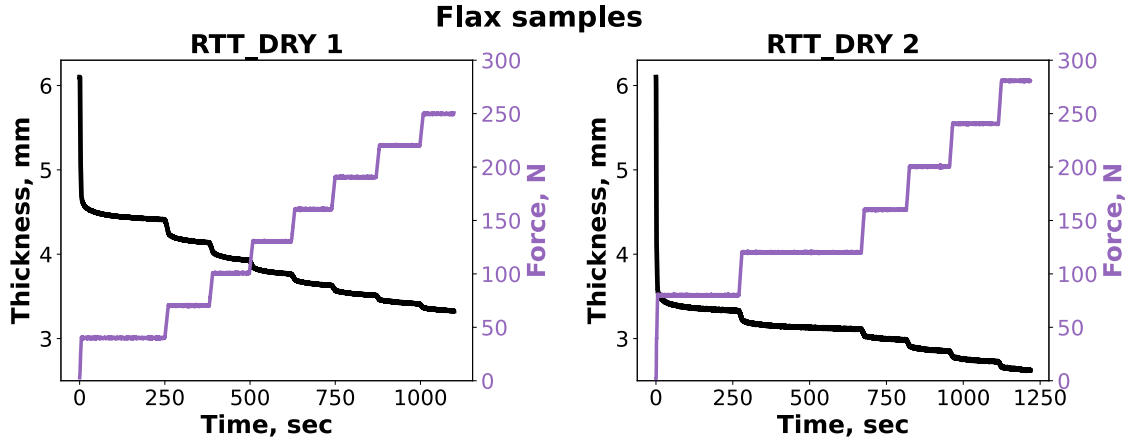

a

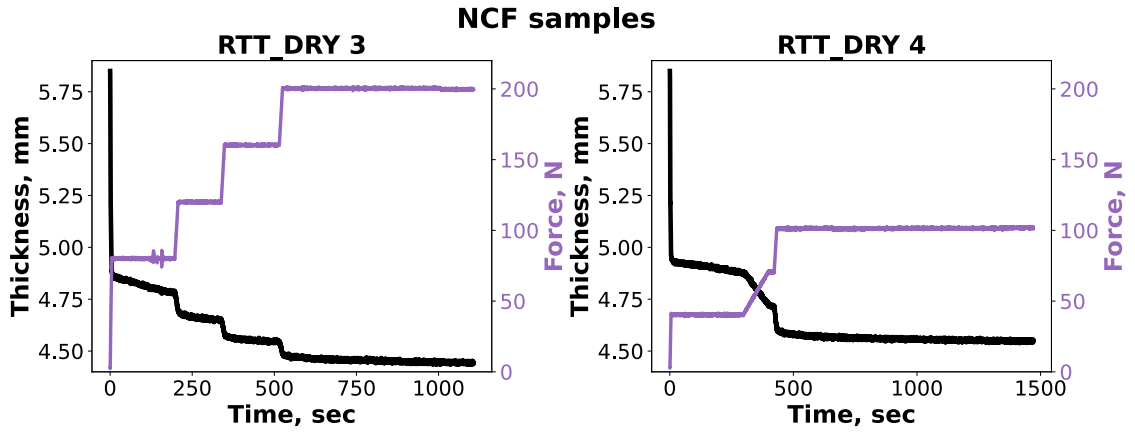

b

Figure 6.20: Dry material testing. Resulting loading programmes and compaction curves. a) Flax samples; b) NCF samples.

The step-by-step parameter extraction routine breakdown for both types of dry material samples is shown in Figure 6.21 (due to the volume of data, only two steps for each material system are shown). The set of favourable candidate models evolved during the testing of flax samples. After the initial load step, the DefGen and percolation models were able to fit the data very well (the prediction curves overlapped with the experimental data). But in the last steps of the test the second-best candidate changed from the percolation to the shear model. Within this research, this was the first instance when the shear model was selected as one of the top two candidates upon the completion of a characterisation test.

For the NCF material the best candidates were consistent throughout the test – DefGen and percolation models (purple and orange curves). Both models demonstrated high accuracy in thickness prediction – the DefGen model showcased the perfect fit to the experimental data and overlapped with the actual compaction curve (the thin purple "DefGen" curve can be seen on top of the thick blue "experimental data" curve). The second-best percolation candidate was able to fit the experimental data with an offset at the stage of the initial load raise (orange curve). The deviation in final thickness prediction for both models was less than 0.1%.

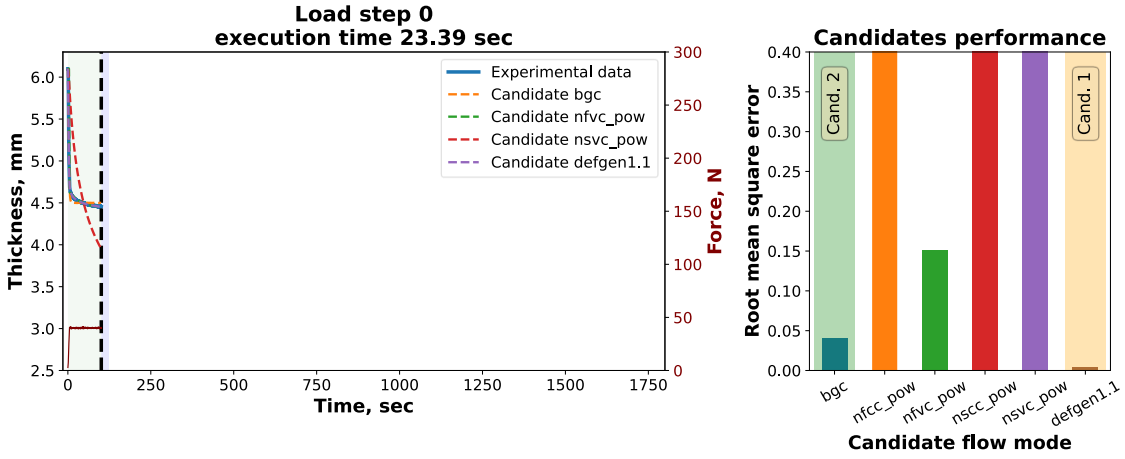

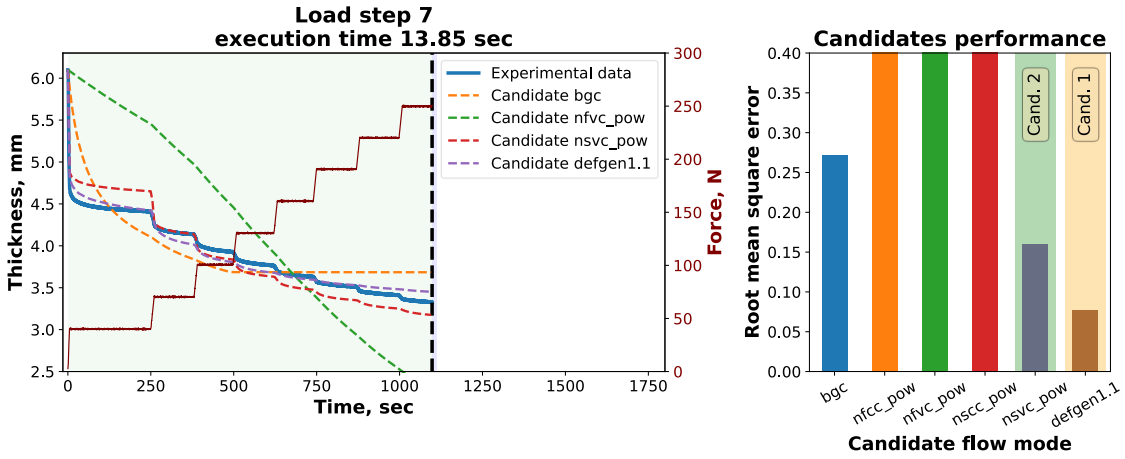

a

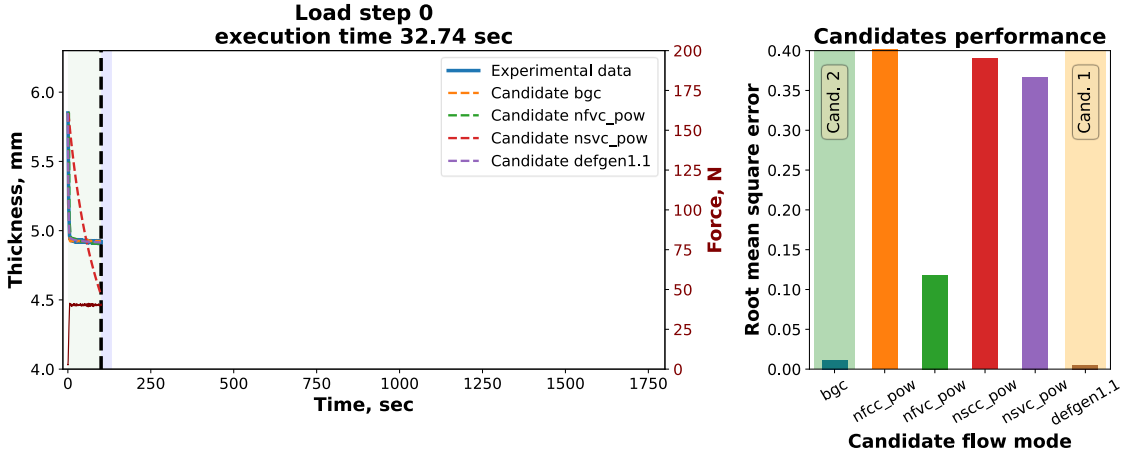

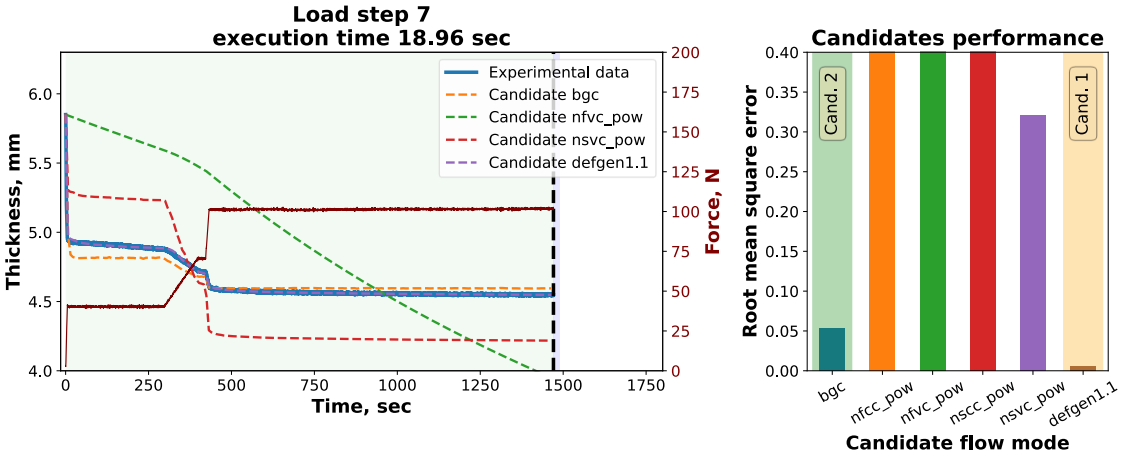

b

Figure 6.21: Step by step experimentation: a) Flax material; b) NCF material. Green region – all previously received data. Blue region (on the right from the vertical black dashed line) – required processing time.

The validation of the obtained models was not performed for this set of materials. The main reason for that is that the current pool candidates is not designed to describe the compaction response of dry materials. Another reason for not conducting the validation process is the variability of the specimens. As discussed in section 6.2.3, dry specimens were laid on top of each other right on the surface of the compression platen. There was no resin which could keep separate plies in place. Inconsistencies in experimentation (in the equipment, specimens' preparation, methodology etc.) for obtaining training or validation compaction datasets may lead to misleading results. In such case, the obtained material model is trained or trialled within features of material behaviour which are not represented in the validation/training sets. As a result, it will perform poorly either due to the insufficiency or irrelevancy of the training dataset.

As it was shown several times in the previous chapters, formidable performance of a candidate model at the training stage is a necessary condition. However, it alone does not provide sufficient cause for making a conclusion about model's feasibility. Even though for certain test/materials scenarios (NCF sample, test RTT_DRY 4) the error in thickness prediction is next-to-zero, there is no guarantee that the derived model would uphold its performance for changed processing conditions.

6.3 Conclusions.

The application of the adaptive consolidation sensor framework to real materials was explored within this chapter. The aspects of performing real-time experimentation on

the universal testing machine, sending/receiving experimental data, possible technical challenges and ways of addressing them were discussed. The final implementation of the setup for the experimentation in the reactive manner represents the proposed framework operating in conjunction with the compression testing rig through the newly developed LabView state machine and the bespoke data acquisition system.

The functionality of the proposed framework was tested within several experimental trials of three different material systems: IMA/M21 prepreg, IM7/8552 prepreg, and dry materials (flax and carbon fibre NCF). For each material type a trend in the shape of the resulting loading programme was observed (load raise-dwell-raise, load plateau, consistent load increase etc.). Changes in the loading programme had a direct effect on the intermediate candidate models' ranking, which was demonstrated in the parameters extraction breakdown. As the compaction response became more complex (various strain rates or achieved compaction levels), the models which performed well at the initial stages of the experiment were moved down to the second place or were even disregarded from the competition. Another interesting observation is that the sequential candidate models update at every load step allowed to correct a non-optimal set of material parameters and to provide an accurate fit of the model in the following steps (IMA/M21 material, DefGen model in test RTT_M21 3).

Upon the completion of each test, the framework successfully identified the most relevant material models and the corresponding set of material parameters. The obtained results for prepreg materials were trialled against the set of tests with predefined loading programmes. The validation process for IM7/8552 material confirmed, that the models trained within the adaptive experimentation showcased a superior performance in comparison with more labour-intensive deterministic training combination. The results for IMA/M21 material system indicated that the expanded set of 3 deterministic programmes was still preferrable, although real-time programmes were more effective than double and single-test combinations.

The characterisation of dry materials was performed to explore the limitations of the proposed approach. The framework showcased a robust performance during training stage by fitting the candidate models to the material's thickness data with no visible offset. The validation of the obtained models was not performed due to the imperfections in dry samples preparation process.

7 CONCLUSIONS

7.1 Original contributions

The main goal of this research was to develop the autonomous unbiased testing system for the characterisation of consolidation mechanisms in composite precursors. The proposed framework demonstrated a significant potential for identification of consolidation models based on the material's feedback in real-time testing. It has the potential to remove the subjective judgement about the material behaviour. The identification of the pure flow modes may also be useful to decode dominant mechanisms at different stages of deformation such as fibre shear, resin bleeding or a transition from one mode to another. In the current research the proposed framework proved its efficiency in handling complex models and developing data-rich testing programmes. The framework demonstrated significant advantages in comparison with the conventional testing approach:

- The designed framework is able to operate autonomously without the researcher's involvement. The test is conducted without any prior assumptions about the material's behaviour. The resulting loading programmes are based on the compaction response of the material.
- The consolidation library can be easily expanded with new models relevant to the studied material.
- The framework allows to access intermediate results. It is possible to see the evolution of models ranking and the influence of the changing load route on the best candidates.
- The framework provides a wide functionality for postprocessing experimental results, such as in-depth analysis of candidate material models' optimisation results, taking advantage of joined datasets from several tests, and conducting validation within independent set of experimental data.

After performing the experimental part of this research, the following challenges in framework's operation became evident:

- If the relevant material models are not represented in the library, the framework will not be able to operate with high level of confidence.
- The result of the real-time experimentation depends on the available computational resources. The processor must have more cores than the number of models in the library to process all candidates concurrently. Besides, weak computational setup will lead to longer processing time, hence longer load dwell stages in the real-time loading programme.
- Sensitivity to inconsistencies in the experimental procedures. There should be no significant scatter in the values of the specimens' initial thickness when processing joined dataset from several experiments. If the model is trained on the dataset which contains systematic bias, it will inherit these features in its behaviour. It is fair to say, that this problem is not specific to the developed testing system alone and is relevant to any model identification procedure

The proposed approach is not limited by consolidation characterisation only. Similar challenges in characterisation of materials can be seen in various other testing campaigns. This includes, for instance, testing of precursors that is required for simulation of AFP deposition/forming/liquid moulding, such as identifying suitable models for the behaviour of prepregs/preforms in in-plane or inter-ply shear, friction, and tack.

The conducted research was multidisciplinary in nature and required a significant amount of effort in various fields of study: the consolidation mechanisms of composites precursors, experimental characterisation of composites, software implementation of the framework, real-time data acquisition and processing. The carried out experimental programme was very labour-intensive. There were more than 200 conducted characterisation tests (140 IMA/M21, 60 IM7/8552, 6 dry specimens). For every test a specimen was carefully manufactured (including cutting plies and performing layup in the clean room). More specimens were required, as every trial attempt during building, adjusting and testing of the real-time setup "cost" one specimen.

The author's main contributions are summarised below in accordance with the chapters of this thesis.

The existing approaches to composites characterisation, technical challenges and the goals of this study were discussed in **Chapter 2**.

In order to conduct the unbiased characterisation study, a set of the most representative consolidation models was discussed within **Chapter 3:**

- The consolidation library with candidate material models was developed. Mathematical formulations of all models were unified within the same notation for further use in this research.
- The importance of the robust characterisation process was demonstrated within two characteristic exercises. Based on the outcomes of those examples, the criteria for material model's performance and the requirements for the robust parameter identification routine were established.

The influence of the completeness of a characterisation programme on the performance of the resulting material model was explored within **Chapter 4**:

- The parameters extraction framework for the model definition from the experimental data was developed in line with the previously defined requirements. The proposed framework employs two-step optimisation routine and is capable of processing the compaction data from several experiments.
- The study on the influence of the data-rich testing programme on the resulting material models was performed. It was established, that more diverse experimental dataset provides more reliable dataset for further model identification. The difference in cumulative error in thickness prediction between the best and the worst models was 27.3%.

The concept of the adaptive consolidation sensor was introduced in **Chapter 5**:

- A novel adaptive consolidation sensor framework was introduced within this chapter. The framework estimates the compaction feedback from the material in real time within each load step and constructs the load route for the next step based on the prediction of candidate models from the library.
- The stated functionality of the framework was challenged within a virtual exercise, where the real material was substituted with a pre-coded module called "BlackBox". The framework successfully managed to investigate hidden consolidation models along with the corresponding set of material parameters. The fidelity of the obtained results was confirmed within the validation exercise for a different set of processing conditions.

The application of the proposed approach to real materials was discussed in **Chapter 6**:

- The technical requirements and the possible challenges for the real-time experimentation were established. The complete setup for the adaptive testing was introduced. The proposed implementation of the system is capable to continuously receive experimental data from the Instron machine and to send the load route commands back.
- The research concluded with the experimentation on three different material systems. The framework proved its ability to operate in a reactive manner and successfully identified proper material models with the corresponding set of parameters. Overall, the real-time loading programmes proved to provide more reliable compaction datasets for further characterisation than their predefined counterparts.

7.2 Future work

Based on the comprehensive experience gained within this research, it is possible to suggest several promising improvements to the current implementation of the framework and new directions for the research. There are two groups of suggestions:

- Methodological:
    - Exploring different load picking logic. As described in chapter 5, the decision about the load programme for further steps was based on the idea of a maximum difference in prediction between best candidate models. It would be interesting to explore a different logic for the load definition. For instance, to add the condition for the load route to cover the maximum space in the load-load rate space. Such development would make the resulting loading programmes more diverse, which may have a positive effect on the models training.
    - Exploring different temperature conditions. All characterisation tests were conducted at the constant temperature of 60℃. Due to the volume of the testing programme other temperature regimes were not explored. For that reason, the obtained models are not guaranteed to perform on the same level within different thermal conditions. The benefit of exploring more temperature regimes, is that it is possible to specify such processing conditions, where the target flow mode would occur explicitly (for instance, resin bleeding out from a specimen).

The possible challenge of taking temperature effects into account is that it would lead to an introduction of temperature-dependent material parameters. Consequently, it would make the characterisation and properties extraction task more challenging due to the increased parameters space.

- Expanding the consolidation library. It is clear that the proposed framework can be reinforced further by enriching the material library. As discussed in chapter 3, the governing equations for the considered flow modes are derived with respect to the specified boundary conditions. By changing the boundary conditions, it is possible to enrich the library with new models (in the same way as Rogers [90] derived the relationships for the shear flow). Besides, the flow models based on different assumptions and laws can be introduced. There is also a potential to include the models represented through fractional derivates [178], [179].
- The proposed adaptive testing approach has a potential for application to various problems beyond the scope of consolidation study for composite precursors. Potentially, it could be relevant for any multi-component compliant material (soils, powders, food etc) which exhibit complex behaviour under processing or service conditions. Applying this methodology to a different multi-material system would require populating the library with the new candidate models which can adequately reflect the response of the studied system. It is also envisaged that this methodology could be applied well beyond the scope of the compaction testing.

- Technical:
  - Different approach to parameter extraction from joint datasets. As described in section 4.7.3, the current approach to processing several tests within one dataset is to reduce the three-dimensional fitting to two-dimensional problem by stacking compaction curves one after another and updating the initial condition $h(t=0)=h_0$. It allows to use a single residual function for further minimisation (parameter extraction). Instead, it is possible to consider the sum of residual functions for separate compaction curves. Such development will save computational

resources (no additional operations needed) and make the framework less sensitive to the variation in samples' initial thickness (as each compaction curve will be processed independently).

- Material parameters' normalisation. For most material models the scale for parameters' values is different. For instance, for the DefGen model *a* and *k* parameters are varied between -1-0 and 5-50 respectively. From the mathematical side of the problem, it may be challenging for the optimiser to operate within such scatter in values. For that reason, input material parameters should be normalised in order to operate within a notionally common scale. Such development has a potential to address the problem of the flat correlation curve, encountered for IMA/M21 material (parameter *a*, the DefGen model) discussed in chapter 6.
- Employing global optimisation algorithms. As stated before, the employed two-stage optimisation routine is not a global optimisation method. It would be interesting to compare the current results with the "global" solution. The implementation of the parameters extraction framework allows to switch between different methods with ease. Global methods require a lot of computational time to converge. Therefore, the comparative analysis is only possible after the experiment is concluded.

The application of these ideas will be explored within the further research and, if useful, the corresponding changes will be implemented in the next generation of the adaptive testing framework.

8 REFERENCES

[1] S. Das, “Life cycle assessment of carbon fiber-reinforced polymer composites,” *Int. J. Life Cycle Assess.*, vol. 16, no. 3, pp. 268–282, 2011, doi: 10.1007/s11367-011-0264-z.

[2] H. E. N. Bersee and A. Beukers, “Consolidation of thermoplastic composites,” *J. Thermoplast. Compos. Mater.*, vol. 16, no. 5, pp. 433–455, 2003, doi: 10.1177/0892705703031862.

[3] P. Šimáček and S. G. Advani, “A continuum approach for consolidation modeling in composites processing,” *Compos. Sci. Technol.*, vol. 186, no. July 2019, 2020, doi: 10.1016/j.compscitech.2019.107892.

[4] T. J. Dodwell, R. Butler, and G. W. Hunt, “Out-of-plane ply wrinkling defects during consolidation over an external radius,” *Compos. Sci. Technol.*, vol. 105, pp. 151–159, 2014, doi: 10.1016/j.compscitech.2014.10.007.

[5] S. Mukhopadhyay, M. I. Jones, and S. R. Hallett, “Compressive failure of laminates containing an embedded wrinkle; Experimental and numerical study,” *Compos. Part A Appl. Sci. Manuf.*, vol. 73, pp. 132–142, 2015, doi: 10.1016/j.compositesa.2015.03.012.

[6] K. Farnand, N. Zobeiry, A. Poursartip, and G. Fernlund, “Micro-level mechanisms of fiber waviness and wrinkling during hot drape forming of unidirectional prepreg composites,” *Compos. Part A Appl. Sci. Manuf.*, vol. 103, pp. 168–177, 2017, doi: 10.1016/j.compositesa.2017.10.008.

[7] D. O’Hare Adams and Hyer M. W., “Effects of layer waviness on the compression strength of thermoplastic composite laminates,” *J. Reinf. Plast. Compos.*, vol. 12, no. 4, pp. 414–429, 1993, doi: 10.1177/073168449301200404.

[8] P. Boisse, N. Hamila, E. Vidal-Sallé, and F. Dumont, “Simulation of wrinkling during textile composite reinforcement forming. Influence of tensile, in-plane shear and bending stiffnesses,” *Compos. Sci. Technol.*, vol. 71, no. 5, pp. 683–692, 2011, doi: 10.1016/j.compscitech.2011.01.011.

[9] P. Hallander, M. Akermo, C. Mattei, M. Petersson, and T. Nyman, “An experimental study of mechanisms behind wrinkle development during forming of composite laminates,” *Compos. Part A Appl. Sci. Manuf.*, vol. 50, pp. 54–64, 2013, doi: 10.1016/j.compositesa.2013.03.013.

[10] J. P. H. Belnoue and S. R. Hallett, “A rapid multi-scale design tool for the prediction of wrinkle defect formation in composite components,” *Mater. Des.*, vol. 187, Feb. 2020, doi: 10.1016/j.matdes.2019.108388.

[11] N. Xie, R. A. Smith, S. Mukhopadhyay, and S. R. Hallett, “A numerical study on the influence of composite wrinkle defect geometry on compressive strength,” *Mater. Des.*, vol. 140, pp. 7–20, 2018, doi: 10.1016/j.matdes.2017.11.034.

[12] M. Nartey *et al.*, “Understanding the impact of fibre wrinkle architectures on composite laminates through tailored gaps and overlaps,” *Compos. Part B Eng.*, vol. 196, 2020, doi: 10.1016/j.compositesb.2020.108097.

[13] H. Hu, D. Cao, Z. Cao, and S. Li, “Experimental and numerical investigations of wrinkle effect on failure behavior of curved composite laminates,” *Compos. Struct.*, vol. 261, 2021, doi: 10.1016/j.compstruct.2021.113541.

[14] M. Y. Matveev *et al.*, “A numerical study of variability in the manufacturing process of thick composite parts,” *Compos. Struct.*, vol. 208, pp. 23–32, Jan. 2019, doi: 10.1016/j.compstruct.2018.09.092.

[15] S. Zhang, L. Zhang, Y. Wang, J. Tao, and X. Chen, “Effect of ply level thickness uncertainty on reliability of laminated composite panels,” *J. Reinf. Plast. Compos.*, vol. 35, no. 19, pp. 1387–1400, 2016, doi: 10.1177/0731684416651499.

[16] M. Li and C. L. Tucker, “Modeling and simulation of two-dimensional consolidation for thermoset matrix composites,” *Compos. - Part A Appl. Sci. Manuf.*, vol. 33, no. 6, pp. 877–892, 2002, doi: 10.1016/S1359-835X(02)00017-9.

[17] M. Hojjati and S. V. Hoa, “Curing simulation of thick thermosetting composites,” *Compos. Manuf.*, vol. 5, no. 3, pp. 159–169, 1994, doi: 10.1016/0956-7143(94)90025-6.

[18] S. Roychowdhury and S. G. Advani, “An experimental investigation of consolidation in thermoplastic filament winding,” *Compos. Manuf.*, vol. 2, no. 2,

pp. 97–104, 1991, doi: 10.1016/0956-7143(91)90186-K.

[19] D. W. Radford and T. S. Rennick, “Separating sources of manufacturing distortion in laminated composites,” *J. Reinf. Plast. Compos.*, vol. 19, no. 8, pp. 621–641, 2000, doi: 10.1177/073168440001900802.

[20] M. R. Wisnom, M. Gigliotti, N. Ersoy, M. Campbell, and K. D. Potter, “Mechanisms generating residual stresses and distortion during manufacture of polymer-matrix composite structures,” *Compos. Part A Appl. Sci. Manuf.*, vol. 37, no. 4, pp. 522–529, 2006, doi: 10.1016/j.compositesa.2005.05.019.

[21] K. Shaker, Y. Nawab, and A. Saouab, “Experimental and numerical investigation of reduction in shape distortion for angled composite parts,” *Int. J. Mater. Form.*, vol. 13, no. 6, pp. 897–906, 2020, doi: 10.1007/s12289-019-01510-6.

[22] C. Bellini and L. Sorrentino, “Analysis of cure induced deformation of CFRP U-shaped laminates,” *Compos. Struct.*, vol. 197, 2018, doi: 10.1016/j.compstruct.2018.05.038.

[23] J. M. Svanberg and J. A. Holmberg, “An experimental investigation on mechanisms for manufacturing induced shape distortions in homogeneous and balanced laminates,” *Compos. - Part A Appl. Sci. Manuf.*, vol. 32, no. 6, pp. 827–838, 2001, doi: 10.1016/S1359-835X(00)00173-1.

[24] P. Hubert and A. Poursartip, “Aspects of the Compaction of Composite Angle Laminates: An Experimental Investigation,” *J. Compos. Mater.*, vol. 35, no. 1, pp. 2–26, Jan. 2001, doi: 10.1177/002199801772661849.

[25] M. R. Wisnom, M. I. Jones, and G. F. J. Hill, “Interlaminar tensile strength of carbon fibre-epoxy - Specimen size, layup and manufacturing effects,” *Adv. Compos. Lett.*, vol. 10, no. 4, pp. 171–177, 2001, doi: 10.1177/096369350101000402.

[26] N. Ersoy, K. Potter, M. R. Wisnom, and M. J. Clegg, “Development of spring-in angle during cure of a thermosetting composite,” *Compos. Part A Appl. Sci. Manuf.*, vol. 36, no. 12, pp. 1700–1706, 2005, doi: 10.1016/j.compositesa.2005.02.013.

[27] P. Causse, E. Ruiz, and F. Trochu, “Spring-in behavior of curved composites manufactured by Flexible Injection,” *Compos. Part A Appl. Sci. Manuf.*, vol. 43, no. 11, pp. 1901–1913, 2012, doi: 10.1016/j.compositesa.2012.06.010.

[28] K. Çinar and N. Ersoy, “3D finite element model for predicting manufacturing distortions of composite parts,” *J. Compos. Mater.*, vol. 50, no. 27, pp. 3791–3807, 2016, doi: 10.1177/0021998315625789.

[29] P. Kim, S. Toll, R. Phillips, and J.-A. E. Manson, “The dimensional stability of composite laminates: sensitivity to gradients in fibre content and misalignment,” *Int. Work. Adv. Mater. High Precis. Detect.*, pp. 123–131, 1994.

[30] L. Jerpdal, M. Åkermo, D. Ståhlberg, and A. Herzig, “Process induced shape distortions of self-reinforced poly(ethylene terephthalate) composites,” *Compos. Struct.*, vol. 193, pp. 29–34, 2018, doi: 10.1016/j.compstruct.2018.03.038.

[31] D. W. Radford, “Cure shrinkage induced warpage in flat uni-axial composites,” *J. Compos. Technol. Res.*, vol. 15, no. 4, pp. 290–296, 1993, doi: 10.1520/ctr10381j.

[32] P. Hubert, R. Vaziri, and A. Poursartip, “A two-dimensional flow model for the process simulation of complex shape composite laminates,” *Int. J. Numer. Methods Eng.*, vol. 44, no. 1, pp. 1–26, 1999, doi: 10.1002/(SICI)1097-0207(19990110)44:1<1::AID-NME481>3.0.CO;2-K.

[33] D. T. Paterson, T. S. Eaves, D. R. Hewitt, N. J. Balmforth, and D. M. Martinez, “Flow-driven compaction of a fibrous porous medium,” *Phys. Rev. Fluids*, vol. 4, no. 7, pp. 1–28, 2019, doi: 10.1103/PhysRevFluids.4.074306.

[34] S. Haghdan, T. Tannert, and G. D. Smith, “Effects of reinforcement configuration and densification on impact strength of wood veneer/polyester composites,” *J. Compos. Mater.*, vol. 49, no. 10, pp. 1161–1170, 2015, doi: 10.1177/0021998314531308.

[35] D. Castellanos, P. J. Martin, J. Butterfield, M. McCourt, M. Kearns, and P. Cassidy, “Sintering and densification of fibre reinforcement in polymers during rotational moulding,” *Procedia Manuf.*, vol. 47, no. 2019, pp. 980–986, 2020, doi: 10.1016/j.promfg.2020.04.301.

[36] J. S. Lightfoot, M. R. Wisnom, and K. Potter, “A new mechanism for the formation of ply wrinkles due to shear between plies,” *Compos. Part A Appl. Sci. Manuf.*, vol. 49, pp. 139–147, 2013, doi: 10.1016/j.compositesa.2013.03.002.

[37] W. -B Young, “Resin flow analysis in the consolidation of multi-directional laminated composites,” *Polym. Compos.*, vol. 16, no. 3, pp. 250–257, 1995, doi:

10.1002/pc.750160309.

[38] P. K. Ivanov Dmitry, Yiqing Li , Ward Carwyn, “Transitional behaviour of prepregs in automated fibre deposition processes,” *Proc. 19th Int. Conf. Compos. Mater.*, 2013.

[39] O. J. Nixon-Pearson, J. P. H. Belnoue, D. S. Ivanov, K. D. Potter, and S. R. Hallett, “An experimental investigation of the consolidation behaviour of uncured prepregs under processing conditions,” *J. Compos. Mater.*, vol. 51, no. 13, pp. 1911–1924, Jun. 2017, doi: 10.1177/0021998316665681.

[40] J. P. H. Belnoue, O. J. Nixon-Pearson, D. Ivanov, and S. R. Hallett, “A novel hyper-viscoelastic model for consolidation of toughened prepregs under processing conditions,” *Mech. Mater.*, vol. 97, pp. 118–134, Jun. 2016, doi: 10.1016/j.mechmat.2016.02.019.

[41] P. V Kaprielian and J. M. O’Neill, “Shearing flow of highly anisotropic laminated composites,” *Composites*, vol. 20, no. 1, pp. 43–47, 1989, doi: 10.1016/0010-4361(89)90681-2.

[42] R. Balasubramanyam, R. S. Jones, and A. B. Wheeler, “Modelling transverse flows of reinforced thermoplastic materials,” *Composites*, vol. 20, no. 1, pp. 33–37, 1989, doi: 10.1016/0010-4361(89)90679-4.

[43] D. J. Groves, “A characterization of shear flow in continuous fibre thermoplastic laminates,” *Composites*, vol. 20, no. 1, pp. 28–32, 1989, doi: 10.1016/0010-4361(89)90678-2.

[44] J. A. Barnes and F. N. Cogswell, “Transverse flow processes in continuous fibre-reinforced thermoplastic composites,” *Composites*, vol. 20, no. 1, pp. 38–42, 1989, doi: 10.1016/0010-4361(89)90680-0.

[45] S. F. Shuler and S. G. Advani, “Transverse squeeze flow of concentrated aligned fibers in viscous fluids,” *J. Nonnewton. Fluid Mech.*, vol. 65, no. 1, pp. 47–74, 1996, doi: 10.1016/0377-0257(96)01440-1.

[46] D. G. Seong, S. Kim, D. Lee, J. W. Yi, S. W. Kim, and S. Y. Kim, “Prediction of defect formation during resin impregnation process through a multi-layered fiber preform in resin transfer molding by a proposed analytical model,” *Materials (Basel).*, vol. 11, no. 10, p. 2055, 2018, doi: https://doi.org/10.3390/ma11102055.

[47] M. R. Wisnom, “The effect of fibre misalignment on the compressive strength of

unidirectional carbon fibre/epoxy," *Composites*, vol. 21, no. 5, pp. 403–407, 1990, doi: 10.1016/0010-4361(90)90438-3.

[48] R. Phillips, D. A. Akyüz, and J. A. E. Månson, "Prediction of the consolidation of woven fibre-reinforced thermoplastic composites. Part I. Isothermal case," *Compos. Part A Appl. Sci. Manuf.*, vol. 29, no. 4, pp. 395–402, 1998, doi: 10.1016/S1359-835X(97)00099-7.

[49] E. L. Wang and T. G. Gutowski, "Laps and gaps in thermoplastic composites processing," *Compos. Manuf.*, vol. 2, no. 2, pp. 69–78, 1991, doi: 10.1016/0956-7143(91)90182-G.

[50] D. S. Ivanov and S. V. Lomov, "Modeling of 2D and 3D woven composites," in *Polymer Composites in the Aerospace Industry (Second Edition)*, P. Irving; and C. Soutis, Eds. Woodhead Publishing, 2019, pp. 23–57.

[51] T. A. Nestor and C. M. O Bradaigh, "Experimental investigation of the intraply shear mechanism in thermoplastic composites sheetforming," *Key Eng. Mater.*, vol. 99, pp. 19–36, 1995, doi: 10.4028/www.scientific.net/kem.99-100.19.

[52] P. A. Hubert Pascal, "A Review of Flow and Compaction Modelling Relevant to Thermoset Matrix Laminate Processing," *J. Reinf. Plast. Compos.*, vol. 17, no. 4, 1998, doi: 10.1177/073168449801700402.

[53] W. F. Stanley and P. J. Mallon, "Intraply shear characterisation of a fibre reinforced thermoplastic composite," *Compos. Part A Appl. Sci. Manuf.*, vol. 37, no. 6, pp. 939–948, 2006, doi: 10.1016/j.compositesa.2005.03.017.

[54] A. Rashidi, H. Montazerian, K. Yesilcimen, and A. S. Milani, "Experimental characterization of the inter-ply shear behavior of dry and prepreg woven fabrics: Significance of mixed lubrication mode during thermoset composites processing," *Compos. Part A Appl. Sci. Manuf.*, vol. 129, 2020, doi: 10.1016/j.compositesa.2019.105725.

[55] K. Vanclooster, S. V. Lomov, and I. Verpoest, "Investigation of interply shear in composite forming," *Int. J. Mater. Form.*, vol. 1, no. 1, pp. 957–960, 2008, doi: 10.1007/s12289-008-0216-8.

[56] Q. Chen, P. Boisse, C. H. Park, A. Saouab, and J. Bréard, "Intra/inter-ply shear behaviors of continuous fiber reinforced thermoplastic composites in thermoforming processes," *Compos. Struct.*, vol. 93, no. 7, pp. 1692–1703, 2011,

doi: 10.1016/j.compstruct.2011.01.002.

[57] M. Danzi, F. Klunker, and P. Ermanni, “Experimental validation of through-thickness resin flow model in the consolidation of saturated porous media,” *J. Compos. Mater.*, vol. 51, no. 17, pp. 2467–2475, Jul. 2017, doi: 10.1177/0021998316671574.

[58] A. Savadori and D. Cutolo, “Impregnation, flow and deformation during processing of advanced thermoplastic composites,” *Makromol. Chemie. Macromol. Symp.*, vol. 68, no. 1, pp. 109–131, 1993, doi: 10.1002/masy.19930680110.

[59] T. G. Gutowski, T. Morigaki, and Z. Cai, “The Consolidation of Laminate Composites,” *J. Compos. Mater.*, vol. 21, no. 2, pp. 172–188, 1987, doi: 10.1177/002199838702100207.

[60] T. G. Gutowski and G. Dillon, “The Elastic Deformation of Lubricated Carbon Fiber Bundles: Comparison of Theory and Experiments,” *J. Compos. Mater.*, vol. 26, no. 16, pp. 2330–2347, 1992, doi: 10.1177/002199839202601601.

[61] T. G. Gutowski, Z. Cai, S. Bauer, D. Boucher, J. Kingery, and S. Wineman, “Consolidation Experiments for Laminate Composites,” *J. Compos. Mater.*, vol. 21, no. 7, pp. 650–669, 1987, doi: 10.1177/002199838702100705.

[62] S. P. Neuman, “Theoretical derivation of Darcy’s law,” *Acta Mech.*, vol. 25, no. 3–4, pp. 153–170, 1977, doi: 10.1007/BF01376989.

[63] K. Terzaghi, *Theoretical Soil Mechanics*. New York: J. Wiley and Sons, Inc, 1943.

[64] M. Wysocki, L. E. Asp, S. Toll, and R. Larsson, “Two phase continuum modelling of composites consolidation,” *Plast. Rubber Compos.*, vol. 38, no. 2–4, pp. 93–97, 2009, doi: 10.1179/174328909X387856.

[65] J. Merotte, P. Simacek, and S. G. Advani, “Resin flow analysis with fiber preform deformation in through thickness direction during Compression Resin Transfer Molding,” *Compos. Part A Appl. Sci. Manuf.*, vol. 41, no. 7, pp. 881–887, Jul. 2010, doi: 10.1016/j.compositesa.2010.03.001.

[66] P. V. Lade and R. De Boer, “The concept of effective stress for soil, concrete and rock,” *Geotechnique*, vol. 47, no. 1, pp. 61–78, 1997, doi: 10.1680/geot.1997.47.1.61.

[67] K. N. Manahiloh, B. Muhunthan, and W. J. Likos, “Microstructure-Based Effective Stress Formulation for Unsaturated Granular Soils,” *Int. J. Geomech.*, vol. 16, no. 6, 2016, doi: 10.1061/(asce)gm.1943-5622.0000617.

[68] M. Imbert, S. Comas-Cardona, E. Abisset-Chavanne, and D. Prono, “Introduction of intra-tow release/storage mechanisms in reactive dual-scale flow numerical simulations,” *J. Compos. Mater.*, vol. 53, no. 1, pp. 125–140, 2019, doi: 10.1177/0021998318780498.

[69] D. Salvatori, B. Caglar, H. Teixidó, and V. Michaud, “Permeability and capillary effects in a channel-wise non-crimp fabric,” *Compos. Part A Appl. Sci. Manuf.*, vol. 108, pp. 41–52, 2018, doi: 10.1016/j.compositesa.2018.02.015.

[70] Y. Inoue, M. Matsumoto, M. Hojo, and K. Ishida, “Microscale simulation of resin-air flow around single fibers,” 2010.

[71] T. A. Cender, P. Simacek, and S. G. Advani, “Resin film impregnation in fabric prepregs with dual length scale permeability,” *Compos. Part A Appl. Sci. Manuf.*, vol. 53, pp. 118–128, 2013, doi: 10.1016/j.compositesa.2013.05.013.

[72] T. D. Papathanasiou, “Flow across structured fiber bundles: A dimensionless correlation,” *Int. J. Multiph. Flow*, vol. 27, no. 8, pp. 1451–1461, 2001, doi: 10.1016/S0301-9322(01)00013-1.

[73] X. Li, S. R. Hallett, and M. R. Wisnom, “Modelling the effect of gaps and overlaps in automated fibre placement (AFP)-manufactured laminates,” *Sci. Eng. Compos. Mater.*, vol. 22, no. 2, pp. 115–129, 2015, doi: 10.1515/secm-2013-0322.

[74] Y. Gu, C. Xin, M. Li, Y. Cheng, and Z. Zhang, “Resin pressure and resin flow inside tapered laminates during zero-bleeding and bleeding processes,” *J. Reinf. Plast. Compos.*, vol. 31, no. 4, pp. 205–214, 2012, doi: 10.1177/0731684411434149.

[75] A. S. Ganapathi, S. C. Joshi, and Z. Chen, “Bleeder thickness optimization for controlling resin content in thick laminated composites,” *Adv. Mater. Res.*, vol. 740, pp. 698–703, 2013, doi: 10.4028/www.scientific.net/AMR.740.698.

[76] S. Thomas, C. Bongiovanni, and S. R. Nutt, “In situ estimation of through-thickness resin flow using ultrasound,” *Compos. Sci. Technol.*, vol. 68, no. 15–16, pp. 3093–3098, 2008, doi: 10.1016/j.compscitech.2008.07.012.

[77] J. Bréard, Y. Henzel, F. Trochu, and R. Gauvin, “Analysis of dynamic flows through porous media. Part II: Deformation of a double-scale fibrous reinforcement,” *Polym. Compos.*, vol. 24, no. 3, pp. 409–421, 2003, doi: 10.1002/pc.10039.

[78] A. A. Somashekar, S. Bickerton, and D. Bhattacharyya, “Exploring the non-elastic compression deformation of dry glass fibre reinforcements,” *Compos. Sci. Technol.*, vol. 67, no. 2, pp. 183–200, 2007, doi: 10.1016/j.compscitech.2006.07.032.

[79] Q. T. Nguyen *et al.*, “Mesoscopic scale analyses of textile composite reinforcement compaction,” *Compos. Part B Eng.*, vol. 44, no. 1, pp. 231–241, 2013, doi: 10.1016/j.compositesb.2012.05.028.

[80] P. Badel, E. Vidal-sallé, E. Maire, and P. Boisse, “Simulation and tomography analysis of textile composite reinforcement deformation at the mesoscopic scale,” *Compos. Sci. Technol.*, vol. 68, no. 12, pp. 2433–2440, 2008, doi: 10.1016/j.compscitech.2008.04.038.

[81] J. P. H. Belnoue, O. J. Nixon-Pearson, A. J. Thompson, D. S. Ivanov, K. D. Potter, and S. R. Hallett, “Consolidation-driven defect generation in thick composite parts,” *J. Manuf. Sci. Eng. Trans. ASME*, vol. 140, no. 7, 2018, doi: 10.1115/1.4039555.

[82] B. Varkonyi, J. P.-H. Belnoue, J. Kratz, and S. R. Hallett, “Predicting consolidation-induced wrinkles and their effects on composites structural performance,” *Int. J. Mater. Form.*, vol. 13, pp. 907–921, Nov. 2019, doi: 10.1007/s12289-019-01514-2.

[83] A. Thompson, J. Belnoue, and S. R. Hallett, “Numerical modelling of defect generation during preforming of multiple layers of 2D woven fabrics,” 2016.

[84] A. J. Thompson, J. R. McFarlane, J. P. H. Belnoue, and S. R. Hallett, “Numerical modelling of compaction induced defects in thick 2D textile composites,” *Mater. Des.*, vol. 196, p. 109088, 2020, doi: 10.1016/j.matdes.2020.109088.

[85] J. P. Belnoue, M. A. Valverde, M. Onoufriou, X. R. Sun, D. S. Ivanov, and S. R. Hallett, “On the physical relevance of power law-based equations to describe the compaction behaviour of resin infused fibrous materials,” *Int. J. Mech. Sci.*, vol. 199, 2021, doi: 10.1016/j.ijmecsci.2021.106425.

[86] T. Kruckenburg and R. Parton, “Compaction of dry and lubricated reinforcements,” *Proc. FPCM-7, Delaware*, pp. 425–436, 2004.

[87] P. Hubert, A. Johnston, A. Poursartip, and K. Nelson, “Cure kinetics and viscosity models for Hexcel 8552 epoxy resin,” *Int. SAMPE Symp. Exhib.*, pp. 2341–2354, 2014.

[88] J. Zhu, S. Wei, A. Yadav, and Z. Guo, “Rheological behaviors and electrical conductivity of epoxy resin nanocomposites suspended with in-situ stabilized carbon nanofibers,” *Polymer (Guildf).*, vol. 51, no. 12, pp. 2643–2651, 2010, doi: 10.1016/j.polymer.2010.04.019.

[89] C. Ghnatios, F. Chinesta, and C. Binetruy, “3D Modeling of squeeze flows occurring in composite laminates,” *Int. J. Mater. Form.*, vol. 8, no. 1, pp. 73–83, 2015, doi: 10.1007/s12289-013-1149-4.

[90] T. G. Rogers, “Squeezing flow of fibre-reinforced viscous fluids,” *J. Eng. Math.*, vol. 23, no. 1, pp. 81–89, 1989, doi: 10.1007/BF00058434.

[91] T. S. Mesogitis, A. A. Skordos, and A. C. Long, “Uncertainty in the manufacturing of fibrous thermosetting composites: A review,” *Compos. Part A Appl. Sci. Manuf.*, vol. 57, pp. 67–75, 2014, doi: 10.1016/j.compositesa.2013.11.004.

[92] A. C. Long, C. E. Wilks, and C. D. Rudd, “Experimental characterisation of the consolidation of a commingled glass/polypropylene composite,” *Compos. Sci. Technol.*, vol. 61, no. 11, pp. 1591–1603, 2001, doi: 10.1016/S0266-3538(01)00059-8.

[93] P. A. Kelly, “A viscoelastic model for the compaction of fibrous materials,” *J. Text. Inst.*, vol. 102, no. 8, pp. 689–699, Aug. 2011, doi: 10.1080/00405000.2010.515103.

[94] G. C. Papanicolaou and S. P. Zaoutsos, *Viscoelastic constitutive modeling of creep and stress relaxation in polymers and polymer matrix composites*, 2nd ed. Elsevier Ltd., 2019.

[95] F. M. Monticeli, H. L. Ornaghi, R. M. Neves, and M. Odila Hilário Cioffi, “Creep/recovery and stress-relaxation tests applied in a standardized carbon fiber/epoxy composite: Design of experiment approach,” *J. Strain Anal. Eng. Des.*, vol. 55, no. 3–4, pp. 109–117, 2020, doi: 10.1177/0309324719892710.

[96] J. H. Almeida, H. L. Ornaghi, N. Lorandi, G. Marinucci, and S. Amico, “On creep, recovery, and stress relaxation of carbon fiber-reinforced epoxy filament wound composites,” *Polym. Eng. Sci.*, vol. 58, no. 10, pp. 1837–1842, 2018, doi: 10.1002/pen.24790.

[97] K. S. Fancey, “A latch-based weibull model for polymerie creep and recovery,” *J. Polym. Eng.*, vol. 21, no. 6, pp. 489–510, 2001, doi: 10.1515/POLYENG.2001.21.6.489.

[98] M. Al-Haik, M. R. Vaghar, H. Garmestani, and M. Shahawy, “Viscoplastic analysis of structural polymer composites using stress relaxation and creep data,” *Compos. Part B Eng.*, vol. 32, no. 2, pp. 165–170, 2001, doi: 10.1016/S1359-8368(00)00042-1.

[99] T. S. Gates and C. T. Sun, “Elastic/Viscoplastic constitutive model for fiber reinforced thermoplastic composites,” *AIAA J.*, vol. 29, no. 3, pp. 457–463, 1991, doi: 10.2514/3.59922.

[100] R. M. Guedes, A. T. Marques, and A. Cardon, “Analytical and Experimental Evaluation of Nonlinear Viscoelastic-Viscoplastic Composite Laminates under Creep, Creep-Recovery, Relaxation and Ramp Loading,” *Mech. Time-Dependent Mater.*, vol. 2, no. 2, pp. 113–128, 1998, doi: 10.1023/a:1009862009738.

[101] P. Hubert and A. Poursartip, “A method for the direct measurement of the fibre bed compaction curve of composite prepregs,” *Compos. Part A Appl. Sci. Manuf.*, vol. 32, no. 2, pp. 179–187, 2001, doi: 10.1016/S1359-835X(00)00143-3.

[102] Q. Govignon, S. Bickerton, and P. A. Kelly, “Simulation of the reinforcement compaction and resin flow during the complete resin infusion process,” *Compos. Part A Appl. Sci. Manuf.*, vol. 41, no. 1, pp. 45–57, 2010, doi: 10.1016/j.compositesa.2009.07.007.

[103] F. Robitaille; and R. Gauvin, “Compaction of textile reinforcements for composites manufacturing. II: Compaction and relaxation of dry and H2O-saturated woven reinforcements,” *Polym. Compos.*, vol. 19, no. 5, pp. 543–557, 1998, doi: 10.1002/pc.10128.

[104] J. Engmann, C. Servais, and A. S. Burbidge, “Squeeze flow theory and applications to rheometry: A review,” *J. Nonnewton. Fluid Mech.*, vol. 132, no.

1–3, pp. 1–27, Dec. 2005, doi: 10.1016/j.jnnfm.2005.08.007.

[105] P. Harrison, M. J. Clifford, A. C. Long, and C. D. Rudd, “A constituent-based predictive approach to modelling the rheology of viscous textile composites,” *Compos. Part A Appl. Sci. Manuf.*, vol. 35, no. 7–8, pp. 915–931, 2004, doi: 10.1016/j.compositesa.2004.01.005.

[106] A. C. Harrison, P., Thije, R.T., Akkerman, R., and Long, “Characterising and Modelling Tool-Ply Friction of Viscous Textile Composites,” *World J. Eng.*, vol. 7, no. 1, pp. 5–22, 2010.

[107] R. Arbter *et al.*, “Experimental determination of the permeability of textiles : A benchmark exercise,” *Compos. Part A*, vol. 42, pp. 1157–1168, 2011, doi: 10.1016/j.compositesa.2011.04.021.

[108] N. Vernet *et al.*, “Experimental determination of the permeability of engineering textiles : Benchmark II,” *Compos. Part A*, vol. 61, pp. 172–184, 2014, doi: 10.1016/j.compositesa.2014.02.010.

[109] S. B. Sharma, M. P. F. Sutcliffe, and S. H. Chang, “Characterisation of material properties for draping of dry woven composite material,” *Compos. Part A Appl. Sci. Manuf.*, vol. 34, no. 12, pp. 1167–1175, 2003, doi: 10.1016/j.compositesa.2003.09.001.

[110] L. Fahrmeir, T. Kneib, and S. Lang, *Regression: Models, Methods and Applications*, 2013th ed. Springer, 2013.

[111] R. Chartrand, “Numerical Differentiation of Noisy, Nonsmooth Data,” *ISRN Appl. Math.*, vol. 2011, pp. 1–11, 2011, doi: 10.5402/2011/164564.

[112] I. Knowles and R. J. Renka, “Methods for numerical differentiation of noisy data,” *Electron. J. Differ. Equations*, vol. 21, pp. 235–246, 2014.

[113] S. N. Wood, *Generalized Additive Models: An Introduction with R*, 1st ed. Chapman and Hall, 2016.

[114] S. L. Brunton, J. L. Proctor, J. N. Kutz, and W. Bialek, “Discovering governing equations from data by sparse identification of nonlinear dynamical systems,” *Proc. Natl. Acad. Sci. U. S. A.*, vol. 113, no. 15, pp. 3932–3937, 2016, doi: 10.1073/pnas.1517384113.

[115] S. H. Rudy, S. L. Brunton, J. L. Proctor, and J. N. Kutz, “Data-driven discovery

of partial differential equations," *Sci. Adv.*, vol. 3, no. 4, pp. 1–7, 2017, doi: 10.1126/sciadv.1602614.

[116] H. R. Hafizpour, M. Sanjari, and A. Simchi, "Analysis of the effect of reinforcement particles on the compressibility of Al – SiC composite powders using a neural network model," *Mater. Des.*, vol. 30, no. 5, pp. 1518–1523, 2009, doi: 10.1016/j.matdes.2008.07.052.

[117] M. Anthony and P. L. Bartlett, *Neural Network Learning: Theoretical Foundations*, 1st ed. Cambridge University Press, 1999.

[118] M. Lefik and M. Wojciechowski, "Artificial Neural Network as a numerical form of effective constitutive law for composites with parametrized and hierarchical microstructure," *Comput. Assist. Mech. Eng. Sci.*, vol. 12, no. 2–3, pp. 183–194, 2005.

[119] T. Qin, K. Wu, and D. Xiu, "Data driven governing equations approximation using deep neural networks," *J. Comput. Phys.*, vol. 395, pp. 620–635, 2019, doi: 10.1016/j.jcp.2019.06.042.

[120] C. González and J. Fernández-León, "A Machine Learning Model to Detect Flow Disturbances during Manufacturing of Composites by Liquid Moulding," *J. Compos. Sci.*, vol. 4, no. 2, p. 71, 2020, doi: 10.3390/jcs4020071.

[121] A. Díaz Lantada, P. Lafont Morgado, J. Luis Muñoz Sanz, J. Manuel Muñoz Guijosa, and J. Echávarri Otero, "Neural Network Approach to Modelling the Behaviour of Ionic Polymer-Metal Composites in Dry Environments," *J. Signal Inf. Process.*, vol. 03, no. 02, pp. 137–145, 2012, doi: 10.4236/jsip.2012.32018.

[122] P. Sangeetha and M. Shanmugapriy, "Artificial neural network applications in fiber reinforced concrete," *J. Phys. Conf. Ser.*, vol. 1706, no. 1, 2020, doi: 10.1088/1742-6596/1706/1/012113.

[123] A. Karpatne *et al.*, "Theory-guided data science: A new paradigm for scientific discovery from data," *IEEE Trans. Knowl. Data Eng.*, vol. 29, no. 10, pp. 2318–2331, Oct. 2017, doi: 10.1109/TKDE.2017.2720168.

[124] R. T. Q. Chen, Y. Rubanova, J. Bettencourt, and D. Duvenaud, "Neural Ordinary Differential Equations," *arXiv Prepr.*, 2018.

[125] S. A. Niaki, E. Haghighat, T. Campbell, A. Poursartip, and R. Vaziri, "Physics-Informed Neural Network for Modelling the Thermochemical Curing Process of

Composite-Tool Systems During Manufacture," *Comput. Methods Appl. Mech. Eng.*, vol. 384, 2020, doi: 10.1016/j.cma.2021.113959.

[126] M. P. Mignolet, "Fiber Clustering: A Comparison of Two Resin Flow Models," *J. Compos. Mater.*, vol. 28, no. 15, pp. 1467–1479, 1994, doi: 10.1177/002199839402801505.

[127] S. Shahsavari and G. H. McKinley, "Mobility of power-law and Carreau fluids through fibrous media," *Phys. Rev. E - Stat. Nonlinear, Soft Matter Phys.*, vol. 92, no. 6, Dec. 2015, doi: 10.1103/PhysRevE.92.063012.

[128] P. 1 Carreau, D. De Kee, and M. Daroux, "An Analysis of the Viscous Behaviour of Polymeric Solutions," *J. Chem. Eng.*, vol. 57, no. 2, pp. 135–140, 1979.

[129] Mario A. Valverde, J. P.-H. Belnoue, R. Kupfer, L. F. Kawashita, M. Gude, and S. R. Hallett, "Compaction behaviour of continuous fibre-reinforced thermoplastic composites under rapid processing conditions," *Compos. Part A Appl. Sci. Manuf.*, vol. 149, 2021, doi: 10.1016/j.compositesa.2021.106549.

[130] J. P. H. Belnoue *et al.*, "Understanding and predicting defect formation in automated fibre placement pre-preg laminates," *Compos. Part A Appl. Sci. Manuf.*, vol. 102, pp. 196–206, Nov. 2017, doi: 10.1016/j.compositesa.2017.08.008.

[131] A. J. M. Spencer, *Deformations of Fibre-Reinforced Materials*. Clarendon Press, Oxford University Press, 1972.

[132] R. B. Pipes, "Anisotropic Viscosities of an Oriented Fiber Composite with a Power-Law Matrix," *J. Compos. Mater.*, vol. 26, no. 10, pp. 1536–1552, 1992, doi: 10.1177/002199839202601009.

[133] C. Servais, A. Luciani, and J.-A. E. Månson, "Squeeze flow of concentrated long fibre suspensions: experiments and model," *J. Nonnewton. Fluid Mech.*, vol. 104, no. 2–3, pp. 165–184, 2002, doi: 10.1016/S0377-0257(02)00018-6.

[134] B. Bird and O. Hassager, *Dynamics of Polymeric Liquids: Fluid Mechanics. Volume 1, 2*. 1987.

[135] F. Lapique and K. Redford, "Curing effects on viscosity and mechanical properties of a commercial epoxy resin adhesive," *Int. J. Adhes. Adhes.*, vol. 22, no. 4, pp. 337–346, 2002, doi: 10.1016/S0143-7496(02)00013-1.

[136] A. Gokce, M. Chohra, S. G. Advani, and S. M. Walsh, “Permeability estimation algorithm to simultaneously characterize the distribution media and the fabric preform in vacuum assisted resin transfer molding process,” *Compos. Sci. Technol.*, vol. 65, no. 14, pp. 2129–2139, 2005, doi: 10.1016/j.compscitech.2005.05.012.

[137] B. T. Åström, R. B. Pipes, and S. G. Advani, “On Flow through Aligned Fiber Beds and Its Application to Composites Processing,” *J. Compos. Mater.*, vol. 26, no. 9, pp. 1351–1373, 1992, doi: 10.1177/002199839202600907.

[138] F. Lionetto, F. Montagna, and A. Maffezzoli, “Out-Of-Plane permeability evaluation of carbon fiber preforms by ultrasonic wave propagation,” *Materials (Basel).*, vol. 13, no. 12, pp. 1–18, 2020, doi: 10.3390/ma13122684.

[139] H. S. Salem, “Application of the Kozeny-Carman equation to permeability determination for a glacial outwash aquifer, using grain-size analysis,” *Energy Sources*, vol. 23, no. 5, pp. 461–473, 2001, doi: 10.1080/009083101300058480.

[140] S. G. Advani and E. M. Sozer, *Process modeling in composites manufacturing*, 2nd ed. CRC Press, 2003.

[141] P. C. Carman, “Fluid flow through granular beds,” *Chem. Eng. Res. Des.*, vol. 15, pp. 150–166, 1937, doi: 10.1016/S0263-8762(97)80003-2.

[142] B. R. Gebart, “Permeability of Unidirectional Reinforcements for RTM,” *J. Compos. Mater.*, vol. 26, no. 8, pp. 1100–1133, 1992, doi: 10.1177/002199839202600802.

[143] M. Sandberg *et al.*, “Permeability and compaction behaviour of air-texturised glass fibre rovings: A characterisation study,” *J. Compos. Mater.*, vol. 54, no. 27, pp. 4241–4252, Nov. 2020, doi: 10.1177/0021998320926703.

[144] T. G. Gutowski, “Resin flow/fiber deformation model for composites,” *SAMPE Q.*, vol. 16, no. 4, pp. 58–64, 1985.

[145] P. Sousa, S. V. Lomov, and J. Ivens, “Methodology of dry and wet compressibility measurement,” *Compos. Part A Appl. Sci. Manuf.*, vol. 128, 2020, doi: 10.1016/j.compositesa.2019.105672.

[146] B. Yenilmez and E. M. Sozer, “Compaction of e-glass fabric preforms in the Vacuum Infusion Process, A: Characterization experiments,” *Compos. Part A Appl. Sci. Manuf.*, vol. 40, no. 4, pp. 499–510, 2009, doi:

10.1016/j.compositesa.2009.01.016.

[147] S. V. Lomov *et al.*, “Compression resistance and hysteresis of carbon fibre tows with grown carbon nanotubes/nanofibres,” *Compos. Sci. Technol.*, vol. 71, no. 15, pp. 1746–1753, 2011, doi: 10.1016/j.compscitech.2011.08.007.

[148] G. Van Rossum and Python Dev Team, *Python 3.6 Language Reference*. Samurai Media Limited, 2016.

[149] J. Martin, D. D. R. de Adana, and A. G. Asuero, “Fitting Models to Data: Residual Analysis, a Primer,” in *Uncertainty Quantification and Model Calibration*, J. P. Hessling, Ed. InTech, 2017.

[150] V. Vijayaraghavan, A. Garg, J. S. L. Lam, B. Panda, and S. S. Mahapatra, “Process characterisation of 3D-printed FDM components using improved evolutionary computational approach,” *Int. J. Adv. Manuf. Technol.*, vol. 78, no. 5–8, pp. 781–793, May 2015, doi: 10.1007/s00170-014-6679-5.

[151] J. Laxalde, C. Ruckebusch, O. Devos, N. Caillol, F. Wahl, and L. Duponchel, “Characterisation of heavy oils using near-infrared spectroscopy: Optimisation of pre-processing methods and variable selection,” *Anal. Chim. Acta*, vol. 705, no. 1–2, pp. 227–234, Oct. 2011, doi: 10.1016/j.aca.2011.05.048.

[152] K. Y. Chan, C. K. Kwong, T. S. Dillon, and Y. C. Tsim, “Reducing overfitting in manufacturing process modeling using a backward elimination based genetic programming,” in *Applied Soft Computing Journal*, Mar. 2011, vol. 11, no. 2, pp. 1648–1656, doi: 10.1016/j.asoc.2010.04.022.

[153] D. Jouan-Rimbaud, D. L. Massart, and O. E. De Noord, “Random correlation in variable selection for multivariate calibration with a genetic algorithm,” *Chemom. Intell. Lab. Syst.*, vol. 35, no. 2, pp. 213–220, 1996, doi: 10.1016/S0169-7439(96)00062-7.

[154] J. Vanhuyse, E. Deckers, S. Jonckheere, B. Pluymers, and W. Desmet, “Global optimisation methods for poroelastic material characterisation using a clamped sample in a Kundt tube setup,” *Mech. Syst. Signal Process.*, vol. 68–69, pp. 462–478, Feb. 2016, doi: 10.1016/j.ymssp.2015.06.027.

[155] J. E. F. Green and A. Friedman, “The extensional flow of a thin sheet of incompressible, transversely isotropic fluid,” *Eur. J. Appl. Math.*, vol. 19, no. 3, pp. 225–257, Jun. 2008, doi: 10.1017/S0956792508007377.

[156] W. Brocks, I. Scheider, and D. Steglich, “Hybrid Methods for Material Characterisation,” *Int. J. Pure Appl. Math.*, vol. 49, no. 4, pp. 553–558, 2008.

[157] D. H. J. A. Lukaszewicz and K. Potter, “Through-thickness compression response of uncured prepreg during manufacture by automated layup,” *Proc. Inst. Mech. Eng. Part B J. Eng. Manuf.*, vol. 226, no. 2, pp. 193–202, Feb. 2012, doi: 10.1177/0954405411411817.

[158] HEXCEL Corporation, “HexPly ® M21 180°C (350°F) curing epoxy matrix. Epoxy Matrix Product Datasheet,” 2015. [Online]. Available: www.hexcel.com.

[159] INSTRON, “5960 Series Dual Column Table Frames Operator’s guide,” 2009. [Online]. Available: www.instron.com.

[160] Instron, “General Purpose Input/Output Option. Reference Manual. M10-16200-EN Revision B.” [Online]. Available: www.instron.com.

[161] Grip-Engineering-GmbH, “Self-aligning compression platens datasheet,” 2020. [Online]. Available: https://grip.de/pdf/THS223_Datasheet.pdf.

[162] Tekscan, “T-Scan Evolution Handle Datasheet.” [Online]. Available: https://www.tekscan.com/products-solutions/electronics/t-scan-evolution-handle.

[163] M. Newville, T. Stensitzki, D. B. Allen, and A. Ingargiola, “LMFIT: Non-Linear Least-Square Minimization and Curve-Fitting for Python,” 2018. doi: 10.5281/zenodo.11813.

[164] F. Gao and L. Han, “Implementing the Nelder-Mead simplex algorithm with adaptive parameters,” *Comput. Optim. Appl.*, vol. 51, no. 1, pp. 259–277, Jan. 2012, doi: 10.1007/s10589-010-9329-3.

[165] C. R. Rao and H. Toutenburg, *Linear Models: Least Squares and Alternatives, Second Edition*. Springer, 1999.

[166] D. J. Wales and J. P. K. Doye, “Global Optimization by Basin-Hopping and the Lowest Energy Structures of Lennard-Jones Clusters Containing up to 110 Atoms,” *J. Phys. Chem. A*, vol. 101, no. 28, pp. 5111–5116, 1997, doi: 10.1021/jp970984n.

[167] R. Storn and K. Price, “Differential Evolution-A Simple and Efficient Heuristic for Global Optimization over Continuous Spaces,” *J. Glob. Optim.*, vol. 11, pp. 341–359, 1997, doi: 10.1023/A:1008202821328.

[168] R. Haberman, *Elementary Applied Partial Differential Equations, with Fourier Series and Boundary Value Problems*, 2nd ed. Pearson, 1986.

[169] E. Bunder and A. J. Roberts, "Numerical integration of ordinary differential equations with rapidly oscillatory factors," *J. Comput. Appl. Math.*, vol. 282, pp. 54–70, 2015, doi: 10.1016/j.cam.2014.12.033.

[170] M. Condon, A. Deaño, and A. Iserles, "On second-order differential equations with highly oscillatory forcing terms," *Proc. R. Soc. A Math. Phys. Eng. Sci.*, vol. 466, no. 2118, pp. 1809–1828, 2010, doi: 10.1098/rspa.2009.0481.

[171] S. Ilie, G. Söderlind, and R. M. Corless, "Adaptivity and computational complexity in the numerical solution of ODEs," *J. Complex.*, vol. 24, no. 3, pp. 341–361, 2008, doi: 10.1016/j.jco.2007.11.004.

[172] K. R. Jackson and R. Sacks-Davis, "An Alternative Implementation of Variable Step-Size Multistep Formulas for Stiff ODEs," *ACM Trans. Math. Softw.*, vol. 6, no. 3, pp. 295–318, 1980, doi: 10.1145/355900.355903.

[173] D. J. Higham and L. N. Trefethen, "Stiffness of ODEs," *BIT Numer. Math.*, vol. 33, no. 2, pp. 285–303, 1993, doi: 10.1007/BF01989751.

[174] L. Ramalho, *Fluent Python: Clear, concise, and effective programming.* O'Reilly Media, Inc., 2015.

[175] NationalInstruments, "LabVIEW User Manual - National Instruments," 2003.

[176] HEXCEL Corporation, "HexPly 8552 ® Epoxy matrix (180°C/356°F curing matrix). Epoxy Matrix Product Datasheet," 2020. [Online]. Available: www.hexcel.com.

[177] Bcomp Ltd., "ampliTex^{TM} 5040 flax fibres fabric. Fabric Product Datasheet." [Online]. Available: www.bcomp.ch.

[178] Y. Jamali and M. A. Matlob, "The Concepts and Applications of Fractional Order Differential Calculus in Modelling of Viscoelastic Systems: A primer."

[179] P. J. Torvik and R. L. Bagley, "On the Appearance of the Fractional Derivative in the Behavior of Real Materials," *J. Appl. Mech.*, vol. 51, no. 2, 1984, doi: 10.1115/1.3167615.